University of Alberta

The Use of the SPT and CPT in Loose Sands

by

Eric Barritt Niven 

A thesis submitted to the Faculty of Graduate Studies and Research in partial fulfillment of the requirements for the degree of *Master of Science*

in

Geotechnical Engineering

Department of *Civil and Environmental Engineering*

Edmonton, Alberta

Spring 2006

Your file Votre référence
ISBN: 0-494-13864-5
Our file Notre référence
ISBN: 0-494-13864-5

ABSTRACT

The SPT and CPT are two commonly used in-situ tests to determine potential for liquefaction in sandy soils. Results from in-situ testing at Syncrude's Aurora Tailings Dam showed conflicting results between the SPT and CPT data. It was found from testing at the Massey Tunnel site that the discrepancy between the SPT and CPT data was likely caused by the weight of the SPT equipment coupled with the generation of excess pore pressures due to the dynamic nature of the SPT.

It was found that the weight of the SPT rods, sampler and hammer have a significant impact on the blow count. Furthermore, it was found that positive or negative excess pore pressures could be generated during the SPT depending on the relative density of the sand.

ACKNOWLEDGEMENTS

There are a number of individuals and organizations that I would like to thank for helping to make this research possible, including:

- Syncrude Canada Ltd. and NSERC for generously funding this research
- Dr. Dave Sego and Dr. Peter Robertson for their ideas and guidance
- ConeTec Investigations Ltd. for field testing support and Adara Systems Ltd. for designing and building the SPTu device
- Ted Lord of Syncrude Canada Ltd.
- My family and friends for their continual support and encouragement

TABLE OF CONTENTS

LIST OF FIGURES

LIST OF TABLES

LIST OF NOMENCLATURE

BBW – Beach below water sand
BAW – Beach above water sand
q_c – Cone tip resistance
q_{c1n} – Cone tip resistance corrected for overburden pressure
(q_{cp} – Cone tip resistance predicted by Schmertmann's method
$(q_{c1n})_p$ – Cone tip resistance predicted by Schmertmann's method, corrected for overburden stress and normalized
q_t – q_c forrected for any unequal area effects: $q_t = q_c (1 – au)$
f_s – Cone penetration test sleeve friction
I_c – Soil classification index
u – Pore water pressure
P_a – Atmospheric pressure
σ'_v – Vertical effective stress
D_r – Relative density of soil
C – unit-less constant dependent on the age of the deposit
n – Stress exponent
N – SPT blow count (blows per 300 mm)
N_{60} – SPT blow count corrected to 60% energy
$(N_1)_{60}$ – SPT blow count corrected for overburden stress and 60% energy
ER – Energy Ratio. Percentage of theoretical maximum energy that reaches the SPT Sampler
$F_{(avg)}$ – The average added quasi-static force during SPT sampling
A – is the constant fraction of maximum theoretical hammer energy
C_1 – Constant that relates quasi-static penetration resistance to cone tip resistance (i.e. $q_{spt} = C_1 q_c$)
C_2 - Constant that relates quasi-static penetration resistance to cone tip resistance (i.e. $f_{spt} = C_2 f_c$)
E' – is the quasi-static energy required for penetration of the sampler from 100 mm to 460 mm below the base of the borehole
$F_{(avg)}$ – average added quasi-static force during SPT sampling
F_e – End bearing force acting on SPT sampler
EBR – Approximate percentage of load due to end bearing resistance
PPV – Peak Particle Velocity
R – Vector distance
M – Explosive charge mass
S – Factor by which mass is scaled
PPR – Pore pressure ratio ($PPR = \Delta u / \sigma'_v$)

LIST OF APPENDICES

Page

1.0 INTRODUCTION

1.1 Background

Syncrude operates the largest oil sands production facility in the world by producing crude oil from tar sands and is responsible for over 13% of Canada's oil production. The oil sand is mined from three mines including the Base Mine, North Mine and Aurora Mine. The tailings resulting from processing of the oil sand are piped as slurry from the processing plant to the tailings ponds where they are deposited.

Normally, tailings would be deposited on a beach via a pipeline where the coarser particles settle out and the majority of the fines and water continue down to the pond. The material that is deposited on the beach slope above the waterline is called 'Beach Above Water' (BAW). The remaining particles that continue to travel down the beach slope and deposit on the underwater beach slope are called 'Beach Below Water' (BBW).

Previous research such as the Canadian Liquefaction Experiment (CANLEX) has shown that sand deposited as beach below water can be very loose and may be susceptible to liquefaction (Robertson et al. 2000). In addition, previous experience at Suncor Energy Inc. showed that rapid construction on top of loose BBW sands could lead to a loss of stability and flow slides into the tailings pond.

In response to the construction of beach below water deposits, Syncrude undertook a field program to evaluate the liquefaction susceptibility of the sand deposits. Such an evaluation is typically conducted using both Standard Penetration Testing (SPT) and Cone Penetration Testing (CPT). The investigation found that the SPT and CPT results did not correlate well with each other.

Lack of correlation between two methods of site investigation (in this case the SPT and CPT) may result in uncertainty in the data. This may result in over conservatism or under conservatism in design depending on which measurements are used in the analysis. The engineer may wonder which results better reflect the actual properties of the soil under investigation.

1.2 Previous Work

The Canadian Liquefaction Experiment (CANLEX) was a major collaborative research project undertaken to study the phenomenon of soil liquefaction in saturated sandy soils.

As part of CANLEX, a study of blast induced liquefaction was also conducted. In the experiment, single and multiple explosive charges were detonated in a level deposit of loose sand in J-Pit at the Syncrude site. At a depth of 6 m, in a level deposit of saturated Syncrude tailings, residual pore pressures were observed

and cyclic liquefaction occurred as a result of single and multiple charge explosions (Al-Qasimi et al. 2005).

After the identification of loose BBW sand, Syncrude performed a field experiment at the Aurora tailings dyke by loading an area of BBW material with a 16 m high embankment, resulting in an increase in effective stress of about 300 kPa on the BBW material. It was hypothesized that the increase in vertical stress in the loose BBW material would result in an increase in the relative density of the material. The results of the test showed an increase in both the cone penetration resistance and the shear wave velocity of the deposit, indicating an increase in density of the material, and that liquefaction of the tailings at the pond load test site was unlikely (Robertson 2004). The results of the site investigations and the Aurora pond load test are further analyzed and discussed in this thesis.

1.3 Objectives

In order to evaluate the potential for liquefaction in the Aurora tailings dyke, Syncrude initiated a field investigation program to ascertain the in situ state of the tailings. The field investigation program consisted of both standard penetration testing (SPT) and cone penetration testing (CPT) which were performed in areas of the dyke where BBW sand was deposited. The results of the investigation indicated two things. Firstly, that the BBW sand deposit may be susceptible to strain softening in undrained simple shear. Secondly, that the SPT and CPT results differed to some degree and did not correlate with each other in a manner consistent with the literature.

SPT and CPT results are normally compared by a ratio of the CPT tip resistance, q_c, to the SPT blow count, N (the q_c/N ratio). Based on previous research presented in the literature, one would expect a q_c/N ratio of 5 for sand (Robertson et al. 1983), when q_c is in units of atmospheric pressure (e.g. bar or tsf). The $q_{c1n}/(N_1)_{60}$ ratio can also be used to compare CPT and SPT results in a similar manner, where q_{c1n} is the normalized cone resistance and $(N_1)_{60}$ is the normalized SPT blow count corrected to 60% energy. At the Aurora tailings dam, $q_{c1n}/(N_1)_{60}$ ratios between 3.7 and 8.2 were measured. Moreover, the $q_{c1n}/(N_1)_{60}$ ratio was found to be dependent on $(N_1)_{60}$.

This observation raises questions over which in-situ test results should be used in a liquefaction analysis. The objective of this research is to evaluate and explain the variation in the $q_{c1n}/(N_1)_{60}$ ratio and its apparent dependence on the blow count, as shown in Figure 3.5 in Section 3.8.

For this research, it is postulated that the SPT test results may be misleading in very loose sands because of either one or both of the following two hypotheses:

1. In very loose sands, the weight of the SPT rods, hammer and sampler can overwhelm the resistance to penetration resulting in lower blow counts relative to the equivalent blow count obtained from the CPT.
2. The SPT itself may cause small zones of liquefaction in and around the sampler shoe in loose BBW sand. It may be that the dynamic nature of the SPT test in loose fine sand may cause a cyclic increase in the pore water pressure around the sampler shoe. If the pore pressure in the sand rises high enough to equal the overburden stress, the effective stress at the test depth could fall to zero causing a condition of cyclic liquefaction. If this were to occur, the measured SPT N-values could appear lower than the equivalent N-values obtained from the CPT and hence, may not represent the actual strength of the sand. It should be noted that it would not be necessary for full cyclic liquefaction to occur for N-values to be affected. Any significant increase in pore pressure due to the test could result in a decrease in effective stress and penetration resistance resulting in a decrease in blow count relative to the equivalent blow count obtained through the CPT (which is essentially a drained test).

The objective of this research was to evaluate the aforementioned hypotheses or to identify an alternate explanation for the observed apparent discrepancy between the CPT and SPT data.

In order to evaluate the first hypothesis mentioned above, an analysis of the Aurora Pond Load Test data was conducted. The effect of the weight of the SPT equipment was also examined based on previous research (Schmertmann 1979). An extension of previous research allowed for the prediction of the penetration of the sampler at the base of a borehole due solely to the weight of the SPT equipment.

In addition, a field program was developed to investigate the second hypothesis. In order to accomplish this, an SPT sampler was designed and constructed with a pore pressure transducer located just above the cutter shoe that allowed measurement of pore water pressure during the SPT. This test will be referred to as the Standard Penetration Test with pore pressure measurement (SPTu).

2.0 LITERATURE REVIEW ON THE SPT AND CPT

2.1 General

This section presents a review of literature on the SPT and CPT, which is deemed relevant to this research.

2.2 Standard Penetration Testing and Factors Affecting its Results

2.2.1 Overview

The standard penetration test (SPT) is the most widely used in-situ soil test in the world. Much research has been presented in the literature concerning the SPT over the last 30 years. The extensive use of the SPT has resulted in a number of useful correlations that allow engineers to apply SPT results directly to design for shallow and deep foundations as well as liquefaction analyses. Unfortunately, there are a number of limitations of the SPT especially concerning the variability and repeatability of results. Such variability in procedure was examined in detail by Kovacs (1981) and others. This section discusses a number of factors, which influence SPT results as well as the use of the SPT in liquefaction evaluations. Figure 2.1 shows a simplified diagram and a photo of an SPT set-up.

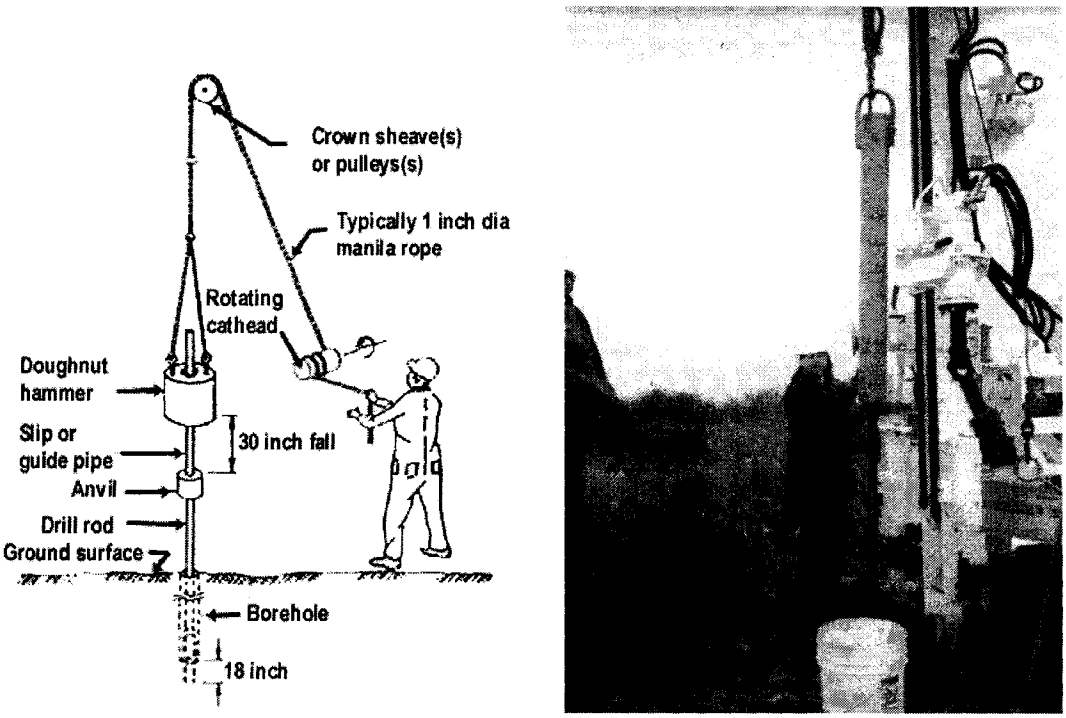

Figure 2.1: Standard Penetration Test

2.2.2 General Considerations

The wash boring technique or rotary drilling with a tricone bit should be used to drill the hole. The hole should be flushed with mud or water and should be maintained up to the ground water level (Skempton 1986).

The SPT should be conducted in boreholes between 65 mm and 150 mm in diameter, though preferably not more than 100 mm in diameter with the casing (if used) not advanced beyond the bottom of the hole (Skempton 1986).

It is now common practice to determine N between 15 and 46 cm (6" and 18") of penetration, as it is recognized that the first 15 cm (6 inches) may be a zone of disturbance from drilling.

2.2.3 Energy

Despite attempts to standardize the SPT, there remains widespread variation in the energy efficiency (energy reaching the sampler compared with the theoretical maximum potential energy of the SPT) of SPT hammer/anvil systems. As a result, it is clear that SPT N values must be corrected to a standard energy ratio (ER). It is standard practice to correct measured N values to an energy ratio of 60% of the potential energy of the hammer at the top of the stroke. In order to accomplish this, the energy reaching the sampler must be measured. The corrected SPT N values then become N_{60} values. Schmertmann and Palacios (1979) showed that the blow count in a given sand is inversely proportional to the drill rod energy. In addition, Robertson et al. (1983) presented SPT data from the same borehole using two different hammer types in alternating tests. They measured significantly higher N values but lower ER in the tests where a donut hammer was used compared to results measured using a safety hammer. When the results were corrected to a constant energy (in their case an ER of 55%), the results showed a consistent SPT profile.

In general, there are two computational procedures to measure the energy efficiency of SPT systems, the force velocity (Fv) method and the F^2 method. Studies have shown that the Fv method is more accurate than the F^2 method, which may result in greater variability (Butler et al. 1998; Farrar 1998). However, it is generally recommended that both Fv and F^2 data should be collected.

2.2.4 Drill Rod Influence

Research conducted by Schmertmann and Palacios (1979) indicates that the theoretical maximum possible energy ratio decreases for decreasing drill rod lengths less than approximately 10 m. The reason for this effect is that there is a reflection of energy in these short rods which result in less energy being used to drive the sampler into the soil (Seed et al. 1985). As such, correction factors should be used when drill rod lengths less than 10 m are used (Skempton 1986). It has been shown by Yokel (1982) that the energy loss effect in short rods is a function of the drill rod weight and the hammer weight. Yokel also suggested that the use of SPT in shallow investigations might be improved by choosing drill

rods with larger cross sectional areas or using a half-weight hammer and running the test with half the standard energy. However, these suggestions have not become standard practice.

The weight and stiffness of the rods appears to have no effect on the energy ratio for loose or dense sands up to a depth of 34 m (Brown 1977; Matsumoto and Matsubara 1982), although Seed et al. (1985) recommends using A or AW rods for holes less than 15 m (50 feet) deep and N or NW rods for holes of greater depths. Seed et al. (1985) proposed that a correction factor of 0.75 be used to correct SPT data from depths of zero to ten metres.

2.2.5 Liners Versus No Liners

SPT samplers are usually built with an inner diameter of the sampler that is slightly larger than the inner diameter of the shoe of the sampler so that a liner may be used in the sampler. However, in North America, the SPT is rarely used with liners in place. Usually the liners have been removed from the sampler. The practice of removing the liners from the sampler results in lower friction inside the sampler and hence, a slightly lower blow count than would be measured if the liners were left in place. On average, a sampler with liners installed will measure 10-30% more blows per 30 cm (foot) of penetration than a sampler without liners installed. The effect is less pronounced in loose sands where the effect is on the order of 10% than in dense sands where the effect may be upwards of 25-30% (Seed et al. 1985). As such, a correction factor should be used to compensate for this effect (Skempton 1986).

Leaving the liners out of SPT samplers makes it easier to remove the soil from the sampler and increases sample recovery. Schmertmann (1979) measured recovery in two boreholes comparing recoveries at the same depth. In all seventeen comparisons, Schmertmann measured greater recovery when not using liners. In fact, he measured 99% soil recovery for tests without liners and only 66% for testing with liners.

2.2.6 Overburden Pressure

The effect of overburden pressure must also be considered when interpreting SPT data. Standard practice is to normalize the SPT N-values to an effective overburden stress of 1 atmosphere (i.e. $\sigma_v' = 100$ kPa), which results in N_1-values where $N_1=C_N N$ (C_N is the correction factor for overburden pressure and N is the measured blow count). Further details regarding the normalization of SPT results will be provided in a later section.

2.2.7 Relative Density

The relative density of a sand refers to its density in relation its loosest and densest possible states as determined (i.e. $D_r = (e - e_{min})/(e_{max} - e_{min})$, where e is the void ratio of the sand, e_{min} is the lowest possible void ratio for the sand as determined by ASTM testing and e_{max} is the highest possible void ratio for the sand as determined by ASTM testing).

Saxena and Srinivasulu (1982) showed that estimation of relative density (D_r) of sands based upon SPT results is unreliable. They showed that the correlations tend to overestimate D_r at shallow depths and underestimate D_r at greater depths. However, the reason for the noted poor correlation was due to the method chosen to correct the field N values for the depth/overburden effects.

2.2.8 Overconsolidation and in-situ stresses

Aside from testing conditions, such as borehole size, or material dependent factors, such as the average particle size, penetration resistance in sands is also controlled largely by the current in-situ stress level (Clayton et al. 1985; Skempton 1986). An increase in penetration resistance can be caused by higher mean effective stresses as a result of over consolidation processes (Skempton 1986). Further, Schmertmann (1979) notes that the N value will vary with the octahedral effective stress and that the horizontal stress has twice the effect of the vertical stress. Clayton et al. (1985) also suggested that the horizontal stress level has twice as much of an impact on the penetration resistance when compared with the vertical stress level.

2.2.9 Borehole Diameter

Borehole diameter may have some effect on the measured blow count. The SPT should be performed in a borehole between 66 mm and approximately 115 mm if possible although in some countries larger boreholes are common (Skempton 1986). Seed et al. (1985) recommends that the borehole diameter be between 102 and 127 mm. While it appears that borehole diameter has little effect in cohesive soils, there is some evidence to suggest that lower blow counts may be recorded in sands where the borehole is larger than recommended (Sanglerat and Sanglerat 1982). Correction factors have been suggested for larger than standard boreholes (Skempton 1986).

2.2.10 Borehole advancement and support

The method of drilling used to advance the hole can also have an impact on the results of the SPT. The wash boring technique or rotary drilling with a tricone and mud flush, water or mud maintained to the groundwater level should be used (Seed et al. 1985; Skempton 1986).

Seed et al. (1988) showed that either water or drilling mud could be used to support the borehole and that SPT results were not dependent on the type of fluid used provided that careful drilling and sampling procedures are employed. However, it should be noted that the use of drilling mud instead of water is often a better choice. In order to avoid hydrostatic imbalance when using water as a drilling fluid, the drill rods must be withdrawn slowly. However, the use of drilling mud helps to reduce the chance of hydrostatic imbalance at the base of the hole since a surface reservoir is usually connected to the borehole which keeps the hole filled with mud at all times (Schmertmann 1989). In sand, SPT results obtained in holes with steel casing may differ from those obtained in holes

supported by drilling mud. Results have been presented which indicate that N values are increased above groundwater level and decreased below ground water level when a steel casing is used to support the hole rather than drilling mud (Whited and Edil 1986).

2.2.11 SPT Hammer Type

Another factor that influences SPT results is the hammer type used. It is well known that using an automatic hammer results in lower SPT N-values compared with results obtained from a safety hammer. The reason for the difference in results due to the hammer type used is due to the energy that is delivered to the sampler shoe (Drumright et al. 1996). The effect of the hammer type can be accounted for simply by measuring the energy ratio (ER_r) of the SPT set-up and correcting the N-values to the energy corrected standard N_{60}.

2.3 Cone Penetration Testing

2.3.1 Overview

The Cone Penetration Test (CPT) is useful in three aspects of site investigation. Firstly, it is a tool that can be used to determine sub-surface stratigraphy. Secondly, the CPT can be used to estimate geotechnical parameters. Thirdly, it can be used to provide results for direct geotechnical design (Robertson 1998). Figure 2.2 shows a diagram and pictures of typical CPT set-ups.

The advantages of the CPT are numerous and include:

1. Its ability to provide a continuous profile of the soil with depth
2. Results with greater reliability and repeatability, when compared to the SPT
3. Results are independent of the operator

One of the often quoted disadvantages of the CPT is its inability to collect soil samples. However, as will be discussed in the following sections, this disadvantage can often be overcome with use of soil behaviour type charts.

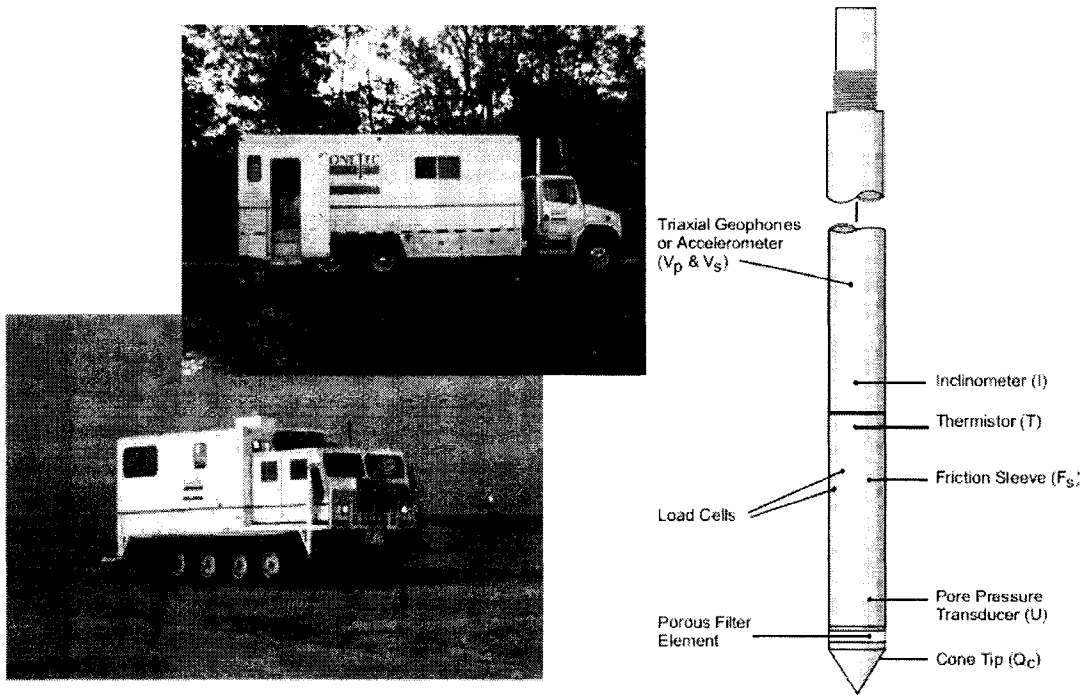

Figure 2.2: Cone penetration testing

2.3.2 Soil Profiling and Classification

One of the most common uses of the CPT is for profiling soil stratigraphy. The application of the CPT for soil profiling is based on extensive published experience, in which the cone penetration resistance is generally high in sands and low in clays while the friction ratio is generally low in sands and high in clays (Robertson 1998).

An extensive base of experience with the CPT has been established over the past 30 years and incorporated into soil behaviour type (SBT) charts. Not to be confused with soil classification, the SBT charts may not identify soils as defined by grain size, but provide an indication of how the soil will behave (Douglas and Olsen 1981). SBT charts that were proposed by Robertson et al. (1986) and Robertson (1990) have become popular in engineering practice.

In areas where there has been little or no experience with the CPT it is advisable to obtain samples to verify the soil classification and soil behaviour. However, in areas where significant experience with the CPT has been accumulated, it may not be necessary to obtain samples and SBT charts can be modified, to fit the local geologic region (Lunne et al. 1997).

SBT can be improved if CPT pore pressure data are also collected by recognizing that high penetration pore pressures are generally measured in soft

clays while in stiff heavily overconsolidated clays, dense silts and silty sands the CPT penetration pore pressures can be small or even negative (Robertson 1998).

Jefferies and Davies (1993) further simplified soil behavioural (SBT) classifications by incorporating the normalized cone resistance, Q, and the normalized friction ratio, F, into one parameter called a soil behaviour type index, I_c. I_c is essentially the radius of concentric circles that represent the boundaries between each SBT zone. This approach simplifies calculations and allows it to be incorporated into a spreadsheet, although I_c does not apply to sensitive fine grained soils, very stiff sand to clayey sands or very stiff fine grained materials, which correspond to SBT 1, 8 and 9 respectively (Robertson 1990).

One of the often-quoted advantages of the SPT over the CPT is the ability to collect samples from the SPT for soil characterization and soil grain size analysis. While the CPT is not capable of collecting samples, research has been conducted over the past fifteen years in an attempt to correlate I_c to the fines content (Kulhawy and Mayne 1990; Robertson and Wride 1998) and other grain characteristics. In geotechnical practice, fines content is generally defined as the fraction of soil smaller than $74(10^{-6})$ m (passing the 200 sieve). However, in the oil sand industry, fines are generally smaller than 44 (10^{-6}) m (passing the 375 sieve. The most popular correlation appears to be that of Robertson and Wride (1998), however the bounds of the correlation are fairly wide since I_c depends on other factors such as plasticity, mineralogy, sensitivity and stress history. As a result of the approximate nature of the correlation, Robertson and Wride (1998) recommend that it be used as a guide. The correlation between fines content and SBT index, I_c, was also verified by Suzuki et al. (1998), who found that fines content increased and mean grain size, D_{50}, decreased with increasing I_c, although the correlation between fines content and I_c showed considerable scatter. It should be noted that the CPT SBT charts do not apply to the following soil types:

- Sensitive, fine grained soils
- Very stiff sand to clayey sand (heavily over consolidated or cemented)
- Very stiff, fine grained soil (heavily over consolidated or cemented)

Baez et al. (2000) attempted to evaluate the correlation proposed by Robertson and Wride (1998) and found that their correlation was suitable for I_c values less than 2.05 but for I_c values greater than 2.05 the correlation proposed by Robertson and Wride (1998) over predicted the fines content. It has been recommended that fines content correlations based on the CPT should not replace the collection of samples and laboratory testing (Baez et al. 2000).

It should be noted that cones of slightly different designs, but still conform with the international standard, may give slightly different values of q_c and f_s, especially in soft clays and silts. Campanella et al. (1982) proposed that the cone resistance, q_c, could be corrected to a total cone resistance, q_t, based on

the pore pressure measured and the net area ratio. The net area ratio is approximated by the square of the ratio between the diameter of the cone load cell support and the diameter of the cone. A similar correction can then be applied to the sleeve friction. However, the corrections are only important in soft clays and silts where high pore pressures and low cone resistances are measured. In sands, the corrections are negligible since penetration is generally drained (meaning that pore pressures dissipate as they are generated) and the cone resistance is large (Robertson 1990).

2.3.3 Factors Affecting CPT results

Robertson (1985) notes that, similar to the SPT, a number of factors influence CPT results including: soil density, soil structure, cementation, aging, stress state and stress history. Much like with the SPT, the CPT cone tip resistance, q_c, must be corrected to an overburden stress level of 100 kPa. The overburden stress correction factors are similar with depth when compared to SPT overburden stress correction factors.

Naturally, the design and specifications of the CPT system have an impact on the CPT results. The standard cone has a 10 cm^2 base area, a 60 degree cone and a 150 cm^2 friction sleeve. Cone penetration systems with other specifications will yield different results. As such, only cone penetration systems that meet the international standard should be used. However, as noted above, Campanella et al. (1982) proposed that the cone resistance, q_c, could be corrected to a total cone resistance, q_t, based on the pore pressure measured and the net area ratio.

CPT results are also affected by the presence of thin layers. Robertson (1985) notes that if a soil layer is less than 10 to 20 cone diameters in thickness, the cone bearing resistance may not represent the true field strength due to influence from adjacent layers. In fact, the CPT penetration resistance represents an average response from the ground within a sphere of influence that can vary from a few cone diameters in soft clay to 20 cone diameters in dense sand (Robertson 1998).

2.4 CPT-SPT Correlations

Despite its known deficiencies, the SPT is one of the most widely used in-situ soil test in the world. The extensive use of the SPT has resulted in a wide variety of correlations, which can be used for geotechnical design. It can sometimes be desirable to use CPT-SPT correlations to estimate equivalent SPT values from the CPT. Hence, some effort has been made to establish CPT – SPT correlations. A number of CPT – SPT correlations have been presented over the past 30 years (Burland and Burbidge 1985; Jefferies and Davies 1993; Kasim et al. 1986; Kruizinga 1982; Meyerhof 1956; Mitchell 1986; Robertson et al. 1983; Schmertmann 1970; Schmertmann 1979; Seed and De Alba 1986; Suzuki et al. 1998). The data are usually expressed as a q_c/N_{60} ratio, where q_c is expressed in bars, kg/cm^2 or tsf.

In early research, Meyerhof (1956) suggested that $q_c/N=4$ on average. Kruizinga (1982) found that the q_c/N relationship was poor at best but noted that q_c/N ratios were an average of $q_c/N=4.5$ in sands and $q_c/N=1.3$ in clays. In (1970), Schmertmann developed a method to compute the static settlement of isolated, rigid, concentrically loaded shallow foundation over sand based on the static cone bearing capacity. In his article, Schmertmann notes that it is possible to convert SPT data to q_c data in order to use his method. Schmertmann (1970) gave approximate q_c/N ratios to convert SPT data for a number of different soil types, and suggested ratios ranging from 2.0 to 6.0 for silts to sands. He also notes that using these ratios to covert SPT data to q_c data results in a more conservative analysis and reduced accuracy.

Schmertmann (1979) presented research which allowed the comparison or prediction of CPT results based on measured SPT results. His theory was based on the limit equilibrium statics of the quasi-static SPT test. His statics theory allowed prediction of the relative magnitudes of the incremental, 15 cm (6 inches), ΔN values in soils as well as the amount of side friction and end bearing resistance for the sampler and the effect of removing the liners from an SPT sampler designed for liners. One notable disadvantage of Schmertmann's (1979) method is that the method is applied to the dynamic SPT while the research was based on the quasi-static SPT.

Another attempt to link the SPT and CPT was made by Robertson and Campanella (1983). They collected data from a number of studies correlating the SPT N value to the CPT cone penetration resistance, q_c. The results of their analysis are shown in Figure 2.3. They were one of the first to suggest that the q_c/N_{60} ratio was a function of the mean grain size (D_{50}) and observed that the q_c/N ratio increased with increasing grain size. Their study assumed that the relationship between the two tests is dependent only on average particle size. The research conducted by Robertson and Campanella appears to be very well accepted in the literature and has been validated by a number of other researchers (Kasim et al. 1986; Suzuki et al. 1998). Very similar data relating soil grain-size to the q_c/N ratio was also presented by Burland and Burbidge (1985). Seed and De Alba (1986) showed another chart similar to that presented by Robertson and Campanella, however, their chart showed smaller q_c/N ratios at large grain sizes and indicated that it would be appropriate to develop site specific correlations for large, high risk projects.

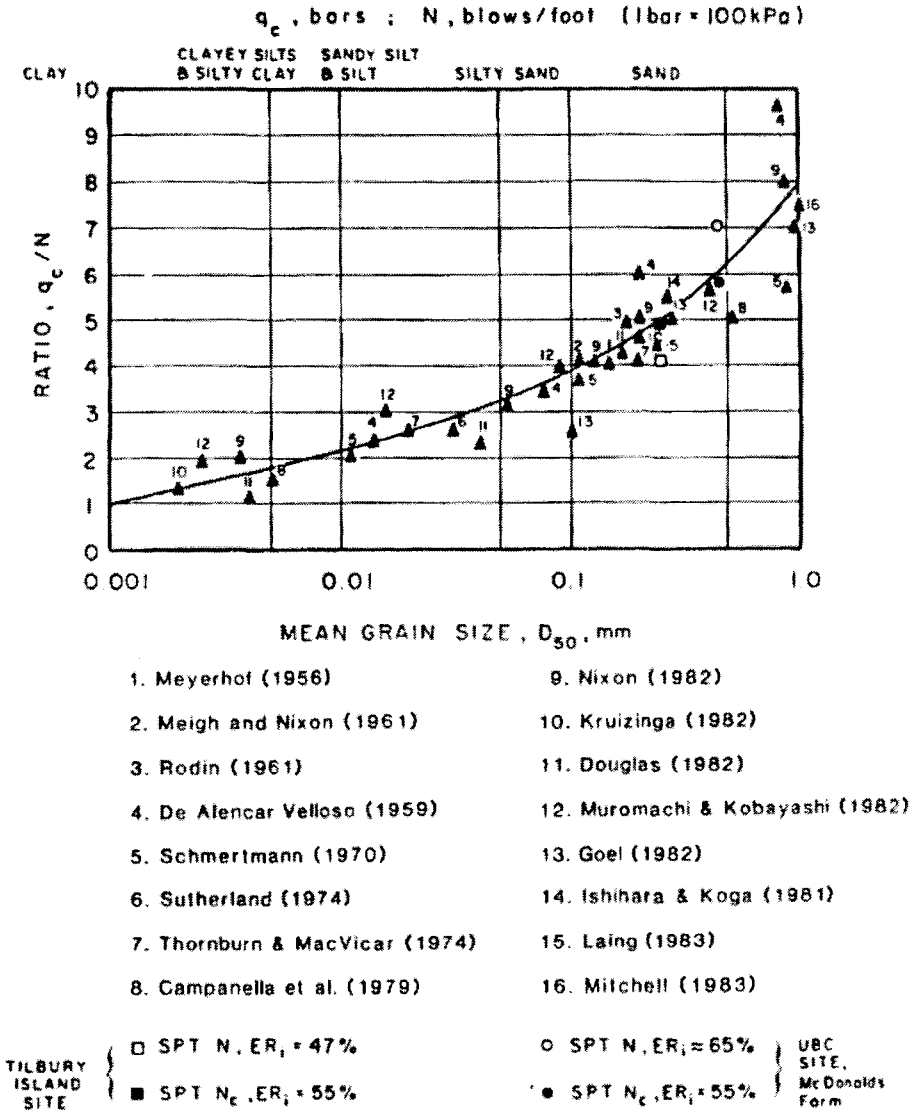

Figure 2.3: Variation in qc/N ratio with mean grain size (modified from Roberson et al. (1983))

Rather than obtaining samples for grain size analysis, the grain size characteristics can be estimated from established CPT-based SBT charts. Robertson (1986) suggested q_c/N_{60} ratios for each SBT using the non-normalized CPT SBT chart. For example, if the data falls within zone number nine on the non-normalized chart (Robertson et al. 1986), it is classified as sand and the suggested q_c/N_{60} ratio to use is 5.

One of the disadvantages of the original correlation suggested by Robertson and Campanella (1983) was that it required nearby sampled boreholes to obtain grain size data. Jefferies and Davies (1993) developed an algorithm using only CPTu

data to estimate equivalent SPT N_{60} data. Using only the CPTu data eliminated potential errors in assuming soil gradation changes between the samples and the collected CPT data. Instead of using the mean grain size, their algorithm relates the q_c/N_{60} ratio directly to the soil behaviour type index, I_c. Another advantage of the algorithm is that it is computationally simple and can easily be incorporated into spreadsheet analyses. Interestingly, Jefferies and Davies found that using the algorithm to estimate SPT data from measured CPTu data resulted in less error than simply using the actual SPT in the same soil. Lunne, et al. (1997) modified the original equation by Jefferies and Davies (1993) to fit the Robertson (1990) normalized SBT chart.

Research conducted by Suzuki et al. (1998) presented q_t/N data that supported Robertson's (1983) SPT-CPT correlation, where q_t is the cone tip resistance in MPa and N is the uncorrected blow count. However Suzuki et al. (1998) also showed that the q_t/N ratio was not just a function of grain size but also of the SPT N-values measured. They found that at a constant D_{50}, the q_t/N ratio increases with decreasing N-values and theorized that the difference might be caused by the different drainage conditions of the two tests noting that the CPT was essentially a drained test while the SPT was essentially an undrained cyclic test.

On a similar note, Kasim et al. (1986) presented data from a site in Alameda, California that indicates that the q_c/N ratio is lower for sands with higher fines contents than for sands with low fines contents at a similar mean grain size. They theorized that the fines fraction affected the sand's permeability, pore pressure distribution, ductility and compressibility. They further noted that the q_c/N ratio was not a function of the cone tip resistance.

The CPT SBT based q_c/N_{60} ratio approach was subsequently verified by Baez et al. (2000) who evaluated case histories and compared the CRR calculated from the CPT and from an equivalent SPT value recommended in the NCEER liquefaction workshop (Youd et al. 2001). Their analysis showed very good agreement between side-by-side SPT and CPT tests with any scatter being attributed to the inconsistency of the SPT results. Furthermore, the research indicated that liquefaction analyses conducted using CPT results were more conservative when the CRR was below 0.23 and that the SPT results were more conservative when the CRR was above 0.23. A $CRR_{7.5}$ of 0.23 corresponds to a normalized SPT blow count of 21. Since most cases of liquefaction occurred in soils where measured normalized blow counts were much lower than 21, it seems reasonable to assert that use of the CPT to assess the potential for liquefaction results in a more conservative analysis and a lower calculated factor of safety. In fact, the data presented by Baez et al. (2000) showed that the data calculated by the CPT liquefaction cyclic resistance ratio may be up to 25% lower than that calculated by the SPT cyclic resistance ratio. Based on these results, Baez et al. (2000) suggested that the CRR_{CPT} base curves from the NCEER workshop were more reliable than the CRR_{SPT} base curves and that the CRR_{SPT} may need some modification below normalized SPT blow counts of 21.

3.0 ANALYSIS OF AURORA POND LOAD TEST DATA

3.1 General

As Syncrude's Aurora tailings dyke was constructed, portions of the dyke were constructed using BBW sand. Sand placed in this manner often results in deposits of lower in situ densities and higher fines contents. Sand placed as BAW often results in a deposit with fewer fines and greater in situ densities. As a result, BBW deposits may be more susceptible to liquefaction than BAW deposits. Syncrude conducted a field test called the Aurora Pond Load Test to determine if an increase in vertical stress under an embankment would result in an increase in the tailings sand, which might result in improved stability in the loose BBW zones. The test consisted of loading a portion of the Aurora tailings dam, which was known to contain BBW sand, with a 16 m high embankment.

This section discusses the Aurora Pond Load Test set up and site investigation. An analysis of the Aurora Pond Load Test data follows. The analysis centres around the $q_{c1n}/(N_1)_{60}$ ratios measured at the site and correlations between the SPT and CPT data collected. The site investigation data collected both before and after the embankment was constructed were analyzed to examine the effect of the embankment on the $q_{c1n}/(N_1)_{60}$ ratio data in particular.

3.2 Test Embankment

The test embankment was constructed over a zone of known loose BBW tailings along the east side of the dyke. The embankment was constructed in two stages, each measuring 8 m high, which brought the total height of the embankment to 16 m. Figure 3.1 shows a conceptual cross section through the Aurora tailings dam and the Aurora pond load test embankment.

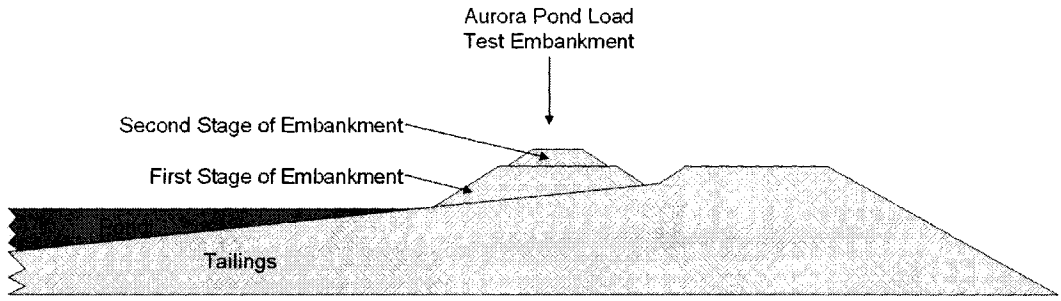

Figure 3.1: Aurora pond load test conceptual cross section (not to scale)

3.3 Site Investigation

Site investigation of the tailings was carried out in three stages. The first stage of the investigation characterized the tailings before placement of the embankment. The second stage of the investigation characterized the tailings after placement of the first stage of the embankment. The third stage of the investigation

characterized the tailings after placement of the second stage of the embankment.

During each stage of site investigation SPT, CPT as well as shear wave velocity measurements were made. The shear wave velocity measurements were made using a Seismic Cone Penetration Test (SCPT). However, this report only considers the SPT and CPT results. The shear wave velocity results are discussed in more detail by Robertson (2004).

3.4 Cone Penetration Testing

The CPT has two main advantages when compared to the SPT test. First, it provides a continuous profile of the soil. Second, results obtained from the CPT test have been observed to be much more repeatable than those obtained with the SPT (Robertson and Wride 1998). Cone penetration testing was carried out as part of the site investigation program for the Aurora Pond Load Test before construction of the embankment as well as after each stage of the embankment construction.

Prior to any embankment construction the CPT profiles measured at the test site, in general, show a layer of dense clean fine tailings sand approximately 6 m thick overlying loose fine tailings sand approximately 13 m thick with numerous layers of thin fine grained material. The elevation of the original tailings surface was about 300 m. The zone of interest for this study was the loose fine sand from an elevation of about 294 m to 281 m. The complete set of CPT and SPT data is presented in Appendix A.

3.5 Cone Penetration Testing Analysis

It is well known that in a clean sand of constant density, the cone penetration resistance (q_c) will increase in a non-linear manner with increasing depth. This can result in incorrect comparisons of CPT logs measured from differing elevations. In order to be able to correctly interpret and compare CPT logs it is necessary to normalize the cone penetration resistance to one atmosphere of effective overburden stress. The resulting cone penetration resistance corrected to a vertical stress of one atmosphere is referred to as normalized cone penetration resistance (q_{c1n}). The normalized cone penetration resistance, q_{c1n}, is dimensionless. The correction is made with the following equation:

$$q_{c1n} = (q_c/P_a)\ (P_a/\sigma'_v)^n \qquad (3.1)$$

Where:

- P_a is atmospheric pressure in the same units as either q_c or σ'_v
- n is a stress exponent, typically 0.5 for clean sand
- σ'_v is the in situ vertical effective stress

The measured layers of soft fine-grained material can also cause problems in comparing CPT logs. The inclusion of such layers might lead to a misleadingly

low average q_{c1n} in the target sand zone of measurement. There are two methods by which the data may be 'cleaned' of these layers. One approach is to convert the 'clay' values to equivalent 'clean sand' values using the approach suggested by Robertson and Wride (1998). The other approach is to simply remove the 'clay' from the dataset altogether. The second approach was chosen for this study since it was deemed less cumbersome than the first approach despite the fact that it would result in fewer data for analysis.

The criteria for what portions of the data were deemed as a 'clay' was taken from Roberson and Wride (1998). They suggest calculating a soil behaviour type index (I_c). The soil behaviour type index is calculated using CPT normalized cone resistance values and friction ratio values. The soil behaviour index, I_c, was defined by Robertson and Wride (1998) as follows:

$$I_c = [(3.47 - \log Q)^2 + (\log F + 1.22)^2]^{0.5} \quad (3.2)$$

Where:

$$Q = [(q_c - \sigma_{vo})/P_{a2}][P_a/\sigma'_{vo}]^n \quad (3.3)$$

And:

- Q is the normalized CPT penetration resistance (dimensionless)
- n is typically equal to 1.0
- $F = [f_s/(q_c - \sigma_{vo})]100\%$ and is the normalized friction ratio in percent
- f_s is the CPT sleeve friction stress
- σ_{vo} and σ'_{vo} are the total and effective overburden stresses, respectively
- P_a is a reference pressure in the same units as σ'_{vo} (i.e., P_a = 100 kPa if σ'_{vo} is in kPa)
- P_{a2} is a reference pressure in the same units as q_c and σ_{vo} (i.e., P_{a2} = 0.1 MPa if q_c and σ_{vo} are in MPa)

The apparent fines content of the soil can then be estimated from the soil behaviour type index. It was decided that all CPT data with fines content greater than 30% would be removed from the dataset. This was achieved using Robertson and Wride's (1998) recommended correlation, which resulted in all data where I_c was greater than 2.5 being removed from the dataset. The remaining data can be referred to as $(q_{c1n})_{Ic<2.5}$. Figure 3.2 shows a typical CPT profile from the Aurora Test site prior to embankment construction, after removing all data where I_c was greater than 2.5.

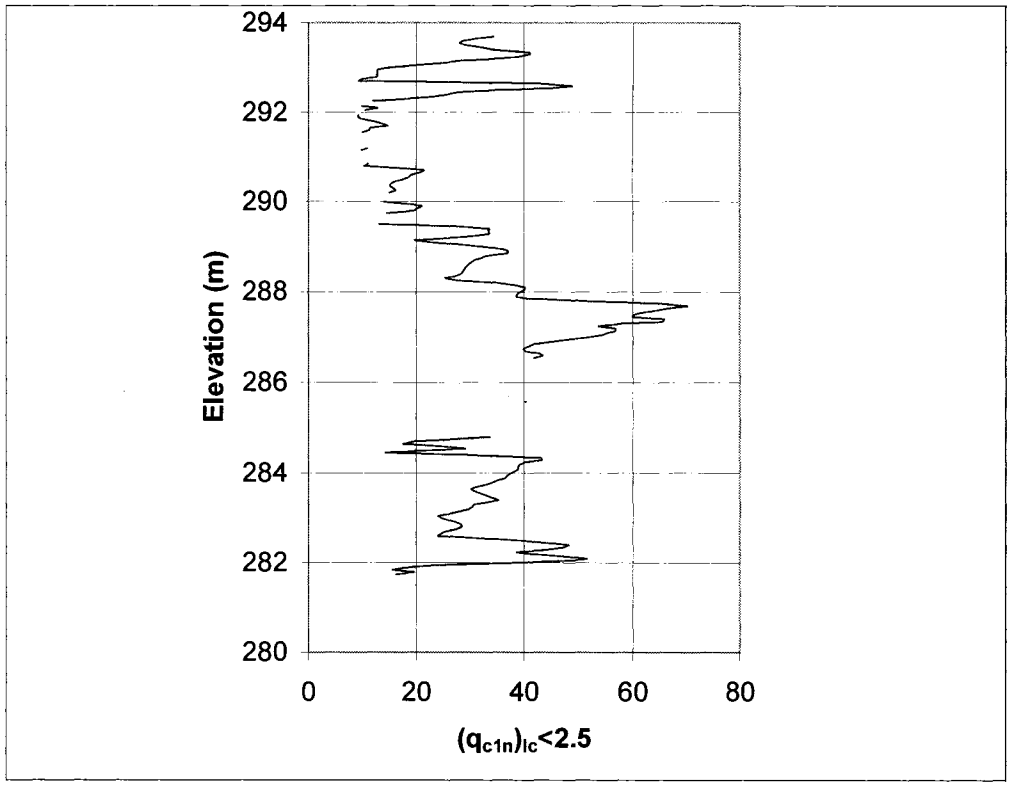

Figure 3.2: Typical Aurora Test site Pre-embankment CPT profile with Ic>2.5 values removed

Values of $(q_{c1n})_{Ic<2.5}$ were calculated for every CPT profile. Finally, an average $(q_{c1n})_{Ic<2.5}$ was calculated by averaging each value measured at each elevation. All 23 CPT profiles were used to determine the mean CPT profile. Figure 3.4 shows the calculated mean CPT profile in the target zone of examination. The mean plus one standard deviation and the mean minus one standard deviation profiles are also shown. The average $(q_{c1n})_{Ic<2.5}$ measured in the zone of interest was 41.8 with an average standard deviation of 14.5. Each point on the average $(q_{c1n})_{Ic<2.5}$ line in Figure 3.4 was calculated from an average of 15 data points.

Normally a slight trend of increasing $(q_{c1n})_{Ic<2.5}$ would be expected as effective stress increases with depth, resulting in a slight increase in the relative density. However, Figure 3.4 shows a slight trend of decreasing $(q_{c1n})_{Ic<2.5}$ with depth indicating decreasing relative density with depth.

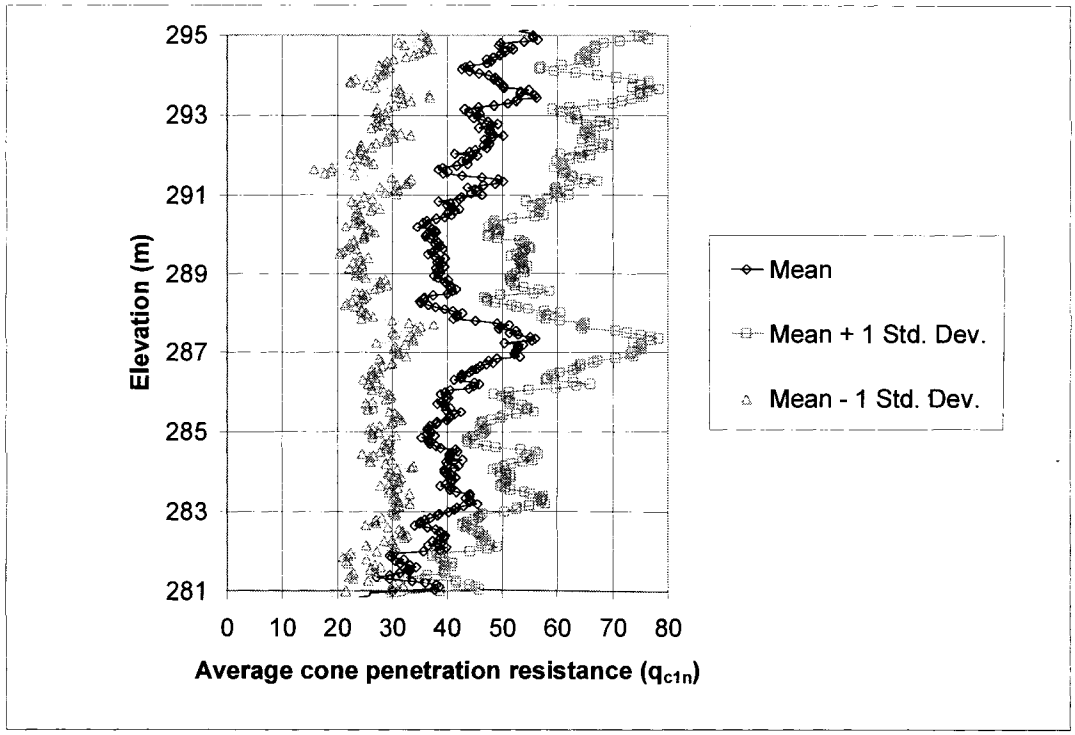

Figure 3.4: Average Aurora Test Site Pre-embankment CPT profile plus and minus one standard deviation (I_c<2.5), based on 23 CPT's

3.6 Standard Penetration Testing

SPT testing was carried out as part of a site investigation program for the Aurora Pond Load test. During the site investigation program, SPT testing was performed at various locations within the test site at 0.76 m (2.5 feet) depth intervals in 21 boreholes. A total of 334 SPT's were performed prior to construction of the embankment. The complete set of SPT data is presented in Appendix A.

3.7 Standard Penetration Testing Analysis

One primary reason for the high variability in SPT results is the wide range of energy that can be delivered to the drill rods from different rigs (Butler et al. 1998). Before the SPT results can be used for interpretation or liquefaction analysis the SPT data must be normalized to a standard energy value. The North American standard is the N_{60}, which corresponds to 60% of the potential energy of the hammer reaching the SPT sampler. The SPT data collected was first normalized to 60% energy, N_{60}, as follows:

$$N_{60} = N(ER_m/60\%) \tag{3.4}$$

Where:

- N is the measured SPT N-value
- ER_m is the measured energy ratio reaching the SPT sampler

In order to determine the energy ratio, two computational procedures can be performed to SPT tests, the F^2 and the Fv methods. At the Aurora Pond Load Test, the energy ratio was measured in 10 holes for a total of 203 measurements. The two methods were in good agreement with the F^2 method producing ER_m of 75.8% while the Fv method produced an ER_m of 74.3%. An overall average ER_m of 75.1% was used to calculate N_{60}.

Just as with the CPT, the SPT results must also be normalized to a reference overburden pressure of one atmosphere, resulting in $(N_1)_{60}$. The calculation to normalize the SPT data to the overburden stress is as follows:

$$(N_1)_{60} = N_{60}(P_a/\sigma'_{vo})^n \quad (3.5)$$

Where:

- σ'_{vo} is the effective overburden stress
- P_a is a reference pressure in the same units as σ'_{vo} (i.e., P_a = 100 kPa if σ'_{vo} is in kPa)
- n is an exponent, usually 0.5 in clean sand

It was also necessary to remove the 'clay' seams from the measured SPT data to avoid comparing it with sand data. With the SPT data, this was done in two ways. Firstly, data was removed from the dataset if the measured fines content in the sample was greater than 30%. Secondly, the borehole logs were checked and any data corresponding to soil classified as organic or clay was removed from the dataset. Figure 3.6 shows an Aurora Test site Pre-embankment typical measured SPT profile.

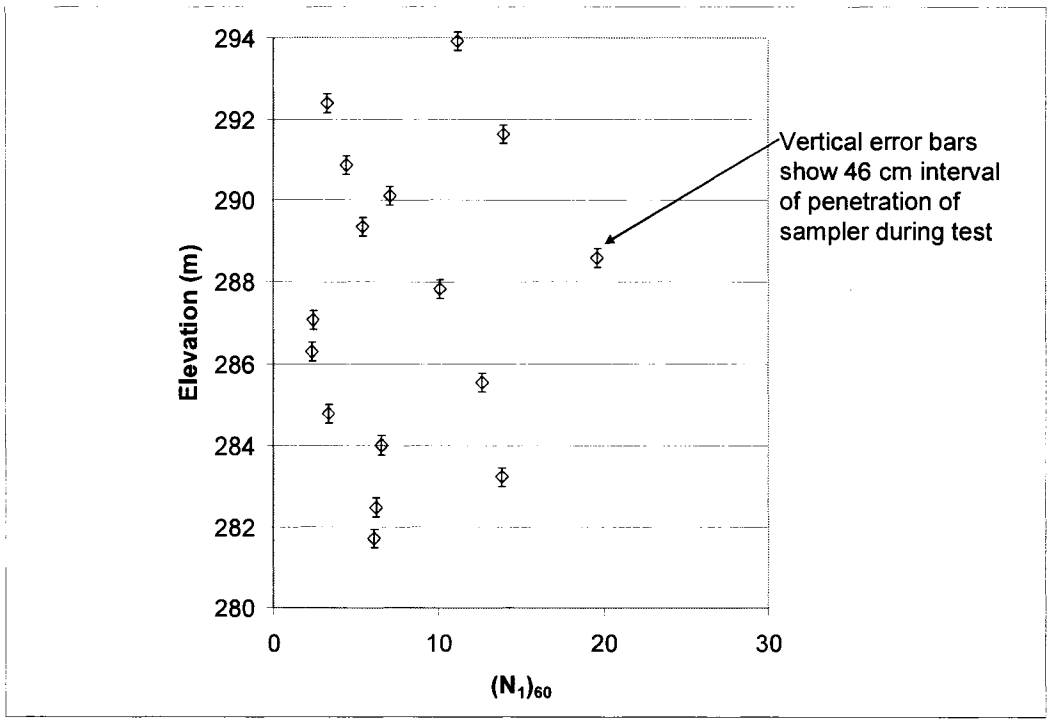

Figure 3.6: Typical Aurora test site Pre-embankment SPT profile

The mean SPT profile was then calculated by averaging all the SPT data within one-metre depth intervals using the average depth during the last 30 cm of penetration (i.e. 30 cm past the start of the test), which would then be assigned the average elevation of the data in the one metre interval. For instance, an average $(N_1)_{60}$ would be obtained for all SPT data occurring between the elevations 284m and 285m, which would then be assigned an average elevation of 284.5m. Figure 3.8 shows the calculated average Pre-embankment SPT $(N_1)_{60}$ profile at the Aurora Test site. The error bars attached to the data points indicate one standard deviation for each data point. The average $(N_1)_{60}$ in the zone of interest was 7.5 with an average standard deviation of 3.8. Hence, 68% of all SPT N-values fall within the range 3.7 to 11.3 (one standard deviation) and 95% of the SPT N-values fall within the range to 0 to 15.1 (two standard deviations). Each average $(N_1)_{60}$ data point in Figure 3.8 was calculated from between 14 and 22 SPT's with an average of 19 SPT's per data point.

It is important to note that Figure 3.8 shows decreasing $(N_1)_{60}$ values with depth. This implies that the relative density of the tailings decreases with depth.

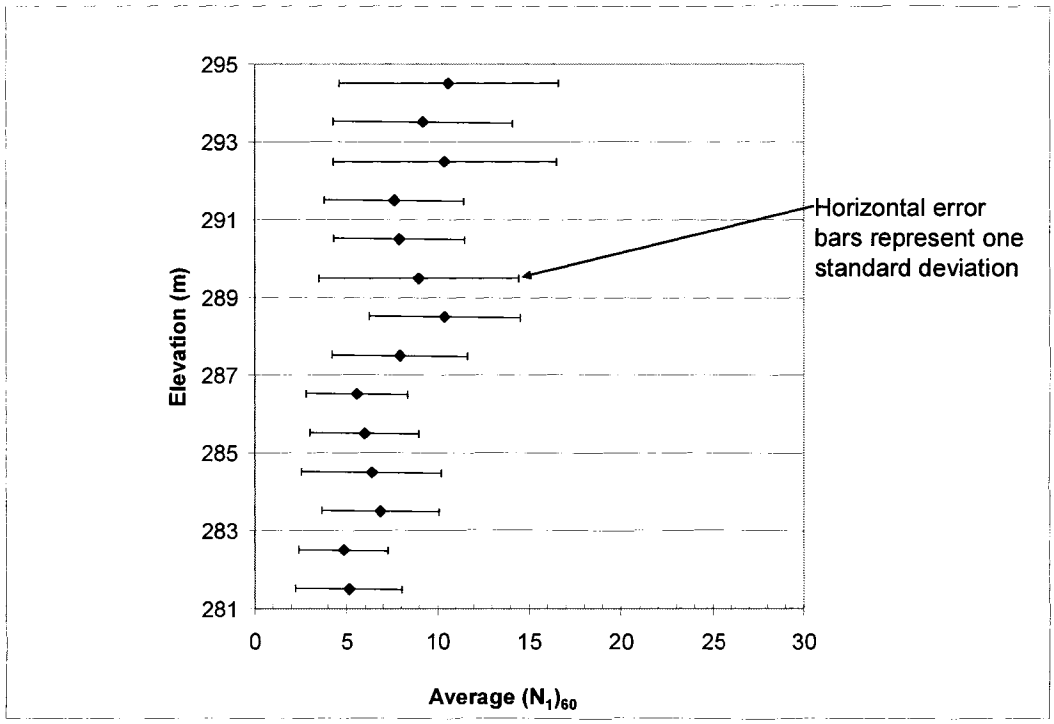

Figure 3.8: Calculated Average Aurora test site pre-embankment SPT Profile (averaged over 1 m depth intervals, total of 334 SPT's in 21 holes)

3.8 SPT-CPT Correlations

The q_c/N ratio is commonly used to compare SPT and CPT data. The $(q_{c1n})/(N_1)_{60}$ ratio can also be used in the same manner, since both sets of data are normalized in the same manner. Robertson et al. (1983) found a relationship between the q_c/N_{60} ratio and the mean grain size (D_{50}), which could then be used to convert CPT data to equivalent SPT data.

Unlike the SPT, the CPT records data every 5 cm. Therefore, in order to compare the two sets of data, both datasets were averaged over 1m intervals. The SPT $(N_1)_{60}$ data was averaged in the manner mentioned in Section 3.7. The CPT was also averaged in a similar manner. For example, between elevations 284 m and 285 m the SPT $(N_1)_{60}$ data was averaged and assigned an elevation of 284.5 m. The CPT q_{c1n} data between the same elevations were also averaged and assigned the elevation of 284.5 m. The quotient of the averaged CPT and SPT data at that depth becomes the ratio $q_{c1n}/(N_1)_{60}$.

Figure 3.11 shows the variation in the $q_{c1n}/(N_1)_{60}$ ratio as a function of $(N_1)_{60}$, and shows that the calculated $q_{c1n}/(N_1)_{60}$ ratio varies between 3.7 and 8.2. Furthermore, the chart shows an inverse relationship between the $q_{c1n}/(N_1)_{60}$ ratio and $(N_1)_{60}$, impling that the cone tip resistance to blow count ratio $(q_{c1n}/(N_1)_{60})$ depends on the blow count. Suzuki et al. (1998) also noticed that the q_t/N ratio tends to decrease with increasing SPT N-value and theorized that this effect may

be caused by drainage conditions between the two tests. However, they did not present any data to support this hypothesis.

An average of 19 SPT blow counts and 365 CPT readings were used to calculate each data point. Many more CPT than SPT readings were averaged in each data point because the CPT makes far more frequent readings. Since the CPT and SPT values are averaged, Figure 3.11 does not reflect the true variability of the tailings deposit. An R^2 value of 0.79 indicates good correlation between $(N_1)_{60}$ and the $q_{c1n}/(N_1)_{60}$ ratio. The trend line in Figure 3.11 is a generic exponential trendline calculated by the program Excel.

The observation of the inverse relationship between the $q_{c1n}/(N_1)_{60}$ ratio and $(N_1)_{60}$ is a source of concern for Syncrude since it raises questions over which in-situ test results should be used in a liquefaction analysis. The objective of this research is to evaluate and explain the variation in the $q_{c1n}/(N_1)_{60}$ ratio shown in along with its dependence on blow count.

Figure 3.12 shows the pre-embankment $(q_{c1n})/(N_1)_{60}$ ratio as a function of normalized cone tip resistance, q_{c1n}. The figure shows a large scatter and essentially no relationship between the $q_{c1n}/(N_1)_{60}$ ratio and q_{c1n}.

Thus, at the Aurora Test site, the pre-embankment $q_{c1n}/(N_1)_{60}$ ratio appears to depend on the SPT blow count, but not on the CPT cone tip resistance. Kasim et. al (1986) also noted that the $q_{c1n}/(N_1)_{60}$ ratio was not a function of the cone penetration tip resistance.

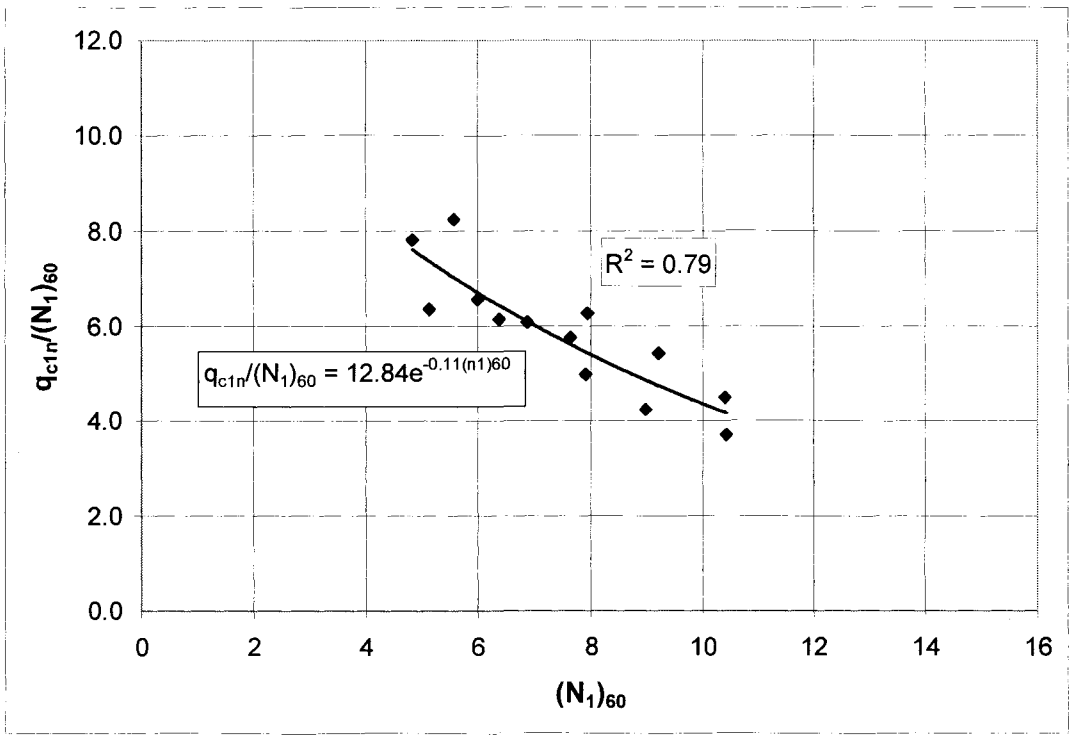

Figure 3.11: Measured Pre-embankment $q_{c1n}/(N_1)_{60}$ ratio at Aurora Test site

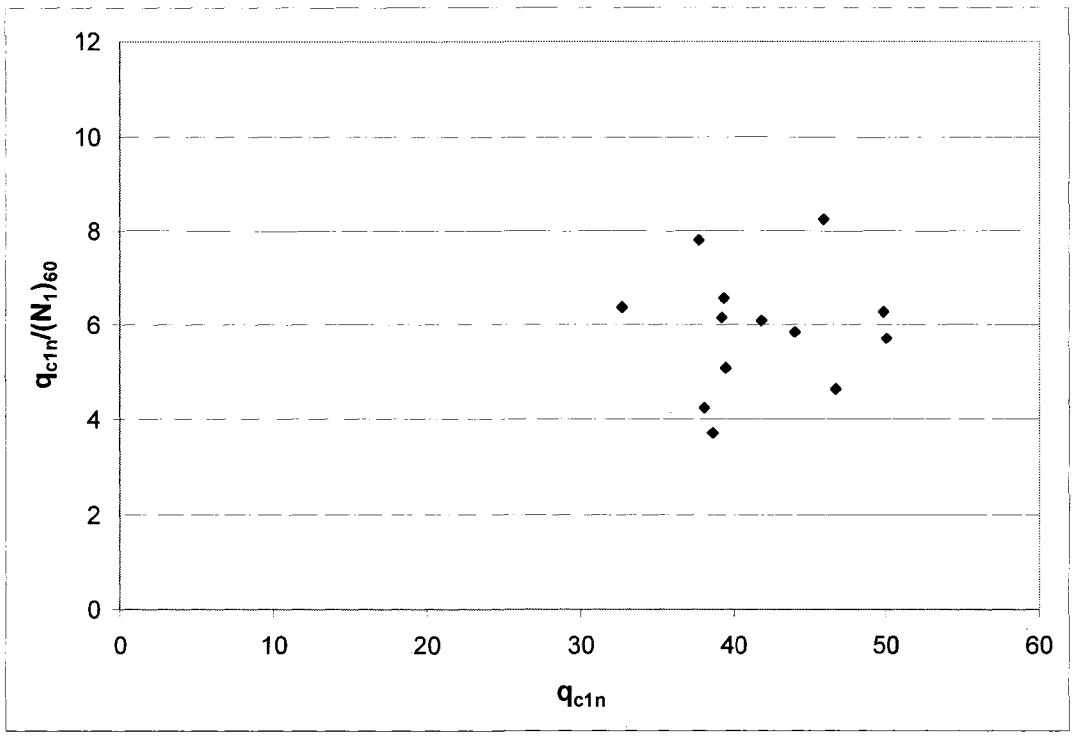

Figure 3.12: The Aurora test site Pre-embankment $q_{c1n}/(N_1)_{60}$ ratio as a function of q_{c1n}

3.9 Post-Embankment Aurora Pond Load Test Data

Figure 3.14 shows both the pre-embankment and post-embankment (full 16 m height) SPT data from the Aurora pond load test. The chart shows a considerable increase in the $(N_1)_{60}$ values measured after the construction of the 16 m high embankment. In fact, in the zone of interest (from 281 m to 294 m), an average increase in $(N_1)_{60}$ of 130% was measured.

Like the pre-embankment data, the post embankment data plotted in Figure 3.14 also show decreasing $(N_1)_{60}$ with depth. However, the post embankment data trend is more distinct. This makes sense since the change in vertical stress would be the greatest nearest to the previous tailings surface (i.e. the pre-embankment tailings surface). The width of the embankment is approximately 50 m while the depth of interest is approximately 20 m from the original tailings surface.

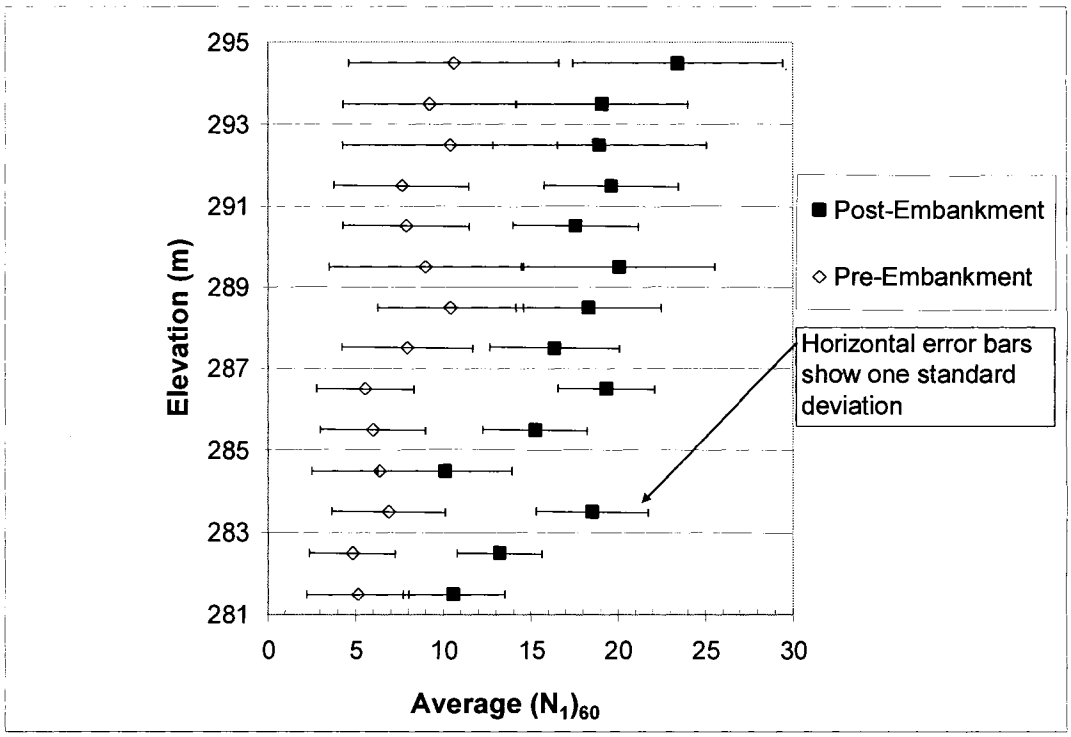

Figure 3.14: Comparison of Aurora test site pre and post-embankment $(N_1)_{60}$ data (mean and standard deviation range)

Figure 3.16 shows both the pre- and post-embankment (again, for the full height embankment) normalized cone tip resistance. Figure 3.16 also shows improvement in the cone tip resistance after the 16m high embankment was constructed. However, Figure 3.16 only shows an average post-embankment increase of 40% in the cone tip resistance compared with an increase of 130% in the SPT $(N_1)_{60}$ data as mentioned above.

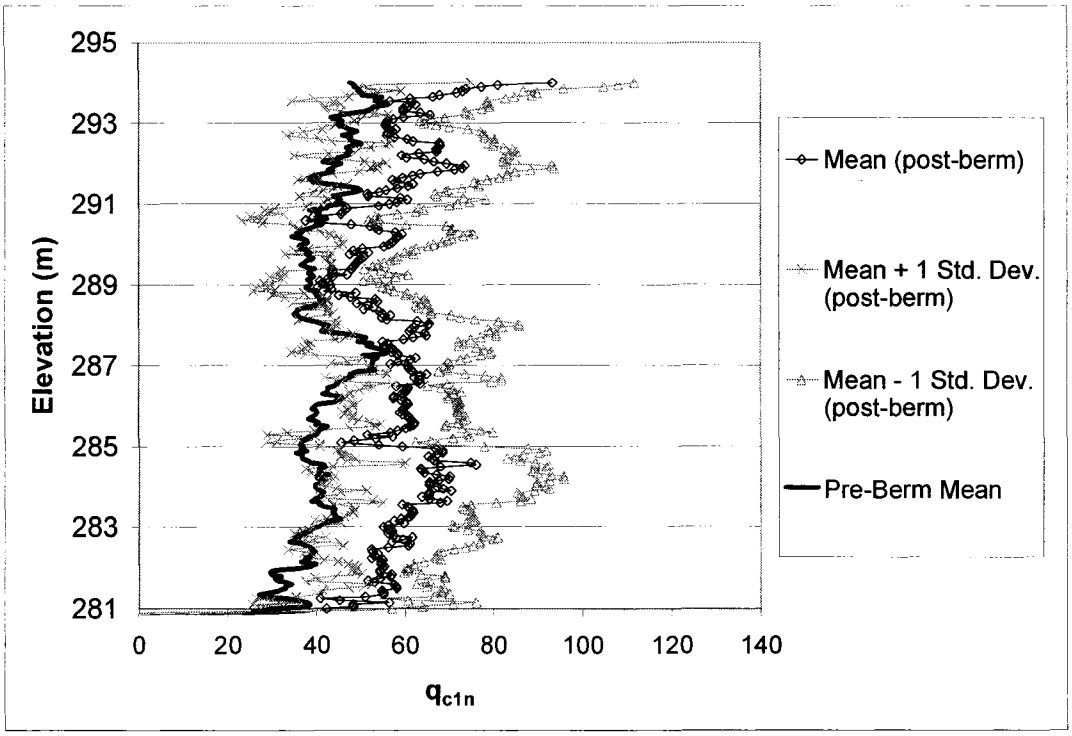

Figure 3.16: Comparison of Aurora test site pre and post embankment CPT data (mean and standard devieation range)

Figure 3.18 shows a comparison of the $q_{c1n}/(N_1)_{60}$ ratio as a function of $(N_1)_{60}$. The same trend between the $q_{c1n}/(N_1)_{60}$ ratio and $(N_1)_{60}$ is seen in the post-embankment data. However, in the post embankment case, the average $q_{c1n}/(N_1)_{60}$ ratio is slightly lower. This may be a result of the fact that the SPT blow count increased by 130%, while the CPT tip resistance increased by only 40%. This makes sense since the SPT blow count is very sensitive to changes in relative density (as will be discussed in greater detail in Section 4). It is possible that both the weight of the SPT equipment and the relative density of the tailings influence the $q_{c1n}/(N_1)_{60}$ ratio. The post-embankment tailings are deeper (hence longer SPT rods) but also denser. It may be that the increased density has off-set the influence of the greater depth to some degree. However, it is not known why much of the post-embankment $q_{c1n}/(N_1)_{60}$ ratio data is less than 4 (the literature review suggests a ratio of 5 should be expected).

Figure 3.20 shows both the pre and post embankment data combined into one data series. A single relationship results from both the pre and post-embankment data. The trend line shows good correlation between the corrected blow count and the $q_{c1n}/(N_1)_{60}$ ratio despite the increase in vertical stress caused by the construction of the embankment.

Figure 3.22 shows the $q_{c1n}/(N_1)_{60}$ ratio plotted as a function of q_{c1n} for both the pre and post-embankment conditions. As can be seen on the chart, there is essentially little or no correlation between the $q_{c1n}/(N_1)_{60}$ ratio and q_{c1n} for either the pre or post-embankment condition.

Figure 3.24 shows the same data as in Figure 3.22 except that the data points were plotted as a single series to allow a trend line to be drawn through it. As is shown, there is little to no correlation between the $q_{c1n}/(N_1)_{60}$ ratio and q_{c1n}. Furthermore, the post-embankment data has a lower average $q_{c1n}/(N_1)_{60}$ ratio compared to the pre-embankment data. As mentioned, this may be a result of the increase in SPT blow count of 130%, while the CPT tip resistance increased by only 40%.

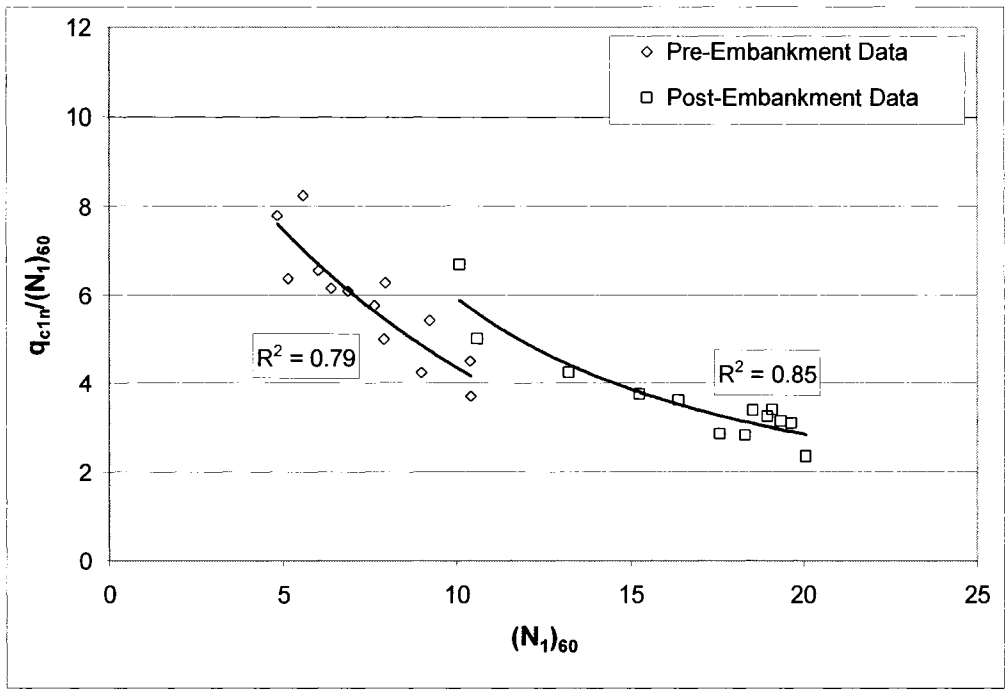

Figure 3.18: Comparison of the Aurora test site pre and post-embankment $q_{c1n}/(N_1)_{60}$ ratio as a function of $(N_1)_{60}$

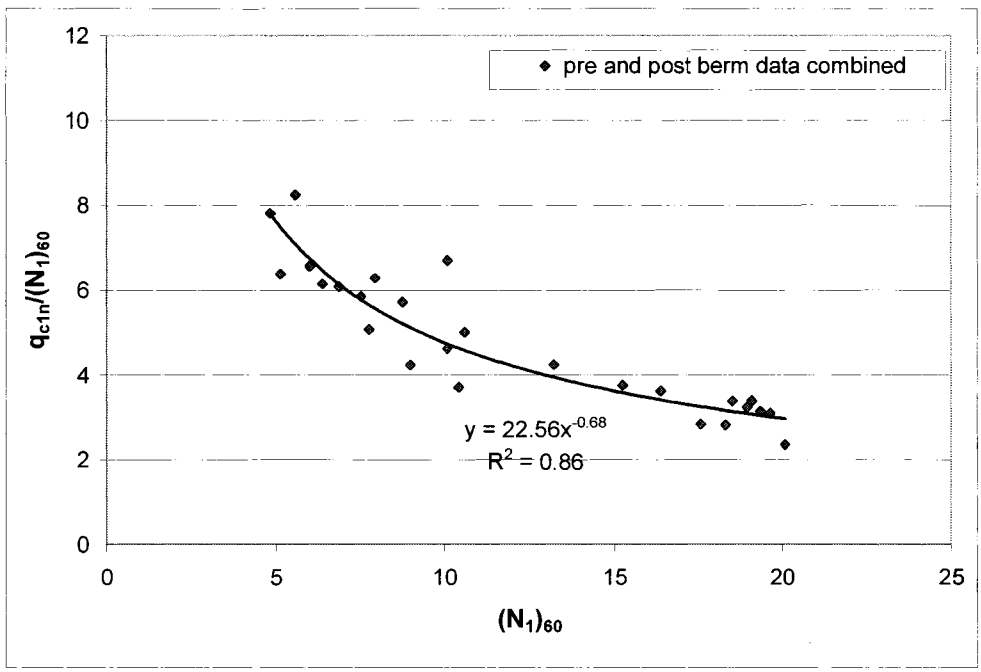

Figure 3.20: The Aurora Test site pre and post-embankment data combined

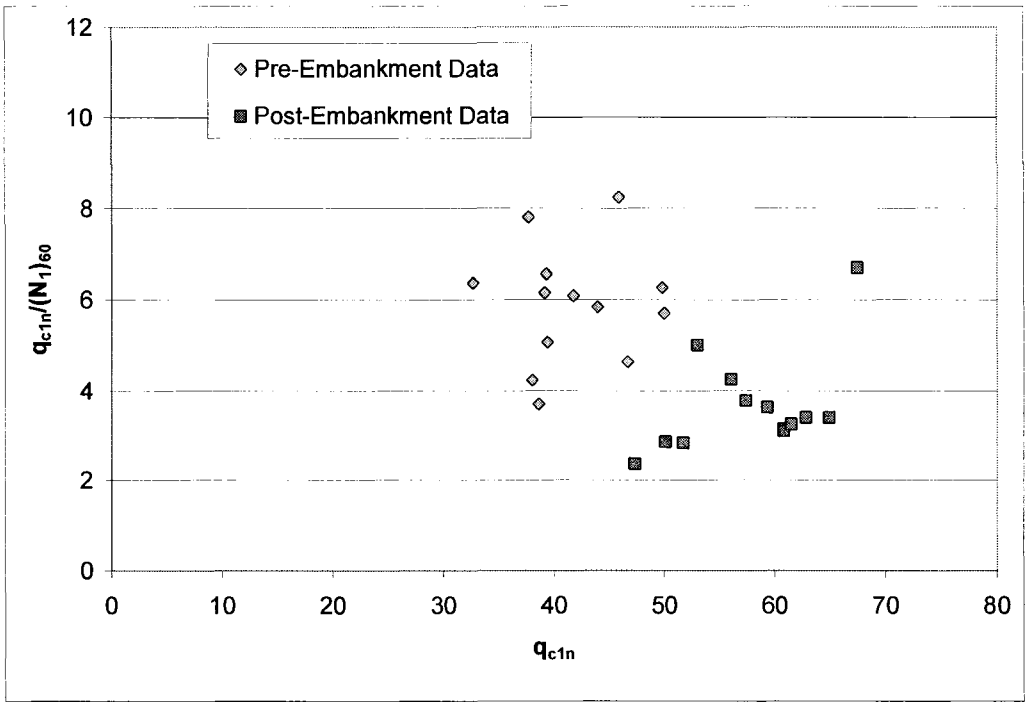

Figure 3.22: Comparison of pre and post-embankment $q_{c1n}/(N_1)_{60}$ ratio as a function of q_{c1n}

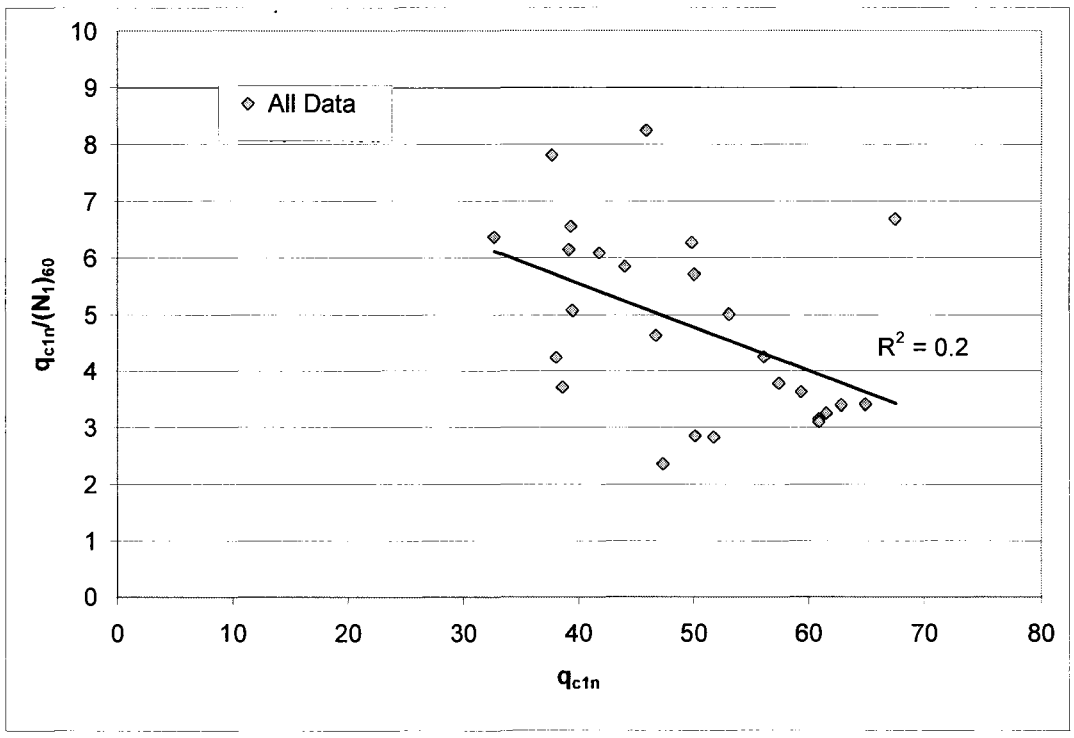

Figure 3.24: Pre and post embankment $q_{c1n}/(N_1)_{60}$ versus q_{c1n} data combined

4.0 SELF WEIGHT PENETRATION OF THE SPT

4.1 General

This section provides a theoretical evaluation of the hypothesis that the weight of the SPT rods and hammer may have an impact on the measured SPT blow count in loose sands. This could result in a lower blow count than would be found by using the CPT to estimate an equivalent SPT blow count.

4.2 Analysis and Statics of the SPT

Schmertmann performed an analysis of the static forces acting on the SPT was conducted quasi-static penetration tests using an SPT sampler in addition to regular SPT's and CPT's. Schmertmann resolved the forces in the SPT (see Figure 4.1) into the following equation, which relates the cone tip resistance to the weight of the rods and the additional quasi-static force needed to advance the sampler by the distance, L:

$$F + W' = [C_1 A_e + (d_i + d_o)\pi L C_2 R_f] q_c \qquad (4.1)$$

Where:

- F is the additional force added to the buoyant weight of rods and sampler that is needed to advance the sampler into the soil. For cases where the blow count is zero, F = 0.
- W' is the Buoyant weight of Rods and Sampler ($W' = W_{rods} + W_{sampler} + W_{hammer} - F_{buoyant}$)
- A_e is the end area of SPT sampler (10.7 cm^2 for a typical sampler)
- d_i and d_o is the inner and outer diameter of sampler, respectively
- L is the depth of penetration of sampler into soil at base of borehole
- R_f is the f_c/q_c the friction ratio
- C_1 and C_2 are constants, which relate the quasi-static penetration resistance and friction resistance of the SPT and the CPT (i.e. $q_{spt} = C_1 q_c$ and $f_{spt} = C_2 f_c$)

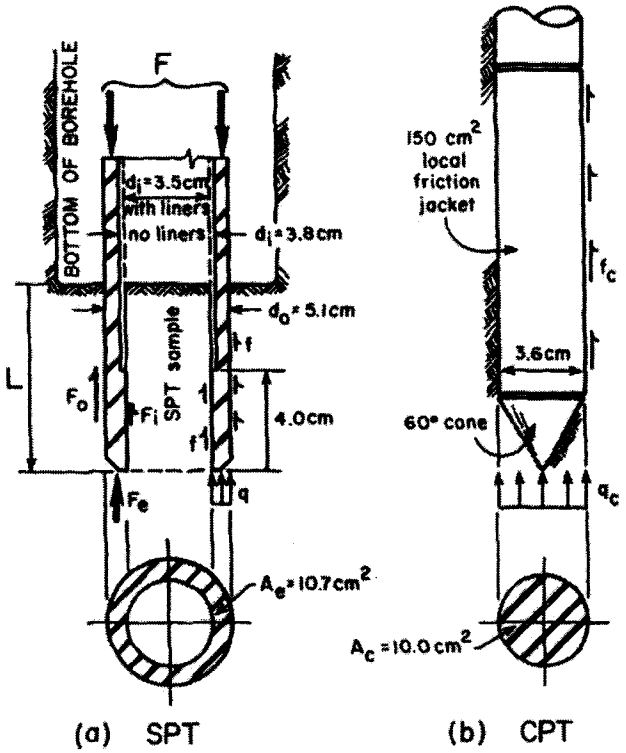

Figure 4.1: Forces acting on quasi-static SPT as well as CPT (Modified from Schertmann, 1979)

In his research, Schmertmann (1979) also found a direct relationship between the blow count from the regular SPT and the added force, F, from the quasi-static SPT required to penetrate the sampler from 15 to 46 cm (6 to 18 inches). He found the direct relationship in the form of the following empirical equation:

$$F_{(avg)} = 623 + \alpha\ 1557\ N \qquad (4.2)$$

Where:

- $F_{(avg)}$ is the average added quasi-static force during SPT sampling. $F_{(avg)}$ is in the units of Newtons.
- α is the constant fraction of maximum theoretical hammer energy. Schmertmann found that α averaged 0.33 in cohesive soils and 0.42 in cohesionless soils.
- N is the blow count from 15 to 46 cm (6 to 18 inches) of penetration in a regular SPT.

Thus, Schmertmann found that N varies directly with the quasi-static energy required to obtain the same sample. This allows Equation 4.1 to be used to estimate the expected cone tip resistance based on the measured blow count, N.

Figure 4.3 shows two sets of relationships in terms of CPT tip resistance versus vertical effective stress. The curved lines show well established relationships

between vertical effective stress and expected cone resistance for a clean sand with a constant relative density (Kulhawy and Mayne 1990). The straight lines show the relationship developed by Schmertmann calculated using Equation 4.1.

As noted, the curved lines in Figure 4.3 showing the Kulhawy and Mayne (1990) relationship were calculated as follows:

$$q_{c1n}/D_r^2 = C \qquad (4.3)$$

Where:

- q_{c1n} is the tip resistance normalized to an overburden stress of 1 atm.
- D_r is the relative density of the sand
- C is a unit-less constant dependent on the age of the deposit (300 to 400 for young to old deposits, respectively)

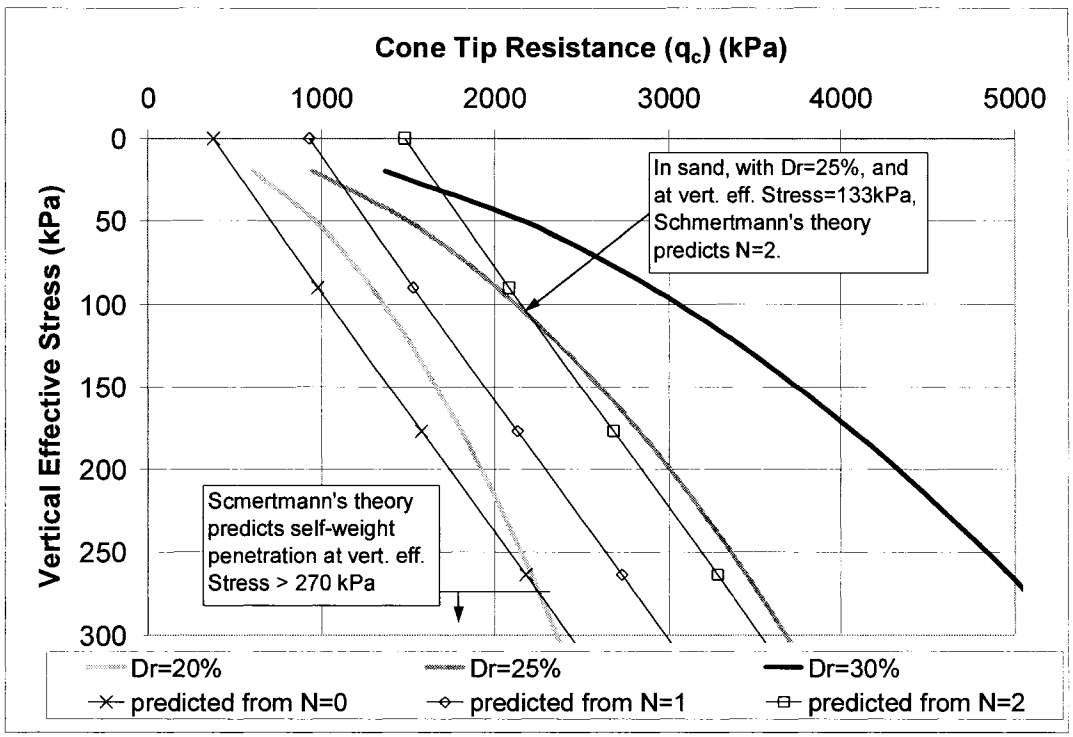

Figure 4.3: Schmertmann predicted cone tip resistance compared to relative density curves for sand

The constant C, for Aurora sand, was estimated to be approximately 340 based on a deposit age between 1 and 10 years of age. Hence, in an Aurora sand deposit with a relative density of 20% the normalized cone resistance would be:

$$q_{c1n} = 340(0.20)^2 = 13.6$$

At a depth where the vertical effective stress would be approximately 133 kPa (i.e. around 15 m), the predicted uncorrected cone tip resistance, q_c, would be (using equation 3.1):

$$13.6(100 \text{ kPa}) / (100 \text{ kPa} / 133 \text{ kPa})^{0.5} = 1568 \text{ kPa}$$

Hence, using the CPT, one would expect to measure a q_c of 1568 kPa at the depth of 15 m assuming that the sand had a relative density of 20%.

The straight line relationships shown in Figure 4.2 were calculated using Schmertmann's static theory from Equation 4.1 for the SPT N-value noted on the chart. Note that in cases where the blow count is not zero, Equation 4.2 can be used to calculate F for use in Equation 4.1.

For example, if one were to consider an SPT performed at a depth of 15 m, where the vertical effective stress is 133 kPa, and the measured SPT blow count is zero, (Figure 4.3) Schmertmann's (1979) theory would predict a cone tip resistance of 1280 kPa.

Note that Figure 4.3 also shows that if the measured SPT N-value was one, Schmertmann's theory would predict a cone tip resistance of 1830 kPa. This means that if the SPT were used in a sand of a relative density of only 20% with blow count of one at this vertical effective stress, Schmertmann's theory would over predict the expected cone penetration resistance (the actual expected cone tip resistance would be 1568 kPa). Said another way, if the expected cone tip resistance was 1568 kPa, Schmertmann's theory would predict a SPT N-value of less than one. This means that some amount of penetration of the sampler in the bottom of the borehole could occur due solely to the weight of the rods and hammer (or "self-weight penetration"). Then after one blow, full penetration would be easily achieved. Hence, some of the energy from the blow would not be needed to achieve the full 45.7 cm (18 inches) of sampler penetration.

Using the SPT-relative density relationship suggested by Skempton (1980) for a clean young fine sand with a relative density of 20%, the expected corrected SPT blow count would be 1.6 ($(N_1)_{60}/Dr^2 = 40$).

It could also be said that for the same depth but in a sand with relative density of 25%, Schmertmann's theory would predict the measurement of N=2 (shown in Figure 4.3 by the intersection of the curved Dr=25% line and the N=2 straight line at the vertical effective stress of 133 kPa).

In addition, it is easy to see that at vertical effective stresses beyond about 270 kPa, measurements of N=0 would be expected for sand with a relative density of 20% or less. This is because the cone tip resistance needed to support the weight of the rods and hammer is greater than what would be predicted for that effective stress level and relative density and hence full self weight penetration

should be achieved. Note that within the zone of interest at the Aurora Test site (pre-embankment) the vertical effective stresses are between 55 kPa and about 177 kPa (a depth range of 6 to 19 m approximately).

Equation 4.1 was re-arranged to solve for L, the length of penetration, in the equation so that self-weight penetration might be predicted:

$$L = [(F + W')/ q_c - C_1A_e] / (d_i + d_o)\pi C_2R_f \quad (4.4)$$

Which equals (when q_c is replaced with q_{c1n}):

$$L = \{ [W'(P_a/\sigma_v')^{0.5} / (q_{c1n} P_a)] - C_1A_e\} / (d_i + d_o)\pi C_2R_f \quad (4.5)$$

In the above equation, F = 0 since for self-weight penetration, no additional force can be added to the weight of the rods, sampler and hammer. q_{c1n} can be replaced by Kulhawy and Mayne's (1990) relative density relationship ($q_{c1n}=CD_r^2$), which yields:

$$L = \{ [W'(P_a/\sigma_v')^{0.5} / (C D_r^2 P_a)] - C_1A_e\} / (d_i + d_o)\pi C_2R_f \quad (4.6)$$

Figure 4.5 shows the magnitude of the predicted self-weight penetration (using Equation 4.5) for sand with D_r of 20% and C assumed to be 340. The constants, C_1 and C_2, have a large impact on the self-weight penetration prediction and the results for $C_1=C_2=0.6$, 0.7 and 0.8 are shown in the Figure 4.5.

Schmertmann made the assumption that the end bearing resistance q over the end area of the SPT sampler equals a constant, C_1, times the static cone end bearing resistance, q_c, (i.e. $q_{spt}=C_1q_c$). He made a similar assumption regarding the friction acting on the SPT sampler and the CPT friction sleeve ($f_{spt}=C_2f_c$).

As can be seen in Figure 4.5, as C_1 and C_2 are increased, the predicted self-weight penetration decreases. Notice that at the surface, the self-weight penetration increases to infinity. This is because at the surface there is zero vertical effective stress, which would, in theory, result in no resistance to penetration. At shallow depths, the results of the equation are dominated by the low effective stress. Thus, equation 4.6 may not be applicable for predicting self-weight penetration of SPT equipment at shallow depths.

As depth and effective stress increase, self-weight penetration decreases to a minimum after which point the weight of the rods, sampler and hammer begin to dominate. Hence, in a very loose sand deposit with a constant relative density of, say 20%, the predicted self-weight penetration is greater at a depth of 30 m than at 15 m because the weight of the rods increases in a linear manner with depth but the penetration resistance increases in a slower non-linear manner with depth, as illustrated in Figure 4.3.

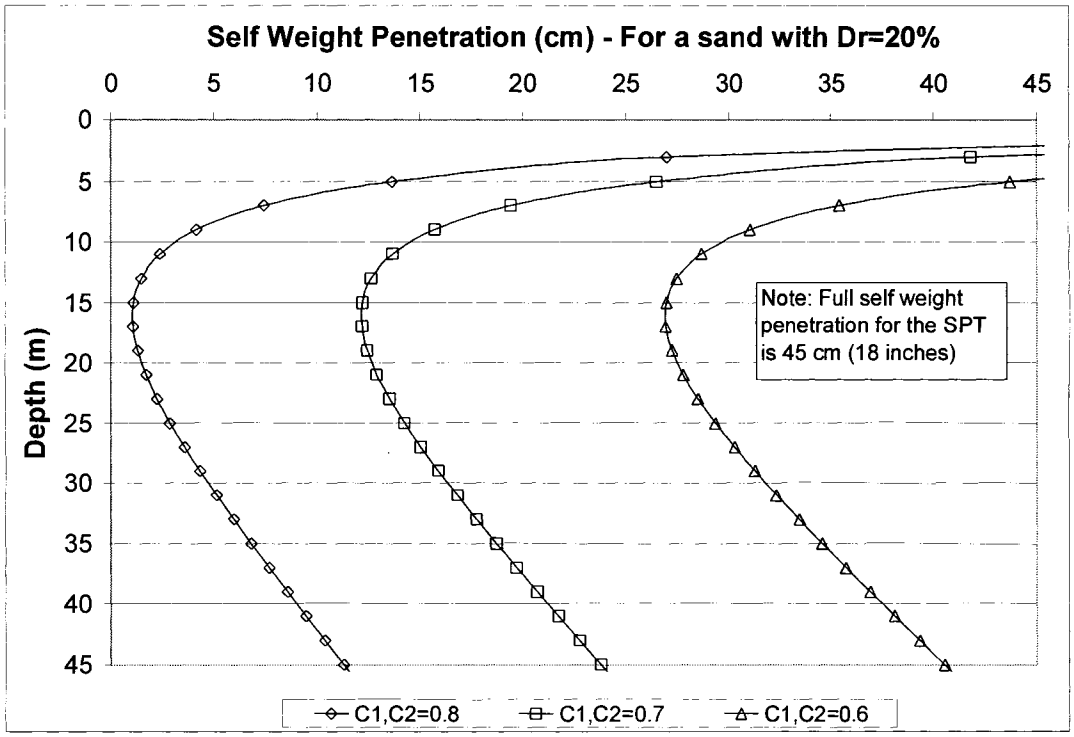

Figure 4.5: Predicted Self-Weight Penetration for a sand with Dr=20%

As it turns out, the self-weight penetration calculation is also sensitive to relative density. Figure 4.7 shows the result if the relative density in the calculation is increased to 21%. As expected, the curves shift to the left, predicting less self-weight penetration with the increase in relative density. Where the equation results in a negative answer (such as for 21% Dr and C_1=C_2=0.8), no self-weight penetration is predicted.

If the relative density is increased to 25%, no self-weight penetration is predicted except in the upper few metres where the low vertical effective stress dominates the self-weight penetration equation. Although the equation requires a sand deposit with a relative density less than about 22% to predict self-weight penetration within the depth range of interest at the Aurora test site, equation 4.6 shows that the weight of the SPT rods, hammer and sampler have a large influence on the blow count.

For a SPT conducted in a sand deposit of 26% relative density at a depth of, say 15 m, no self-weight penetration would be predicted. However, it is clear that the weight of the SPT components would put the sampler/soil interface at a condition near static equilibrium and that one blow would likely result in full penetration.

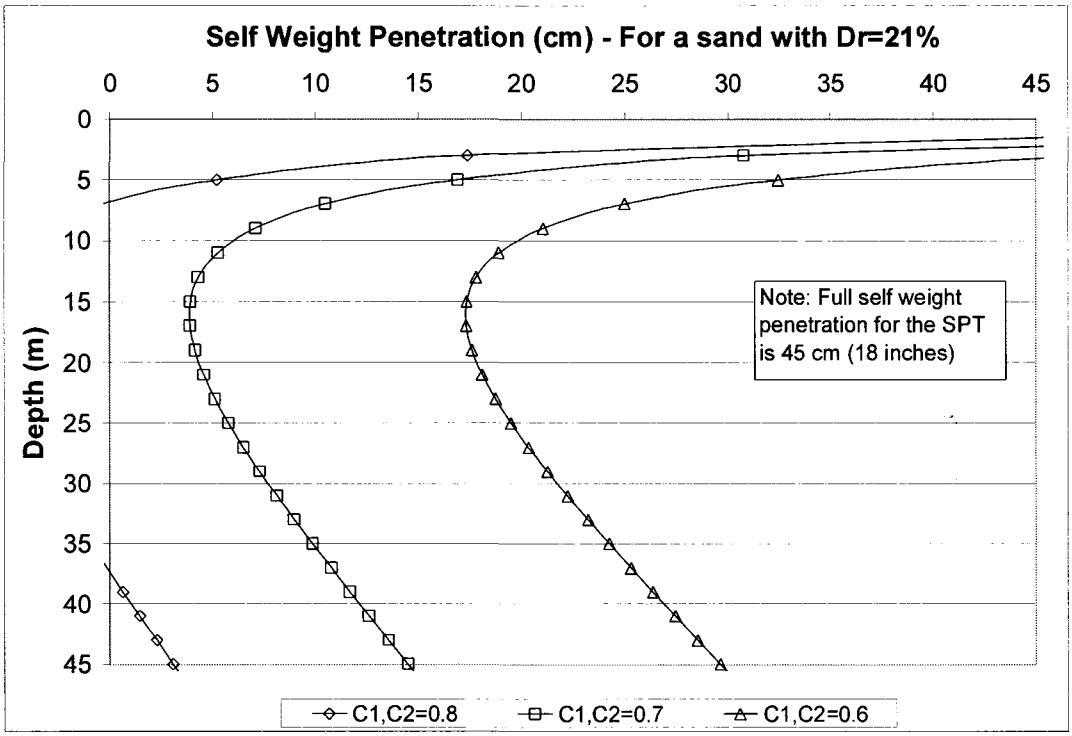

Figure 4.7: Predicted Self-Weight Penetration for a sand with Dr=21%

Figure 4.9 shows the variation in the calculated $q_{c1n}/(N_1)_{60}$ ratio with depth from the Aurora site (Pre-embankment). While there is some scatter in the data due to variation in the relative density of the sand, the overall trend of increasing $q_{c1n}/(N_1)_{60}$ ratio with depth is clear. This data supports the discussion regarding the self-weight penetration equation (equation 4.6). As mentioned, a possible reason for the trend is that as the depth increases, the weight of the SPT equipment grows at a faster rate than the penetration resistance of the sand resulting in lower blow counts relative to the cone tip resistance. It should be noted that much of the research presented in the literature concerning the q_c/N ratio was collected from reasonably shallow depths (typically less than 10 m). However, at the Aurora tailings dam, the zone of interest is from a depth of about 6 m to 20 m, so the weight of the SPT equipment may have a larger influence on the blow count. For the post-embankment condition, the depth range increases to between 22 and 36.

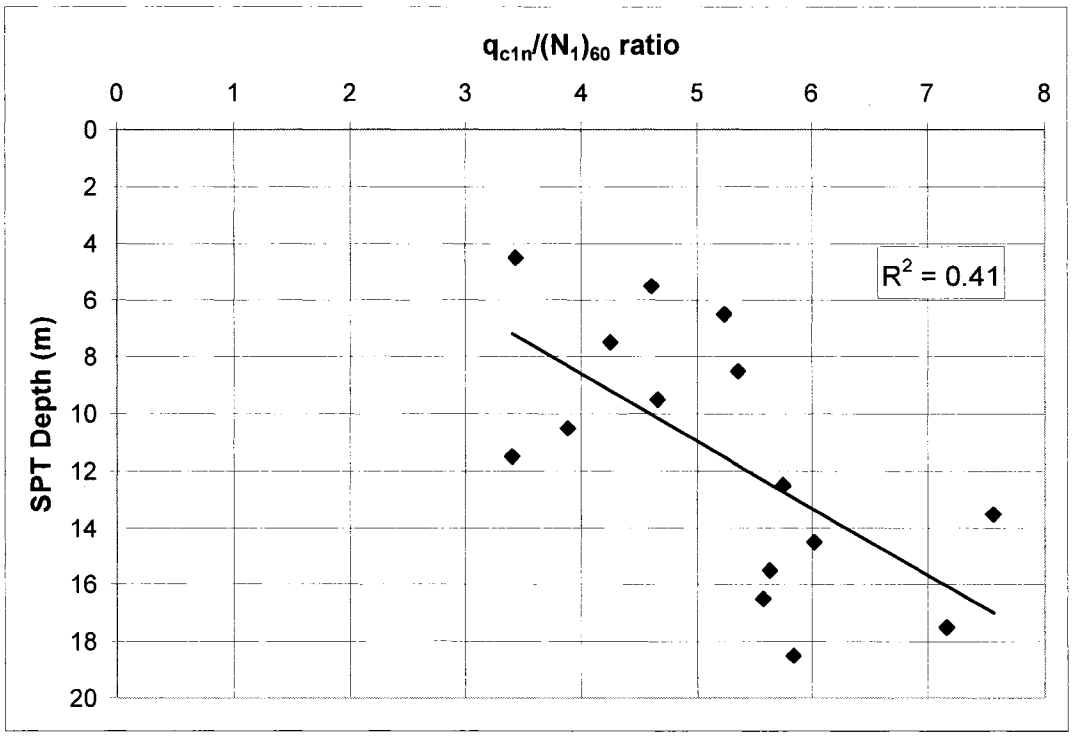

Figure 4.9: Calculated variation in the $q_{c1n}/(N_1)_{60}$ ratio with depth at Aurora test site (Pre-embankment)

4.3 Self-Weight Penetration Applied at Aurora

In the example of an SPT performed at a depth of 15 m, a relative density of 20% was assumed, which resulted in a predicted q_{c1n} of 13.6. However, at Aurora, at a depth of 15m, the average q_{c1n} measured was 44 with a standard deviation of 17. Therefore, 68% of the measured data at that depth fell within the range of q_{c1n} of 27 to 61. Thus, an effort was made to use the actual measured q_{c1n} in the self-weight penetration calculations, rather than predicted values. The results are shown in Table 4.1.

The value of C chosen in the relative density equation was also found to have a large impact on the calculation. Based on the relative density with deposit age relationships put forth by Jamiolkowski et al. (1988), Kulhawy and Mayne (1990) and the CANLEX data (Wride et al. 2000), C may range from about 200 to 380. Jamiolkowski et al. (1988) recommends a C of approximately 200 for a deposit with an age similar to Aurora (approximately 4 years). Kulhawy and Mayne recommend a C of approximately 340 for the same deposit. The CANLEX data suggests a much more rapid variation with age than either Kulhawy and Mayne or Jamiolkowski et al. Based on the CANLEX data, the choice of C in a range from 220 to 300 seems reasonable.

Table 4.1 shows that using the actual normalized CPT data results in predictions of relative densities between 24% to 47% and hence lower self-weight penetration. For instance, the average q_{c1n} minus one standard deviation at a depth of 15 m was 27, meaning that only 16% of all data collected at this depth was smaller than 27. The resulting relative density may vary from 27% to 37% depending on the choice of C for the deposit. At such a relative density, no self-weight penetration is predicted.

4.1: Self-Weight Penetration Predictions at Aurora

Depth (m)	Measured qc1n	qc1n (mean or mean minus one std. Dev.)	Constant C	Predicted Dr	Predicted Self-Weight Penetration (cm)
15	44	Mean	200	47%	0
15	44	Mean	340	36%	0
15	44	Mean	380	34%	0
15	27	Mean minus one Std. Dev.	200	37%	0
15	27	Mean minus one Std. Dev.	340	28%	0
15	27	Mean minus one Std. Dev.	380	27%	0
19.4	27	Mean	200	37%	0
19.4	27	Mean	340	28%	0
19.4	27	Mean	380	27%	0
19.4	22	Mean minus one Std. Dev.	200	33%	0
19.4	22	Mean minus one Std. Dev.	340	25%	0
19.4	22	Mean minus one Std. Dev.	380	24%	0

Even an examination of the loosest sand at Aurora and assuming the worst conditions regarding the choice of constants C, C_1 and C_2 it was found that SPT self-weight penetration is unlikely. For instance, at a depth of 19.4 m, using the mean q_{c1n} minus one standard deviation value of 22, and using the highest reasonable value for C, 380, yields a relative density of 24%. Assuming the worst conditions for $C_1=C_2=0.6$ still results in a prediction of no self-weight penetration.

Furthermore, if one were to assume a C=290 (the average of all values reported) and a very loose sand of 20% relative density at a depth of 15m, the corresponding q_{c1n} (based on the $q_{c1n}/D_r^2=C$ relationship) would be approximately 12. However, only 3% of all q_{c1n} measurements at that depth were smaller than 12.

4.4 Remarks on the self-weight penetration of the SPT

The above analysis shows that no SPT self-weight penetration was likely to have been observed at the Aurora test site. However, the weight of the SPT rods and hammer likely influenced the measured SPT blow count resulting in smaller measured N values than the equivalent N-values obtained from the CPT. As

mentioned earlier, the influence of the weight of the SPT equipment would increase with increasing depth.

The above analysis has shown that in very loose sand deposits with a relative density around 20% (specifically less than about 22%), self-weight penetration of the SPT sampler into the base of the borehole may be possible. Furthermore, the analysis has shown that particularly at depths greater than 15 m, the weight of the rods, sampler and hammer, will have a dramatic influence on the SPT resulting in lower blow counts relative to the equivalent SPT blow counts obtained from CPT testing. Even if no self-weight penetration is predicted, it is clear that in loose sands, the weight of the rods, hammer and sampler are a major contributor towards lower blow counts relative to equivalent SPT blow counts obtained from CPT testing.

4.5 Predicting Cone Penetration Resistance with SPT data

Schmertmann (1979) found a direct relationship between the SPT N-value and quasi-static energy required for the same sampler penetration from 15 to 46 cm (6 to 18 inches) below the bottom of the borehole. As noted earlier, Schmertmann's work allows prediction of CPT results based on SPT blow counts.

4.5.1 Schmertmann's (1979) Method

The average quasi-static energy required to advance the sampler during sampling is (Schmertmann 1979):

$$E' = 190 + \alpha\, 475\, N \qquad (4.7)$$

Where:

- E' is the quasi-static energy required for the penetration of the sampler from 100 to 460 mm (6 to 18 inches) in joules
- 190 Joules is a constant resulting from the 63.5 kg (623 Newtons, or, 140 lb) hammer always having a net drop of 300 mm (12 inches) during the interval in which the blows are counted
- α is a constant fraction of maximum deliverable hammer energy (α=0.42 and 0.33 for cohesionless and cohesive soils respectively) that is required for *quasi-static* sampling. The energy required for normal dynamic penetration of the sampler (energy ratio of the SPT rig) usually exceeds that required for quasi-static penetration (α) because of dynamic losses due to ground quake, viscous effects, etc. (Schmertmann 1979)
- N is the blow count
- 475 (joules) is the maximum possible amount of dynamic energy in the 63.5 kg (140 lb) SPT hammer at impact after falling the specified 76 cm (30 inches) (equal to 475 J, or 4200lb-inches)

The average added quasi-static force for penetrating 100 to 460 mm (6 to 18 inches) is then E'/0.305 m, which yields Equation 4.2, as stated earlier:

$$F_{(avg)} = 623 + \alpha\ 1557\ N \quad (4.8)$$

Where:

- $F_{(avg)}$ is the average added quasi-static force during SPT sampling. $F_{(avg)}$ is in the units of Newtons.
- 623 Newtons equals 190 Joules divided by 0.305 m (12 inches)
- 1557 Newtons equals 475 Joules divided by 0.305 m (12 inches)
- α is the fraction of maximum theoretical hammer energy required to obtain the sample. Schmertmann found that α averaged 0.33 in cohesive soils and 0.42 in cohesionless soils.
- N is the blow count from 100 to 300 mm (6 to 18 inches) of penetration.

Schmertmann then calculates the end bearing force on the sampler as:

$$F_e = [\ z(5.95\ kg/m) + (EBR)F_{(avg)}\ ]\ 9.81\ m/s^2 \quad (4.9)$$

Where:

- F_e is the end bearing force on the SPT sampler
- z is the depth of sample in metres
- EBR is the approximate percentage of load due to end bearing resistance
- $F_{(avg)}$ is an estimate of the average added quasi-static force during SPT sampling
- 5.95 kg/m (4 lb/ft) is the approximate weight of the rods and sampler per metre of length

Using Schmertmann's technique, predicted CPT q_c values, $(q_c)_p$, can be obtained from F_e and compared with the measured CPT q_c data as follows:

$$(q_c)_p = [\ F_e / (A_e)_{SPT}\ ] \quad (4.10)$$

Where:

- $(q_c)_p$ is the cone tip resistance predicted by Schmertmann's method
- F_e is the end bearing force on the SPT sampler
- $(A_e)_{SPT}$ is the end area of the SPT sampler (usually 10.7 cm^2)

The Schmertmann predicted data were normalized for vertical effective stress using the commonly accepted formula:

$$(q_{c1n})_p = [(q_c)_p / Pa][Pa/\sigma'_v]^n \quad (4.11)$$

Where:

- Pa is atmospheric pressure in the same units as either q_c or σ'_v
- n is a stress exponent, typically 0.5 for clean sand
- σ'_v is the in-situ vertical effective stress

- $(q_c)_p$ is the cone penetration resistance predicted by Schmertmann's theory
- $(q_{c1n})_p$ is the cone penetration resistance predicted by Schmertmann's theory, normalized for overburden stress.

Figure 4.6 shows the measured normalized SPT data on the x-axis and the corresponding Schmertmann predicted normalized cone tip resistance on the y-axis. As can be seen in the figure, the relationship between the corrected blow count and the Schmertmann predicted normalized cone tip resistance is linear with an intercept at an SPT $(N_1)_{60} = 0$. As an example, if one were to measure a $(N_1)_{60}$ of 10, the corresponding normalized cone tip resistance predicted by Schmertmann's theory would be about 53, which appears reasonable (i.e. $q_{c1n}/(N_1)_{60} = 5.3$). However, it is more important to note the offset/intercept near the origin of the chart. This shows that while a SPT blow counts of zero might be measured, Schmertmann's theory does not predict cone tip resistances (q_c) of zero. This reflects reality since blow counts as low as 1 was measured at Aurora, while cone tip resistances of less than 20 are rarely measured in practice. The offset near the origin is actually due to Schmertmann's inclusion of the weight of the SPT equipment in his static theory.

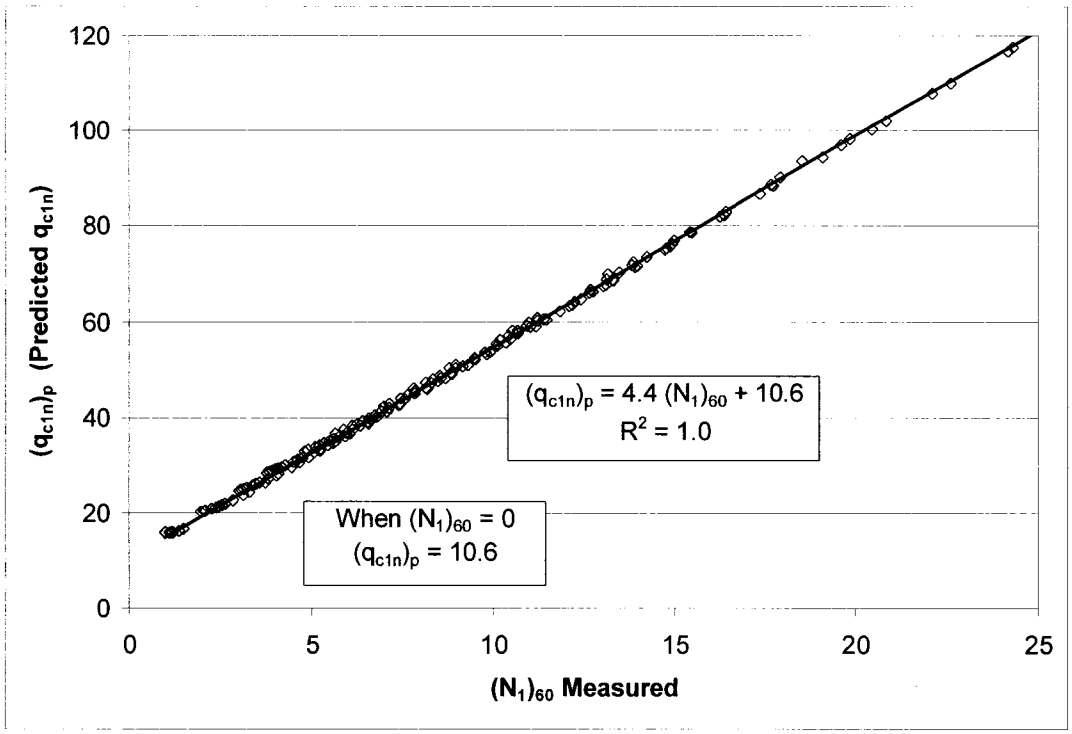

Figure 4.11: Relationship between measured $(N_1)_{60}$ and predicted $(q_{c1n})_p$

If the y-axis on Figure 4.11 is divided by $(N_1)_{60}$, the result is the $(q_{c1n})_p/(N_1)_{60}$ ratio predicted by Schmertmann's work. Schmertmann's technique can also be used to predict how the $q_{c1n}/(N_1)_{60}$ ratio changes with increasing $(N_1)_{60}$, as shown in Figure 4.13. The figure shows the $(q_{c1n})_p/(N_1)_{60}$ ratio (subscript $_p$ denotes 'predicted') predicted by Schmertmann's technique. As the blow count decreases to zero, the $(q_{c1n})_p/(N_1)_{60}$ ratio increases to infinity as a result of the offset shown in Figure 4.11 (i.e. the best fit line not passing through the origin). As noted, the offset and hence the inverse relationship in Figure 4.13 is caused by Schmertmann's inclusion of the weight of the SPT equipment in his theory linking the SPT and CPT.

In very loose sands, where the measured $(N_1)_{60}$ value would be less than 10, Schmertmann's static theory predicts increasing $(q_{c1n})_p/(N_1)_{60}$ ratios from about 6 to 14 as the $(N_1)_{60}$ measured values drop to around 1. It is also worth noting that as $(N_1)_{60}$ increases to values greater than about 10, the predicted $(q_{c1n})_p/(N_1)_{60}$ ratio approaches 5 (within the zone of engineering interest where $(N_1)_{60}$ is less than 30-40). A $(q_{c1n})_p/(N_1)_{60}$ ratio of 5 would seem to agree with the work conducted by Robertson and Campanella (1983) and other researchers as noted in Section 2.4

Thus, based on Schmertmann's theory, one would expect that the weight of the SPT equipment would have a larger impact on the measured $q_{c1n}/(N_1)_{60}$ ratio in very loose sands where the blow count is less than 10. In medium dense or dense sand (where blow counts are greater than 10) one would not expect the weight of the SPT equipment to have a significant impact on the measured $q_{c1n}/(N_1)_{60}$ ratio.

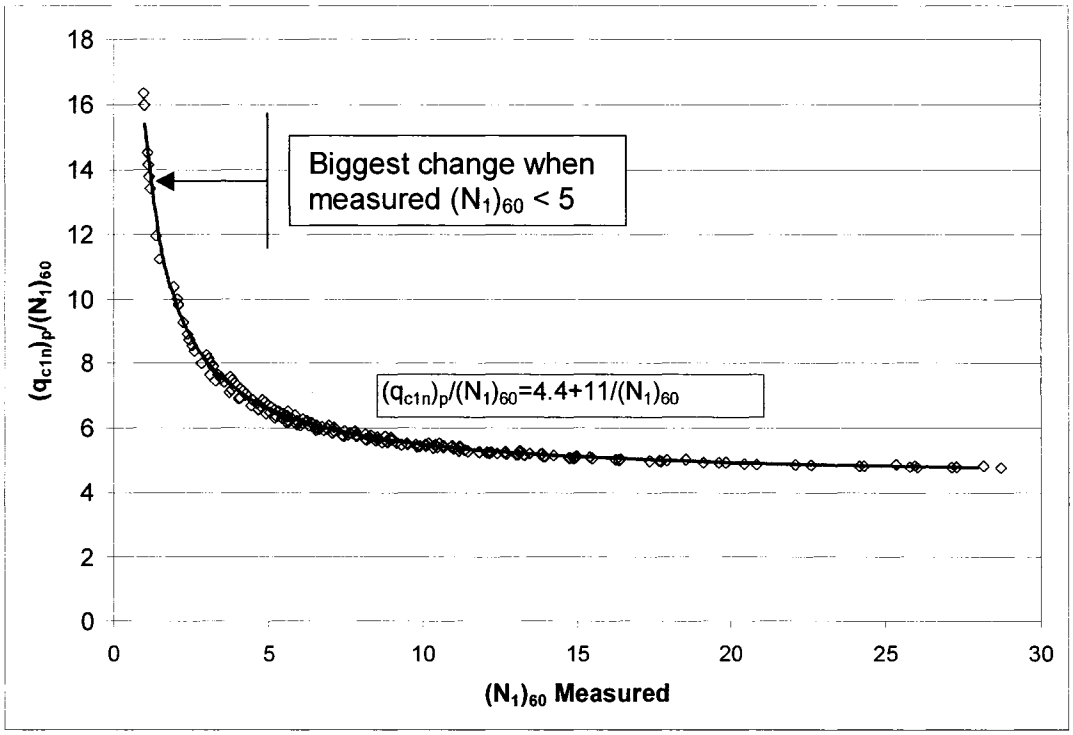

Figure 4.13: $(q_{c1n})_p/(N_1)_{60}$ ratio predicted by Schmertmann's technique

It should be noted that for the Aurora field load test there were 334 SPT's performed prior to construction of the embankment. Of those 334 SPT's, 10.5% resulted in a normalized blow count ($(N_1)_{60}$) less than 3, 28% resulted in a normalized blow count less than 5 and 61% resulted in a corrected blow count less than 8. Thus, the weight of the SPT equipment may have influenced the blow count on a significant percentage of the tests.

Figure 4.15 shows a comparison between the actual $(q_{c1n})/(N_1)_{60}$ ratio measurements from the Aurora test site (with the pre- and post embankment plotted as one series) and the Schmertmann predicted $(q_{c1n})_p/(N_1)_{60}$ ratio. The relationship suggested by Idriss and Boulanger (2004) is also shown on the figure for comparison. The Idriss and Boulanger relationship was developed by combining relationships between cone tip resistance and relative density and blow count and relative density. Idriss and Boulanger theorized that their relationship was consistent with the drainage conditions in each in-situ test. They speculated that since the SPT was a largely undrained test, it would develop positive excess pore pressures in loose sand and negative excess pore pressures in dense sand.

The Idriss and Boulanger relationship predicts much higher $(q_{c1n})/(N_1)_{60}$ ratios than either the Schmertmann's static theory or what was observed in the field

although it approaches a value of about 6 at $(N_1)_{60}$ values greater than about 20, which is not unreasonable.

Figure 4.13 and Figure 4.15 help to illustrate that in loose sand (i.e when $(N_1)_{60} <$ 10), the influence of the weight of the hammer, sampler and rods has a significant effect on the measured $(N_1)_{60}$ and the resulting $(q_{c1n})_p/(N_1)_{60}$ ratio.

Figure 4.17 shows the $(q_{c1n})_p/(N_1)_{60}$ ratio if the weight of the hammer, sampler and drill rods are ignored in Schmertmann's calculations compared to when they are not ignored. The figure shows a constant $(q_{c1n})_p/(N_1)_{60}$ ratio of 4.4 when the weight of the SPT equipment is ignored.

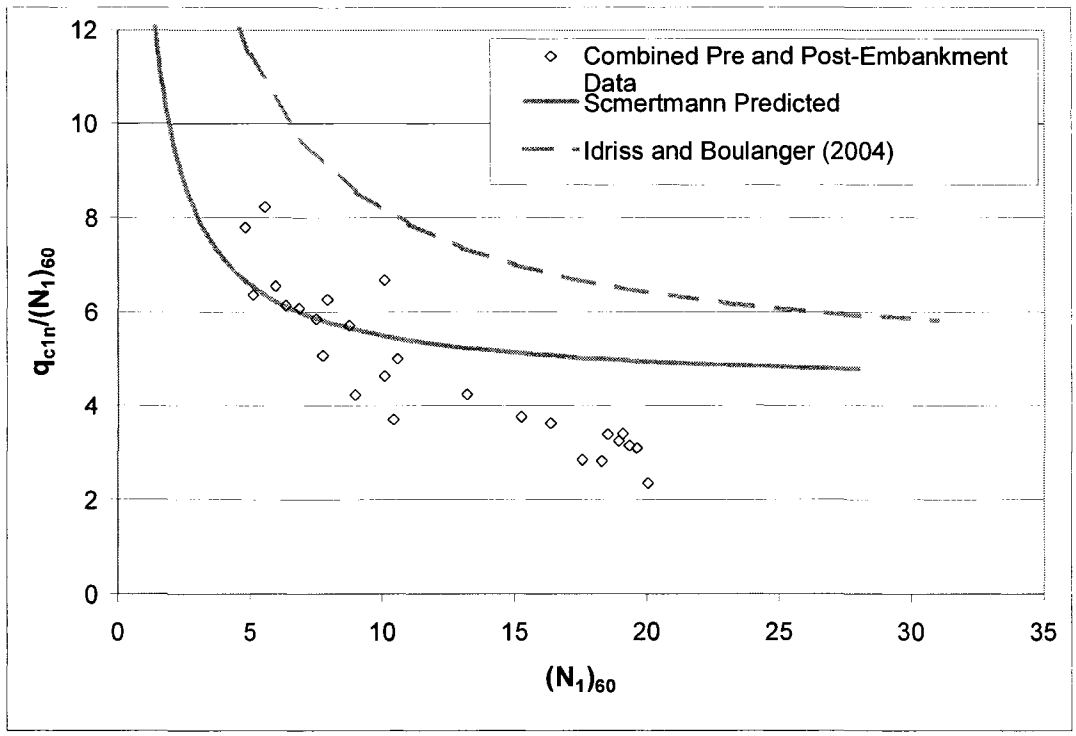

Figure 4.15: Change in measured Aurora test site (both pre- and post embankment) $(q_{c1n})/(N_1)_{60}$ ratio compared to Schmertmann predicted $(q_{c1n})_p/(N_1)_{60}$ ratio

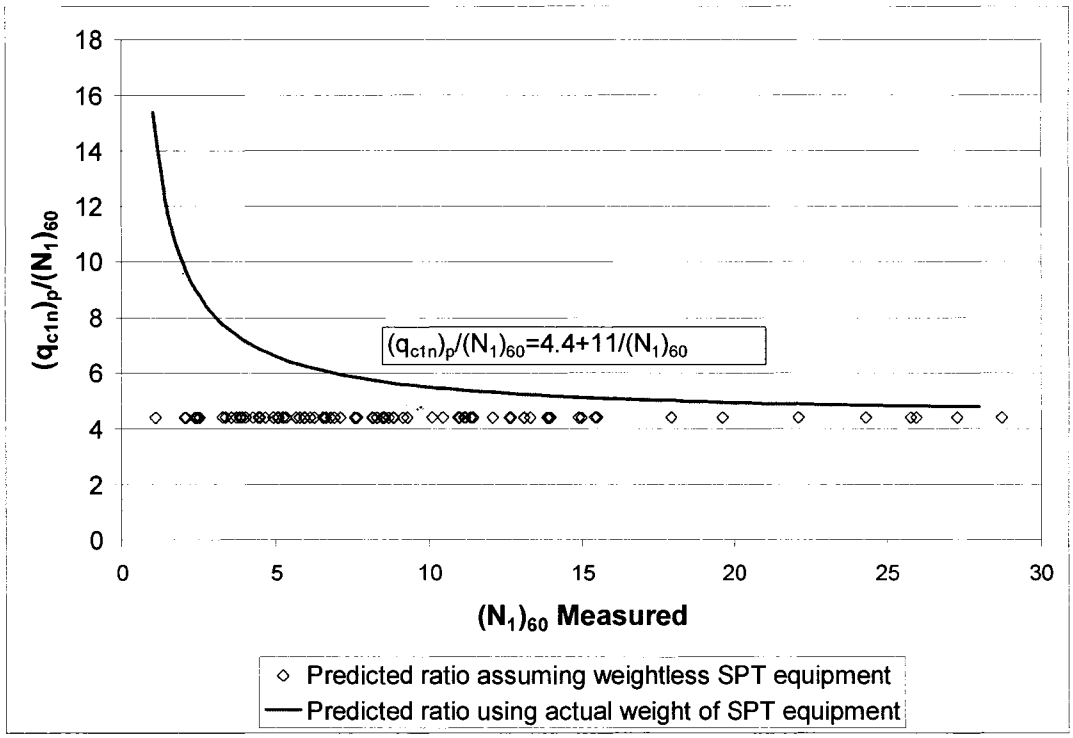

Figure 4.17: $(q_{c1n})_p/(N_1)_{60}$ ratio predicted by Schmertmann's technique ignoring the effect of hammer, sampler and drill rod weight

5.0 SPTu FIELD TESTING PROGRAM

5.1 General

A field in situ testing program was undertaken to confirm or reject the second hypothesis put forth earlier in this thesis. In an effort to determine if the SPT, in fact, does cause increased pore pressures during the test, a standard split spoon sampler was outfitted with a pore pressure measurement device. The SPT with pore pressure measurement will be referred to as the SPTu. The modified split spoon sampler was designed and manufactured by Adara Systems Ltd.

5.1.1 Preliminary SPTu testing and related research

Daniel et al. (2003) analyzed SPT stress wave data using the CASE method. They found that the effect of rod couplings could be predicted and was not negligible. More importantly, they also observed considerable soil softening, the calculated soil resistance often dropping to zero, after the initial cycle of loading. This effect was more pronounced in soils with a low blow count. They hypothesized that the softening was caused by the occurrence of short-term liquefaction of the soil around the base of the sampler. In soils with high blow counts, softening was still observed but soil resistance did not drop to zero.

Preliminary testing using a SPT sampler outfitted with a pore pressure measurement device was conducted in September and October of 2004 at the Massey tunnel site, which was studied in great detail during CANLEX (ConeTec 2004). Researchers from the University of British Columbia conducted additional tests to facilitate interpretation of the pore pressure data (Daniel and Howie 2004). Daniel and Howie (2004) calculated the energy absorbed by the soil from the Dynamic Energy Monitoring (DEM) data as a function of sampler penetration and their results are shown in Figure 5.1.

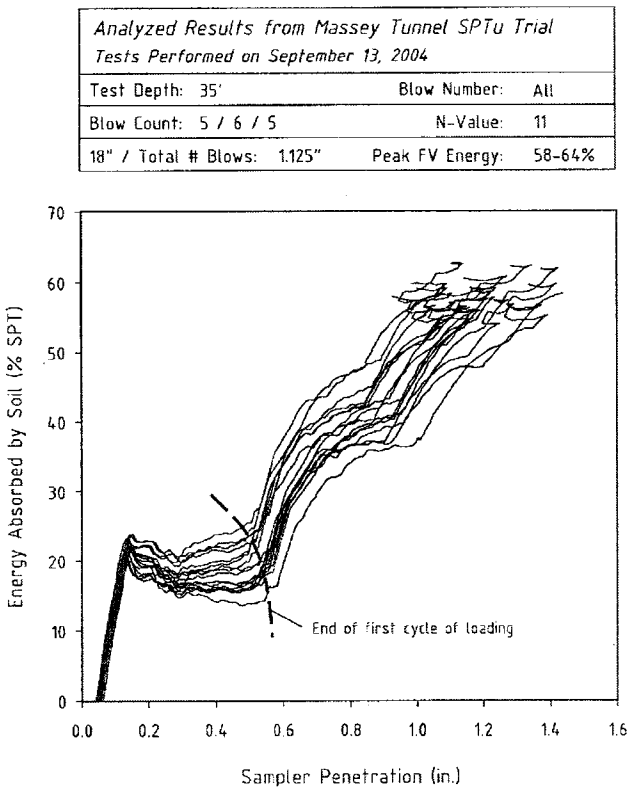

Figure 5.1: Absorbed energy versus sampler displacement relationships for 16 hammer blows at 10.7 m (35') depth, calculated from DEM data (modified from Daniel and Howie (2004))

They observed a stiff initial response (steep curve) where between 20 and 25% of the SPT hammer potential energy was absorbed by the soil for a penetration of about 3 mm (0.1 inch). This steep portion of the curve was followed by a very soft response, for which little or no energy was absorbed by the soil for approximately 10 mm (0.4 inches) of penetration. This portion of the curve was followed by another steep section, which indicated the second arrival of the original stress wave at the sampler-soil interface (Daniel and Howie, 2004).

Daniel and Howie (2004) noted that during previous studies, the initial stiff response of the soil was insensitive to the blow count. They postulated this portion of the curve may represent an initial shock loading during which the soil resistance is largely derived from the relatively incompressible pore fluids. They further noted that the average slope of the second portion of the curve was dependent on the blow count and that the slope typically reduces to zero for blow counts of about 10. In these cases, Daniel and Howie (2004) felt that the initial shock loading may be initiating liquefaction of the soil, which would explain the increase in penetration of the sampler with no increase in the energy absorbed by the soil.

Based on their observations of absorbed energy versus sampler displacement (shown in Figure 5.1), Daniel and Howie (2004) theorized that the pore pressure history at the sampler location would progress through two stages. The first stage, during the peak loading, would be characterized by a brief high pore pressure seen as the stress wave transfers from the SPT sampler to the pore fluid. The second stage, during the post-peak loading stage, would be characterized by a period of lower pore pressure magnitudes between the peak loading stage and the next cycle of loading. They noted that the pore pressure response in this stage of loading may depend on the soil response to shear loading and whether its response would be dilative or contractive.

5.1.2 SPTu Field Investigation Site Selection

A field-testing program using the SPTu device was to take place on December 7, 2004 at the Aurora Pond Load Test site as part of Syncrude's regular SPT program. However, due to very cold weather, the drilling and testing proceeded slower than hoped and imposed considerable time constraints on the testing. One SPTu was performed at a depth of 1.52 m (approximately 0.5 m above the water table) in order to establish the baseline pore pressure transducer response, at which point the testing program had to be abandoned.

The field-testing of the SPTu was completed in Vancouver at the Massey Tunnel site between January 20 and 21, 2005.

The Massey Tunnel site was selected due to a combination of the warm weather, nearby availability of a drill rig and CPT and the fact that the Massey site is a well-known loose sand deposit, which was heavily investigated during the CANLEX project.

5.1.3 Setup

ConeTec Investigations performed the SPTu and energy measurement testing. An M10 drill rig was used to drill an auger hole in which to perform the SPTu. For the first two SPTu's performed, a multi-truck CPT/drill rig was used to push a blast probe outfitted with a pore pressure sensor and a triaxial accelerometer.

For the first two SPTu's, the blast probe was driven approximately 1.12 m away (in plan view) from the auger/SPTu hole. The blast probe was oriented so that the SPT testing would be directly in line with its x-axis as is normally done for particle acceleration measurements. The blast probe was driven 23 cm (9 inches) past the depth that the SPTu started so that the end of the sampler would pass it exactly half way through the test.

For the remaining five SPTu's, the blast probe was driven at a distance of just 0.29 m (11.5 inches) away (in plan view). It was believed that this would allow measurement of stronger particle acceleration measurements and the possibility of measuring elevated pore pressures because of the SPTu. As in the first two

tests, the blast probe was driven 23 cm (9 inches) past the starting depth of the SPTu.

A diagram of the SPTu set up is shown in Figure 5.3.

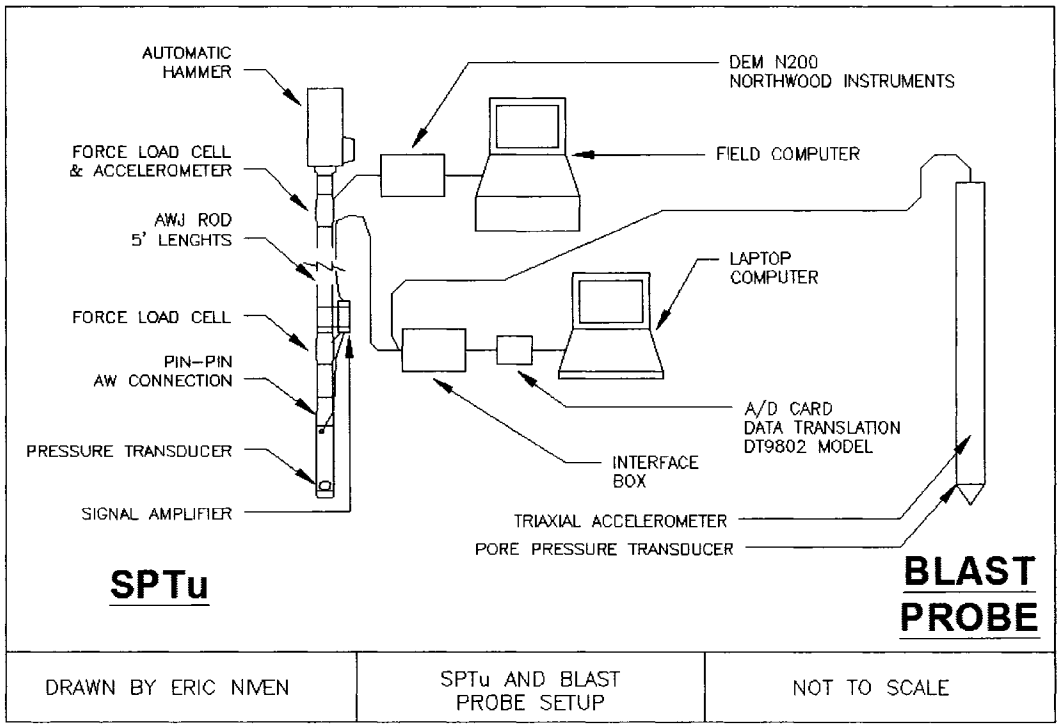

Figure 5.3: Diagram of SPTu Set-Up

The pore pressure transducer was located inside the split spoon sampler barrel. The connecting wire ran out through a hole in the barrel of the sampler and into a down-hole signal amplifier. The connection from the down-hole force load cell also ran into the amplifier. The amplifier was taped to the drill rod. A single cable, which was taped at 1.5 m (5 ft) intervals, ran up the drill string and out of the hole. The cable then ran into a ConeTec interface box. The signal from the interface box then ran into a Data Translation DT9802 model A/D card, which then ran into a laptop computer outfitted with Data Translation signal acquisition software.

A force load cell and accelerometer was also located up-hole, just below the anvil on the drill string in order to measure the energy of the SPT automatic hammer. The signal from the load cell and accelerometer ran into a Northwoods Instruments Dynamic Energy Monitoring (DEM) N200 Model and from there into a Field Computer.

The blast probe was outfitted with a pore pressure sensor and a triaxial accelerometer. The signal from the blast probe ran into the same ConeTec interface box that was used for the SPTu signals and from there, the signal passed through the same A/D card and into the laptop as is shown in Figure 5.3.

5.1.4 SPTu Assembly and Set-up

The SPTu device consisted of a standard split spoon sampler outfitted with a pore pressure transducer to measure the water pressure changes during the test. The SPTu device was designed and manufactured by Adara. Schematics of the design of the SPTu modified split spoon sampler are shown in Appendix B.

A small hole was machined into one side of the split spoon barrel approximately 9.9 cm above the cutting edge of the sampler shoe. The hole measured approximately 0.7 cm wide by 2.4 cm tall. The hole was covered with a fine mesh screen, which interfaces the soil, however it was supported by a coarser screen.

The pore pressure transducer was located inside the split spoon barrel. The cable from the transducer traveled up and out of the sampler through a hole in the split barrel sampler. The cable was protected from being cut by the edges of the hole by a Kevlar sleeve.

The electrical connections between the transducer and down-hole load cell and the down-hole signal amplifier were packed with o-ring grease to prevent infiltration of water. The connections were then further protected by being carefully wrapped in electrical tape to provide another seal against water infiltration. Then the cables and down-hole signal amplifier were securely taped to the side of the drill stem just above the split spoon sampler using more electrical tape. The cable was then taped to the drill stem at 1.52 m (5 foot) intervals. After each test, the entire assembly had to be taken apart to remove the sample and then reassembled and carefully re-taped to ensure integrity of the system.

5.1.5 SPTu Test procedures

The test began by auger drilling to a depth of 1.52 m (5 ft). This depth was known to be above the water table. This provided a suitable location to establish the response of the pore pressure transducer to the stresses of the SPT without the measurement of water pressure. As mentioned, the blast probe was driven 1.12 m away (in plan view) from the auger hole and to a depth of 23 cm (9 inches) past where the SPTu test began.

Self-weight penetration was measured before each test was performed. This was accomplished by taking the known depth of the hole added to the length of the rods above the hole and subtracting that from the total length of the SPT drill assembly. This procedure was performed with the hammer resting on the anvil.

A piece of duct tape was then placed on the rod string just above the collar of the hole. The 0.15 m (6 inch) intervals for the test were marked on the tape. Baseline readings were then measured and recorded for each instrument.

With each blow during the test, the tape was marked on the tape at the drill stem collar to indicate the distance of penetration after each blow. After the test, the penetration intervals were measured to the nearest centimetre and recorded.

The SPTu was performed using a 63.5 kg (140 lb) automatic hammer owned by ConeTec Investigations. Data acquisition began approximately 20 seconds before the test started. Once the test was started, as mentioned, the level of the drill hole collar was recorded on a piece of duct tape attached to the drill stem to measure the distance of penetration for each blow. After each SPTu test was completed, data acquisition continued for approximately 20 seconds. The extra data was collected before and after the test in order to examine any changes in the baseline data just before, during and after the test.

After the test, the split spoon SPTu apparatus had to be carefully disassembled to avoid ripping or cutting the wires and to avoid any more disturbance of the sample. Sample recovery was also measured and recorded.

5.2 SPTu Field Testing Program Experimental Results

5.2.1 Massey SPTu Results

In total, seven trials with the SPTu device were performed at various depths in the same borehole. The measured blow count and corrected $(N_1)_{60}$ values are presented in Table 5.1. The blow count was corrected for vertical effective stress and energy ratio (ER).

The sampler used in the SPTu's was not outfitted with liners. Normally the use of a sampler without liners would require a correction by a factor of between 1.1 and 1.3. However, the pore pressure transducer for the SPTu sampler was located inside the sampler barrel in a metal casing. The result would be a decrease in the volume inside the sampler and an increase in the friction forces and penetration resistance on the sampler. While it is not known if the effect of the transducer exactly offsets the effect of having liners in the sampler, it was assumed that the difference between the two would be small and hence no correction for using a sampler without liners was made.

In the table, the column labelled 'recorded' denotes the number of blows that were recorded by the instrumentation attached to the SPT. In a few cases, an extra blow was applied after the full 46 cm (18 inches) of penetration was achieved because the automatic hammer was not shut off fast enough. The average energy ratio calculated by the F-v maximum method was used to correct the N-values to a standardized energy of 60%. While the energy ratio using the F^2 method was also measured, the F-v energy method was used to correct the N-values since it is widely regarded to be more accurate.

As is shown in Table 5.1, very high energy ratios were calculated for the SPTu testing performed at the Massey site. Calculated energy ratios ranged from 75.2% to 122.8% and averaged 108.6%. Equation 3.4 in Section 3.7 was used to correct the SPT N-values to obtain $(N_1)_{60}$ values. As a result of the very high energy efficiency of the automatic hammer (compared to the accepted standardized value of 60%), large corrections were made to the SPT N-values to obtain $(N_1)_{60}$ values. In fact, for the fourth test at a depth of 9.33 m, an energy efficiency of 115.1% was calculated. Therefore, a correction factor of 1.92 had to be applied to the N-value to obtain an $(N_1)_{60}$ value as follows:

$$(N_1)_{60} = C_n \, ER \, N \qquad (5.1)$$

$$(N_1)_{60} = 1.0 \; (115.1\% / 60\%) \; 5 = 9.2$$

$$(N_1)_{60} = 9.2$$

5.1: SPTu measured and corrected N-values

	SPT Blow Counts									
Depth (m)	A 0-152mm (0-6")	B 152-305mm (6-12")	C 305-457mm (12-18")	N (B+C)	Vert. Eff. Stress (kPa)	Cn*	ER (%) Fv (Max)	$(N_1)_{60}$	Total Blows (A+B+C)	Recorded Blows
1.52	3	4	4	**8**	30	1.8	75.2	**18.4**	11	11
7.72	4	3	3	**6**	94	1.0	112.8	**11.6**	10	12
8.56	2	3	4	**7**	101	1.0	98.4	**11.4**	9	9
9.33	2	2	3	**5**	108	1.0	115.1	**9.2**	7	8
10.80	3	3	4	**7**	121	0.9	121.0	**12.8**	10	10
12.41	3	2	5	**7**	135	0.9	122.8	**12.3**	10	11
13.92	5	5	8	**13**	148	0.8	115.2	**20.5**	18	19

*Cn is the overburden stress correction factor. i.e. $(N_1)_{60}$ = Cn N ER

A profile of the SPT $(N_1)_{60}$ values is shown in Figure 5.5 along with the uncorrected SPTu N-values and the equivalent $(N_1)_{60}$ values obtained from the CPT, which was conducted 1 m away from the SPTu hole. The equivalent $(N_1)_{60}$ values were calculated from measured CPT data using the equation presented by Jefferies and Davies (1993) as follows:

$$N_{60} = q_c / [0.85 (1 - I_c / 4.75)] \quad (5.2)$$

Where:

- q_c is the measured cone tip resistance in units of MPa
- N_{60} is the predicted corrected blow count in units of number of blows per 300mm

N_{60} was then corrected for vertical effective stress using the following equation (Robertson and Wride 1998):

$$(N_1)_{60} = N_{60} [100 / \sigma_{vo}']^{0.5} \quad (5.3)$$

Where:

- σ'_{vo} is the effective overburden stress

From CANLEX, it is known that the zone of interest for liquefaction potential evaluations is from approximately 7.92 and 13.11 m at the Massey site. The $(N_1)_{60}$ values in this depth range varied between 9.2 and 12.8 and averaged 11.5. With an average $(N_1)_{60}$ value of 11.5, this deposit can be classified as loose. At a depth of 13.72 m, the $(N_1)_{60}$ value measured increases to 20.5 indicating an increased density.

It should be noted that the large difference between the uncorrected N values and the corrected $(N_1)_{60}$ values is mainly due to the high energy ratios measured for the SPT rig. In most cases, the correction made to the data was quite large, and in some cases was as large as 84% of the original value.

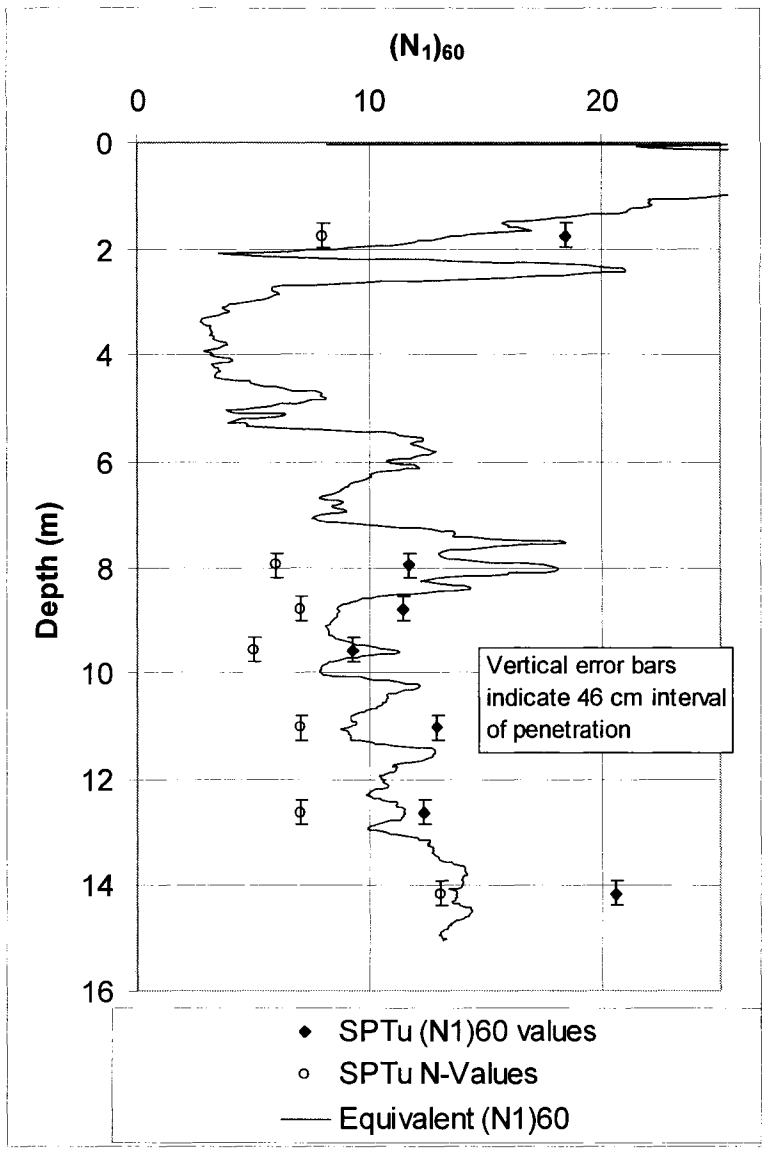

Figure 5.5: Profile of SPTu N-values at Massey Site

5.2.2 Massey CPT Results

After the SPTu was performed, a single CPT was performed nearby at a distance of 1 m from the SPTu hole. The CPT profile is shown in Figure 5.7. The CPT profile is representative of loose sand, particularly from 4.57 to 7.32 m and from 8.53 to the end of the log at almost 15.24 m. Note that the 'gap' in the CPT data is due to removal of data where I_c was greater than 2.5. However, no SPTu's were performed at the depths where the data were removed.

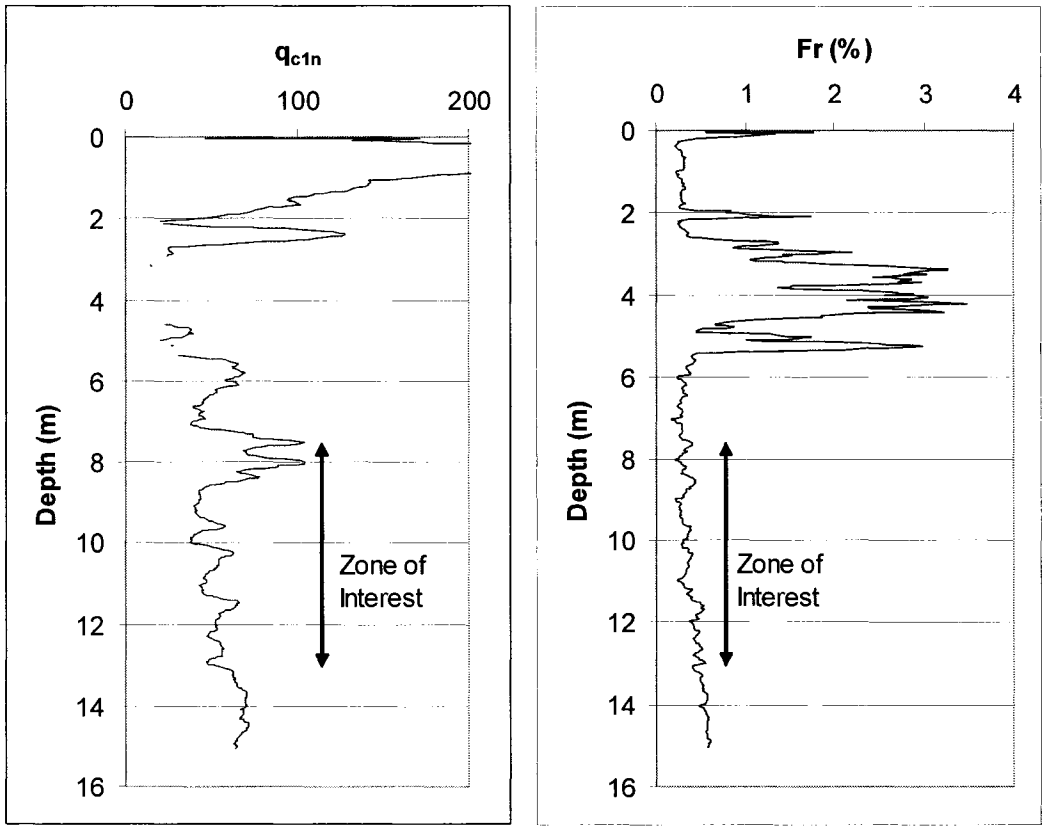

Figure 5.7: Massey CPT Profile

5.2.3 $(q_{c1n})/(N_1)_{60}$ Ratio at the Massey Site

Figure 5.9 shows the variation in the $(q_{c1n})/(N_1)_{60}$ ratio with increasing $(N_1)_{60}$ values at the Massey site compared to the Aurora site. The CPT q_{c1n} data was averaged over one meter, from half a meter above to half a meter below the SPTu test depth, then divided by the $(N_1)_{60}$ value at that particular depth. The SPTu test depth is noted for each data point on the chart.

Upon examination of Figure 5.9 it can be seen that six of the seven points show a $(q_{c1n})/(N_1)_{60}$ ratio between approximately 4.5 and 5.5.

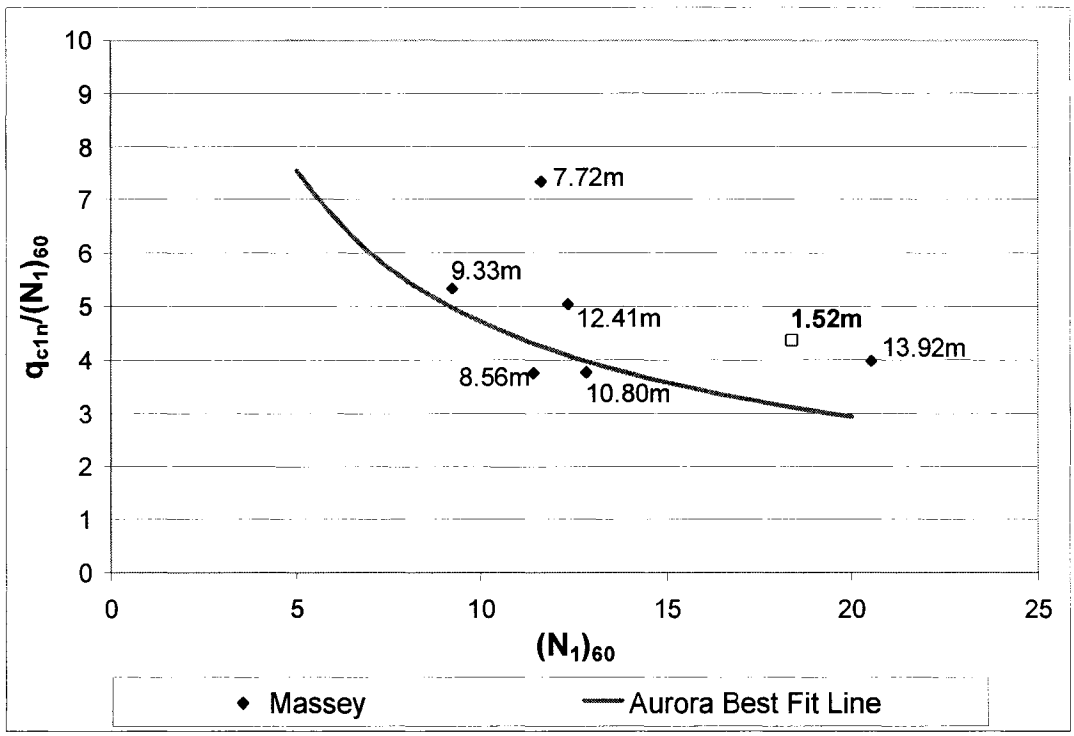

Figure 5.9: $q_{c1n}/(N_1)_{60}$ ratio at Massey Compared to Aurora

5.2.4 SPTu Pore Pressure Response

This section discusses the pore pressure measurements made during the SPTu's. Unfortunately, the pore pressure measurement system did not function properly for the tests at depths of 7.72, 8.56 and 9.33 m. It was later discovered that the down-hole signal amplifier was not functioning properly for those tests. Adara Systems personnel were able to change the amplifier and data was obtained for the successive three tests.

5.2.4.1 SPTu at 1.52 m

As mentioned, the first SPTu was performed at a depth of 1.52 m, which was above the ground water table. The purpose of the test was to establish the response of the SPTu pore pressure transducer to the stresses imposed on it

during the test. The blow counts for the first, second and third 152 mm (6 inch) intervals of penetration were 3, 4 and 4 for an N of 8 and an $(N_1)_{60}$ of 18.4 when corrected for the measured energy ratio, and the overburden stress. The overall baseline pore pressure response (on a macro scale) of the transducer is shown in Figure 5.11.

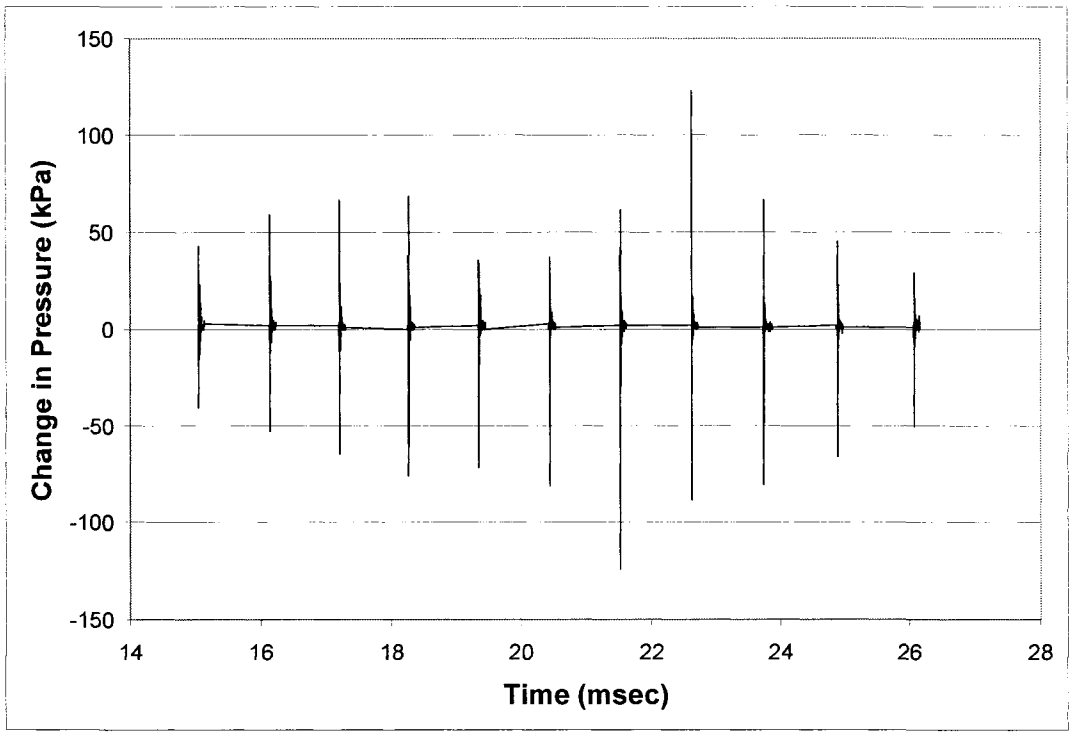

Figure 5.11: SPTu Pore Pressure Response (depth 1.52 m)

The figure shows very large spikes of as much positive and negative 125 kPa relative to the baseline pore pressure. At a depth of 1.52 m, the vertical effective stress is approximately 30 kPa so the figure shows pressure spikes as high as four times the vertical effective stress.

Figure 5.13 shows the SPTu pore pressure response on a much smaller time scale for the first of eleven blows at a depth of 1.52 m. The response from the other 10 blows is shown in Appendix C. The down hole force load cell response is also plotted on the chart to illustrate the lack of time lag between the force reaching the sampler and the time for pore pressure response.

There are a few important features to note about the pore pressure response shown in Figure 5.13. As mentioned, the magnitude of the positive and negative pore pressure 'peaks' is much greater than the actual effective vertical stress at this depth. There is little to no time lag between the force reaching the sampler and the pore pressure response (less than 1 msec response). No residual pore pressure was measured on this particular blow (or any blow at this depth). That

is, no sustained pore pressure increase was measured during any of the blows at a depth of 1.52 m. Just after the blow, the pore pressure response is very cyclical, attenuating over time to no residual pressure. In reality, much of the cyclical response is due to the stress wave in the drill rods and the motion of the pore pressure transducer. It is believed that the pore pressure transducer acts as an accelerometer and as a result, much of the cyclical response just after the blow is due to the shaking of the device. Adara tested a number of SPTu sampler prototypes in hopes of eliminating this effect. However, in the interests of saving time and money on the development of the device, it was not possible to eliminate this effect. It may be possible to eliminate this effect by placing an actual accelerometer down the hole near the sampler and developing a correction to the pore pressure response based on the measured acceleration of the sampler.

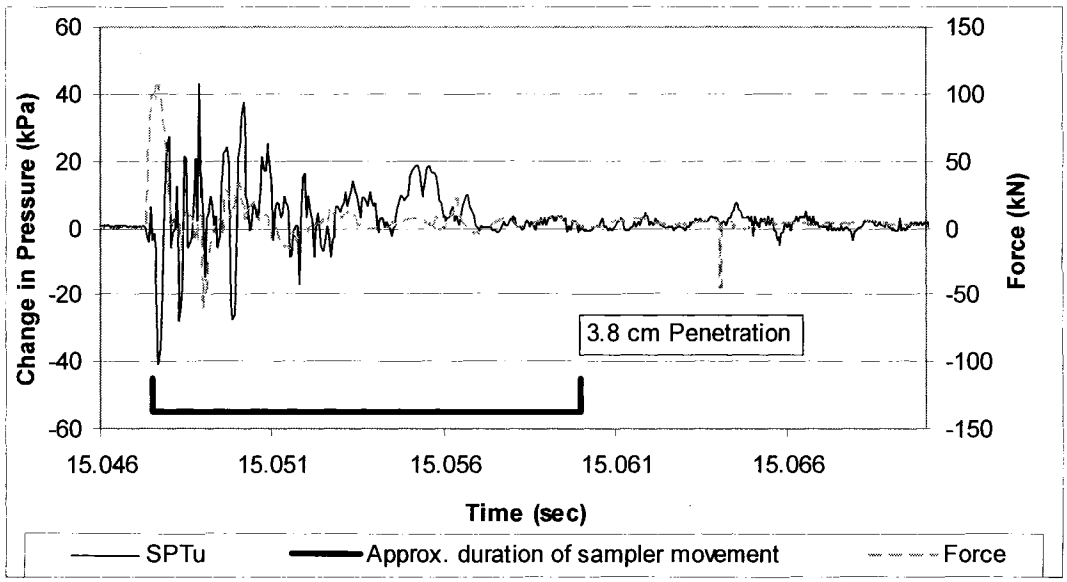

Figure 5.13: SPTu response (Depth 1.52 m (5'), blow 1 of 11; 3.8 cm of sampler penetration)

5.2.4.2 SPTu at 7.72 m

The second SPTu was performed at a depth of 7.72 m. The blow counts for the first, second and third 152 mm (6 inch) intervals of penetration were 4, 3 and 3 respectively for an N value of 6 and an $(N_1)_{60}$ value of 11.6 when corrected for measured energy ratio and overburden stress. The pore pressure response at this depth for all blows is shown in Figure 5.15.

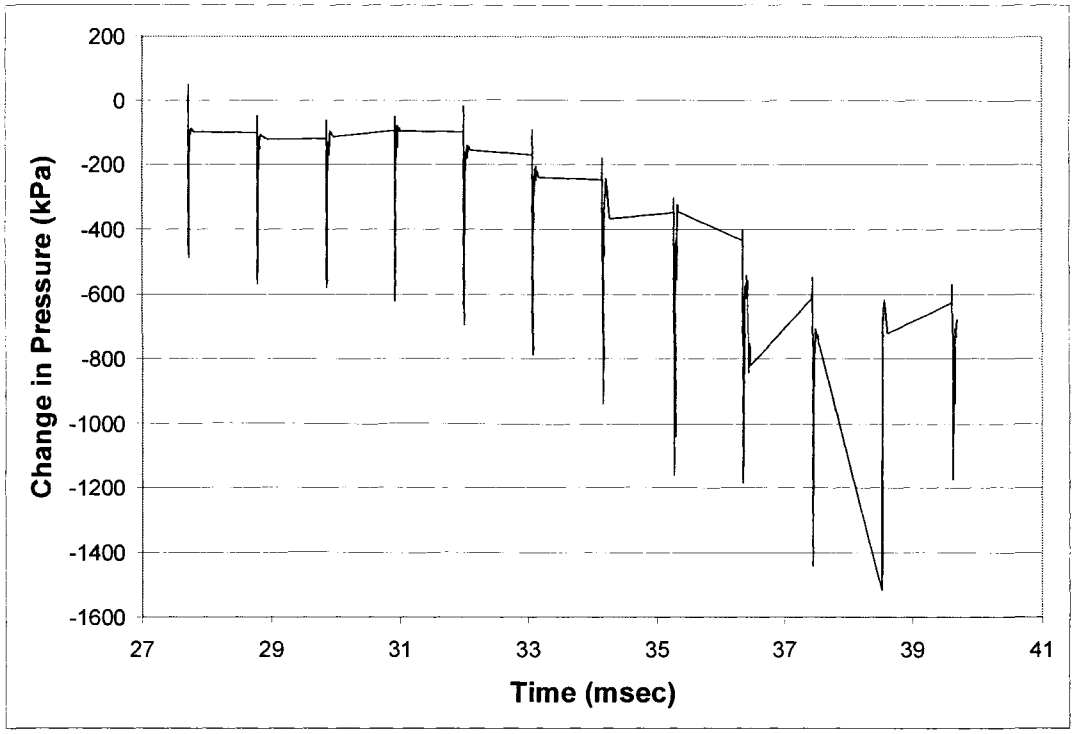

Figure 5.15: SPTu Pore Pressure Response (depth 7.72 m)

It is quite clear from Figure 5.15 that the pore pressure transducer failed to work properly for this test at a depth of 7.72 m. Measured pore pressures as low as -1500 kPa relative to the in-situ pore pressure were measured, but are clearly not realistic. It was later found that the down-hole signal amplifier had somehow been damaged during the testing and that this was the reason for the erratic pore pressure transducer response.

5.2.4.3 SPTu at 8.56 m

The pore pressure transducer was also not functioning properly for the SPTu performed at 8.56 m deep. The pore pressure transducer response for each blow is shown in Appendix C. As mentioned in the previous section, the down-hole signal amplifier was damaged, which was the reason for the unreliable pore pressure results at this depth.

5.2.4.4 SPTu at 9.33 m

The pore pressure transducer was also not functioning properly for the SPTu performed at 9.33 m deep. The pore pressure transducer response for each blow is shown in Appendix C. As mentioned, the down-hole signal amplifier was damaged, which was the reason for the unreliable pore pressure results at this depth.

5.2.4.5 SPTu at 10.80 m

The fifth SPTu was performed at a depth of 10.80 m. Prior to this test, the down hole signal amplifier was replaced, which resulted in the measurement of reasonable data. The blow counts for the first, second and third 152 mm (6 inch) intervals of penetration were 3, 3 and 4 respectively for an N value of 7 and an $(N_1)_{60}$ value of 12.8 when corrected for measured energy ratio and overburden stress. The pore pressure response at this depth for all blows is shown in Figure 5.17.

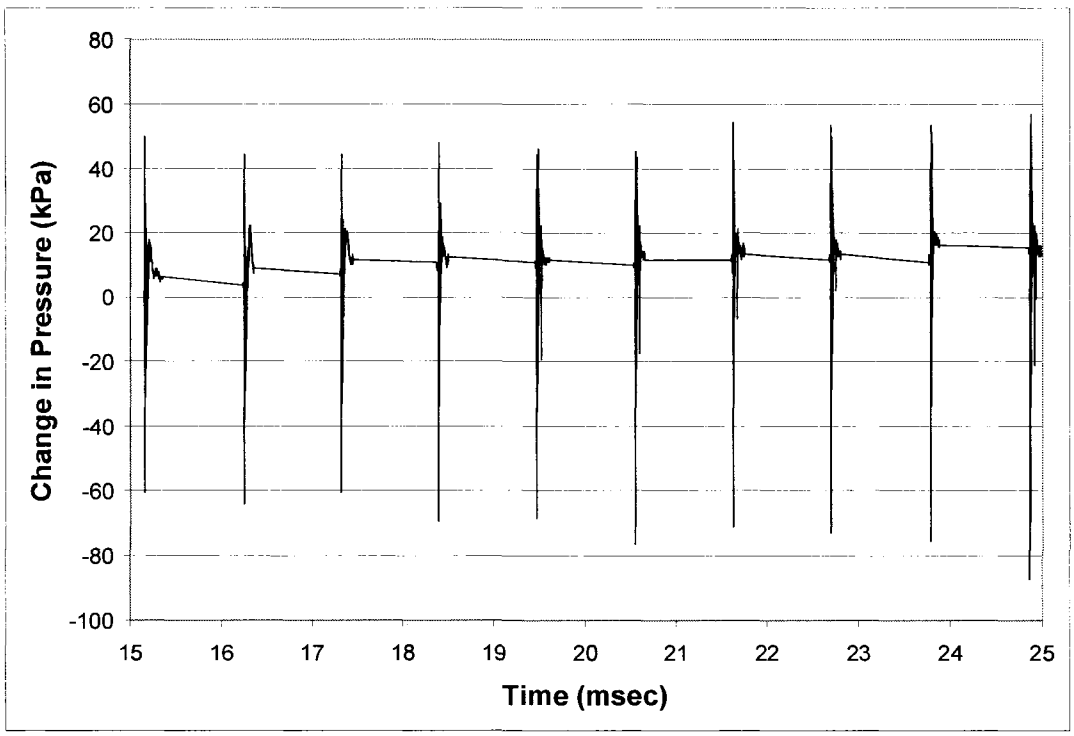

Figure 5.17: SPTu Pore Pressure Response (depth 10.80 m)

The above figure shows very large spikes as great as positive 55 kPa and negative 87 kPa relative to the baseline pore pressure. It is important to note the rising residual pore pressure. Figure 5.17 shows a rising residual pore pressure after each blow for the first seven blows after which, the rising residual pore pressure levels off. After the ten blows, the measured residual pore pressure rose to almost 20 kPa, which corresponds to a pore pressure ratio of 0.17.

Figure 5.19 shows the SPTu pore pressure response on a much smaller time scale for the first of ten blows at a depth of 10.80 m. The force load cell response is also plotted on the chart to illustrate the lack of significant time lag between the force reaching the sampler and the time for pore pressure response.

There are a few important features to note about the pore pressure response shown in Figure 5.19. The magnitude of the positive and negative pore pressure

'peaks' are much greater than the actual effective vertical stress at this depth. As noted earlier, it is believed that much of the cyclical response is due to the shaking of the pore pressure transducer, which appears to be acting as an accelerometer. How much of the cyclical response is due to the actual pore pressure and how much is due to shaking of the transducer is not known. However, the approximate duration of the bulk of sampler penetration is also shown on the chart and was estimated from work conducted by Daniel and Howie (2004). It is shown on the chart that much of the cyclical response occurs during penetration of the sampler, and attenuates quickly after penetration of the sampler ceases. It should be noted though, that this is a very rough estimate of the duration of sampler penetration. For future research studies using the SPTu device, it may be useful to use the wave equation to better understand how the pore pressure responds to the amount and duration of sampler penetration.

Figure 5.19 shows that the cyclical pore pressure response attenuates into a reasonably smooth and constant positive residual pore pressure of about 15 kPa above the initial in-situ pore pressure.

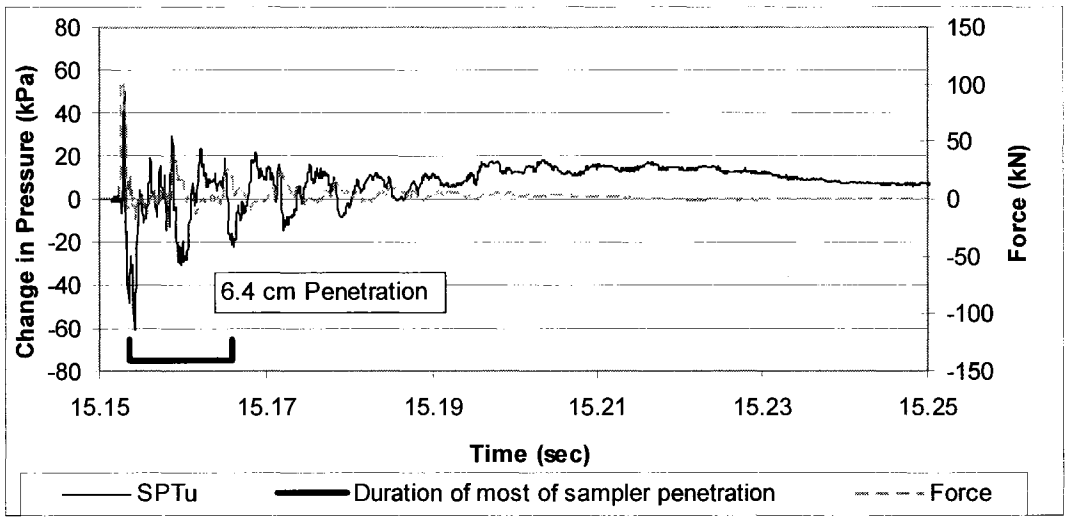

Figure 5.19: SPTu response (Depth 10.80 m, blow 1 of 10; 6.4 cm of sampler penetration)

Figure 5.21 shows the last blow from the test at 10.80 m deep. The measured pore pressure just before the blow is approximately 14.5 kPa (relative to the initial in-situ pore pressure) and after the blow, the residual pore pressure rises to almost 20 kPa.

The pore pressure response from the other blows at this depth is shown in Appendix C.

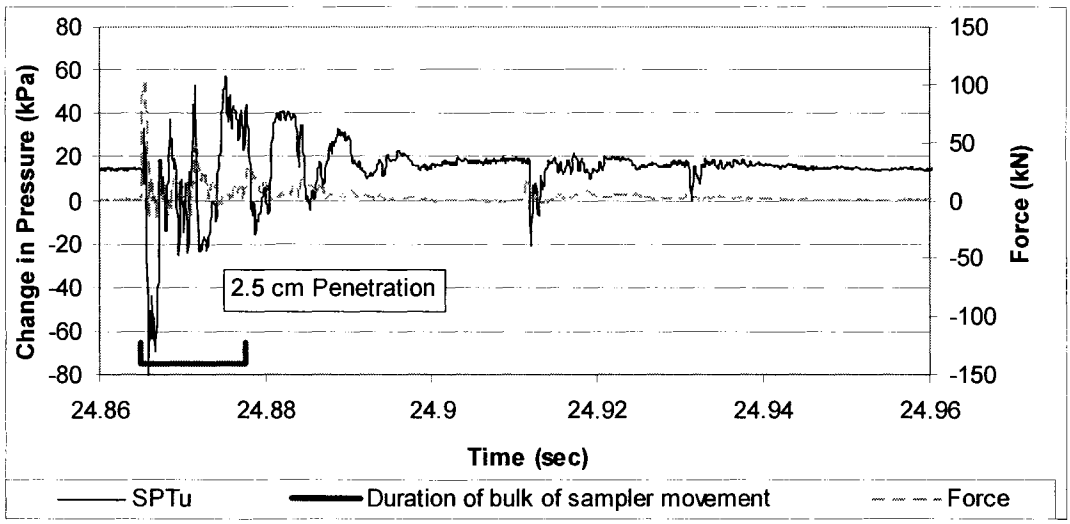

Figure 5.21: SPTu response (Depth 10.80 m, blow 10 of 10; 2.5 cm of sampler penetration)

Figure 5.24 illustrates the change in residual pore pressure as the SPTu test proceeds. The upper line shows the change in residual pore pressure during the SPTu if the residual is defined as the pressure attained as the cyclical pore pressure response attenuates into an essentially smooth residual pressure. The lower line shows the residual pore pressure taken just before the *next* blow. Thus, the chart shows that, as expected, the residual pore pressure decreases between blows as dissipation of the pore pressure occurs.

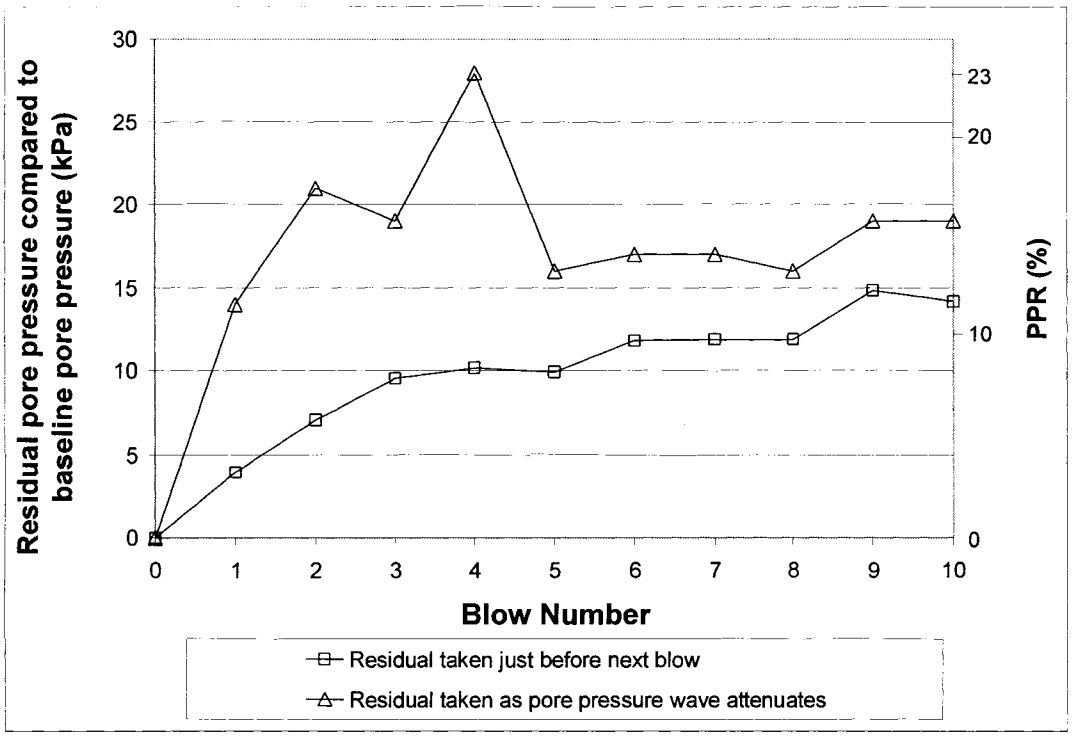

Figure 5.24: Change in residual pore pressure during SPTu (Depth 10.80 m)

The Pore Pressure Ratio (PPR) is defined as the ratio between the change in pore pressure relative to the in-situ pore pressure and the vertical effective stress ($PPR=\Delta u/\sigma_v'$). Thus, for liquefaction around the sampler to be measured, the PPR must equal one.

For the SPTu conducted at a depth of 10.80 m, the measured peak residual pressure of 28 kPa equates to a PPR of 0.23. Therefore, while liquefaction did not occur at the location where the pore pressure is measured (about 10 cm above the bottom of the sampler shoe), the 28 kPa peak change in pore pressure represents a 23% reduction in the vertical effective stress. This is a significant reduction in vertical effective stress and is likely to have an impact on the penetration resistance of the sand for successive blows. In addition, it is well known that penetration resistance is controlled more by horizontal in situ stress than vertical stress (Schmertmann 1979). Thus, for the case of an embankment dam, such as at Aurora, where the horizontal stress is lower than the vertical effective stress, the 28 kPa peak change in pore pressure would actually represent a much larger reduction in the horizontal effective stress. If the horizontal stress is equal to half the vertical effective stress, the 28 kPa peak would represent a 46% reduction in horizontal effective stress. This reduction in horizontal effective stress may result in a substantial decrease in penetration resistance.

Furthermore, pore pressure in the SPTu was measured 9.9 cm above the base of the sampler shoe. Higher pore pressures may exist nearer to the end of the sampler shoe where compressive stresses are higher. In the cone penetration test, the largest pore pressures are measured in the zone beneath the cone where the compressive stresses are the largest. The normal stresses dominate the pore water pressure response beneath the cone, while the shear stresses dominate the response along the shaft (Lunne et al. 1997). Thus, it seems likely that the shear stresses along the sampler wall dominate the pore pressure response during the SPTu. Therefore, even higher pore pressures may be generated beneath the sampler shoe where the normal stresses and stress change are greater.

5.2.4.6 SPTu at 12.41 m

The sixth SPTu was performed at a depth of 12.41 m. The blow counts for the first, second and third 152 mm (6 inch) intervals of penetration were 3, 2 and 5 respectively for an N value of 7 and an $(N_1)_{60}$ value of 12.3 when corrected for measured energy ratio and overburden stress. The pore pressure response at this depth for all blows is shown in Figure 5.26. Note that for this test an extra blow was recorded after the full 46 cm (18 inches) of penetration due to the hammer not being shut off fast enough. The vertical effective stress at this depth is approximately 135 kPa.

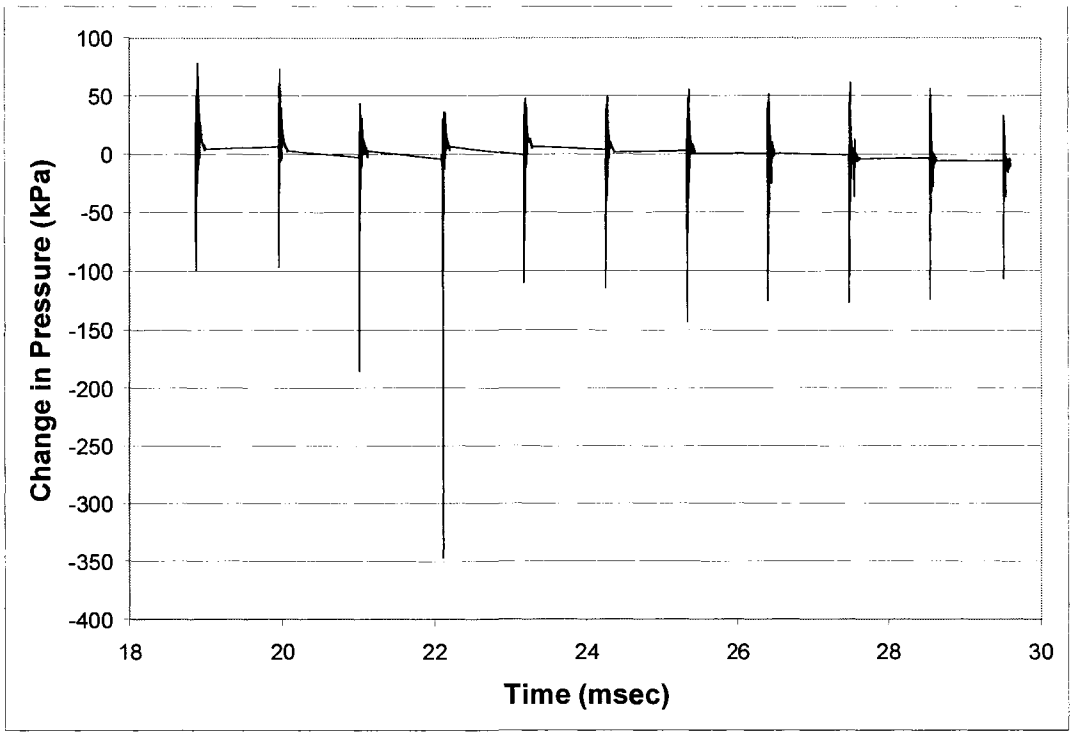

Figure 5.26: SPTu Pore Pressure Response (depth 12.41m)

The above figure shows measured pore pressure peaks of as high as 80 kPa. Most measured pore pressure lows were between –100 and –150 kPa relative to the baseline pore pressure, however one measurement was as low as –350 kPa. However, as mentioned earlier, these peaks probably do not reflect the actual pore pressure in the sand. Rather, they probably reflect the shaking of the pore pressure transducer.

Figure 5.28 shows the same cyclical pore pressure response shown earlier, that attenuates after approximately 50 milliseconds into a residual pore pressure of approximately 20 kPa relative to the initial in-situ pore pressure.

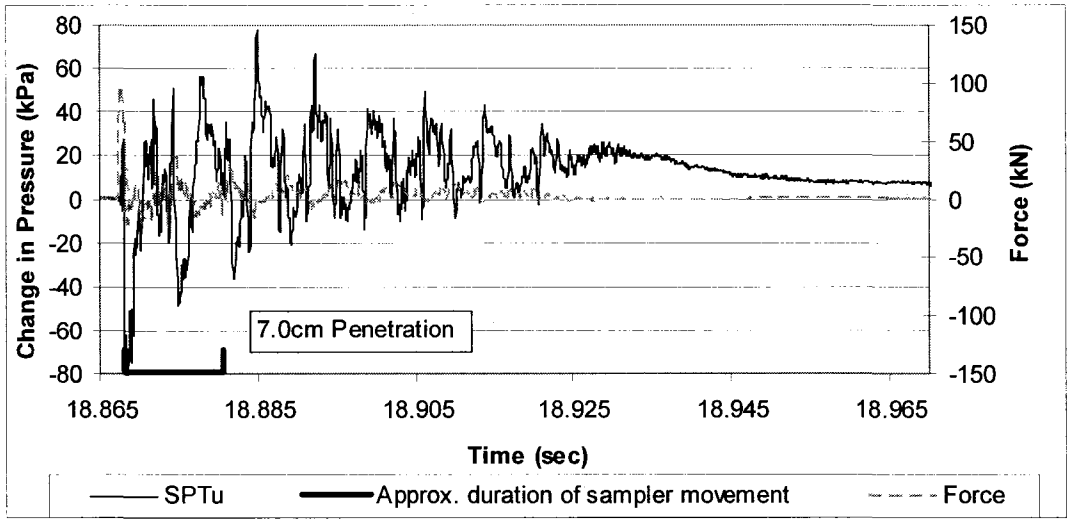

Figure 5.28: SPTu response (Depth 12.41m, blow 1 of 11; 7cm of sampler penetration)

Figure 5.31 shows the pore pressure trace from the last blow of the test at 12.41 m (40'8"). Figure 5.31 is plotted on the same time scale as Figure 5.28 and shows that the pore pressure response for the last blow at this depth attenuates much more rapidly than of first blow.

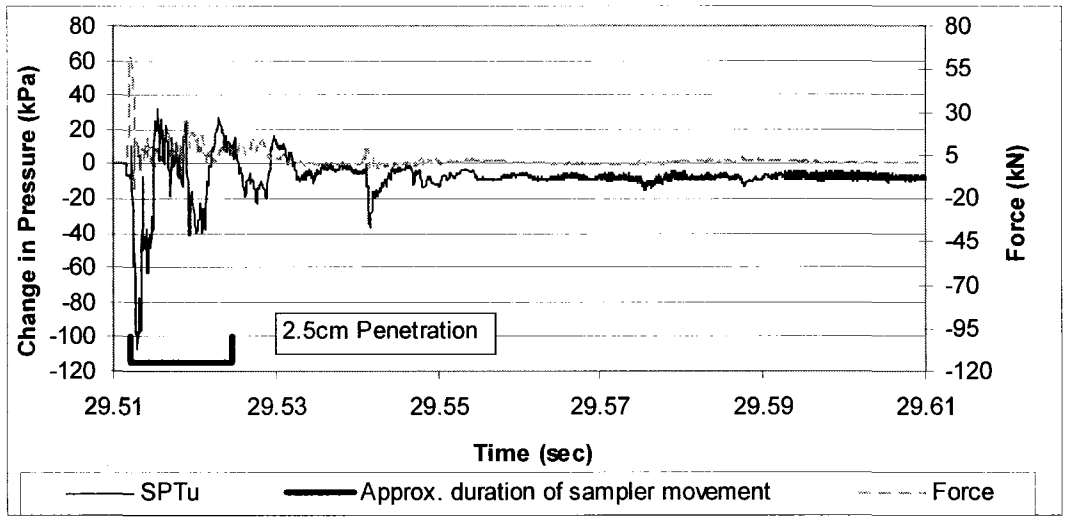

Figure 5.31: SPTu response (Depth 12.41m, blow 11 of 11; 2.5 cm (1") of sampler penetration)

At the end of the final blow shown in Figure 5.31, the residual pore pressure fell to approximately -8 kPa relative to the initial in-situ measured pore pressure. Figures showing the pore pressure response for the other blows at this depth are shown in Appendix C.

Figure 5.34 illustrates the change in residual pore pressure as the SPTu test proceeds. As noted in the test for the previous depth, the upper line shows the residual pore pressure taken just as the cyclical response attenuates while the lower line shows the residual pressure taken just before the *next* blow. In this case, the chart shows a spike in the residual pore pressure to a high of 23 kPa on the first blow, which is equal to a PPR of 0.16. The residual pore pressure then decreases steadily finally reaching -8 kPa relative to the initial in-situ pore pressure after the final blow.

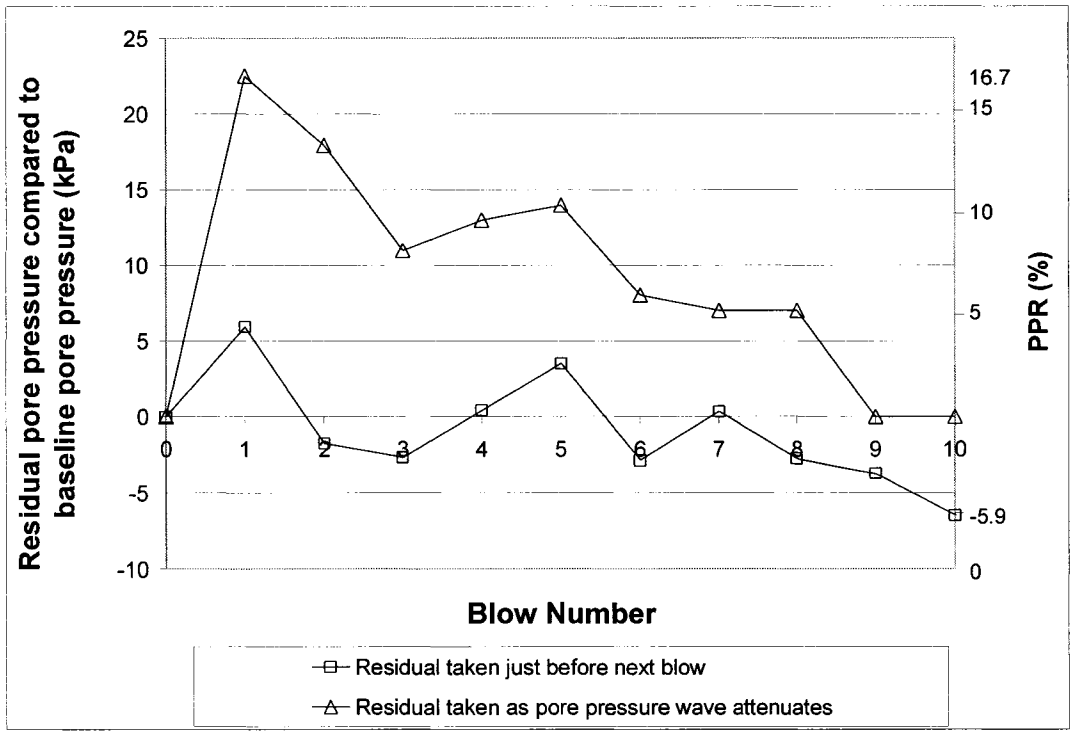

Figure 5.34: Change in residual pore pressure during SPTu (Depth 12.41m)

5.2.4.7 SPTu at 13.92 m

The seventh and final SPTu was performed at a depth of 13.92 m. The blow counts for the first, second and third 15 cm (6 inch) intervals of penetration were 5, 5 and 8 respectively for an N value of 13 and an $(N_1)_{60}$ value of 20.5 when corrected for measured energy ratio and overburden stress. The pore pressure response at this depth for all blows is shown in Figure 5.36. Note that for this test an extra blow was recorded after the full 457 mm (18 inches) of penetration due to the hammer not being shut off fast enough. The vertical effective stress at this depth is approximately 148 kPa.

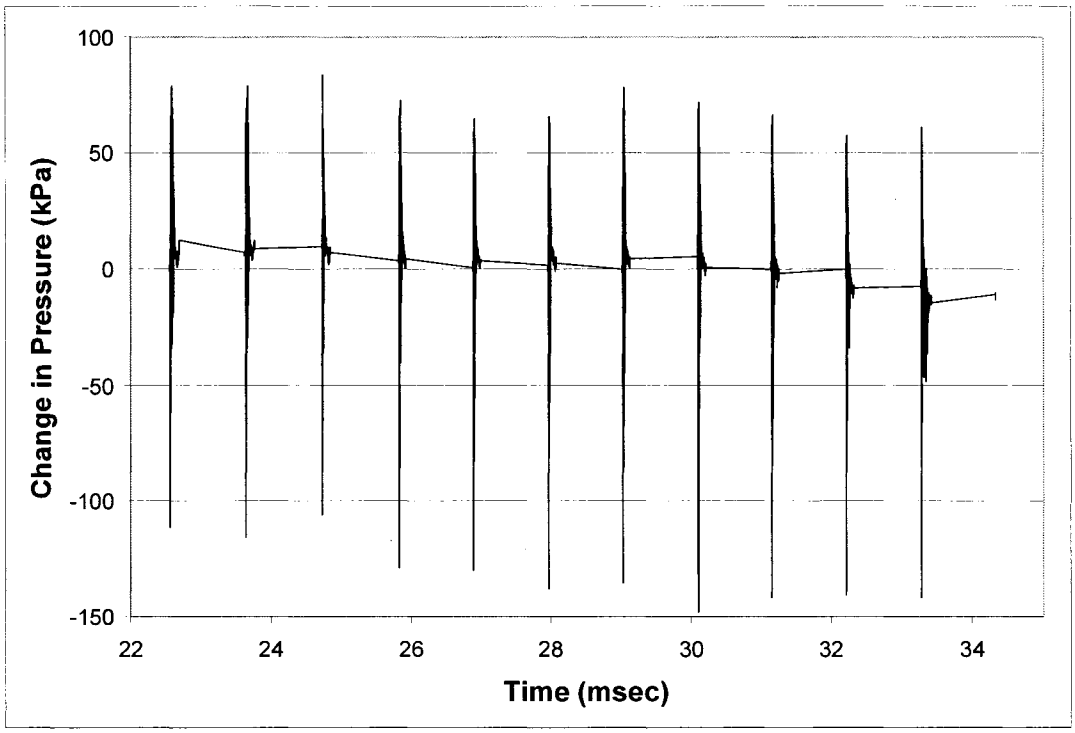

Figure 5.36: SPTu Pore Pressure Response (depth 13.92m)

Figure 5.39 shows the same cyclical pore pressure response seen in other blows that attenuates after approximately 50 milliseconds and shows a rise in pore pressure to a residual pore pressure of approximately 10 kPa. The 10 kPa rise in pore pressure represents a PPR of 0.07.

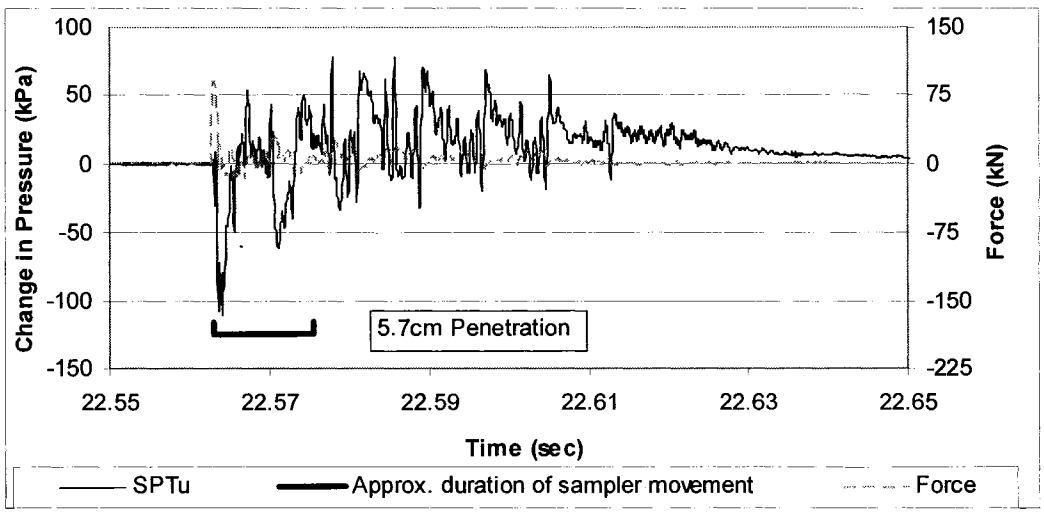

Figure 5.39: SPTu response (Depth 13.92m, blow 1 of 19)

By the final and 19th blow, shown in Figure 5.42, the measured increase in residual pore pressure had decreased to -50 kPa relative to the initial baseline pore pressure. Again, note that Figure 5.39 and Figure 5.42 are on the same time scale and show that the pore pressure response for the last blow at this depth attenuates much more rapidly than that of the first blow.

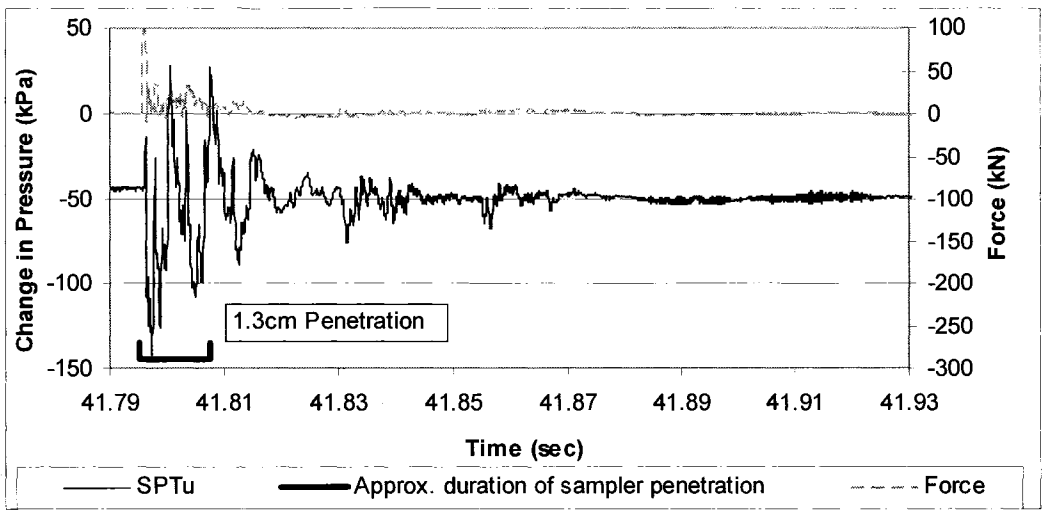

Figure 5.42: SPTu response (Depth 13.92m, blow 19 of 19)

Figure 5.45 illustrates the change in residual pore pressure measured as the SPTu test proceeds. As noted earlier, the upper line shows the change in residual pore pressure taken just as the cyclical pore pressure response attenuates, while the lower line shows the residual pore pressure response taken just before the next blow. In this case, the chart shows a spike in the residual pore pressure to a peak of 20 kPa on the first blow (equivalent to a PPR of 0.14). The residual pore pressure then decreases steadily finally reaching approximately –50 kPa relative to the initial in-situ pore pressure after the final blow. Thus, by the final blow, a substantial increase in effective stress was measured. Since the initial vertical effective stress at this depth was 148 kPa, the negative 50 kPa residual pore pressure represents a 33% increase in the effective stress.

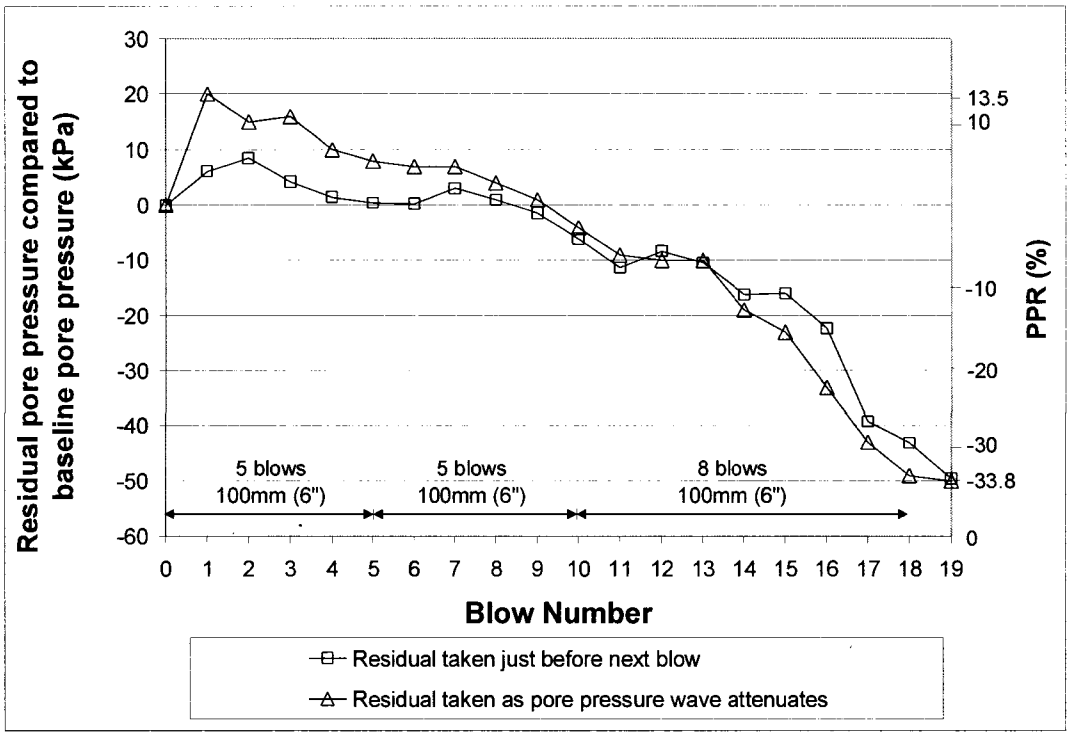

Figure 5.45: Change in residual pore pressure during SPTu (Depth 13.92m)

Figure 5.24, Figure 5.34 and Figure 5.45 show how the residual pore pressure changes with increasing blows during the SPTu (for depths 10.80 m, 12.41 m and 13.92 m respectively). At a depth of 10.80 m, the residual pore pressure increased steadily for the duration of the test. For the next test at a depth of 12.41 m, positive residual pore pressures were initially measured, but with increasing blows, the residual pore pressures decreased finally ending in a slightly negative residual pore pressure. For the final test at a depth of 13.92 m, again positive residual pressures were measured on the first blow, but with successive blows, the residual pore pressure steadily decreased until the final

blow where a residual pore pressure of negative 50 kPa was measured relative to the initial in-situ pore pressure.

However, upon examination of the relative density determined from the CPT (shown in Figure 5.47), it can be seen that the approximate relative density increased from about 45% at a depth of 10.80 m to 48% at a depth of 12.41 m to 56% at a depth of 13.92 m.

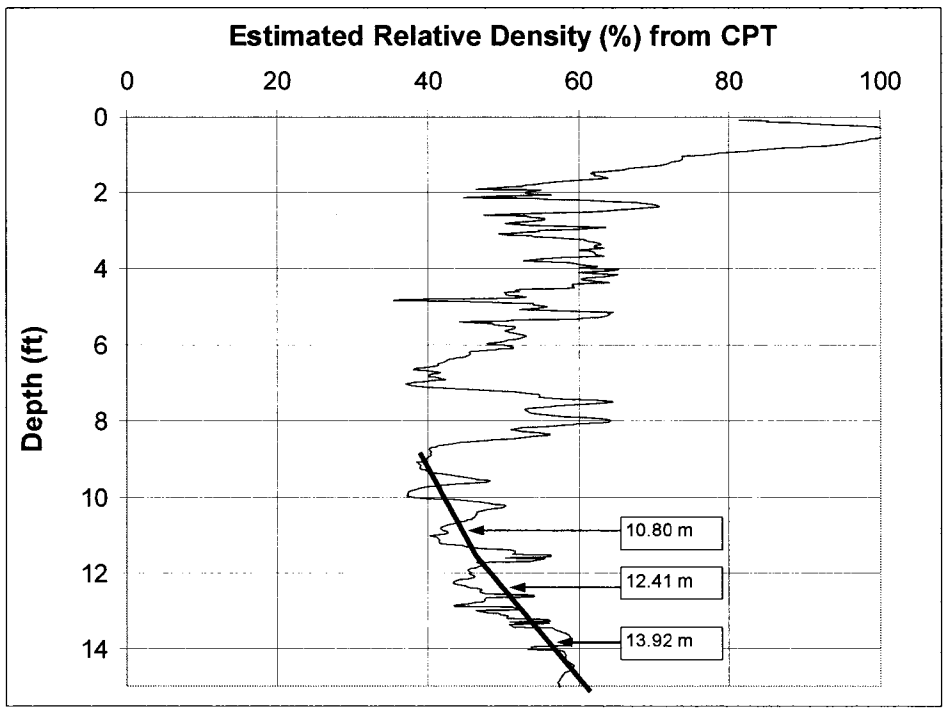

Figure 5.47: Change in approximate relative density with depth (Massey Site)

Thus, it may be that for the first SPTu at a depth of 10.80 m, the sand was loose enough to act in a contractant manner for the entire duration of the test. This would result in positive excess pore pressures being generated during the test. However, by the final SPTu at a depth of 13.92 m, the sand may have acted in a contractant manner on the first few blows, before quickly changing to a dilatant response on successive blows. In this case, negative excess pore pressures would be expected. For the test at 12.41 m deep, the pore pressure response appeared to be in between the other two tests, which makes sense since the relative density at that depth was in between the relative density of the other two tests.

The apparent response of the pore pressure to the density of the sand makes sense when the SPT is compared to the CPT. It was noted earlier that shear stresses dominate the pore pressure response along the cone shaft. For the

CPT, shear stresses may induce either positive or negative pore pressure changes, depending on the dilatantcy properties and the shear stress levels in the soil (Lunne et al. 1997). Thus, it seems likely that this would also apply to the SPT with the pore pressure response being dominated by shear stresses along the sampler barrel wall and the dilatancy properties of the soil.

In addition, disturbance due to drilling and loosening of the sand at the base of the borehole may have resulted in positive excess pore pressures being generated for the first few blows. In each case the largest positive change in pressure occurred on the first blow, which occurred in the disturbed (and probably loosened) sand. Then as penetration progressed, the density of the sand may have increased in each case, resulting in either lesser positive changes in pore pressure or negative changes in pore pressure depending on the test.

5.2.5 Blast Probe Pore Pressure Measurements

For the first two tests at 1.52 m and 7.72 m respectively, the blast probe was located at a distance of approximately 1.1 m away from the drill hole (in plan view) and 22.9 cm (9 inches) below the beginning depth for each of the SPTu tests. The blast probe was outfitted with a pore pressure transducer as well as a triaxial accelerometer.

For the first two SPTu tests, the blast probe did not measure any noticeable change in pore pressure during the tests. Figures that illustrate this can be seen in Appendix D. The likely reason that no pore pressure change was measured is that the energy and shock wave created in the soil and pore fluid was not great enough to result in a measurable increase in pore pressure at a distance of 1.1 m away.

For the five remaining SPTu's, the blast probe was moved to a new location approximately 29.2 cm (11.5 inches) from the SPTu hole in plan view and kept at the same depth arrangement (22.9 cm below the SPTu starting test depth). It was hoped that by moving the blast probe closer that a higher quality acceleration trace would be obtained and that there might be a chance of measuring a pore pressure increase due to the SPTu testing.

5.2.5.1 Blast Probe Pore Pressure at 8.56 m

At a depth of 8.56 m, the blast probe did record changes to the measured pore pressure during the test. A typical example is shown in Figure 5.50. The down hole force is also shown on the chart to illustrate when the stress wave reached the sampler and when the sampler began to move. The figure shows that immediately following the blow, there was a small increase in pore pressure from 59 kPa to 60 kPa. This was followed by a sharp decrease in pore pressure from 60 kPa to 54.5 kPa after which point the pore pressure rose more slowly to a peak of 61 kPa at a time of 28.88 seconds. The other blast probe pore pressure traces from the other blows can be found in Appendix D.

The 1 kPa increase in pore pressure is quite small in relation to the in-situ pore pressure (59 kPa). However, the reading was made from a distance of approximately 30 cm away and one would expect higher pore pressures nearer to the test.

It should be noted that Figure 5.50 shows a typical test from a depth of 8.56 m. Typical characteristics to note are the small increase, sharp decrease and sharp increase in pore pressure followed by a more gradual increase above the initial in-situ pressure.

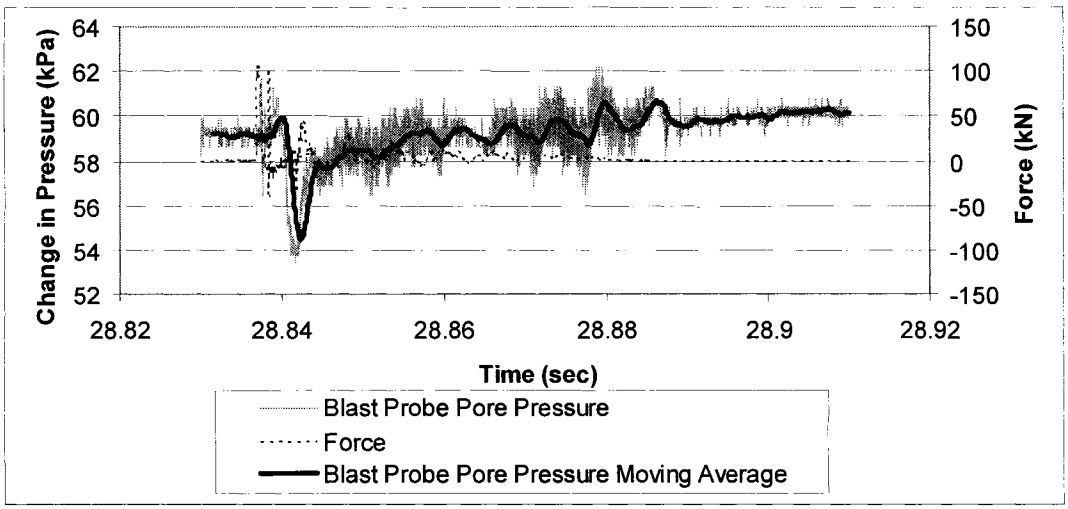

Figure 5.50: Blast probe pore pressure response (Depth 8.56 m, blow 4 of 9)

5.2.5.2 Blast Probe Pore Pressure at 9.33 m

At a depth of 9.33 m, the blast probe did record changes to the measured pore pressure during the test. An example of this is shown in Figure 5.52. The down hole force is also shown on the chart to illustrate when the stress wave reached the sampler and when the sampler began to move. The figure shows that after the first blow, the pore pressure at the blast probe increased from 63 kPa to 65 kPa. However, this increase in pore pressure was not sustained between blows. Thus, the measured pore pressure before each blow was 63 kPa and no sustained residual increase in pore pressure was measured. The other blast probe pore pressure traces from the other blows can be found in Appendix D.

While an increase in pore pressure of 2 kPa may not seem like much, it should be noted that the measurement was made from a distance of about 30 cm (a foot) away from the SPTu. Thus, much higher pore pressures would be expected nearer to the SPTu.

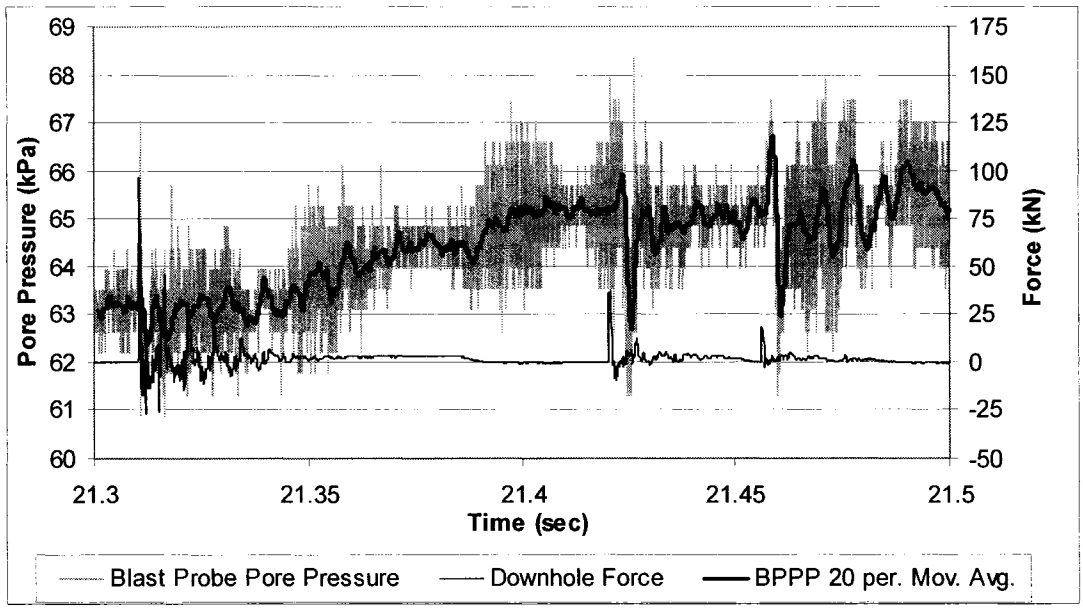

Figure 5.52: Blast probe pore pressure response (Depth 9.33 m, blow 1 of 8)

It should also be noted that two bounces of the hammer (in addition to the initial blow) were recorded by the down-hole transducer and are shown in Figure 5.52. As can be seen in the figure, the pore pressure response to the hammer bounces occurs quite quickly. In fact, the pore pressure responds after just two milliseconds in both cases. Thus, the velocity of the pressure wave is about 150 m/s (v=d/t where d=30.5 cm (12 inches) and t=0.002 sec). This agrees well with the expected shear wave velocity of loose sand. Thus, the blast probe measured pore pressure changes due to the generation of shear waves rather than compressive waves.

5.2.5.3 Blast Probe Pore Pressure at 10.80 m

The blast probe pore pressure results from a depth of 10.80 m are shown in Figure 5.54. In this case it was felt that the results from the first blow were not representative of the majority of the blows. The blast probe pore pressure trace shown in Figure 5.54 is very similar to blows three through 10. With the exception of the first blow, every blow shows a small and sudden decrease in pore pressure of approximately 3 kPa followed by a slower rise in pore pressure to between 2-4 kPa above the initial baseline pore pressure. The increase in pore pressure was not sustained between blows so the measured pore pressure before each blow was 81 kPa and no residual increase in pore pressure was measured. The other blast probe pore pressure traces from the other blows can be found in Appendix D.

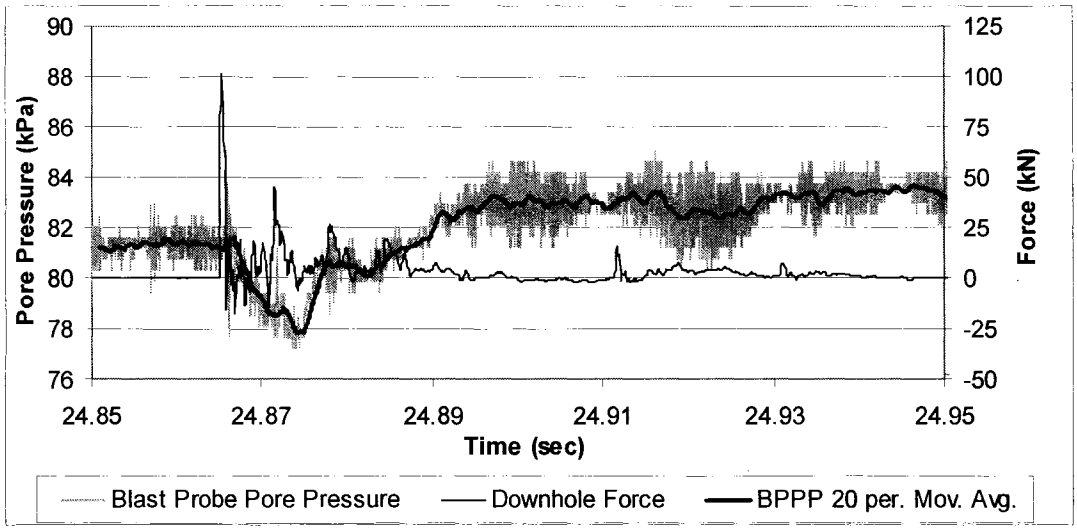

Figure 5.54: Blast probe pore pressure response (Depth 10.80 m, blow 2 of 10)

5.2.5.4 Blast Probe Pore Pressure at 12.41 m

The blast probe pore pressure results from 12.41 m deep are considerably more erratic and unpredictable than for the previous test. A good example of this type of response is illustrated by Figure 5.56, which shows the response from the fourth blow of ten blows. The figure shows a sharp dip in pore pressure approximately 5 milliseconds after the stress wave reached the sampler, much like the test at the previous depth. However, Figure 5.56 shows a very erratic pore pressure response that varied by as much as 5 kPa in places – a great deal more than for either of the previous two tests. In addition, it is much harder to qualitatively identify a pattern between the SPT blow and the pore pressure response measured by the blast probe. The difficulty in interpreting the blast probe pore pressure response may be due, in part, to the increased density of the sand at this depth.

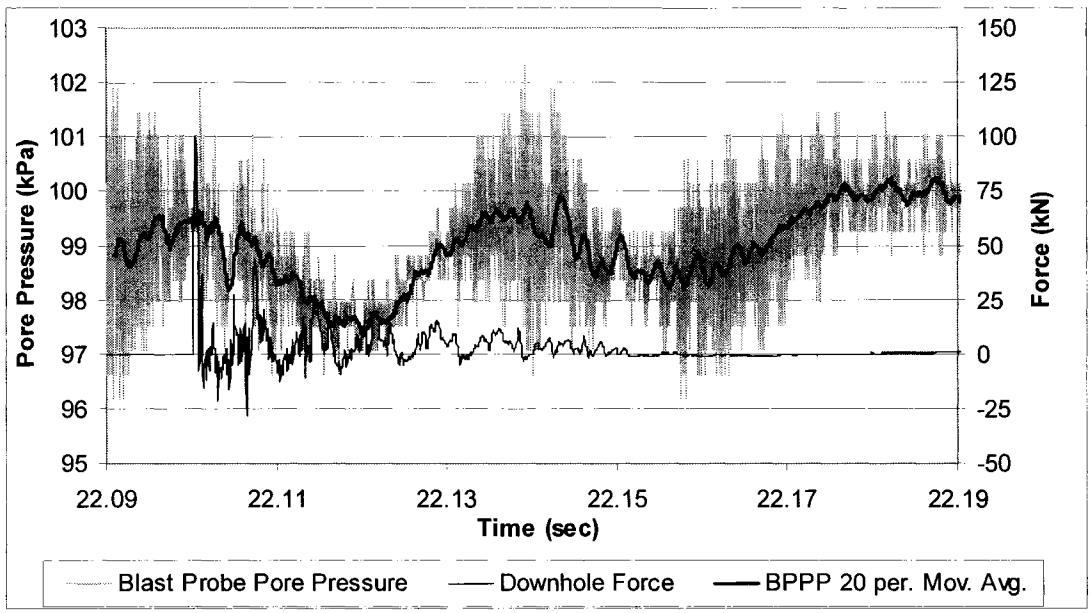

Figure 5.56: Blast probe pore pressure response (Depth 12.41 m, blow 4 of 10)

5.2.5.5 Blast Probe Pore Pressure at 13.92 m

Very little correlation was observed between the SPTu blows and the blast probe pore pressure response. Evidence of this lack of correlation is illustrated in Figure 5.58, which shows a blast probe pore pressure response for blow 15 of 19 and is typical of most blows from the test depth of 13.92 m. The blast probe pore pressure response is similarly erratic when compared to the test from a depth of 12.41 m. This figure also shows the sharp dip in pore pressure approximately 5 milliseconds after the stress wave reached the sampler. In addition, Figure 5.58 also shows a very erratic pore pressure response that varies by as much as four kPa in places. With the exception of the characteristic dip in pore pressure just after the SPTu blow, it is very difficult to discern any reasonable correlation between the SPTu blow and any change in the blast probe pore pressure response. The difficulty in interpreting the blast probe pore pressure response may be due, in part, to the increased density of the sand at this depth.

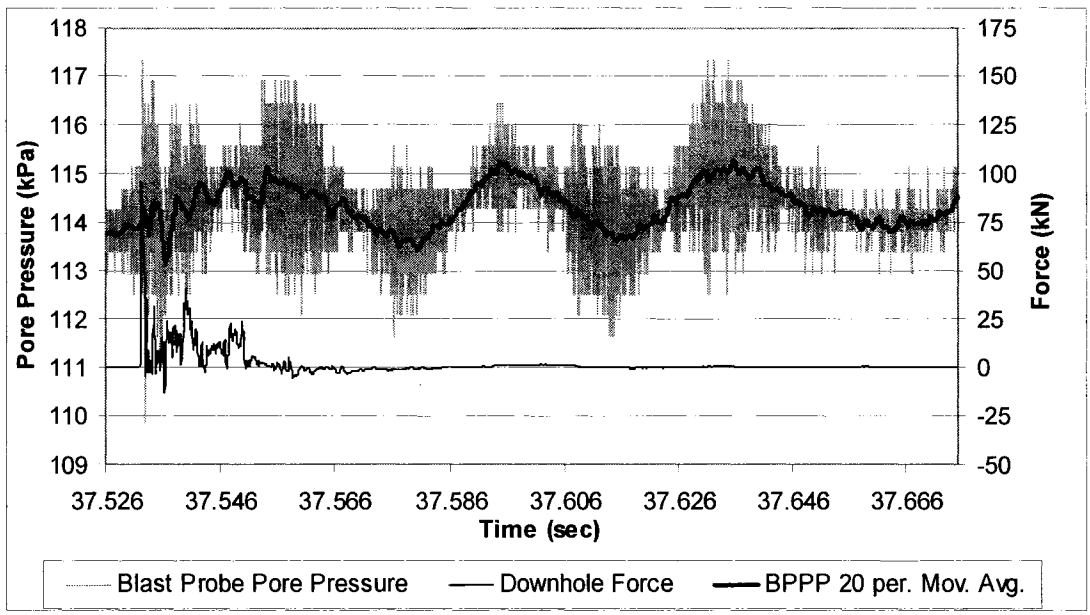

Figure 5.58: Blast probe pore pressure response (Depth 13.92 m, blow 15 of 19)

5.2.6 Peak Particle Velocity

In addition to making pore pressure measurements, the blast probe was also equipped with a triaxial accelerometer. Results from the accelerometer were integrated to obtain particle velocity at the blast probe location.

Typical particle velocity measurements during a SPT blow are shown in Figure 5.60. The figure shows the results from the last of ten blows from a depth of 10.80 m. Figure 5.60 shows a peak particle velocity of approximately 0.35 mm/sec. To see the particle velocity traces for each blow at each depth, refer to Appendix E.

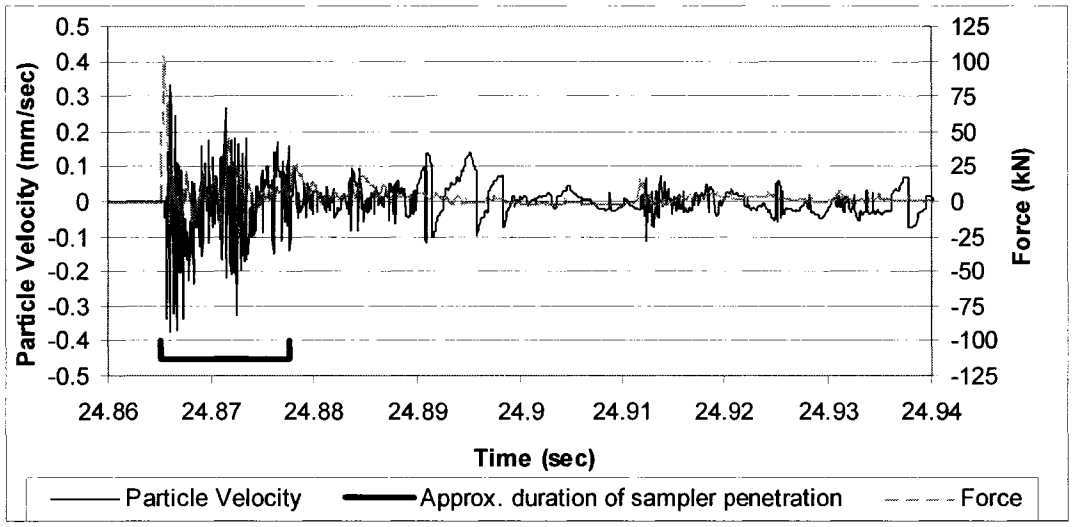

Figure 5.60: Peak particle velocity measurement from test at 10.80 m (blow 10 of 10)

The relationship between SPTu blow number and peak particle velocity is shown in Figure 5.62 for all SPTu's performed. The figure shows a strong trend, in most cases, between increasing blow numbers and decreasing peak particle velocities measured. It should be noted that for the test depth of 1.52 m and 7.72 m the blast probe was located 1.12 m away from the test, while for the remainder of the tests the blast probe was located much closer at a distance of only 29 cm. For the latter 5 tests where the probe was located at a distance of 29 cm away from the SPTu, correlation coefficients range from 0.75 to 0.96 indicating good to excellent correlation between decreasing peak particle velocity as blows increase as the test proceeds.

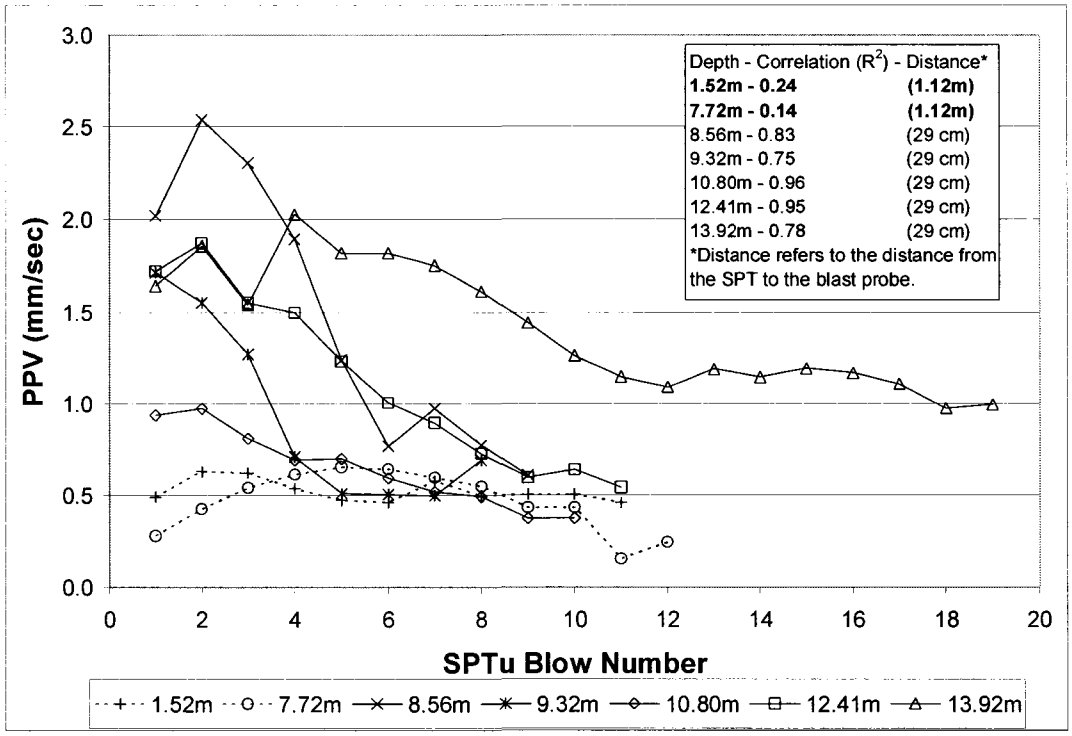

Figure 5.62: Correlation between blow number and peak particle velocity

A number of researchers have conducted research on problems of blast induced liquefaction (Al-Qasimi et al. 2005; Charlie et al. 1992; Veyera and Charlie 1988; Veyera and Charlie 1990). Residual pore pressures and liquefaction may be generated in saturated sand by one or more cycles of compressive strain, which may be followed by one or more cycles of shear strain that may be generated by detonation of explosives.

The scaled distance is a parameter that is often useful for comparing one set of vibration results to others. The ratio R/M^s is the scaled distance, where:

- R is the vector distance between the explosive source and the point of vibration monitoring in m
- M is the charge mass in kg
- S is a scaling constant, typically ½ but may be 1/3 in some cases

When ½ is used as the scaling constant, it is called square root scaling and when 1/3 is used as the scaling constant, it is called cubed root scaling. Square root scaling ($R/M^{1/2}$) is used in most cases of blasting regulations. Cubed root scaling ($R/M^{1/3}$) is often used in construction blasting at distances under 6 m (Lucca 2003) or for very large explosives such as nuclear blasts, or where the explosive acts as a point charge rather than a cylindrical charge like in most boreholes.

In addition to blasting applications, vibrations monitoring and commonly used blasting relationships are often applied on construction jobs where piles are being driven. It was thought that these relationships may be applicable to the SPT and that measured particle velocity data might be able to be used to estimate generated pore pressure changes due to the test.

Most relationships for blasting relate the charge weight, M, and vector distance, R, to peak particle velocity. The SPT cannot directly be expressed as a charge mass, however, an attempt to express the SPT as an equivalent charge mass was made.

It is well documented that 1 kg of TNT has 4,186,800 J of energy. The SPT is capable of imparting a maximum theoretical energy of 474 J (63.5 kg hammer mass times 76 cm fall height = 474 J). This means that the theoretical energy of the SPT is equivalent to the energy of 1.1×10^{-4} kg of TNT. However, at the Massey Site the average measured energy of the SPTu was 113% in the zone of interest. In all calculations, the SPT's equivalent charge mass of TNT was corrected for the actual energy of the SPT rig and used to calculate the scaled distance.

Figure 5.64 and Figure 5.66 show the measured peak particle velocity versus the scaled distance for each blow on each test. Equation 5.4 and Equation 5.5 represent the upper and lower bounds of best-fit lines to predict peak particle velocity based on the known scaled distance. These equations are empirical and were developed from previous field explosive tests (Charlie et al. 1992; Drake and Little 1983). Although the equations are empirical they do have some theoretical basis. The exponents (-2.5 and -2.06) account for material properties and shock dissipation within the material and incorporate reduction of the charge mass from a squared root to a cubed root. The constants (5.6 and 8.75) are a function of the material properties of the soil.

$$PPV = 5.6(R/M^s)^{-2.5} \quad \text{(Drake and Little 1983)} \quad (5.4)$$

$$PPV = 8.75(R/M^s)^{-2.06} \quad \text{(Charlie et al. 1992)} \quad (5.5)$$

Where:

- PPV is peak particle velocity (m/sec)
- R is the vector distance in m
- M is the explosive mass in kg
- S is the factor by which the mass is scaled. Typically, s is ½ or 1/3.

In this case, the measured vector distance is 1.1 m and 0.29 m (11.5") for the first two and last five tests respectively. Since the distance is much less than 6 m, one might assume that cubed root scaling would be appropriate, however the energy imposed on the soil by the SPTu is typically 0.01% of the energy of one

kilogram of TNT and thus, the cubed root scaling may not be appropriate in this case. Both the square and cubed root scaling methods were examined.

Figure 5.64 shows the scaled distance versus measured peak particle velocity data if squared root scaling is used. Figure 5.66 shows the scaled distance versus measured peak particle velocity data if cubed root scaling is used.

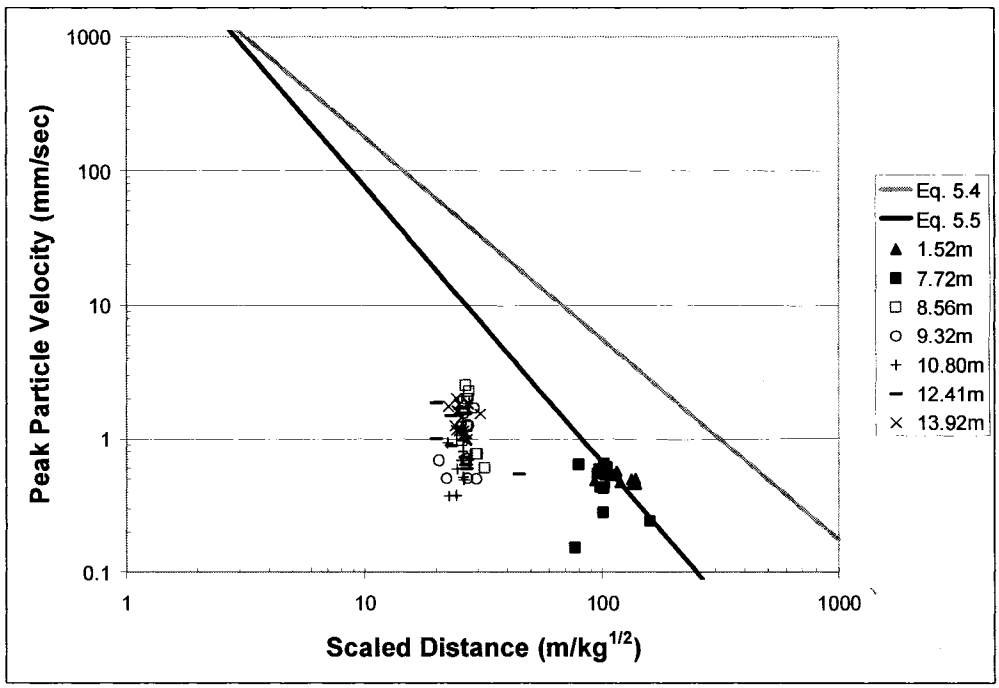

Figure 5.64: Scaled distance and measured peak particle velocity (squared root scaling)

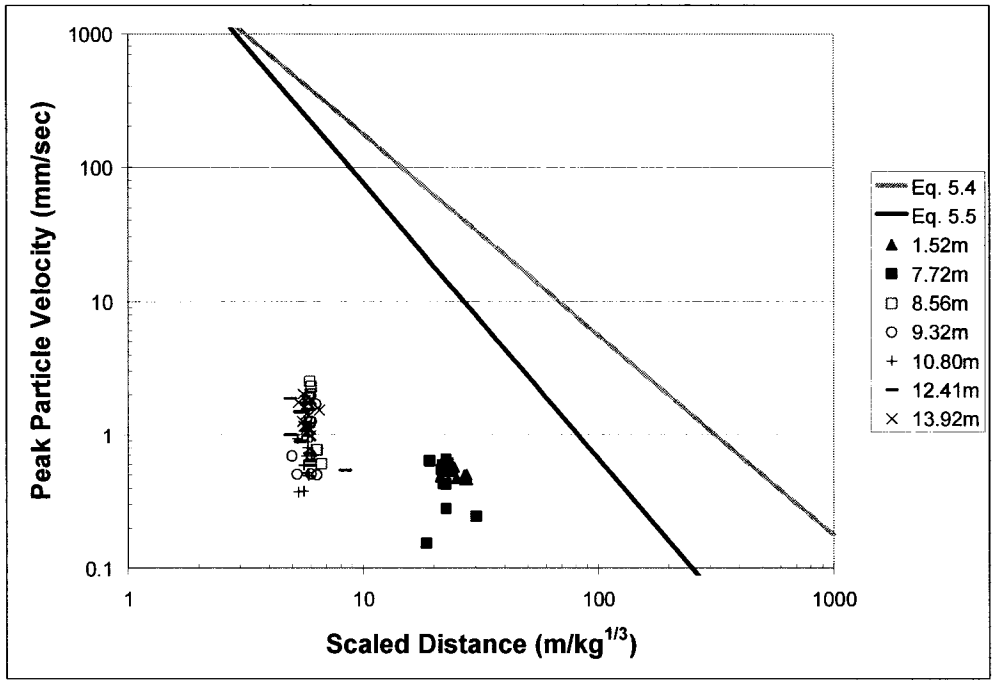

Figure 5.66: Scaled distance and measured peak particle velocity (cubed root scaling)

If Figure 5.64 and Figure 5.66 are compared, it is easily seen that squared root scaling yields better agreement with equations 5.4 and 5.5. This is likely because the SPT generates four orders of magnitude less energy than one kilogram of TNT. In fact, it may even be appropriate to use an exponent larger than ½ to scale the equivalent charge weight of the SPT because of the difference in energy between it and using explosives.

Al-Qasimi et al. (2005) developed a relationship between peak particle velocity and pore pressure ratio measured after detonation of explosives in saturated Syncrude tailings sand as follows:

$$PPR = 1.32(PPV)^{0.65} \quad (5.6)$$

Where:

- PPR is the pore pressure ratio ($PPR=\Delta u/\sigma_v'$)
- PPV is the peak particle velocity in m/sec

The above equation was used to approximate pore pressure ratios from the measured peak particle velocity from the Massey site and the result is shown in Figure 5.68.

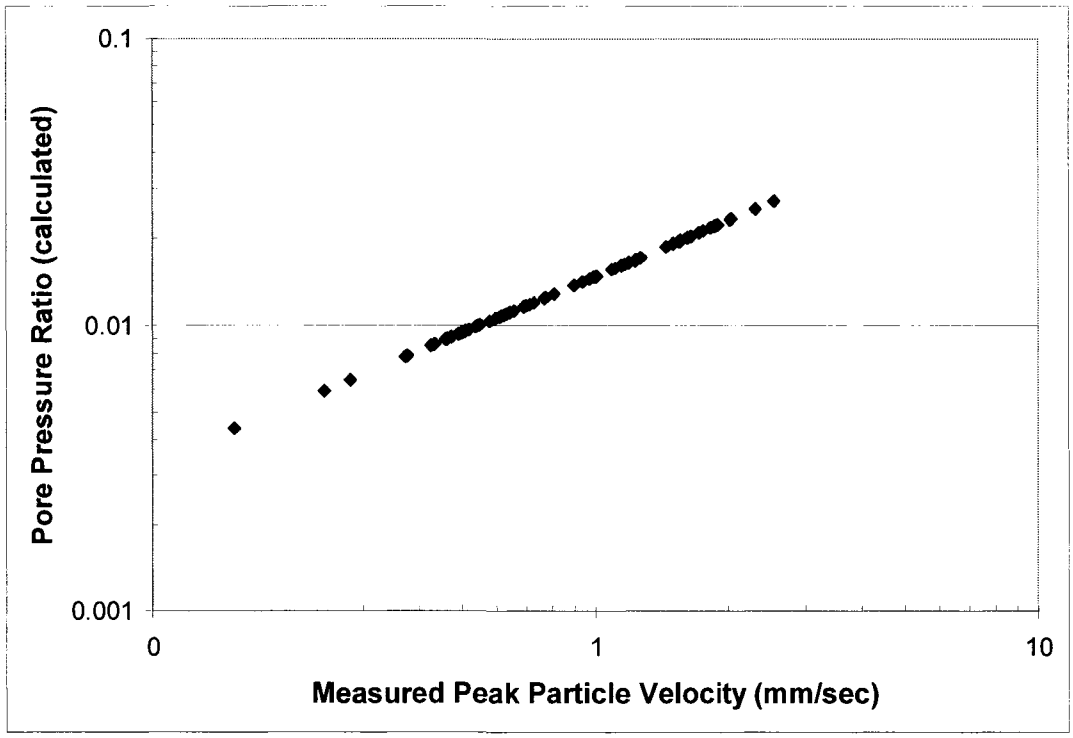

Figure 5.68: Relationship between PPR and PPV (PPR = 1.32(PPV)$^{0.65}$) (Al-Qasimi et al. 2005)

Figure 5.68 shows that Equation 5.6 calculates pore pressure ratios ranging from 0.004 to 0.03. The smallest calculated PPR's are from the first two SPTu tests for which the blast probe was located at a distance of 1.1 m away. The larger PPR's were calculated from vibration data collected during the third through seventh SPTu test for which the blast probe was located much closer at a vector distance of 29 cm away. Thus, Equation 5.3 calculates that pore pressure ratios of 0.01 to 0.03 may be expected up to a 30 cm away from an SPT test in loose sand. Assuming an average vertical effective stress in the zone of interest of 130 kPa, a PPR of 0.01 equates to a change in pore pressure of 1.3 kPa. A change in pore pressure of 1.2 kPa is in reasonable agreement with the pore pressure changes measured by the blast probe.

Since Equation 5.6 predicts pore pressure ratios of up to 0.03 at a distance of about a 29 cm away from an SPT test in loose sand, an effort was made to estimate the pore pressure ratio much closer to the test where much higher PPR's would be expected and to see if the blast induced liquefaction relationships would allow estimation of the pore pressures generated near to the SPT cutter shoe.

At a distance of 5 cm from the SPT, the scaled distance drops to 4.4 m/kg$^{0.5}$ when squared root scaling is used. An extrapolated best-fit line through the data shown in Figure 5.70 indicates that a peak particle velocity of 4.5 mm/sec might be expected at a distance of 5 cm from the SPT.

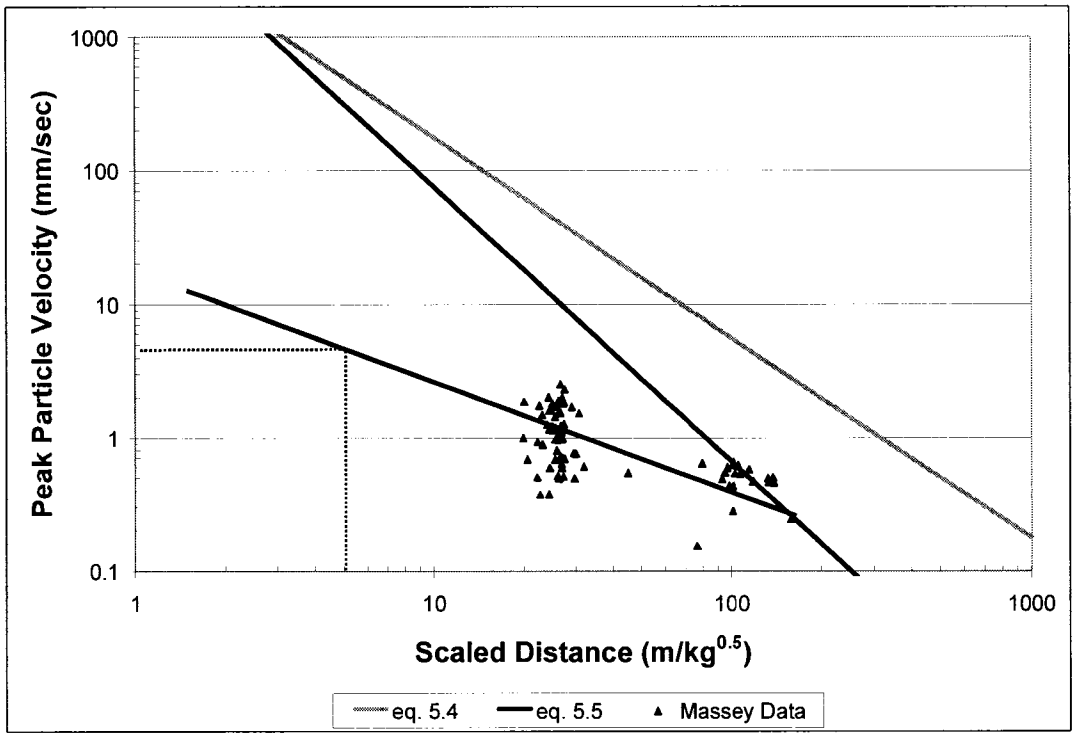

Figure 5.70: Extrapolating measured data to estimate PPV 5 cm from the SPT

Figure 5.72 shows the same chart as Figure 5.68, except that a best-fit line through the data was extrapolated to estimate the PPR at a distance of 5 cm from the SPT. At a distance of 5 cm from the SPT, it was noted that a PPV of almost 4.5 mm/sec would be expected. From the extrapolated relationship in Figure 5.72, a PPR of 0.04 would be predicted at a distance of 5 cm from the SPT. At a vertical effective stress of 130 kPa, this equates to a change in pore pressure of 5.2 kPa. This result is not in good agreement with results from the SPTu testing, which measured much greater pore pressure changes.

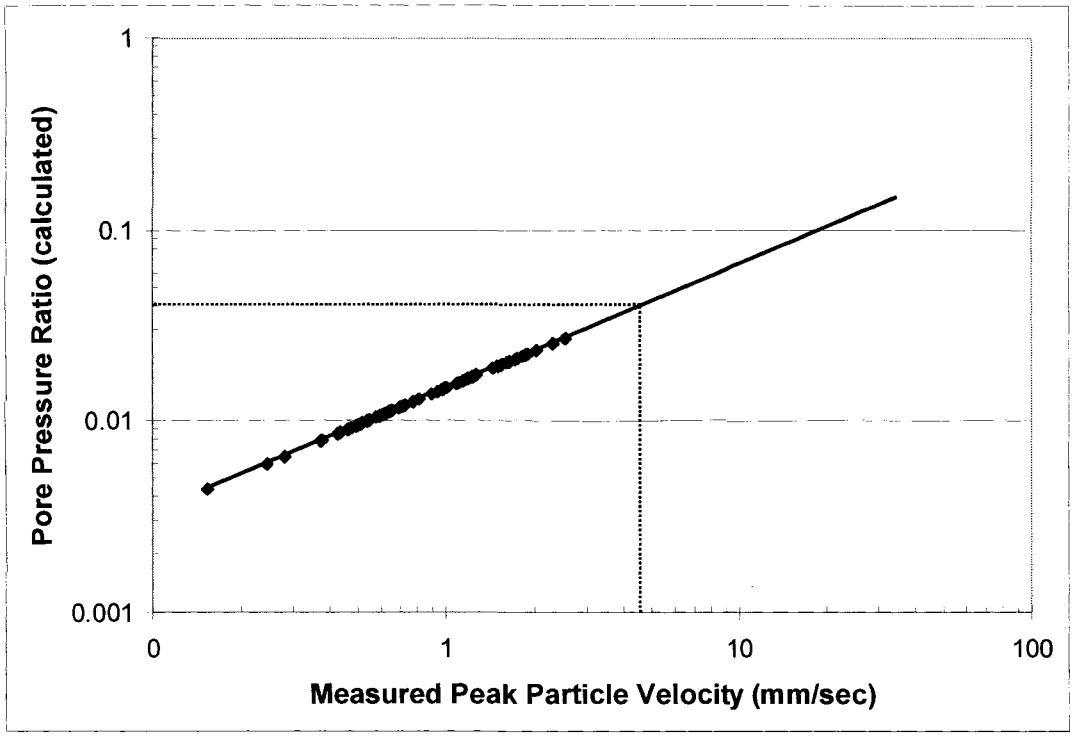

Figure 5.72: Extrapolating to estimate PPR 5 cm from the SPT

Another relationship to calculate PPR was developed by Al-Qasimi et al. (2005) based on scaled distance rather than measured peak particle velocity. In Equation 5.4, SD stands for scaled distance. In this case, square root scaling was used to calculate scaled distance since it provided a better fit between the SPT data and the blasting data.

$$PPR = 16.27\,[SD]^{-1.52} \qquad (5.7)$$

The results of Equation 5.4 are shown in Figure 5.74. The chart shows that PPR's as large as 0.2 are calculated at a distance of 30 cm away from the SPT. Again, assuming an average vertical effective stress of 130 kPa, this equates to a change in pore pressure of 26 kPa, which does not agree well with the pore pressure measurements from the blast probe, which were about an order of magnitude lower.

As indicated in Figure 5.74, the equation calculates a PPR of one when the scaled distance equals approximately 6 $m/kg^{1/2}$. That equates to a PPR of one at a distance of approximately 6.8 cm. Thus, using this equation, one would expect liquefaction of the sand at a distance of 6.8 cm from the SPT sampler. This result seems completely unrealistic for the SPT, especially when compared to the pore pressures measured with the SPTu device.

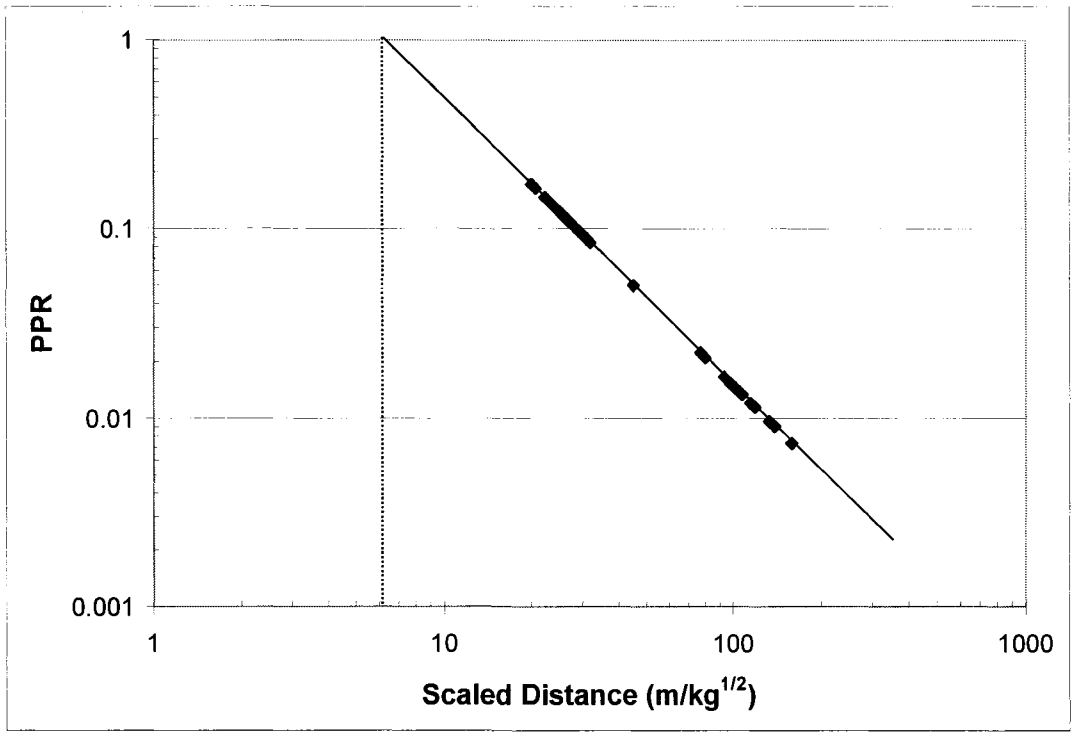

Figure 5.74: Calculated PPR based on Scaled Distance

5.2.6.1 Remarks on Particle Velocity Measurements

Equation 5.6 was used to calculate the expected PPR close to the SPTu device based on the measured peak particle velocity. As noted, the equation results in reasonable calculation of PPR.

Equation 5.7 was also used to calculate the PPR close to the SPTu device based on the calculated scaled distance. As noted, the equation results in gross over prediction of the PPR compared with results measured with the SPTu device.

Use of relationships between PPV, PPR and scaled distance developed for blast induced liquefaction should probably not be applied to the SPT. The energy of the SPT is a several magnitudes smaller than the energy of actual explosive blasts. In studies of blast-induced liquefaction, measurements of pore pressure were made from much greater distances compared to the SPTu testing and the scale effects of applying blast-induced liquefaction relationships to the SPTu are not known.

In addition, it was previously noted that either positive or negative excess pore pressures could be generated from the SPT depending on the stress level and dilatancy of the soil. However, the literature generally only considers the blast-induced pore pressure changes are generally only positive away from the blast. As a result, the blast-induced liquefaction relationships are not able to capture the effects of the stress level and dilatancy close to the SPTu device. In addition,

blast induced liquefaction relationships are not capable of correctly predicting the negative pore pressures, which may be generated by the SPT.

6.0 SUMMARY AND CONCLUSIONS

Syncrude initiated a site investigation program to study loose beach below water deposits of sand in areas of the Aurora tailings dam to determine whether or not there might be potential for liquefaction of the BBW sand.

During the site investigation, it was discovered that the SPT and CPT results did not correlate well with each other. The cone tip resistance to blow count ratio ($q_{c1n}/(N_1)_{60}$) was found to vary substantially. Moreover, it was found that the $q_{c1n}/(N_1)_{60}$ ratio was dependent on the blow count, but not on the cone tip resistance.

The objective of this thesis was to find an explanation for the observed discrepancy between the CPT and SPT data at Aurora and find an explanation for the observed dependence of the $q_{c1n}/(N_1)_{60}$ ratio on the SPT blow count.

It was postulated that either one or both of the following two hypotheses might explain the observed data:

1. In loose sands where the blow count is expected to be low, the weight of the rods, sampler and hammer overwhelms the sand's resistance to penetration resulting in lower than expected blow counts relative to the CPT data. The effect of the weight of the rods would be more pronounced in loose sand compared to dense sand.
2. The SPT itself may cause small zones of liquefaction in and around the sampler shoe in the loose BBW sand. It may be that the dynamic nature of the SPT may cause a cyclic increase in the pore water pressure in the loose fine sand around the sampler shoe. A rise in the pore pressure around the sampler shoe would result in a decrease in effective stress and thus, penetration resistance. This would result in a low blow count relative to the equivalent blow count obtained from the CPT. It would not be necessary for actual liquefaction to occur for the SPT blow count to be affected. Any significant increase in pore pressure due to the test would result in a decrease in effective stress and a decrease penetration resistance and blow count.

In order to confirm or reject the first hypothesis, the work of Schmertmann (1979) was first examined. Schmertmann developed a theory based on the static forces acting on the SPT and CPT that linked the two tests and allowed prediction of the cone tip resistance based on the measured blow count. Because Schmertmann included the weight of the SPT rods, sampler and hammer in his static theory, a blow count as low as zero might be measured but a cone tip resistance of zero is not predicted by his theory. As a result, when Schmertmann's work is used to predict the $q_{c1n}/(N_1)_{60}$ ratio, the ratio increases to infinity as the blow count drops to zero. However, at blow counts greater than about 10, Schmertmann's work predicts a $q_{c1n}/(N_1)_{60}$ ratio of about 5, which agrees well with what is observed from the literature.

It was also postulated that in very loose sand, one might observe some amount of penetration in the borehole due solely to the weight of the SPT equipment, termed "self-weight penetration". Schmertmann's theory was extended and an equation to predict self-weight penetration in loose sands was developed. The equation is dominated by low vertical effective stresses near to the surface, which, theoretically, would result in large self-weight penetration predictions. However, at greater depths for sand with a constant relative density, the equation predicts increasing self-weight penetration with depth. The reason for this is that the weight of the rods increases in a linear manner with depth, while the expected cone tip resistance increases at a slower, non-linear manner with depth (for a deposit with constant relative density). As a result, one would expect that the weight of the SPT rods would have a much larger impact on the blow count with increasing depth and hence, higher $q_{c1n}/(N_1)_{60}$ ratios would be seen. This prediction was supported by data collected from the Aurora site. Data were presented that shows an overall trend of increasing $q_{c1n}/(N_1)_{60}$ ratio with depth.

In order to evaluate the second hypothesis, a field-testing program was developed to monitor the pore water pressure during the SPT. A standard split spoon sampler was outfitted with a pore pressure transducer and this test was termed the SPTu. The SPTu device was developed by Adara and a number of prototypes were tested before arriving at a final design where the pore pressure transducer was located inside the split spoon sampler and measured the pore pressure on the outside of the sampler wall through a small screen.

Changes in pore pressure during Standard Penetration Tests were measured with the SPTu device. Positive residual pore pressures as high as 28 kPa above the initial in-situ stress were measured in the test at a depth of 10.80 m, which equates to a PPR of 0.23. While actual liquefaction was not measured with the SPTu device, it seems likely that the 23% reduction in vertical effective stress was likely to have an impact on the penetration resistance for successive blows. In addition, it is well known that the horizontal stresses have approximately twice the effect of the vertical stresses (Schmertmann 1979). Since the horizontal stresses are lower than the vertical effective stresses in an earth dam, one would expect that the 23% reduction in vertical stress represents a much greater reduction in horizontal effective stress and hence penetration resistance.

For the next two tests at depths of 12.41 and 13.92 m, positive residual pore pressures were measured on the first couple of blows, which then decreased with successive blows and ended in negative residual pore pressures in both tests. Residual pore water pressures of –8 kPa and –50 kPa relative to the initial in-situ pore pressure were measured for the tests at 12.41 and 13.92 m, respectively.

Upon examination of the CPT data collected at the Massey site it was found that the relative density increased from a depth of 10.80 m to 12.41 m and increased further from a depth of 12.41 m to 13.92 m.

Therefore, it may be that for the test at 10.80 m deep, the sand may have acted in a contractive manner for the entire duration of the SPT. As the sand contracted due to its collapse, positive residual pore pressures would be built up.

For the tests at 12.41 and 13.92 m deep, the sand may have initially acted in a contractive manner generating positive residual pore pressures and then on further penetration of the sampler was forced to dilate generating negative residual pore pressures.

The blast probe was used to measure pore pressure changes away from the SPTu. Data was presented that shows that the blast probe measured pore pressure increases of up to 2 kPa as a result of the SPTu blows. While 2 kPa might not seem like much, the blast probe was located at an average distance of approximately 29 cm away from the SPTu. Therefore, one would expect to measure much higher residual pore pressures if it was possible to locate the blast probe even closer to the SPTu.

Relationships between PPV, PPR and scaled distance, which were developed for analysis of blast induced liquefaction, were used in an attempt to predict the pore pressure response measured by the blast probe. However, it was found that the blast-induced liquefaction relationships could not predict the pore pressure response as a result of dynamic nature of the SPT for the two reasons. Firstly, that the relationships were developed using explosives with several orders of magnitude more energy than the SPT and measurements were made from much greater distances from the energy source. Secondly, the relationships are not able to predict negative pore pressures, which may be generated in dense sand.

No amount of self-weight penetration was measured during the SPTu testing at the Massey Tunnel site. However, it was shown through the self-weight penetration equation that no self-weight penetration was predicted for the Massey site. The calculations showed that in order to measure any significant self-weight penetration, the SPT would have to be conducted in sand with a relative density of less than about 22%. From CANLEX it was determined from testing on high quality undisturbed samples that the average relative density of the Massey deposit was 33%. Furthermore, the Massey sand was deposited approximately 200 years ago and is aged, which would further increase penetration resistance and decrease self-weight penetration predictions.

This research has shown that the range of $q_{c1n}/(N_1)_{60}$ ratio data and their dependence on the blow count observed at Aurora can be explained by the effect of the weight of the SPT hammer, rods and sampler. In fact, the dependence of the $q_{c1n}/(N_1)_{60}$ ratio on the blow count and high $q_{c1n}/(N_1)_{60}$ ratios should be expected any time the SPT is used in very loose sands, particularly where the depth of the testing exceeds approximately 10 m.

At shallow depths (less than 10 m) where the rods are short, the SPT equipment weighs less and has less of an impact on the blow count. In addition, in medium dense to dense sands (where blow counts are greater than 10), the weight of the SPT equipment has less of an impact on the blow count.

For loose sands, where the relative density is less than about 40%, the weight of the SPT equipment appear to decrease the measured blow counts when the depth is greater than about 10 m. One would expect the blow counts to decrease as the relative density of the sand decreases and the depth increases. Ultimately, it would appear to be possible for blow counts of 0 to be measured where the sand is very loose and the depth of testing is very large.

In medium dense to dense sands, where the relative density is greater than about 40%, the measured $q_{c1n}/(N_1)_{60}$ ratio appears to decrease with increasing relative density.

In addition, while more testing with the SPTu device would be recommended, this research has also shown that it is possible that the dynamic nature of the SPT may result in positive residual pore pressures being generated relative to the initial in-situ pore pressure. Any increase in pore water pressure around the SPT sampler shoe would result in a decrease in effective stress and the blow count, which in turn may contribute to high $q_{c1n}/(N_1)_{60}$ ratios. As one would expect, the highest sustained pore pressure increases were measured in the loosest sand tested, while negative residual pore pressures (relative to the in-situ pore pressure) were measured in denser sand. Since the Massey sand is denser and older than the Aurora tailings sand, one might expect that greater positive residual pore pressures might be observed if the SPTu device were to be tested at Aurora.

The SPT probably should not be thought of as being more sensitive to loose sand than the CPT. In fact, one might suggest that the opposite is true since the weight of the SPT equipment plays such a major role in reducing the blow count in very loose sands, while having much less impact in denser sands. It could be said that the weight of the SPT equipment overwhelms the penetration resistance of very loose sand especially at depths that exceed 10m.

The problems with the SPT are well documented throughout the literature. The CPT is clearly the more reliable and repeatable of the two tests. Nevertheless, the SPT is still often used in liquefaction investigations as a primary or secondary means of conducting a liquefaction screening on a sand deposit. If the SPT is to be used for investigations in loose sand at depths greater than about 10 m, the engineer must keep in mind the effect of the weight of the SPT equipment on the blow count. The engineer must realize that in loose sands, the SPT and CPT data may not correlate well with each other and higher than expected $q_{c1n}/(N_1)_{60}$ ratios should be expected due to the effect of the weight of the SPT equipment on the blow count. In very loose sands, pore pressure increases as a result of

the dynamic action of the SPT may further contribute to higher $q_{c1n}/(N_1)_{60}$ ratios. However, as noted, the pore pressure change appears to depend on the density and stress state of the sand.

In essence, this research has served to point out two more factors to add to the already long list of factors that have an impact on SPT results. The weight of the SPT equipment and the potential changes in pore pressure around the SPT sampler shoe due to the dynamic nature of the SPT both clearly have an impact on the blow count in loose saturated sand, which may result in a decrease in measured blow count and an increase in the expected $q_{c1n}/(N_1)_{60}$ ratio.

Unfortunately, it would probably be difficult to develop yet another correction to the blow count to account for the weight of the rods since its effect would depend on the relative density of the sand, which is often very difficult to determine with a high degree of accuracy. In addition, it seems that it would be even more difficult to develop a correction for the blow count to account for changes in pore pressure (that might be positive or negative depending on the relative density of the deposit), which occur during the test.

6.1 Summary of Conclusions

1. The variation in the $q_{c1n}/(N_1)_{60}$ ratio and its dependence on the blow count can be explained by the effect of the weight of the SPT equipment. The weight of the SPT equipment was found to have an increasing impact on the blow count with depth. High $q_{c1n}/(N_1)_{60}$ ratios should be expected when the SPT is used in very loose sands (i.e. $(N_1)_{60} \leq 10$) where the depth of testing exceeds approximately ten metres (>10m).
2. It is possible that the dynamic nature of the SPT may result in some excess (positive or negative) residual pore pressure generation.
    - Any increase in pore water pressure around the SPT sampler shoe would result in a decrease in effective stress, penetration resistance and blow count relative to CPT results, which in turn would contribute to high $q_{c1n}/(N_1)_{60}$ ratios. Conversely, the generation of negative excess pore pressures in denser sand would result in an increase in blow count and possibly lower $q_{c1n}/(N_1)_{60}$ ratios.
3. If the SPT is to be used for investigations in loose sand at depths greater than about 10 m, the engineer should be aware of the effect of the weight of the SPT equipment on the blow count. The engineer should realize that in loose sands, higher than normal $q_{c1n}/(N_1)_{60}$ ratios can be expected due to the effect of the weight of the SPT equipment on the blow count. In very loose sands, pore pressure increases as a result of the dynamic action of the SPT may further contribute to higher $q_{c1n}/(N_1)_{60}$ ratios. However, the changes in pore pressure are difficult to quantify.
4. In essence, this research has served to point out two additional factors to add to the already long list of factors that have an impact on SPT results.

6.2 Recommended Future Work

Recommended future work could include:

- To the author's knowledge, only one other instance of the relationship between the $q_{c1n}/(N_1)_{60}$ ratio and the blow count has been reported. Thus, it would be useful to obtain additional data from different sands at other sites.
- Additional testing with the SPTu device for the purpose of:
    - Measuring the pore pressure response of the SPTu device at other depths in different sand with different relative density.
    - Better defining the SPTu's pore pressure response to the relative density of the sand. More test data could aid in defining the transition from dilative pore pressure response (negative residual pore pressures being generated in dense sand) to contractive pore pressure response (positive residual pore pressures being generated in loose sand).
    - It would also be valuable, though difficult, for future research to eliminate the cyclical pore pressure response that was measured by the SPTu device and is thought to be the result of stress waves and shaking of the SPT sampler.

7.0 REFERENCES

Al-Qasimi, E.M.A., Charlie, W.A., and Woeller, D.J. 2005. Canadian Liquefaction Experiment (CANLEX): Blast-Induced Ground Montion and Pore Pressure Experiments. Geotechnical Testing Journal, **28**(1): 1-13.

Baez, J.I., Martin, G.R., and Youd, T.L. 2000. Comparison of SPT-CPT Liquefaction Evaluations and CPT Interpretations. *In* Geotechnical Special Publication #97, Proceedings of sessions of Geo-Denver 2000. *Edited by* P.W. Mayne and R. Hyrciw. Denver, Co. American Society of Civil Engineers, pp. 17-32.

Brown, R.E. 1977. Drill Rod Influence on Standard Penetration Test. Journal of Geotechnical and Geoenvironmental Engineering, ASCE, **103**(11): 1332-1336.

Burland, J.B., and Burbidge, M.C. 1985. Settlement of foundations on sand and gravel. Proceedings of the Institution of Civil Engineers, **78**: 1325-1381.

Butler, J.J., Caliendo, J.A., and Goble, G.G. 1998. Comparison of SPT energy measurement methods. *In* Geotechnical Site Characterization. *Edited by* P.K. Robertson and P.W. Mayne. Atlanta, Georgia. A.A.Balkema, Vol.1, pp. 901-905.

Charlie, W.A., Jacobs, P.J., and Doehring, D.O. 1992. Blast-Induced Liquefaction of an Alluial Sand Deposit. Geotechnical Testing Journal, **15**(1): 14-23.

Clayton, C.R.I., Hababa, M.B., and Simons, N.E. 1985. Dynamic penetration resistance and the prediction of the compressibility of a fine-grained sand - a laboratory study. Geotechnique, **35**(1): 19-31.

ConeTec, I. 2004. SPT Pore Pressure Measurement Data: October 14, 2004, p. Personal Communication.

Daniel, C.R., and Howie, J.A. 2004. Preliminary Research Summary: Massey Tunnel SPTu Trial, September 13, 2004, UBC, Vancouver.

Daniel, C.R., Howie, J.A., and Taylor, B. 2003. Analysis of spt stress wave data using the case method. *In* 56th Canadian geotechnical conference. Winnepeg, Manitoba. Canadian Geotechnical Society, Vol.???????????, p.????????????

Douglas, B.J., and Olsen, R.S. 1981. Soil Classification Using Electric Cone Penetrometer. *In* ASCE National Convention. St. Louis. American Society of Civil Engineers (ASCE), pp. 209-227.

Drake, J.L., and Little, C.D. 1983. Ground Shock from Penetrating Conventional Weapons. *In* Symposium of the Interaction of Non-Nuclear Munitions with Structures. Colorado Springs, CO. U.S. Air Force Academy, pp. 1-6.

Drumright, E.E., Pfingsten, C.W., and Lukas, R.G. 1996. Influence of Hammer Type on SPT Results. Journal of Geotechnical and Geoenvironmental Engineering, ASCE, **122**(7): 598-599.

Farrar, J.A. 1998. Summary of standard penetration test (SPT) energy measurement. *In* Geotechnical Site Characterization. *Edited by* P.K. Robertson and P.W. Mayne. Atlanta, Georgia. A.A. Balkema, Vol.1, pp. 919-926.

Idriss, I.M., and Boulanger, R.W. 2004. Semi-Empirical Procedures for Evaluating Liquefaction Potential During Earthquakes. *In* Joint conference: 11th International Conference on Soil Dynamics & Earthquake Engineering and the 3rd International Conference on Earthquake Geotechnical Engineering. Berkeley, California, pp. 32-56.

Jefferies, M.G., and Davies, M.P. 1993. Use of CPTu to estimate equivalent SPT N60. Geotechnical Testing Journal, **16**(4): 458-468.

Kasim, A.G., Chu, M., and Jensen, C.N. 1986. Field Correlation of Cone and Standard Penetration Tests. Journal of Geotechnical and Geoenvironmental Engineering, ASCE, **112**(3): 368-372.

Kovacs, W.D. 1981. Results and Interpretation of SPT Practice Study. Geotechnical Testing Journal, **4**(3): 126-129.

Kruizinga, J. 1982. SPT-CPT Correlations. *In* The Second European Symposium on Penetration Testing; ESOPT II. *Edited by* A. Verruijt, F.L. Beringen, and E.H.D. Leeuw. Amsterdam. A.A.Balkema, Vol.1, pp. 91-94.

Kulhawy, F.H., and Mayne, P.W. 1990. Manual on Estimating Soil Properties for Foundation Design. Electric Power Research Institute.

Lucca, F.J. 2003. Tight Construction Blasting: Ground Vibration Basics, Monitoring and Prediction. Terra Dinamica L.L.C.

Lunne, T., Robertson, P.K., and Powell, J.J.M. 1997. Cone Penetration in Geotechnical Practice. Blacki Academic and Professional, London, UK.

Matsumoto, K., and Matsubara, M. 1982. Effects of Rod Diameter in the Standard Penetration Test. *In* The Second European Symposium on Penetration Testing/ESOPT. *Edited by* A. Verruijt, F.L. Beringen, and E.H.D. Leeuw. Amsterdam. A.A. Balkema, Vol.1, pp. 107-112.

Meyerhof, G.G. 1956. Penetration Tests and Bearing Capacity of Cohesionless Soils. Journal of Soil Mechanics and Foundations Division, ASCE, **82**(SM1): 1-19.

Mitchell, J.K. 1986. Ground Improvement Evaluation by In-Situ Tests. *In* Use of In Situ Tests in Geotechnical Engineering (In Situ '86). *Edited by* S.P. Clemence. Blacksburg, Virginia. American Society of Civil Engineers (ASCE), pp. 221-237.

Robertson, P.K. 1990. Soil classification using the cone penetration test. Canadian Geotechnical Journal, **27**: 151-158.

Robertson, P.K. 1998. Cone Penetration Testing Geotechnical Applications Guide. ConeTec Investigations Ltd. & Gregg In-situ Inc.

Robertson, P.K. 2004. Aurora Tailings Pond Load Test: CPT and SCPT Data Analysis. Report, Syncrude Canada Ltd., Edmonton.

Robertson, P.K., and Wride, C.E. 1998. Evaluating cyclic liquefaction potential using the cone penetration test. Canadian Geotechnical Journal, **35**: 442-459.

Robertson, P.K., Campanella, R.G., and Wightman, A. 1983. SPT-CPT correlations. Journal of Geotechnical and Geoenvironmental Engineering, ASCE, **109**(11): 1449-1459.

Robertson, P.K., Campanella, R.G., Gillespie, D., and Greig, J. 1986. Use of Piezometer Cone Data. *In* In-Situ '86, Use of in-situ testing in geotechnical engineering, ASCE Specialty Conference. Blacksburg. American Society of Civil Engineers (ASCE), pp. 1263-1280.

Sanglerat, G., and Sanglerat, T.R.A. 1982. Pitfalls of the SPT. *In* The Second European Symposium on Penetration Testing; ESOPT II. *Edited by* A. Verruijt, F.L. Beringen, and E.H.D. Leeuw. Amsterdam. A.A. Balkema, Vol.1, pp. 143-145.

Saxena, K.R., and Srinivasulu, G.T. 1982. Prediction of Engineering Behaviour of Sands from Standard Penetration Tests. *In* The Second European Symposium on Penetration Testing; ESOPT II. *Edited by* A. Verruijt, F.L. Beringen, and E.H.D. Leeuw. Amsterdam. A.A.Balkema, Vol.1, pp. 153-158.

Schmertmann, J.H. 1970. Static Cone to Compute Static Settlement Over Sand. Journal of the Soil Mechanics and Foundations Division, ASCE, **96**(SM3): 1011-1043.

Schmertmann, J.H. 1979. Statics of SPT. Journal of Geotechnical and Geoenvironmental Engineering, ASCE, **105**(GT5): 655-670.

Schmertmann, J.H. 1989. Discussion of "Effects of Borehole Fluid on Standard Penetration Test Results" by R.B. Seed, L.F. Harder, Jr., and T.L. Youd. Geotechnical Testing Journal, **12**(3): 250-151.

Schmertmann, J.H., and Palacios, A. 1979. Energy dynamics of SPT. Journal of Geotechnical and Geoenvironmental Engineering, ASCE, **105**(GT8).

Seed, H.B., and De Alba, P.A. 1986. Use of SPT and CPT tests for Evaluating the Liquefaction Resistance of Sands. *In* Use of In Situ Tests in Geotechnical Engineering; In Situ '86. *Edited by* S.P. Clemence. Blacksburg, Virginia. American Society of Civil Engineers (ASCE), pp. 281-302.

Seed, H.B., Tokimatsu, K., Harder, L.F., and Chung, R.M. 1985. Influence of SPT Procedures in Soil Liquefaction Resistance Evaluations. Journal of Geotechnical and Geoenvironmental Engineering, ASCE, **111**(12): 1425-1445.

Seed, R.B., Harder, L.F., and Youd, T.L. 1988. Effects of Borehole Fluid on Standard Penetration Test Results. Geotechnical Testing Journal, **11**(4): 248-256.

Skempton, A.W. 1986. Standard penetration test procedures and the effects in sands of overburden pressure, relative density, particle size, ageing and overconsolidation. Geotechnique, **36**(3): 425-447.

Suzuki, Y., Sanematsu, T., and Tokimatsu, K. 1998. Correlation between SPT and Sesismic CPT. *In* Geotechnical Site Characterization. *Edited by* P.K. Robertson and P.W. Mayne. Atlanta, Georgia. A.A.Balkema, Vol.1, pp. 1375-1380.

Veyera, G.E., and Charlie, W.A. 1988. Laboratory Study of Compressional Liquefaction. Journal of Geotechnical and Geoenvironmental Engineering, ASCE, **115**(5): 790-804.

Veyera, G.E., and Charlie, W.A. 1990. An Experimental Laboratory Facility for Studying Shock-Induced Liquefaction. Geotechnical Testing Journal, **13**(4): 312-323.

Whited, G.C., and Edil, T.B. 1986. Influence of Borehole Stabilization Techniques on Standard Penetration Test Results. Geotechnical Testing Journal, **9**(4): 180-188.

Wride, C.E., Robertson, P.K., Biggar, K.W., Campanella, R.G., Hofmann, B.A., Hughes, J.M.O., Kupper, A., and Woeller, D.J. 2000. Interpretation of in situ test results from the CANLEX sites. Canadian Geotechnical Journal, **37**(3): 505-529.

Yokel, F.Y. 1982. Energy transfer in standard penetration test. Journal of Geotechnical and Geoenvironmental Engineering, ASCE, **108**(9): 1197-1202.

Youd, T.L., Idriss, I.M., Andrus, R.D., Arango, I., Castro, G., Christian, J.T., Dobry, R., Finn, W.D.L., Harder, L.F., Hynes, M.E., Ishihara, K., Koester, J.P., Liao, S.S.C., Marcuson, W.F., Martin, G.R., Mitchell, J.K., Moriwaki, Y., Power, M.S., Robertson, P.K., Seed, R.B., and Stokoe, K.H. 2001. Liquefaction Resistance of Soils: Summary Report from the 1996 and 1998 NCEER/NSF Workshops on Evaluation of Liquefaction Resistance of Soils. Journal of Geotechnical and Geoenvironmental Engineering, ASCE, **127**(10): 817-833.

APPENDIX A: AURORA POND LOAD TEST DATA

Pre-Embankment Aurora Pond Load Test SPT Data

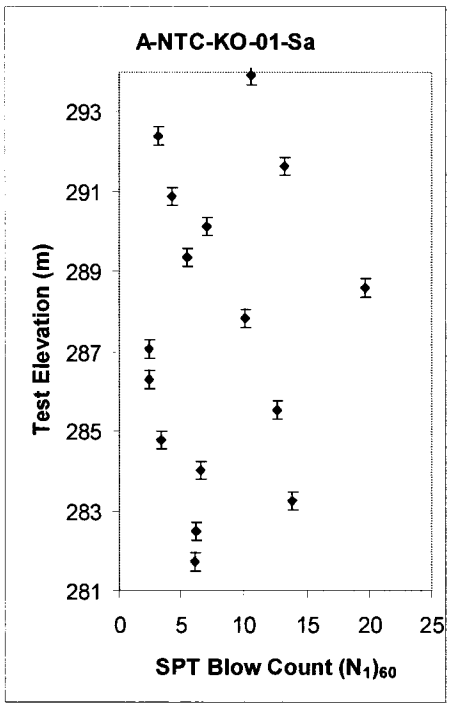

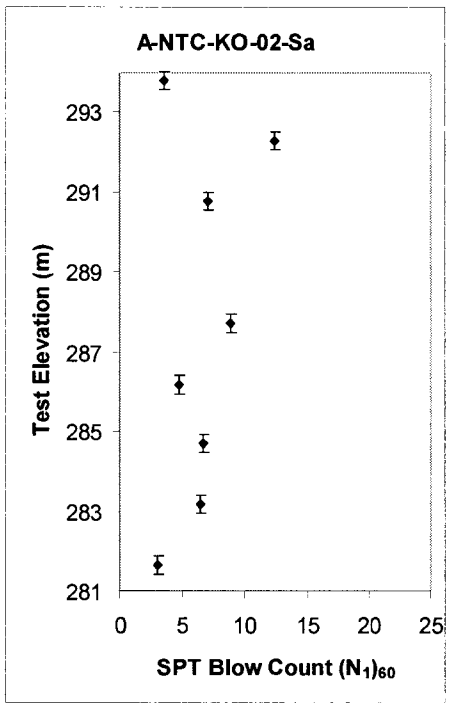

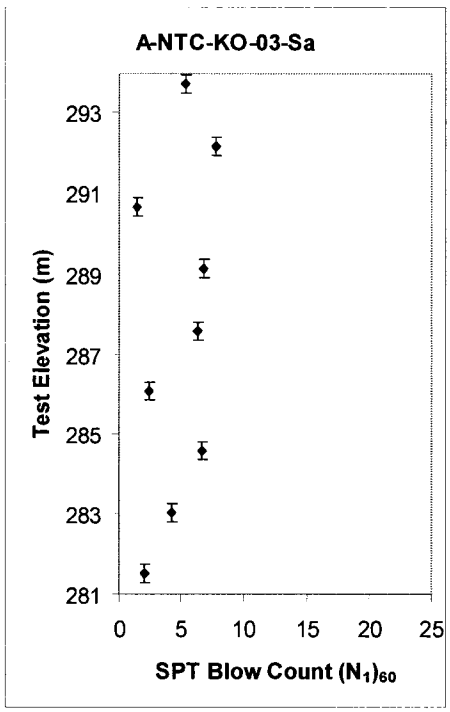

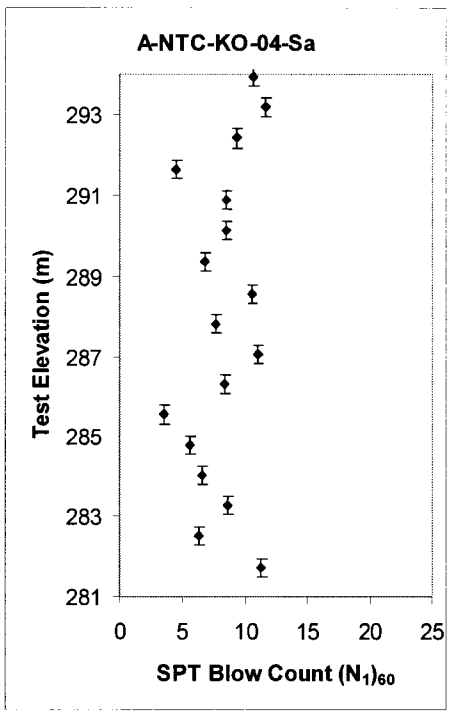

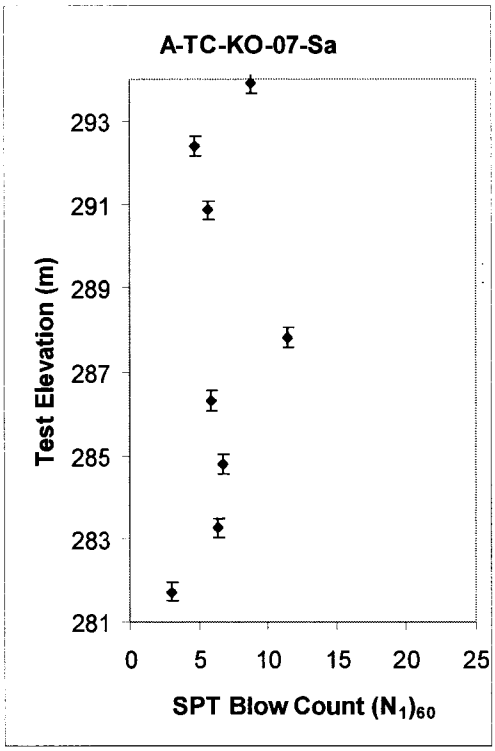

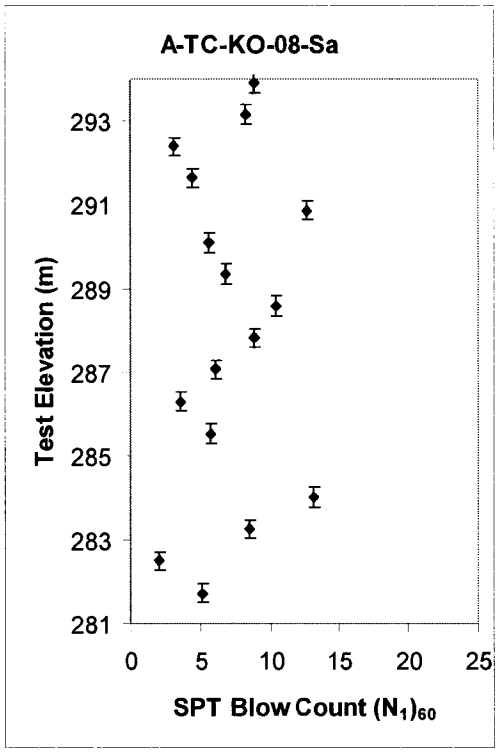

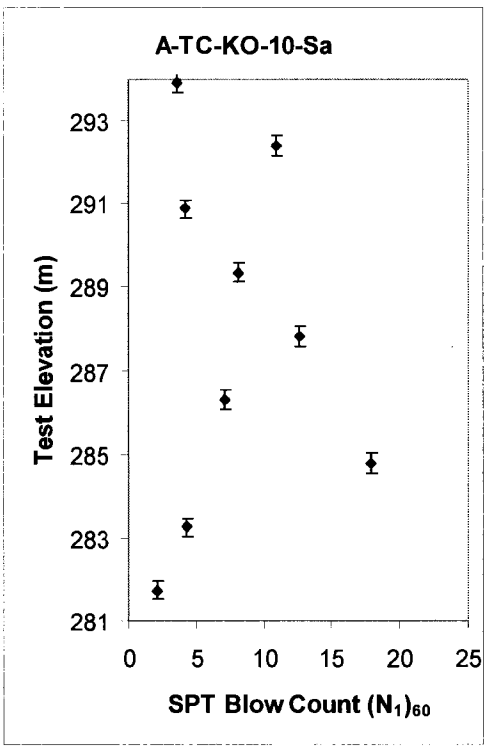

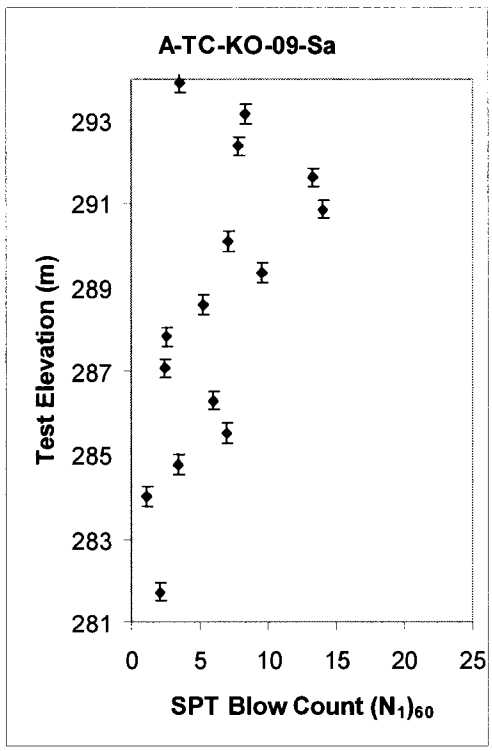

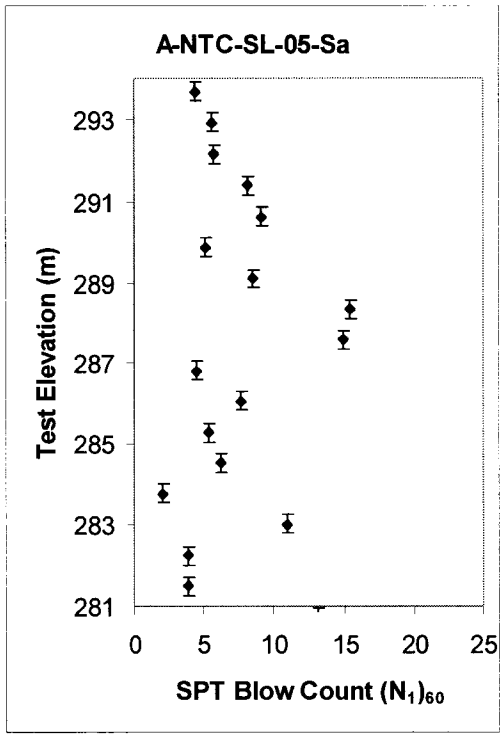

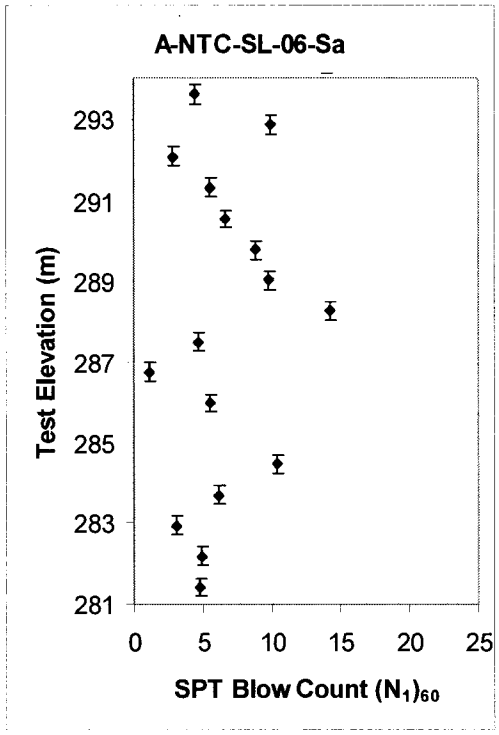

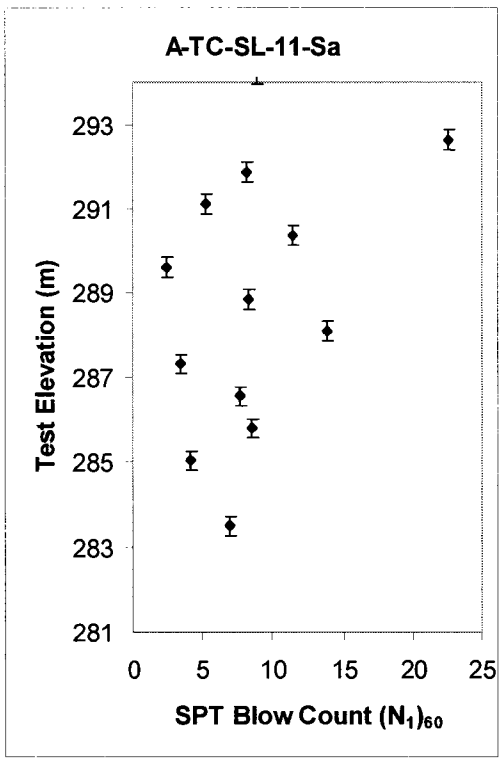

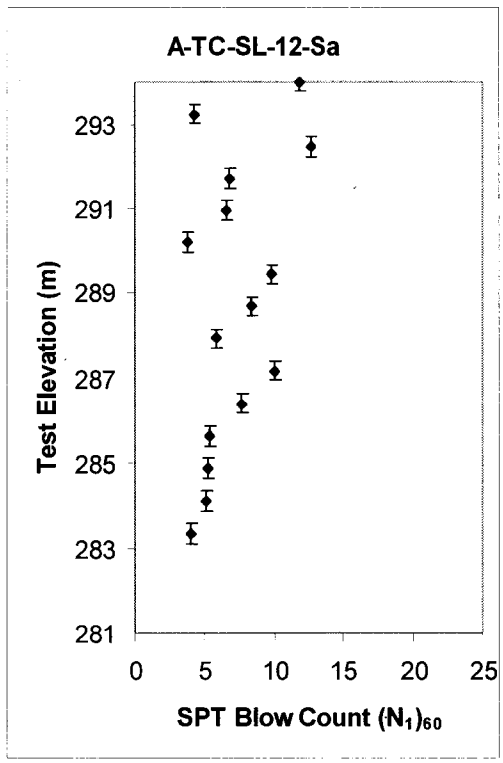

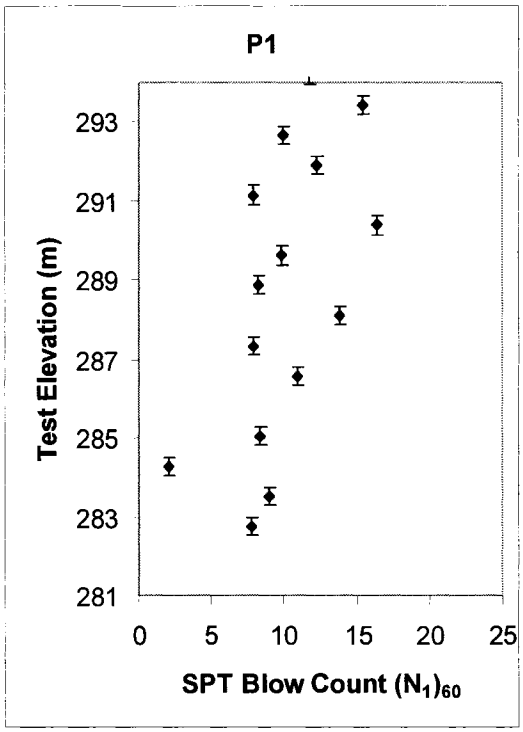

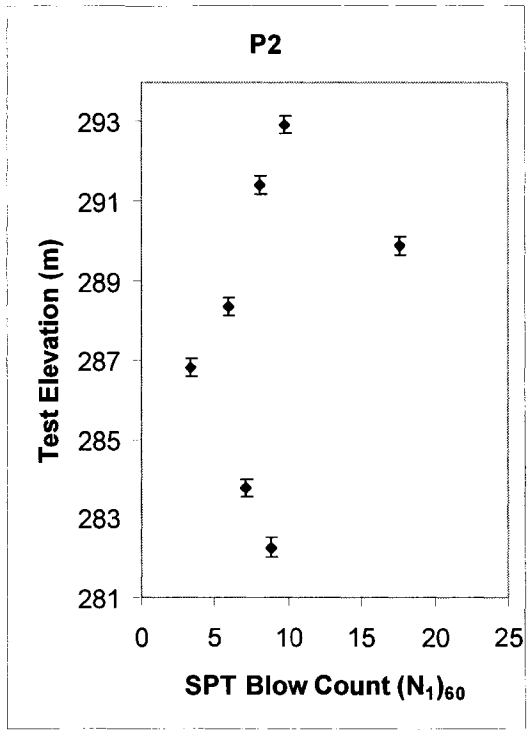

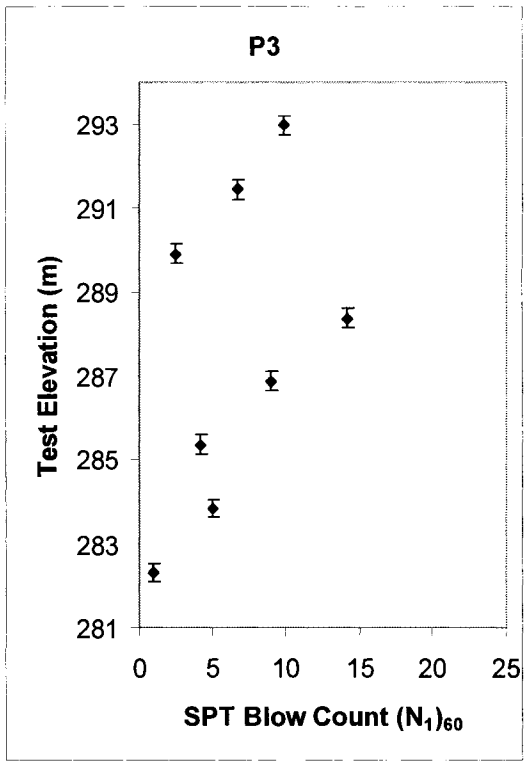

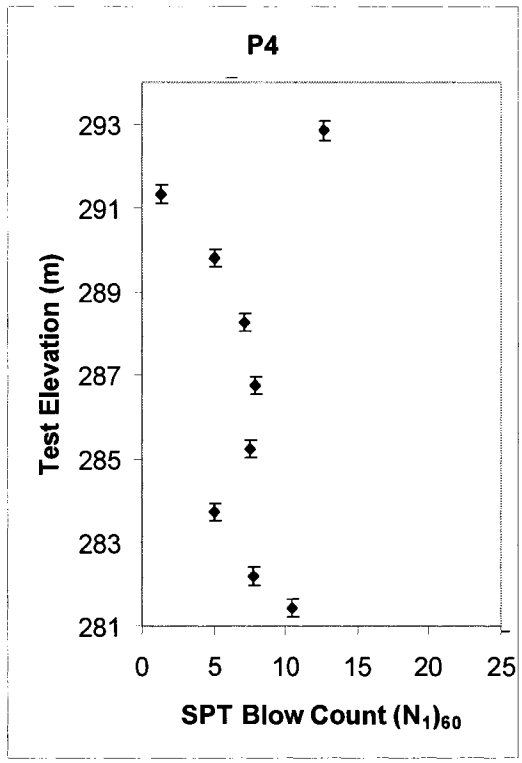

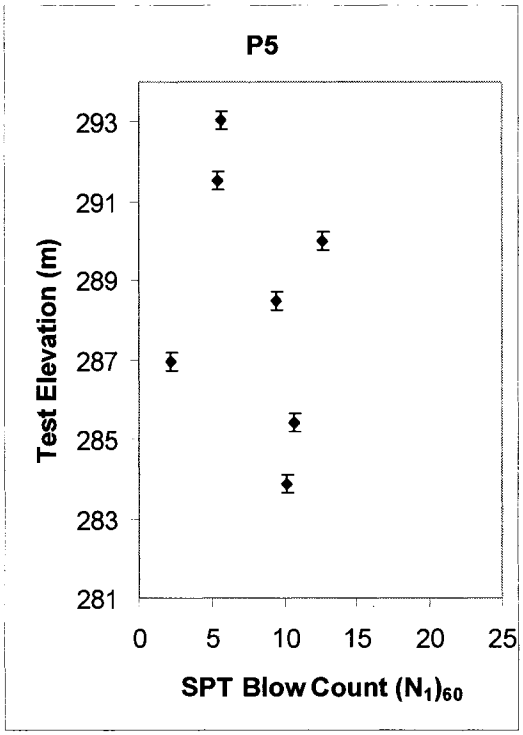

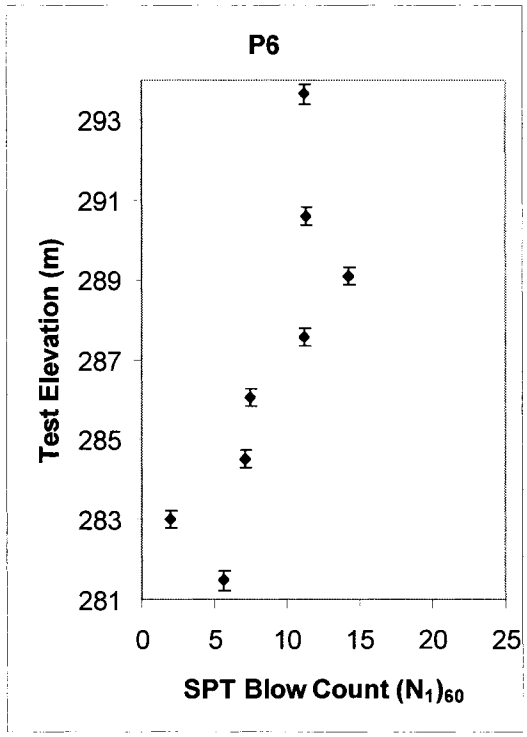

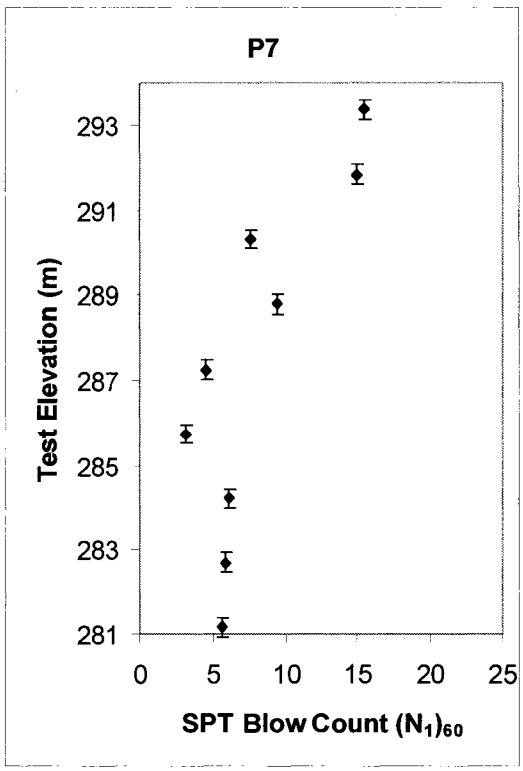

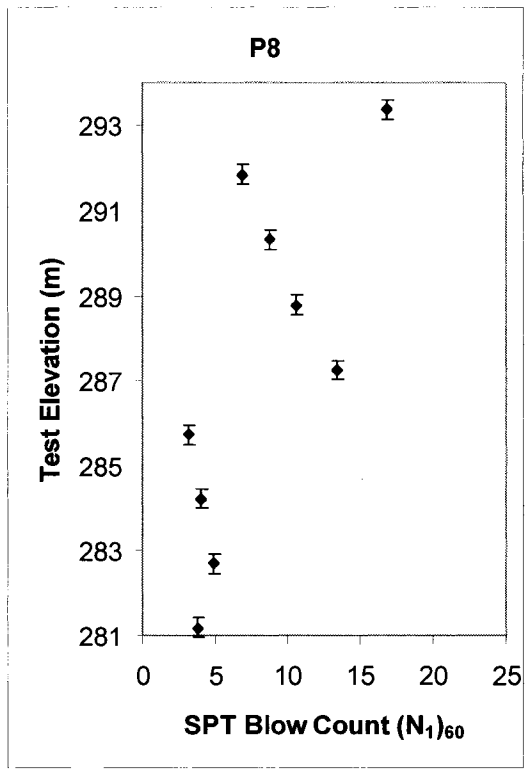

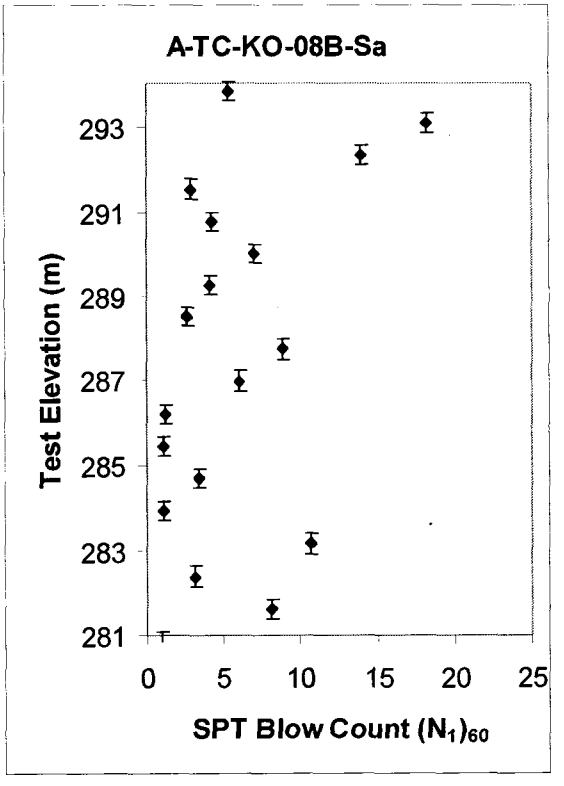

Post-Embankment Aurora Pond Load Test SPT Data

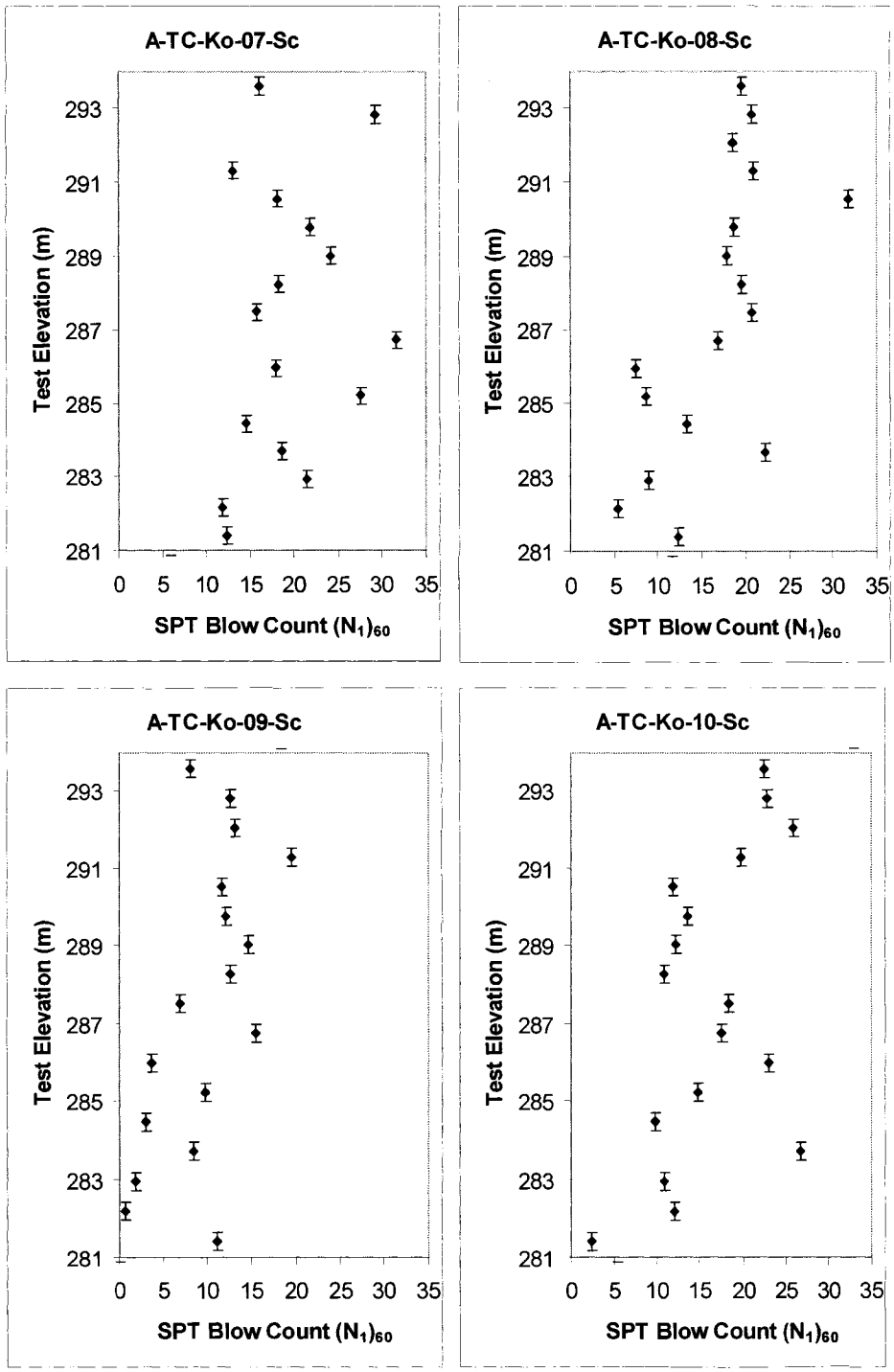

Pre-Embankment Aurora Pond Load Test CPT Data

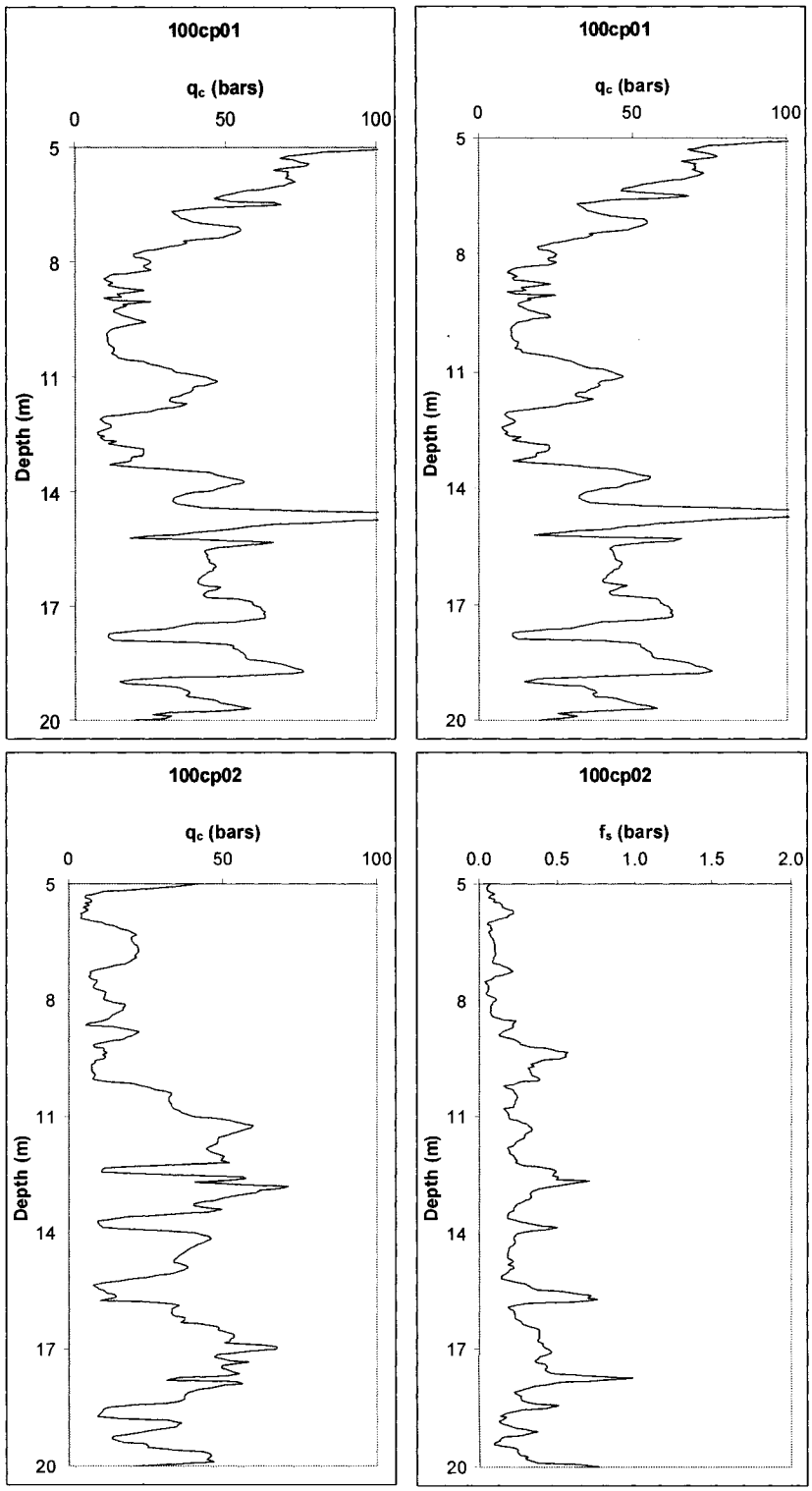

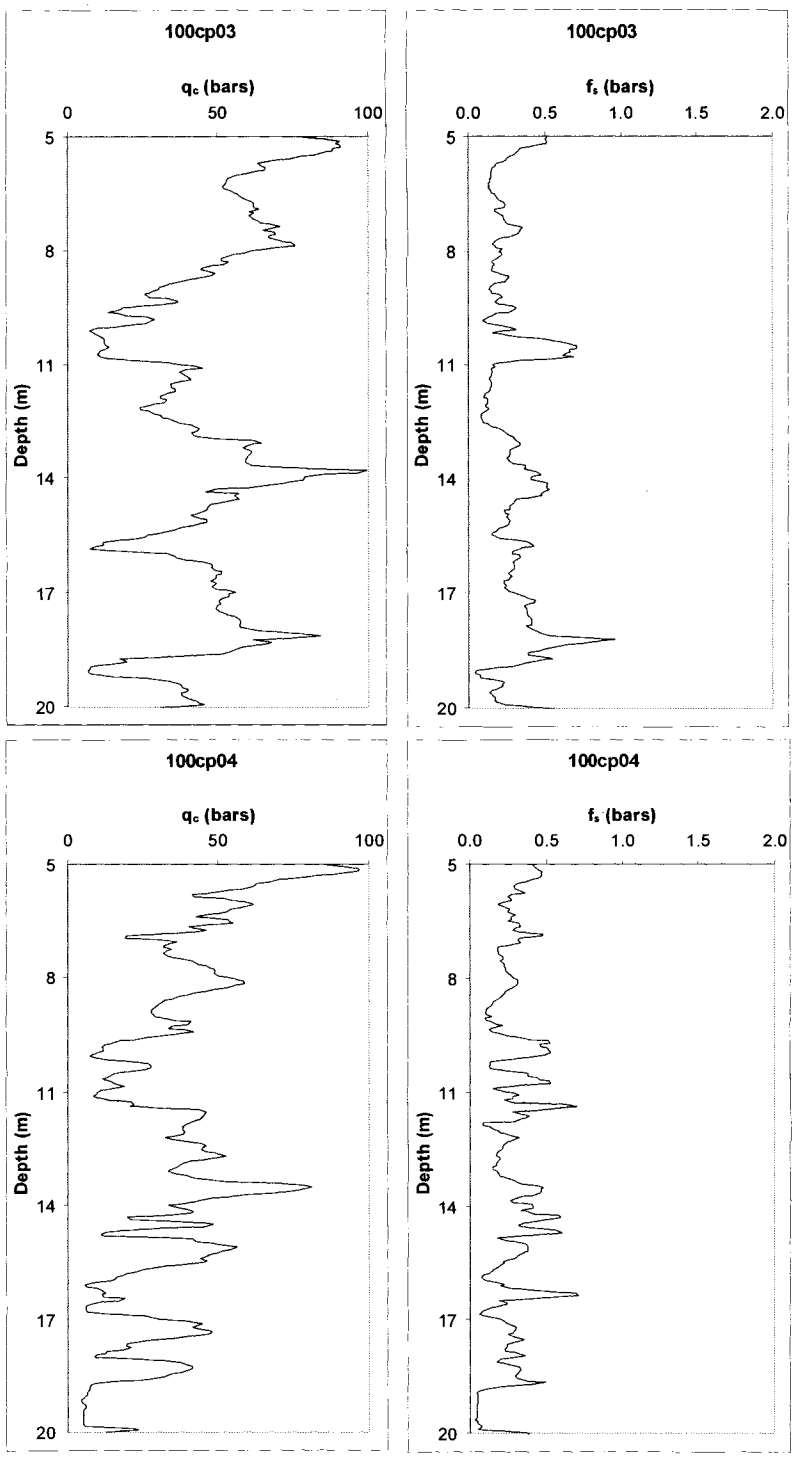

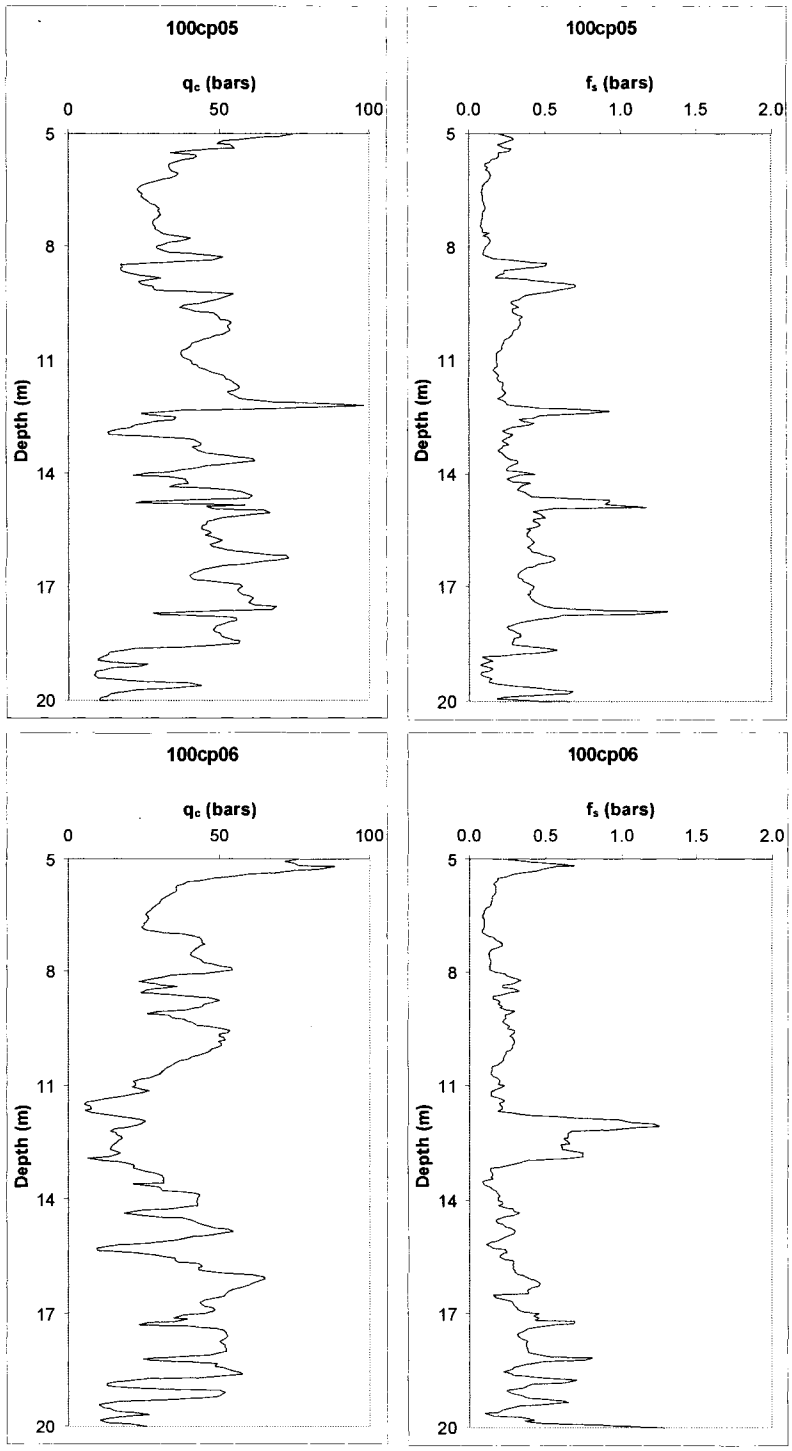

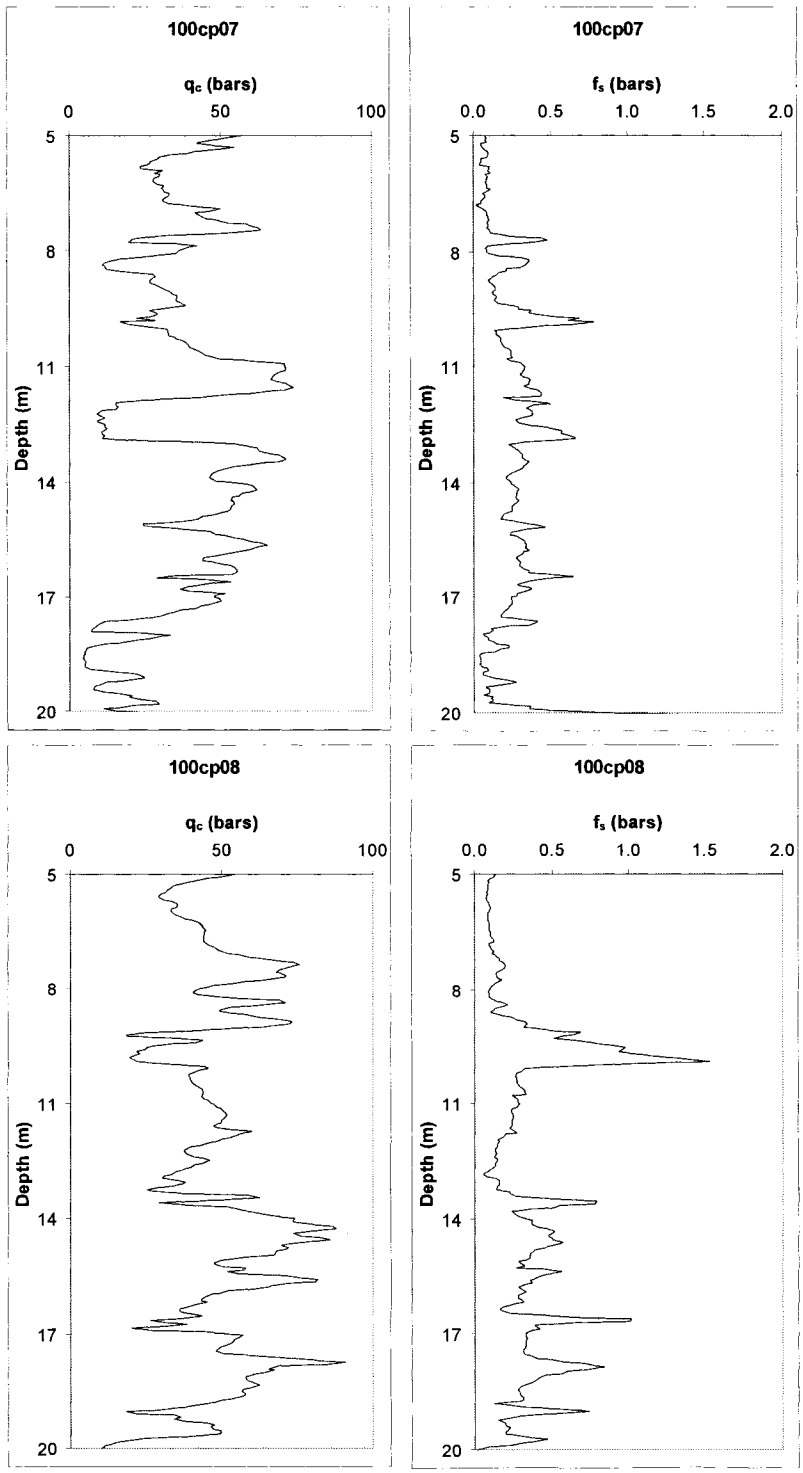

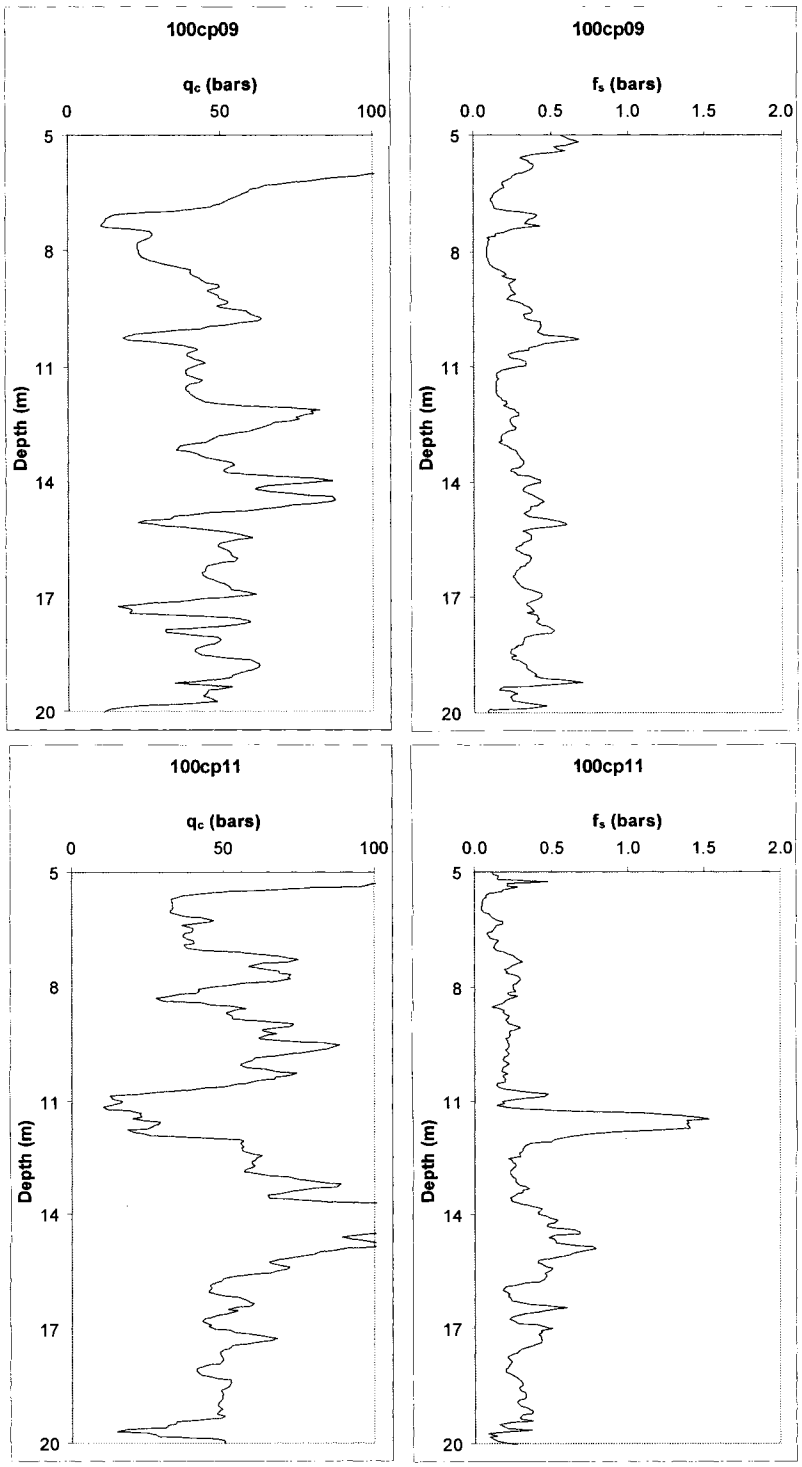

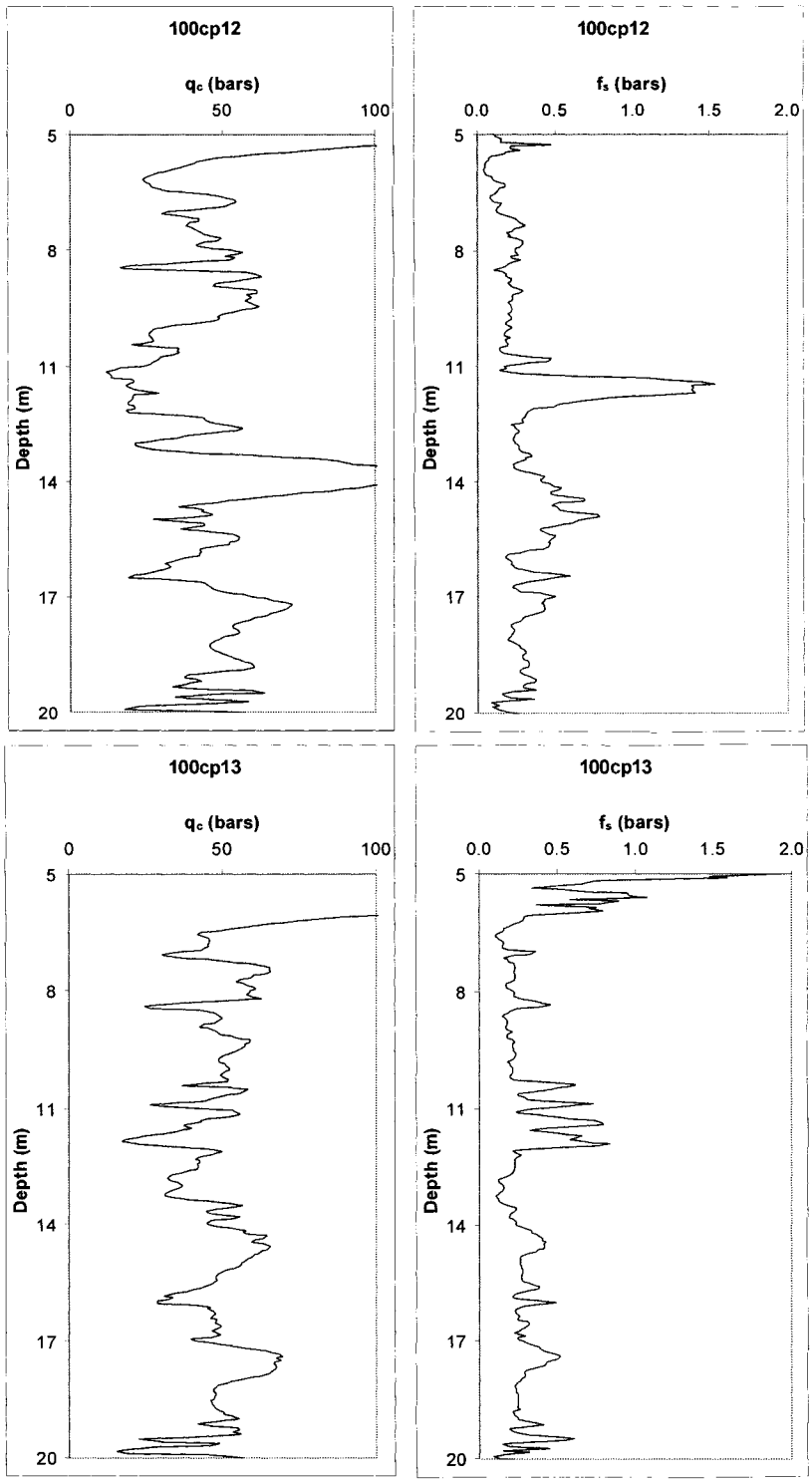

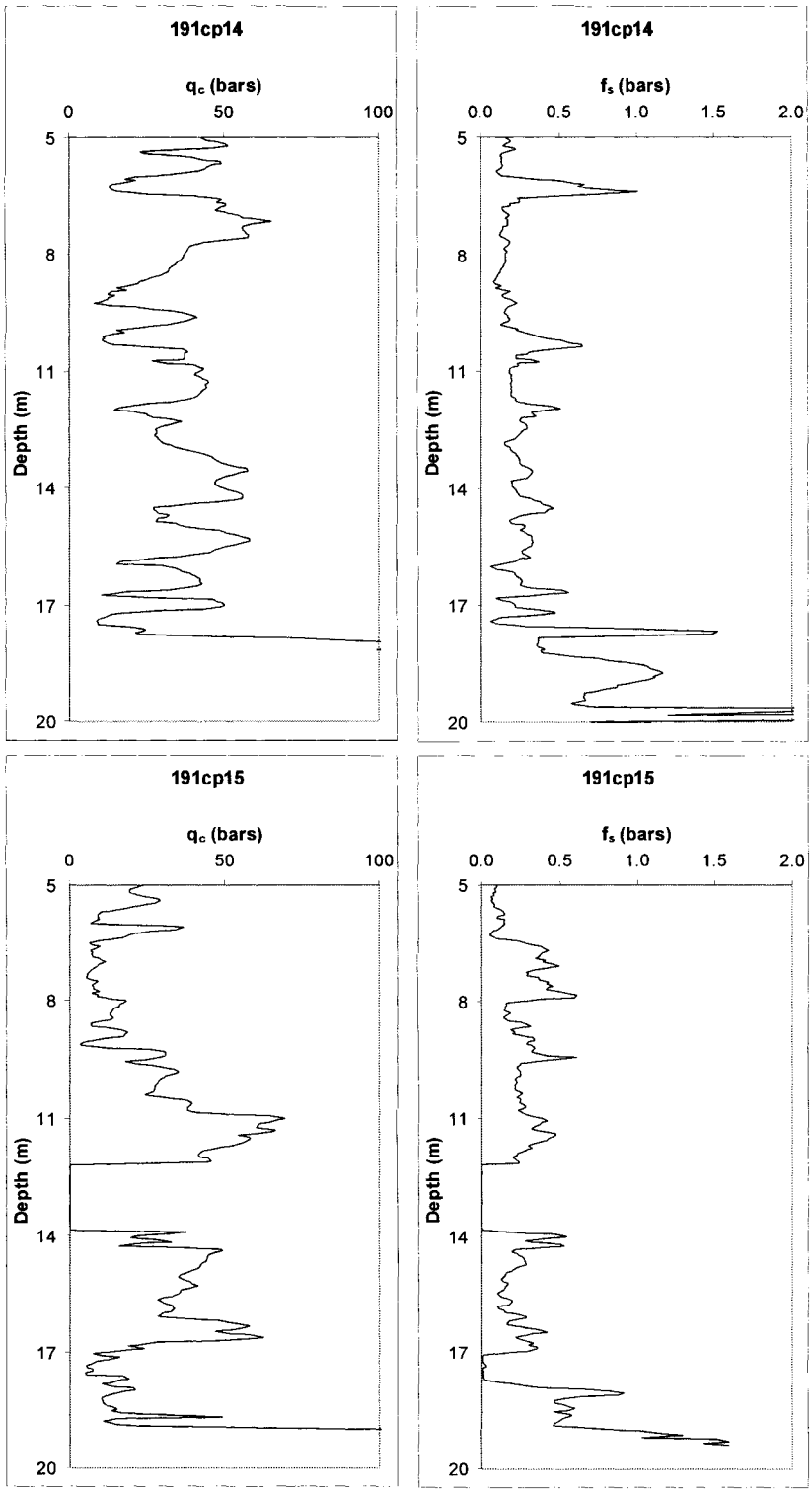

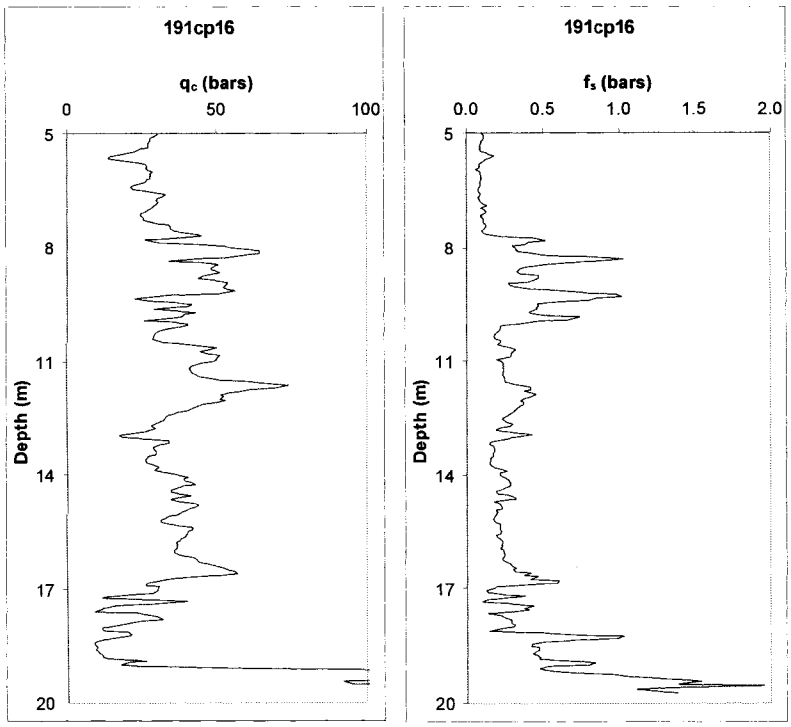

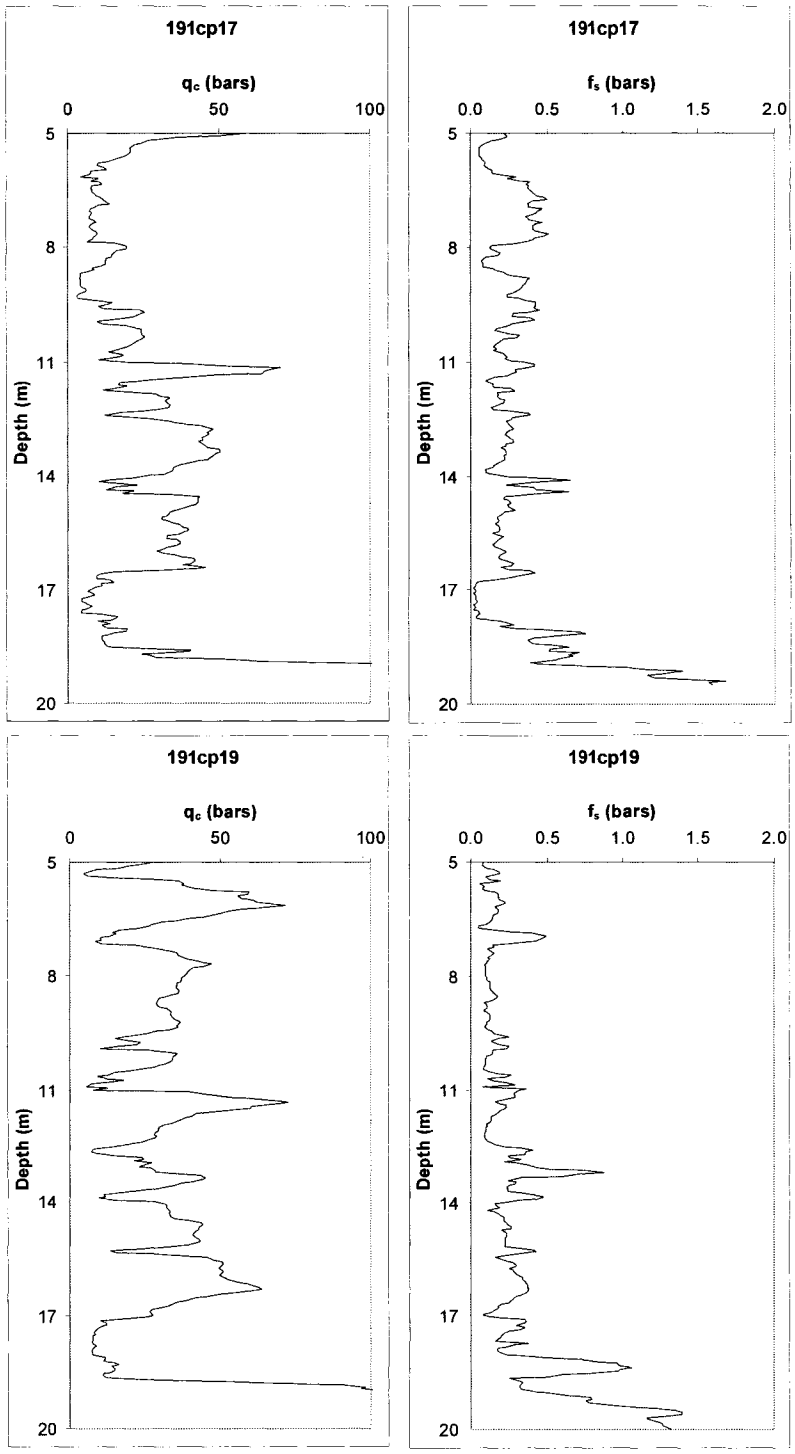

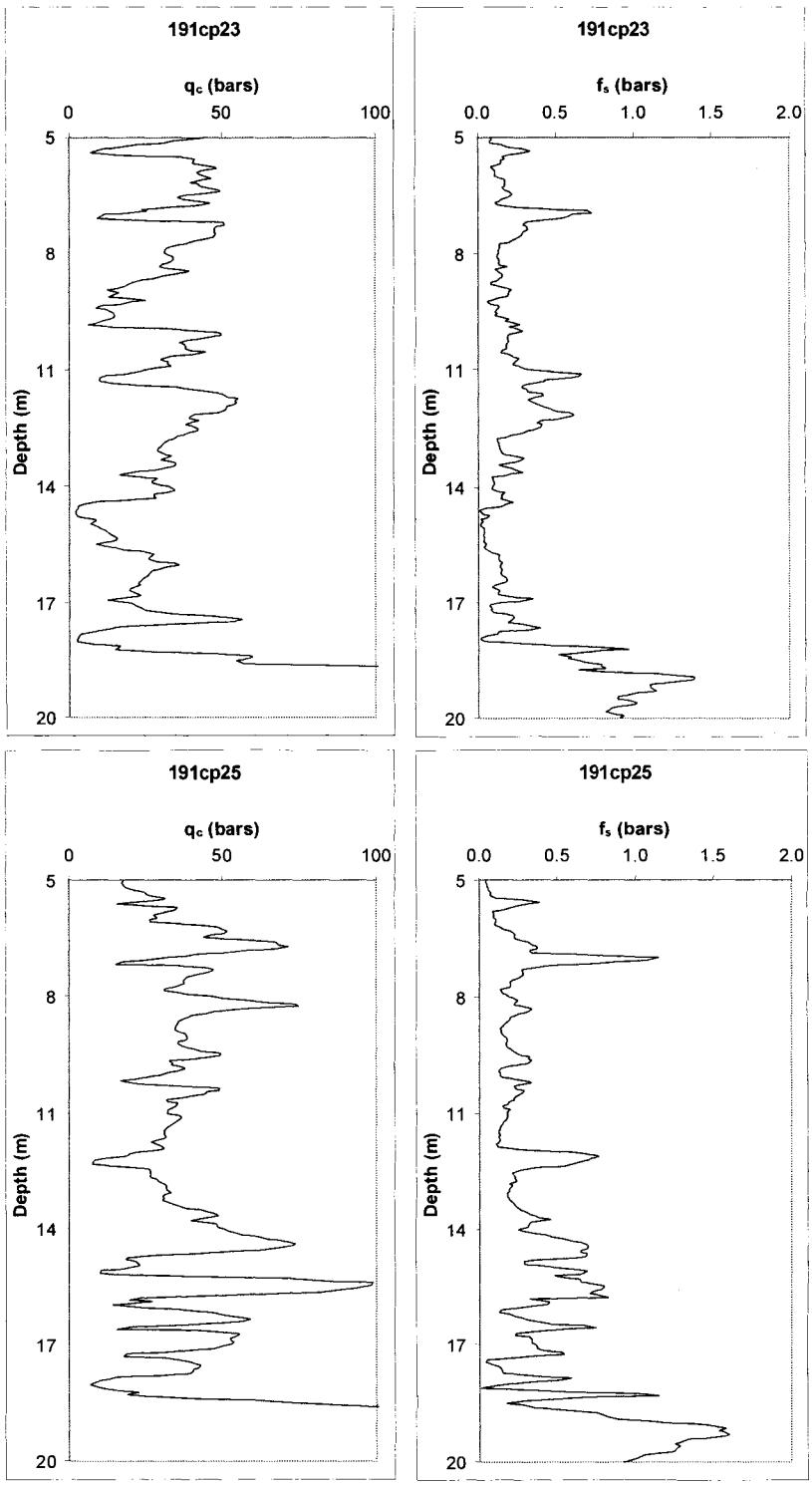

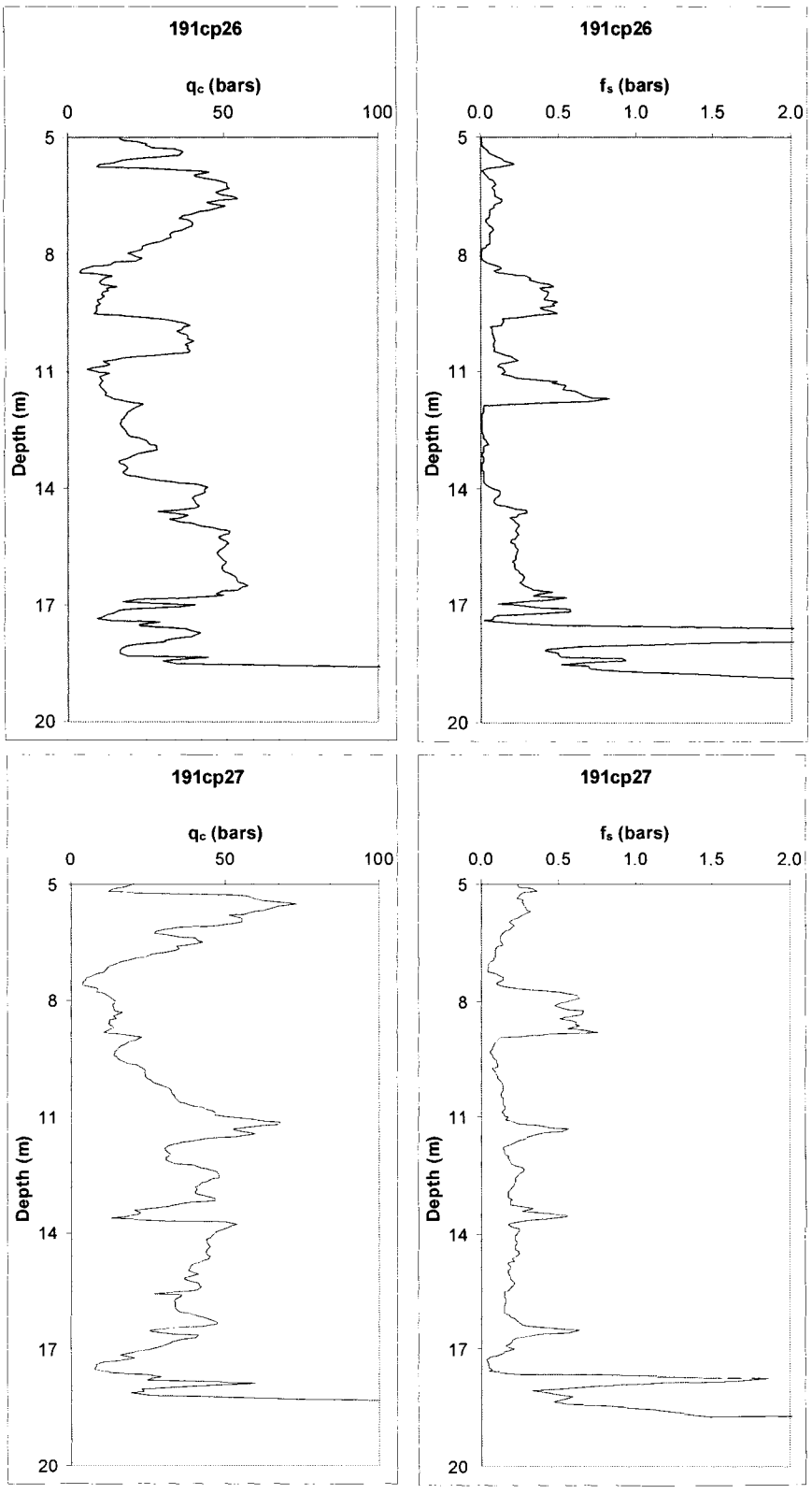

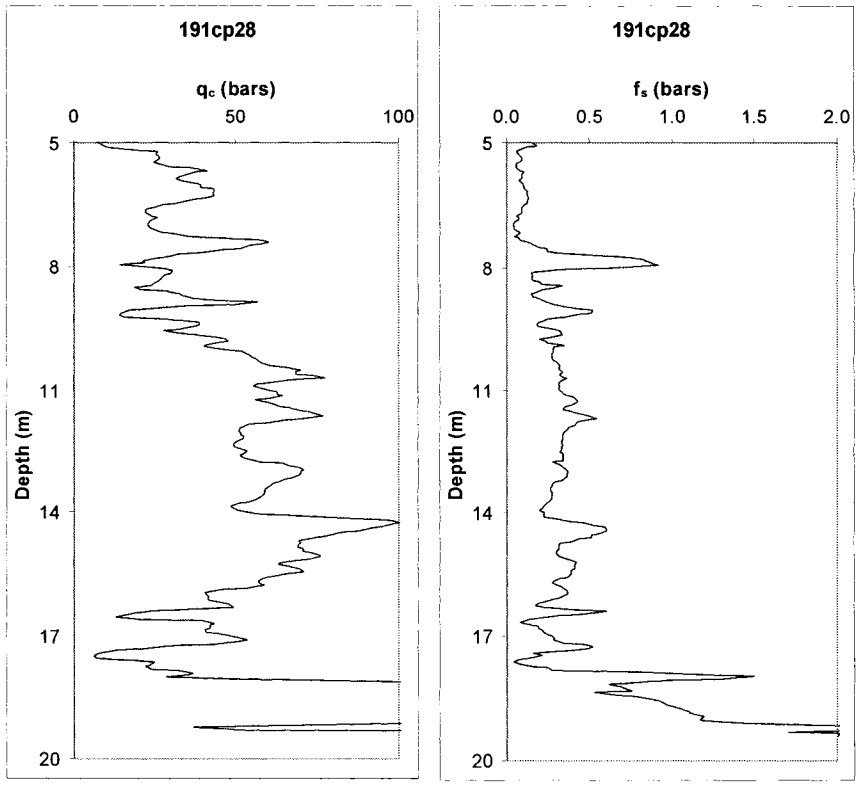

Post-Embankment Aurora Pond Load Test CPT Data

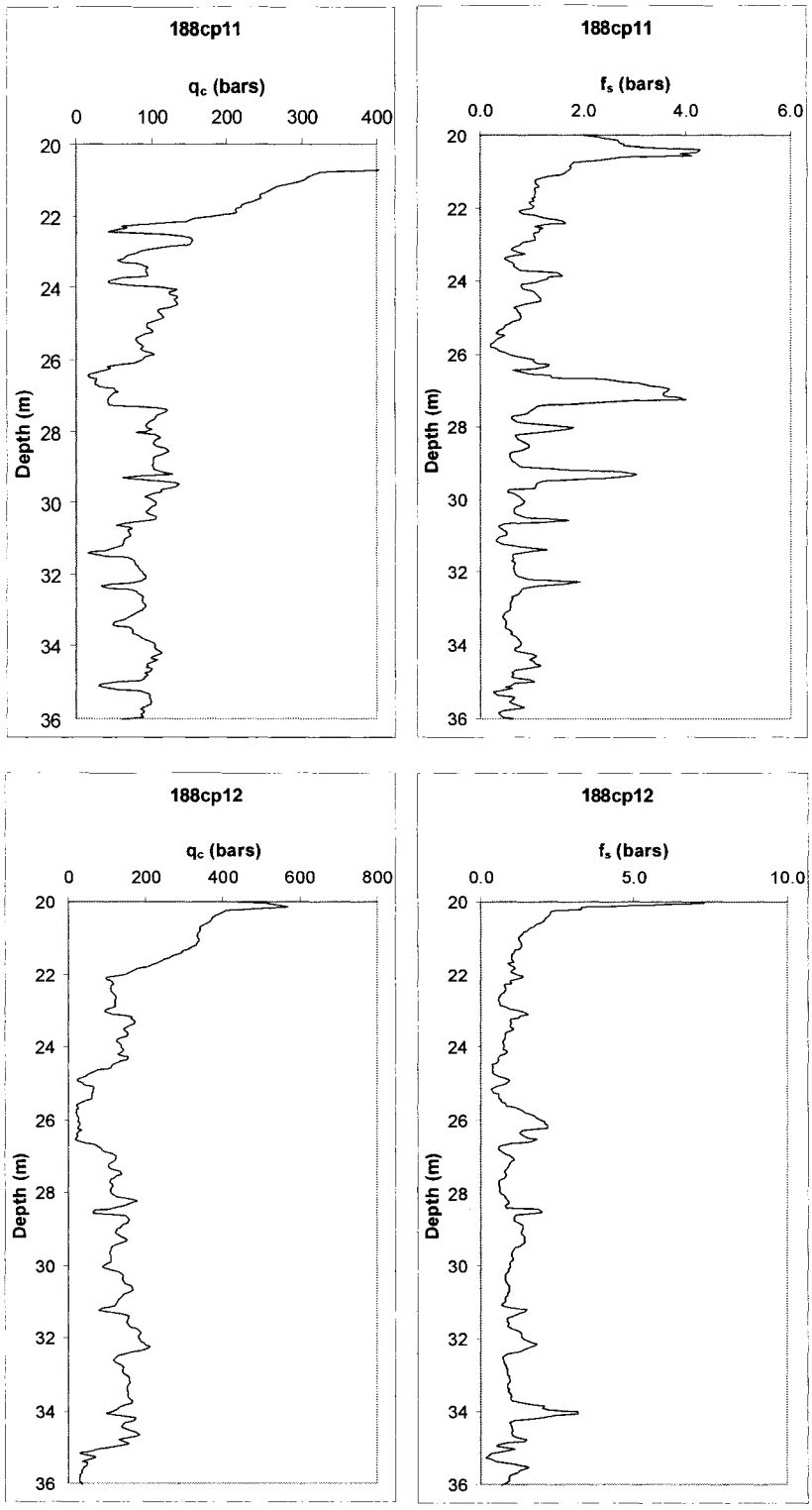

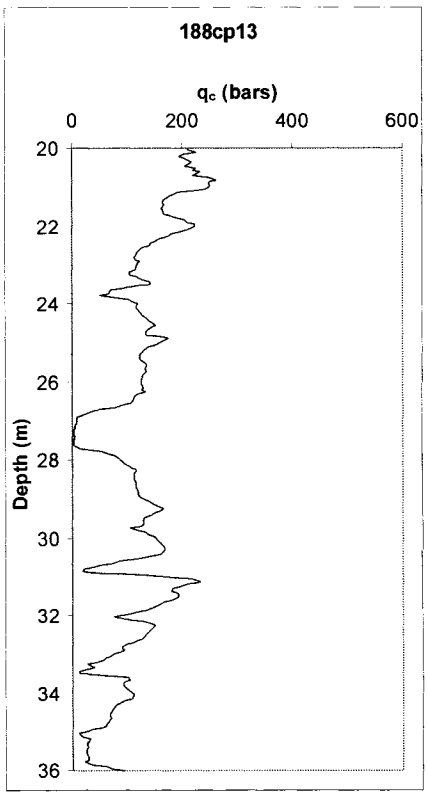

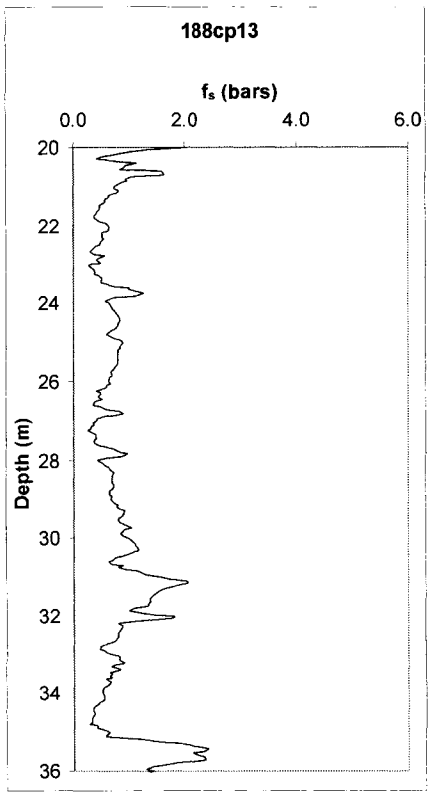

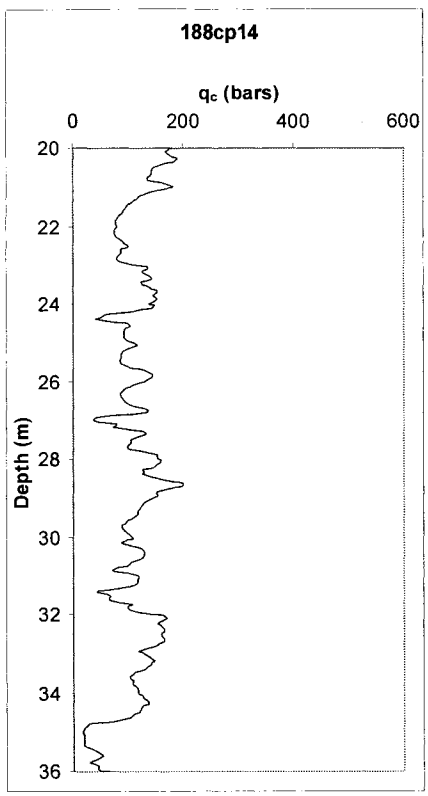

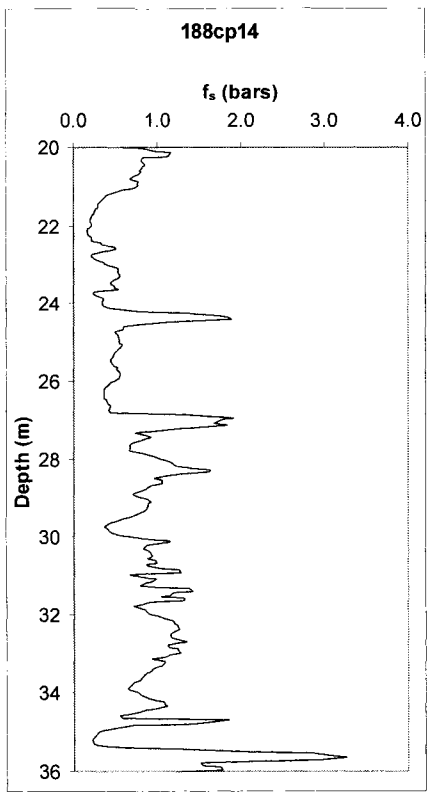

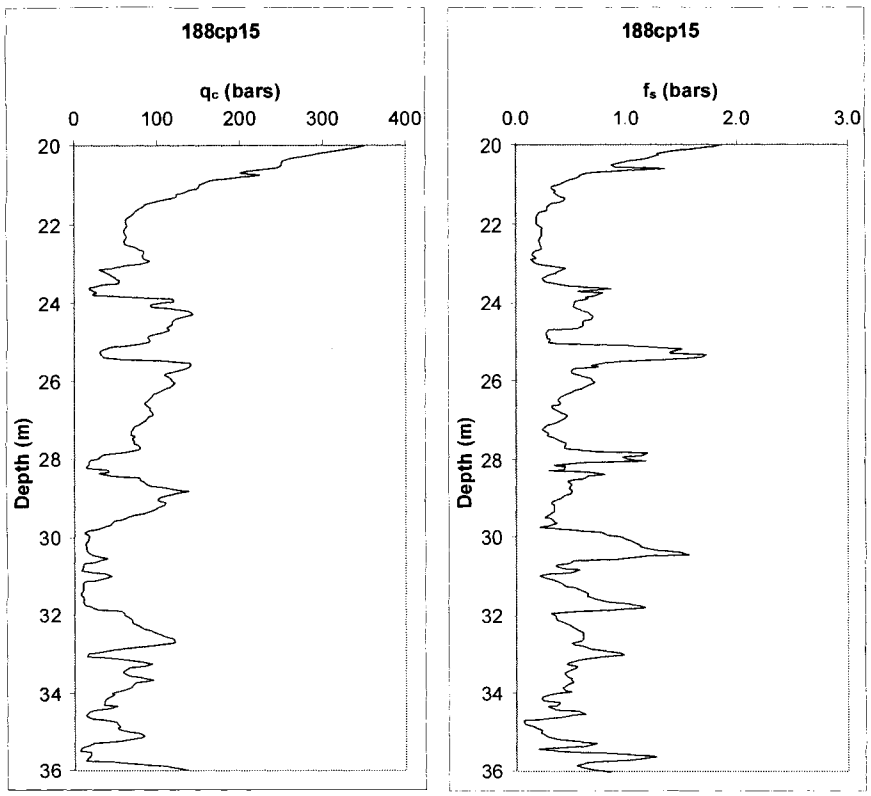

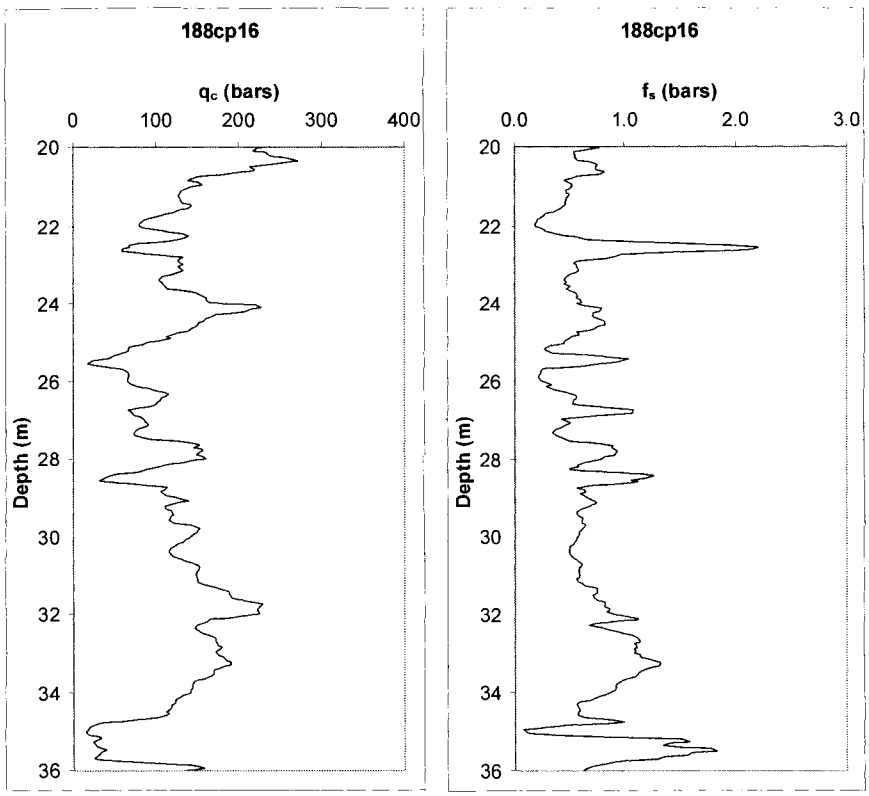

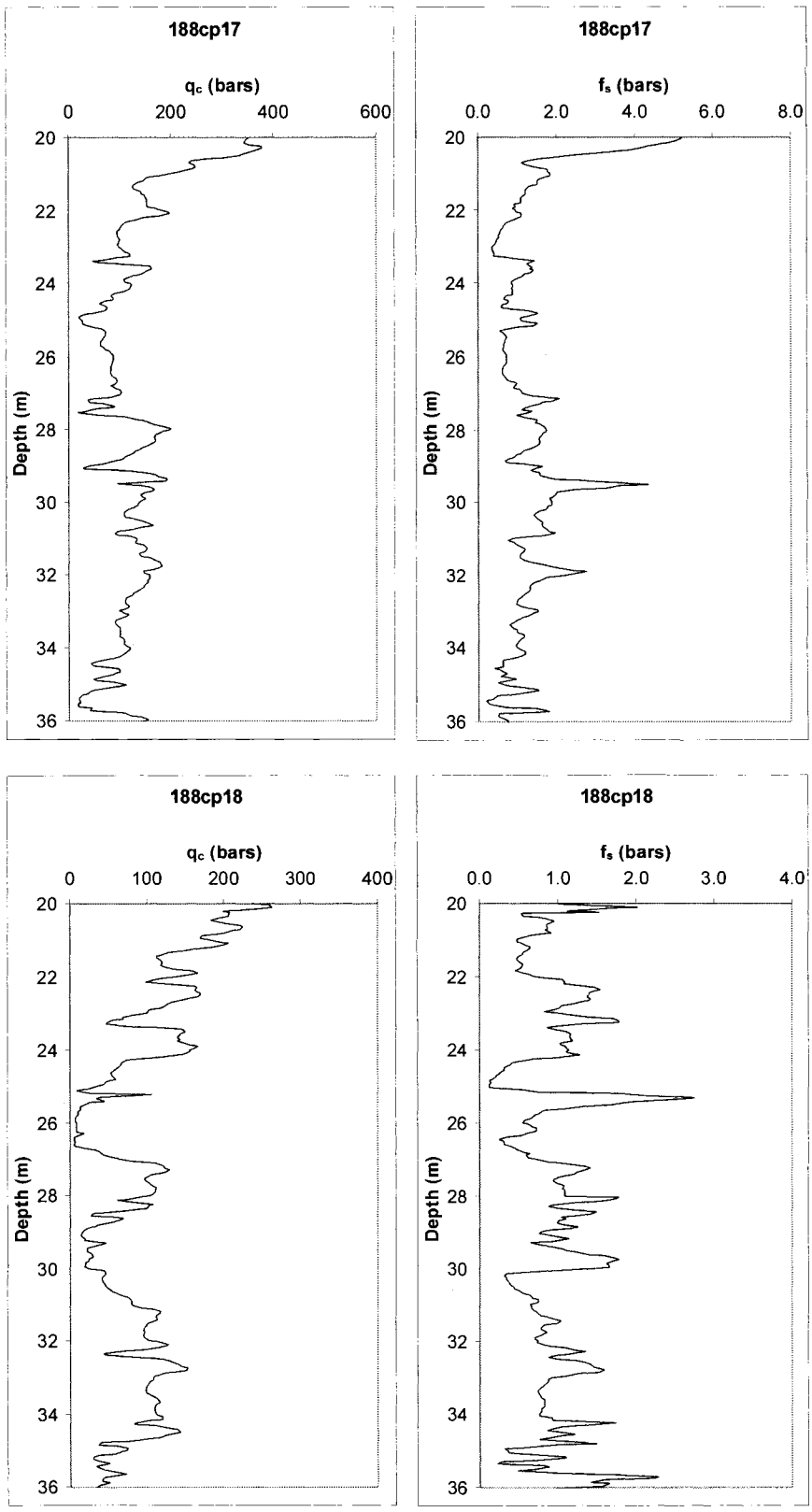

APPENDIX B: SPT_U DESIGN AND ASSEMBLY

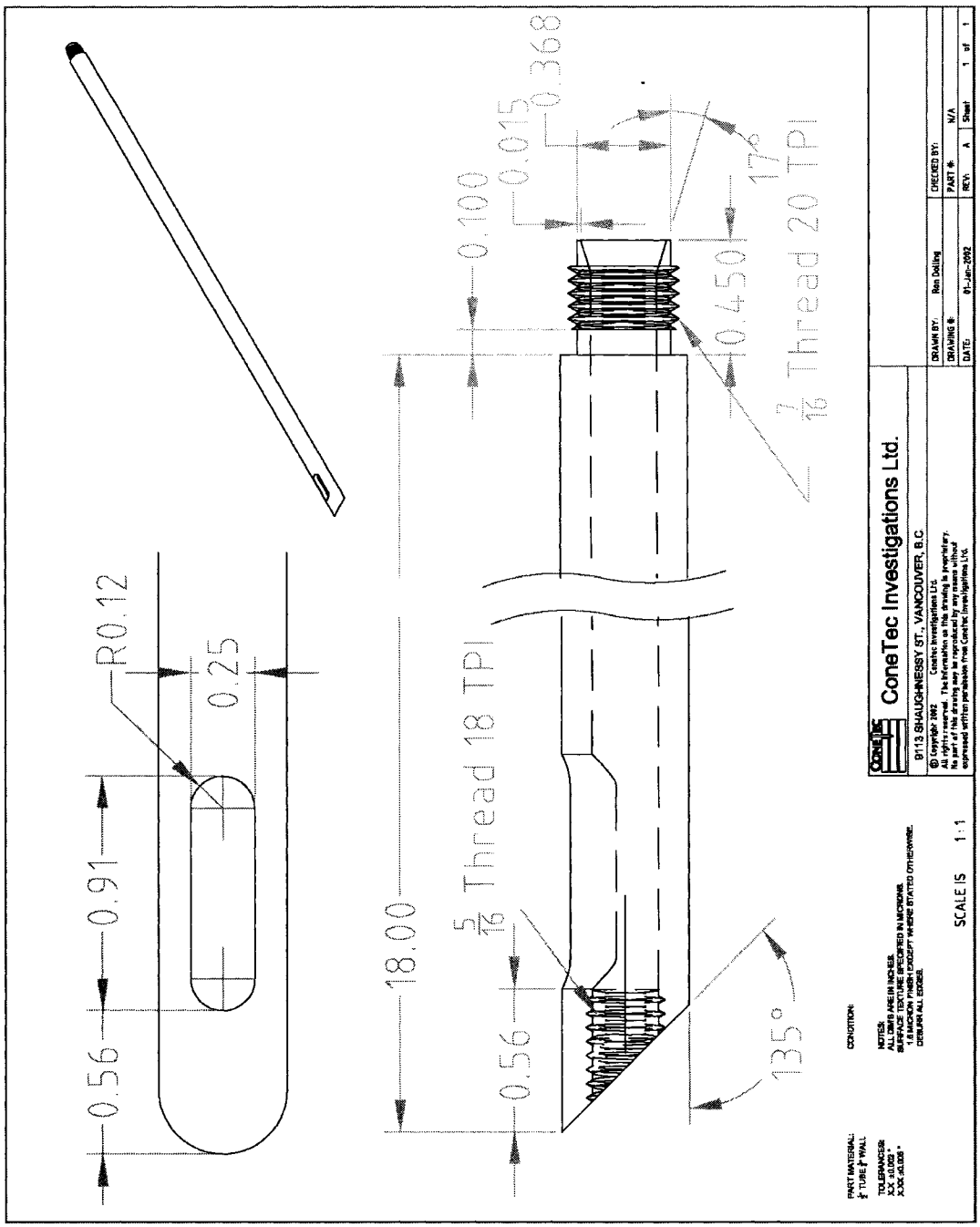

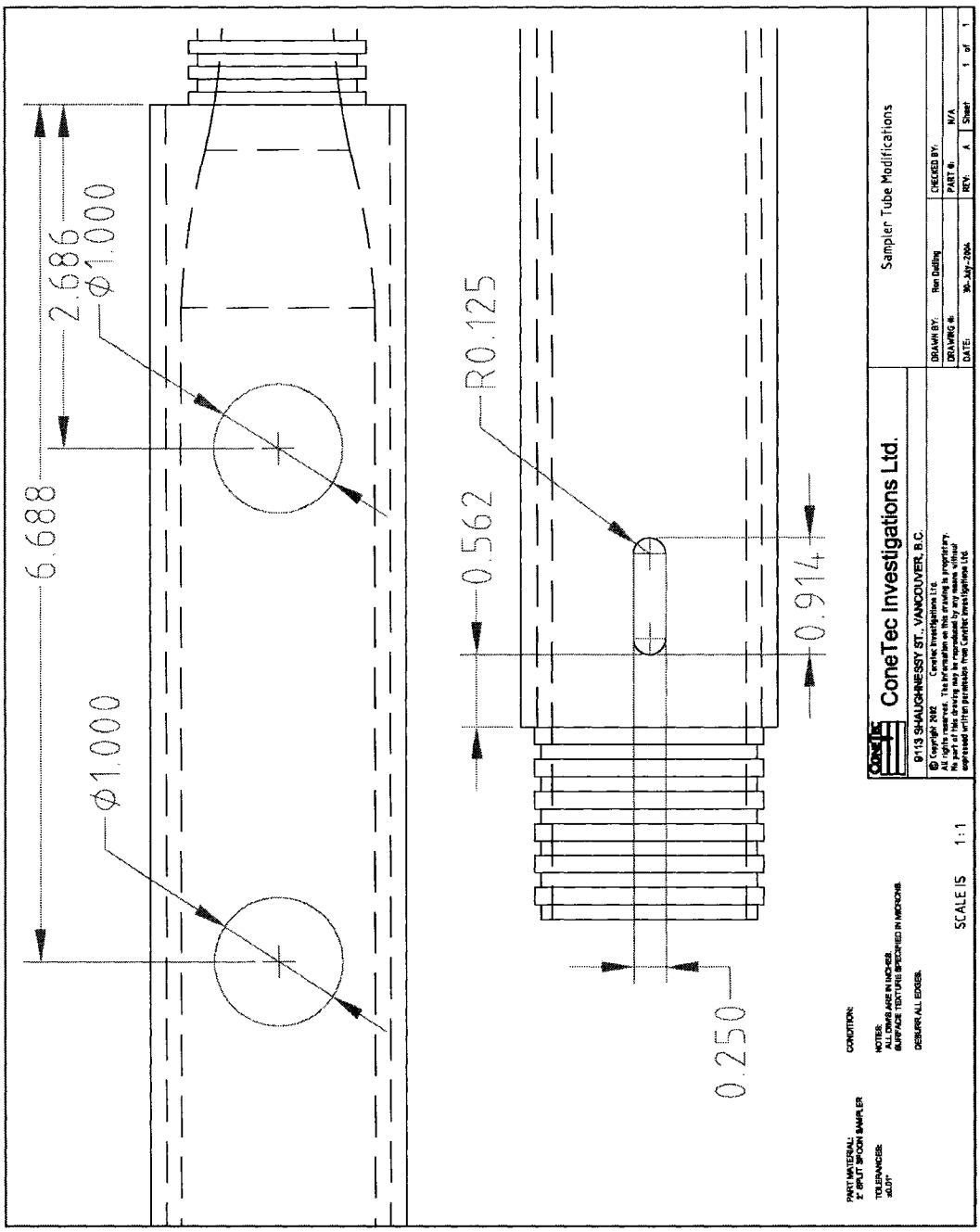

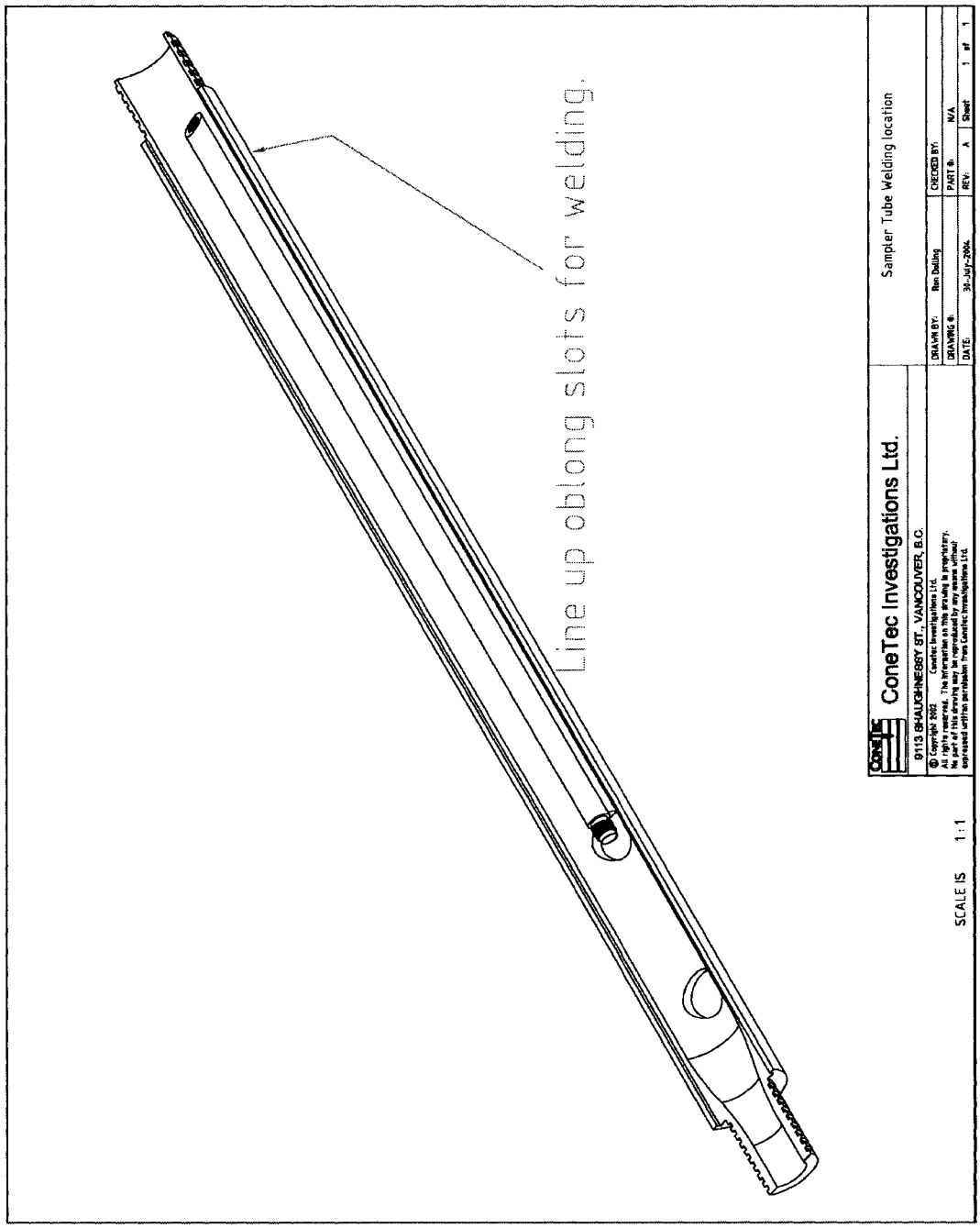

APPENDIX C: SPT_U PORE PRESSURE RESPONSE

SPTu Pore Pressure Response From 1.52 m Depth

Blow 1 pore pressure response:

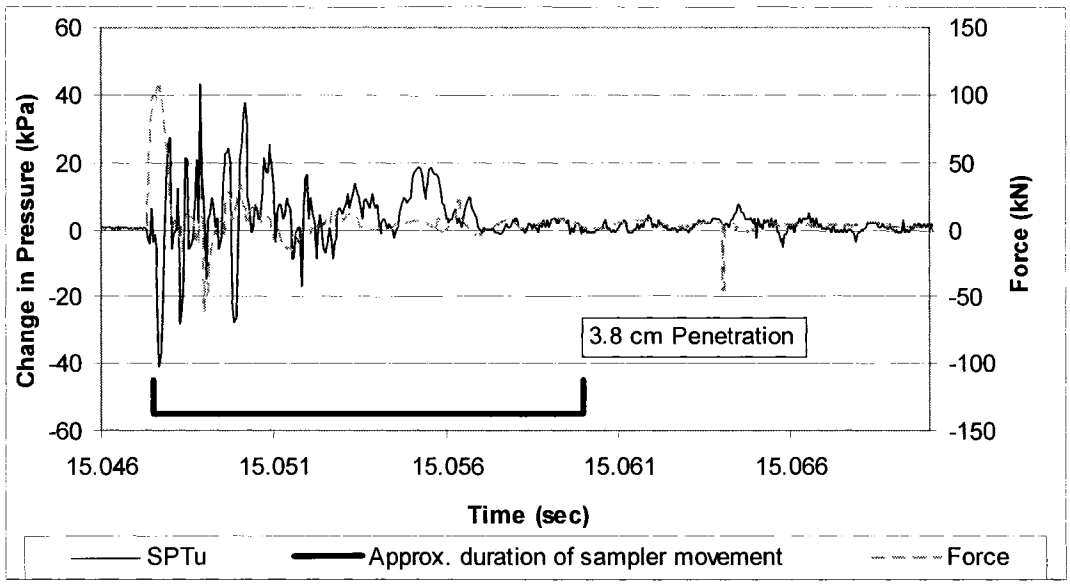

Blow 2 pore pressure response:

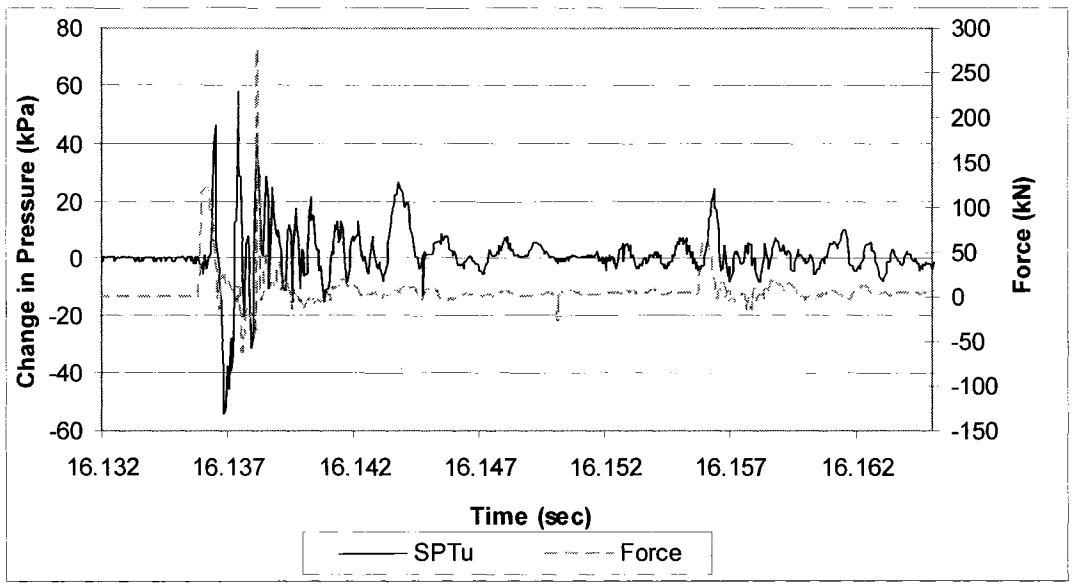

Blow 3 pore pressure response:

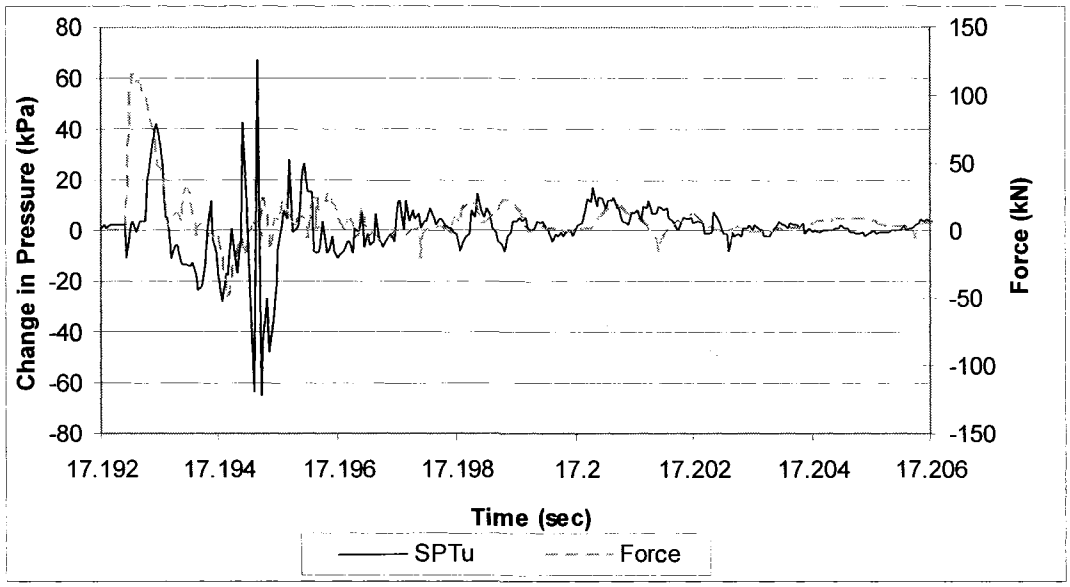

Blow 4 pore pressure response:

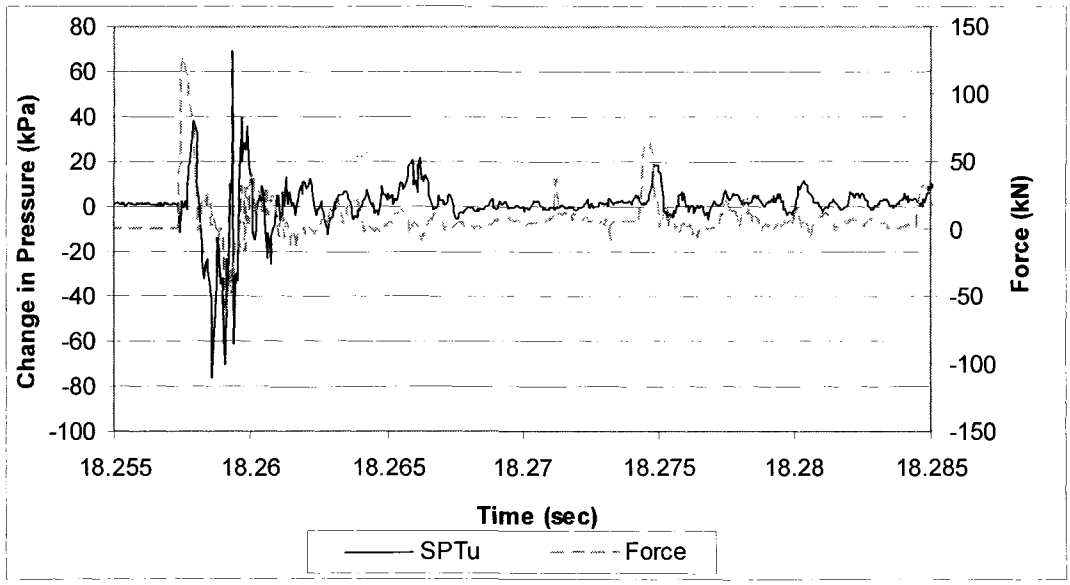

Blow 5 pore pressure response:

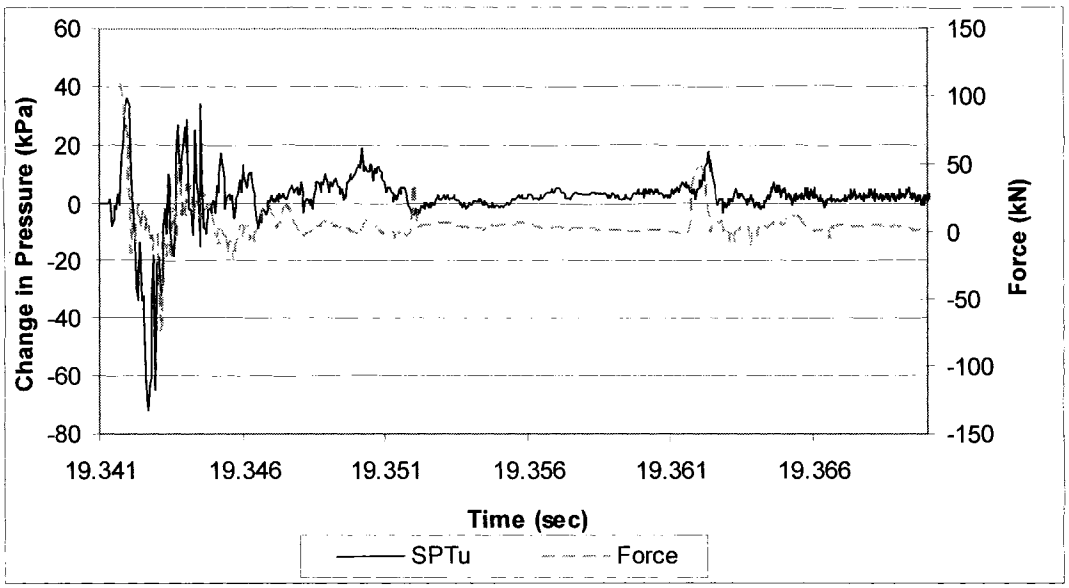

Blow 6 pore pressure response:

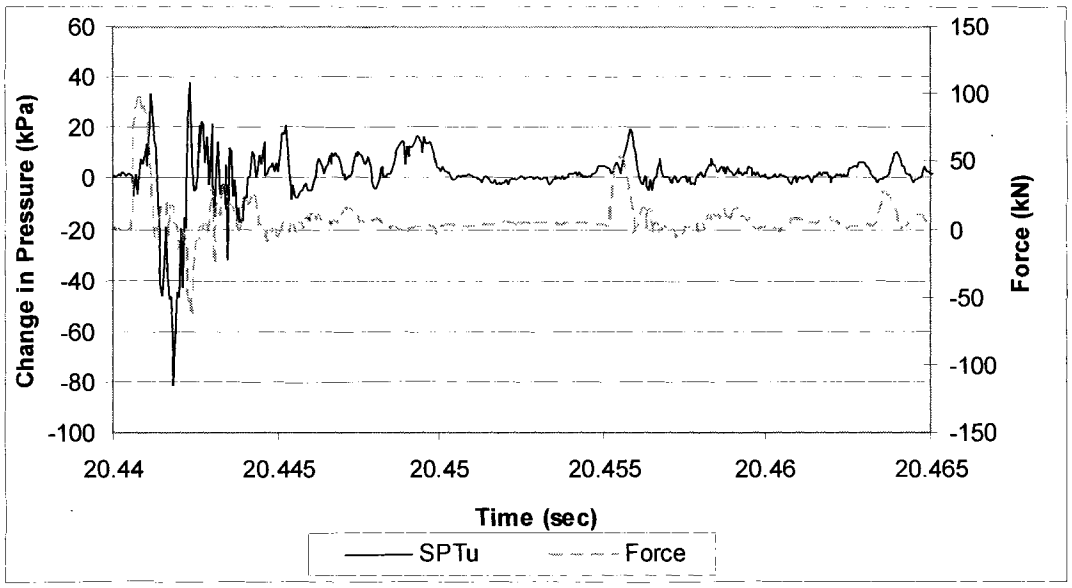

Blow 7 pore pressure response:

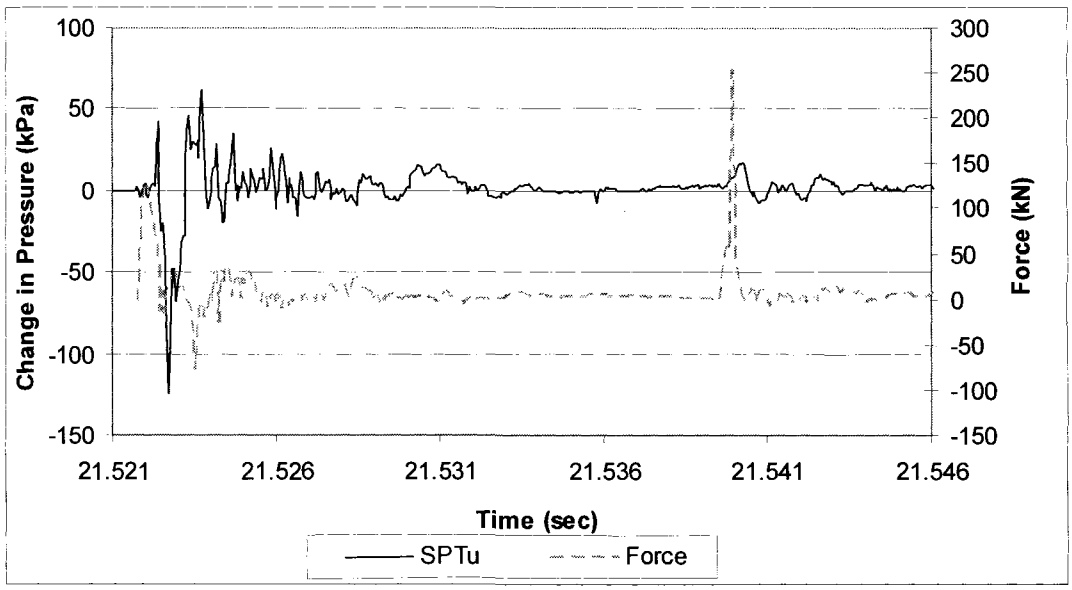

Blow 8 pore pressure response:

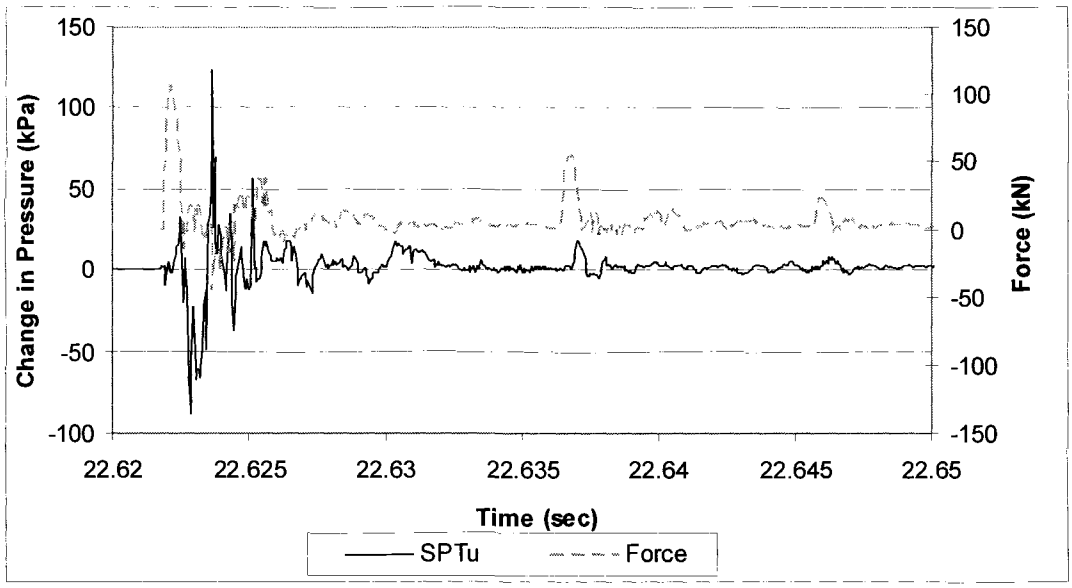

Blow 9 pore pressure response:

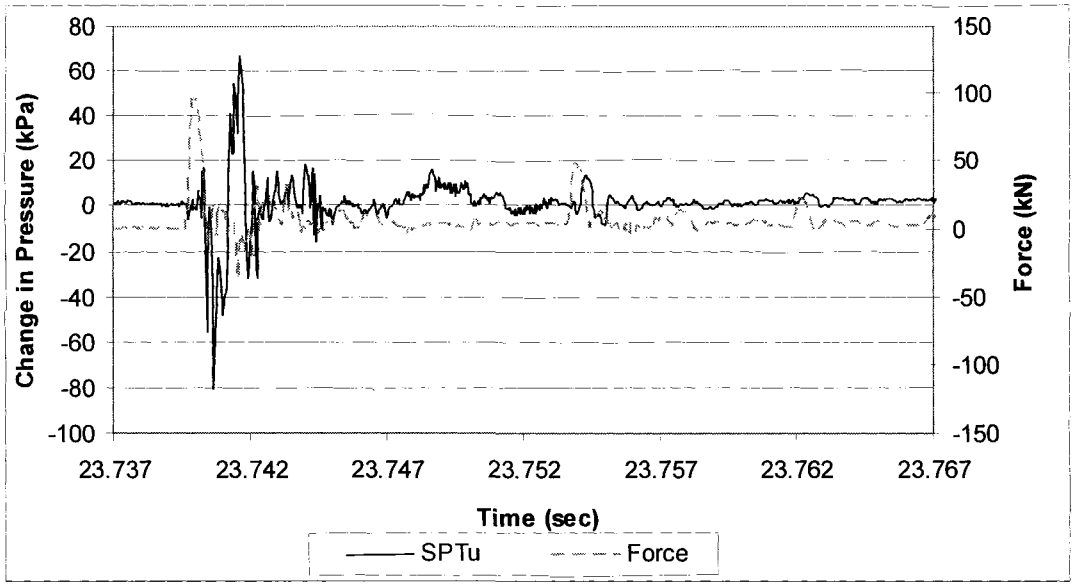

Blow 10 pore pressure response:

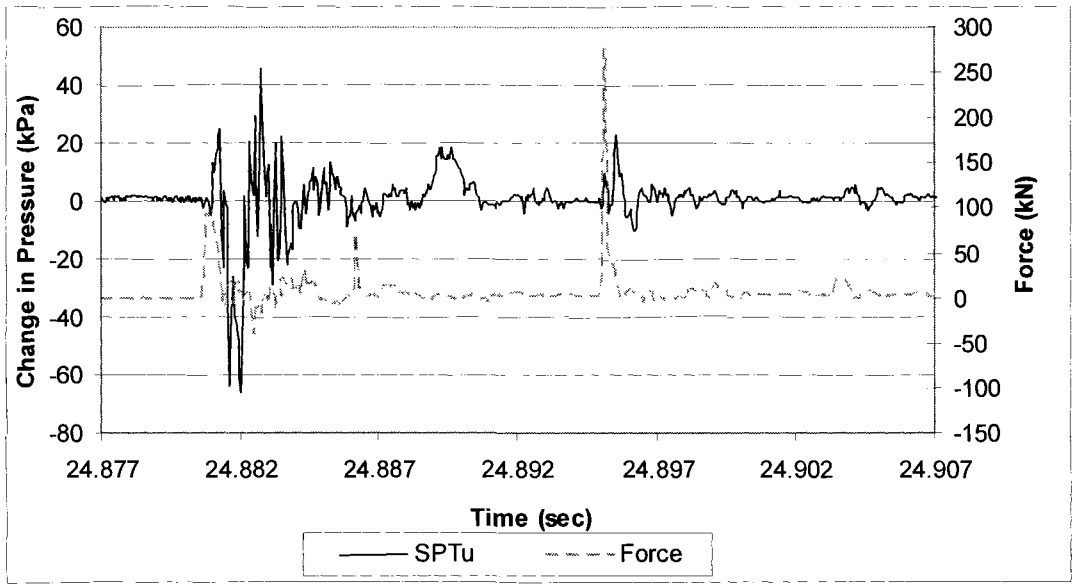

Blow 11 pore pressure response:

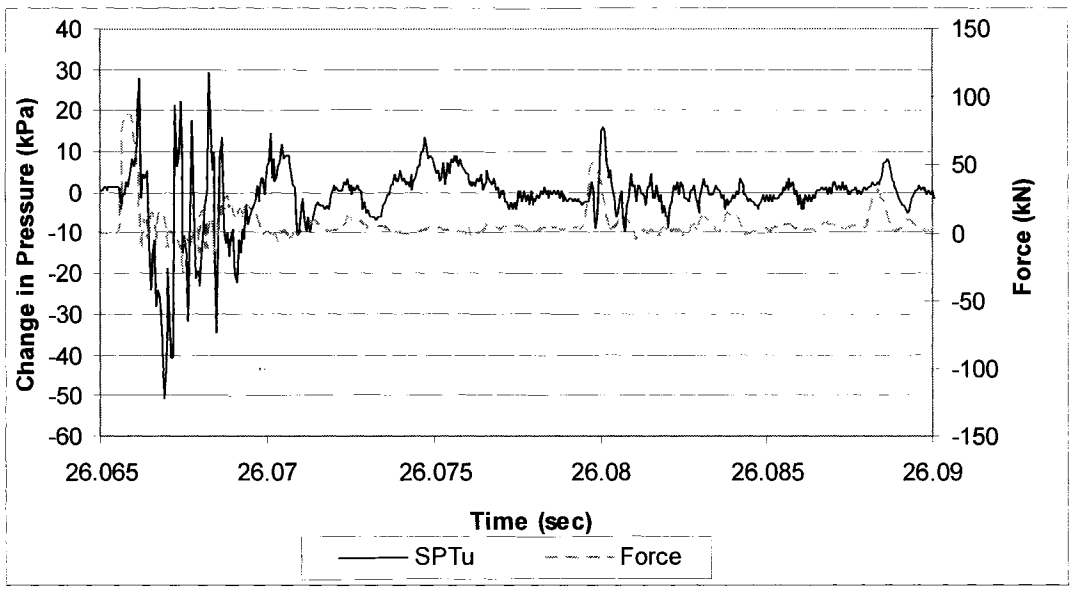

SPTu Pore Pressure Response From 7.72 m Depth

Blow 1 pore pressure response

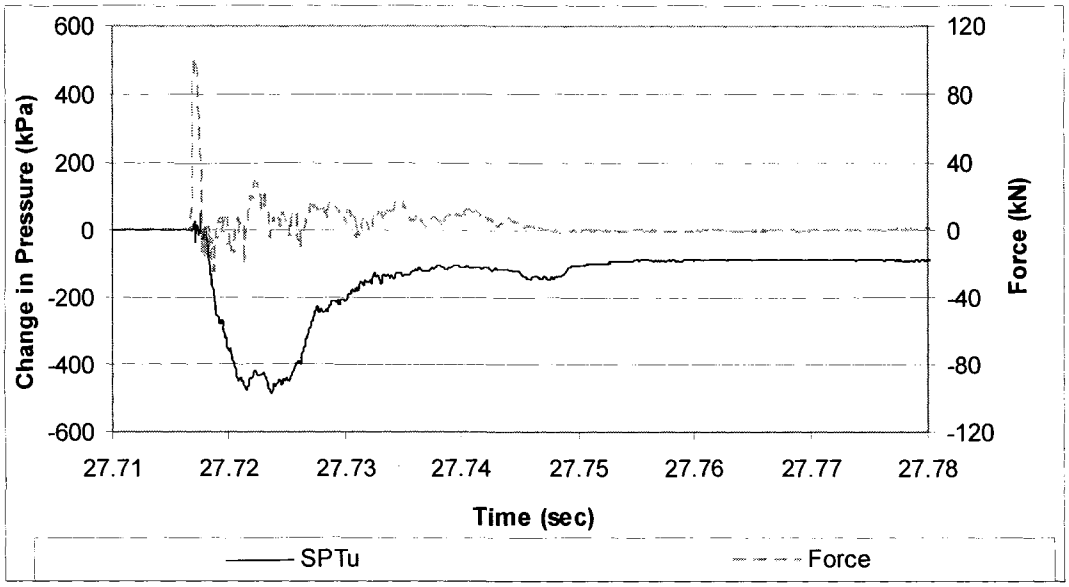

Blow 2 pore pressure response

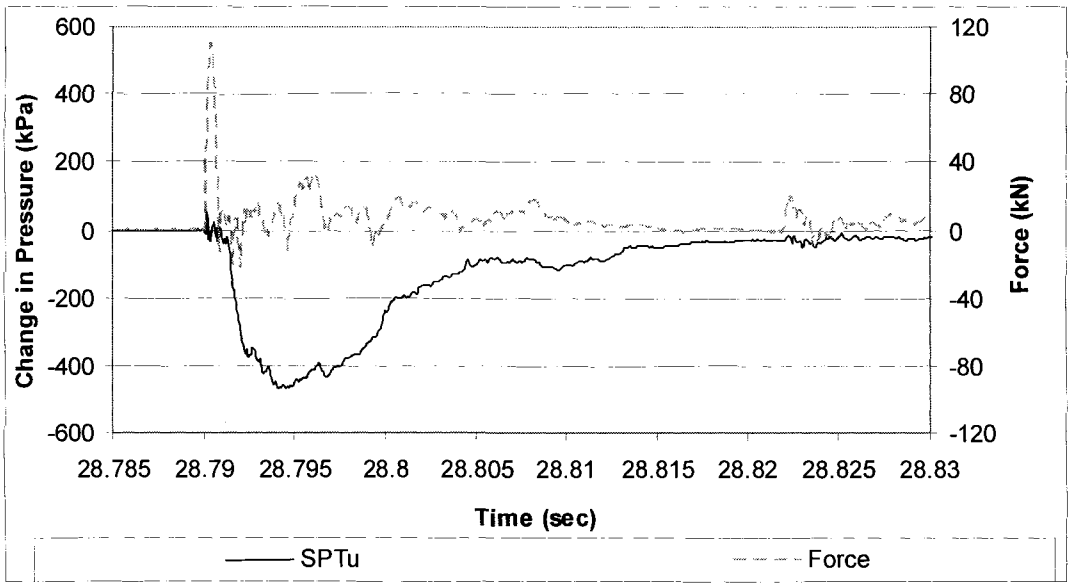

Blow 3 pore pressure response

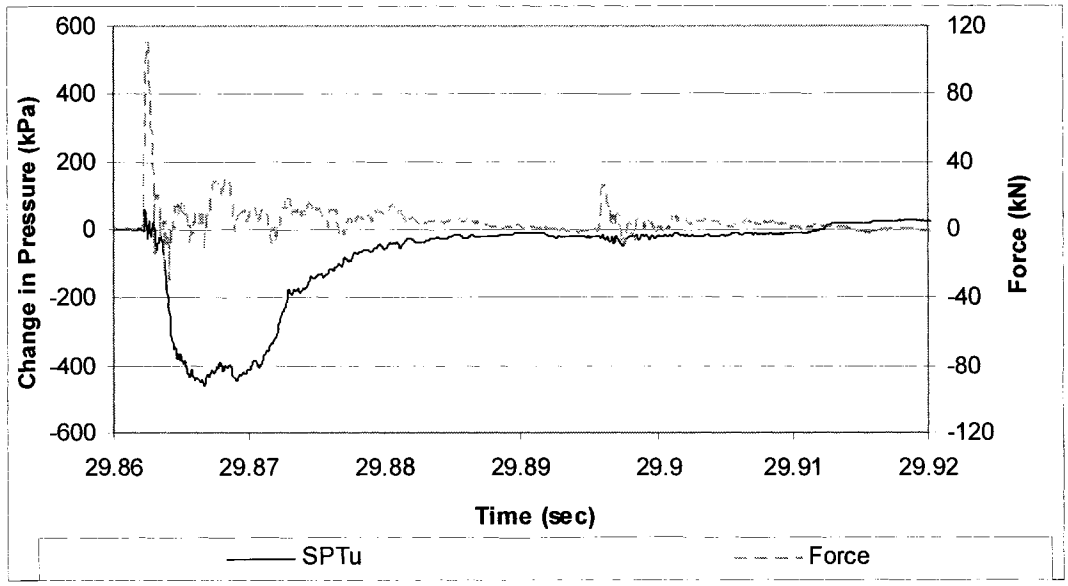

Blow 4 pore pressure response

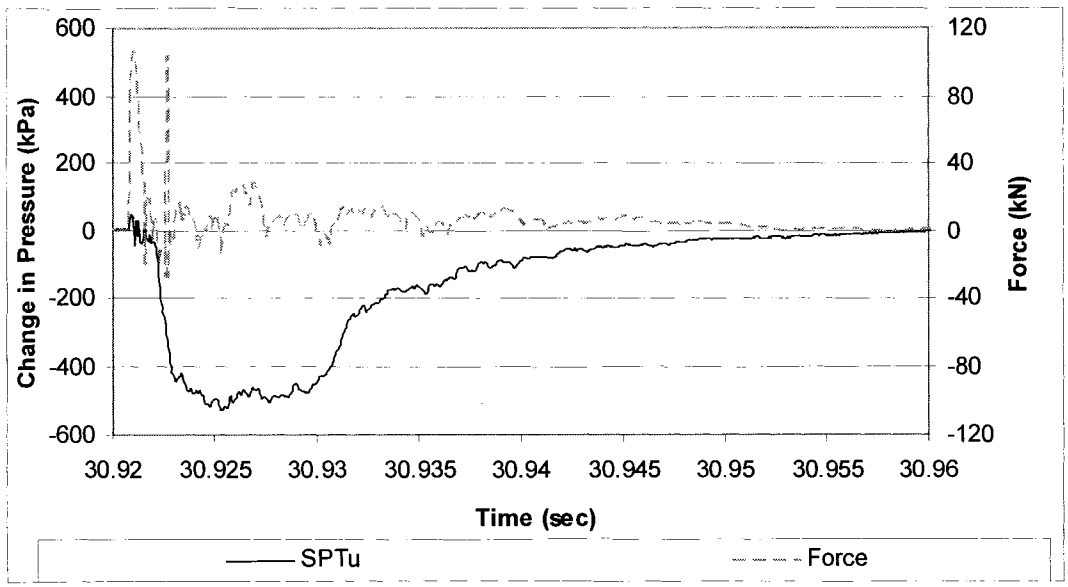

Blow 5 pore pressure response

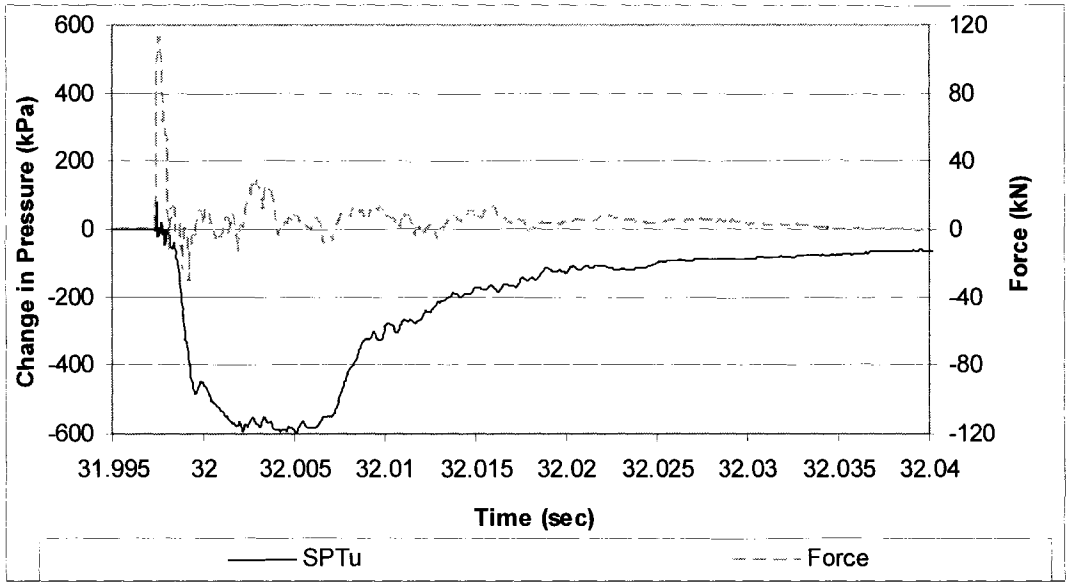

Blow 6 pore pressure response

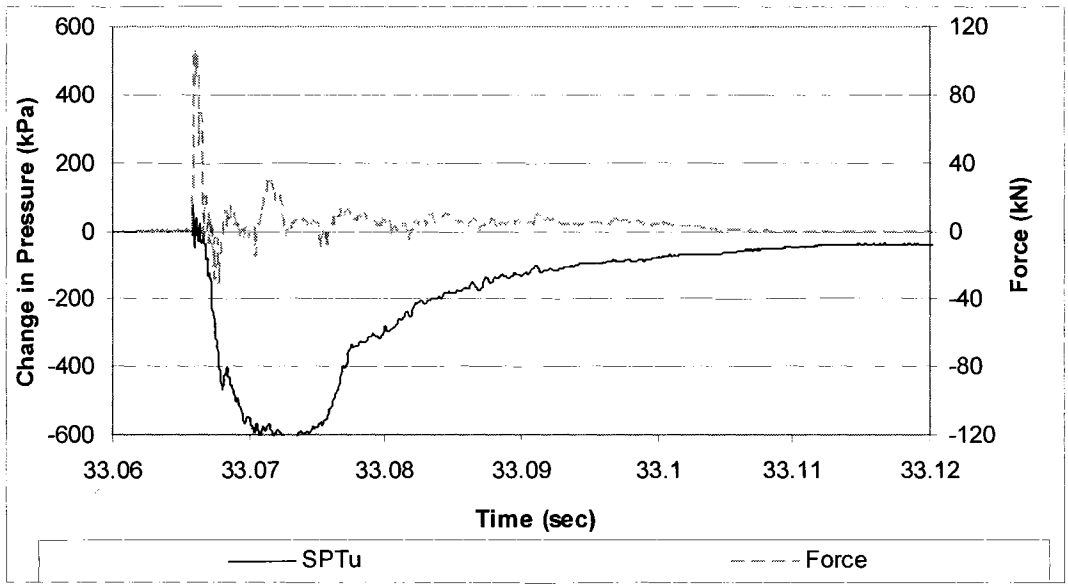

Blow 7 pore pressure response

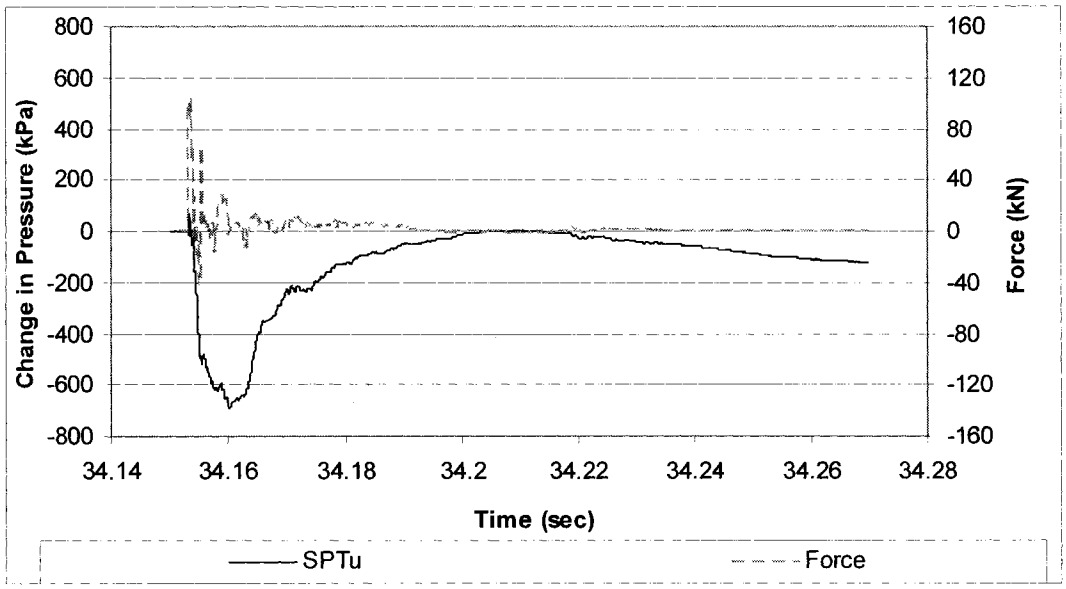

Blow 8 pore pressure response

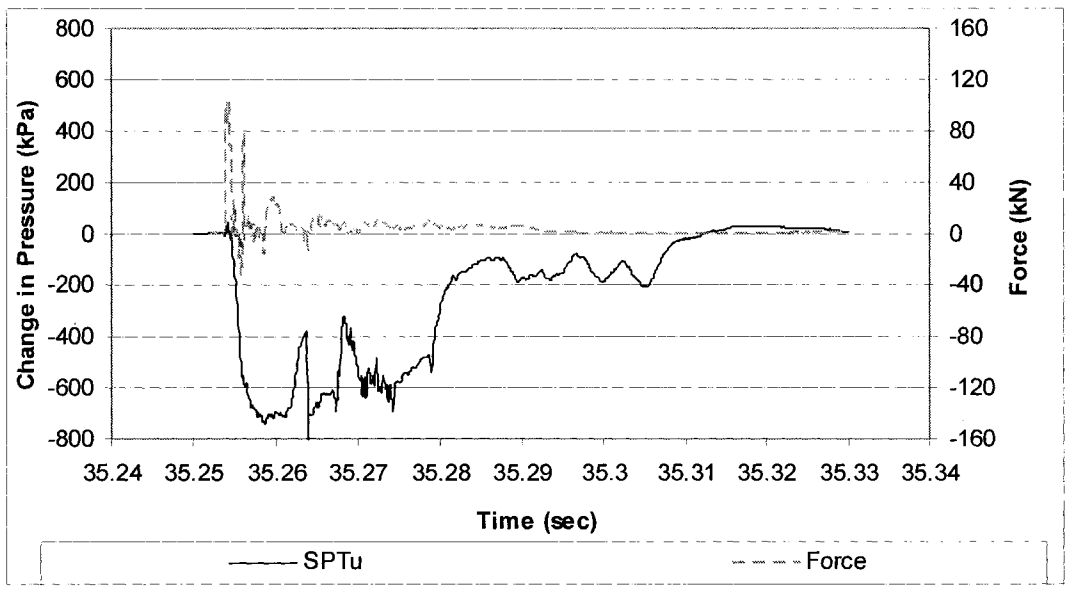

Blow 9 pore pressure response

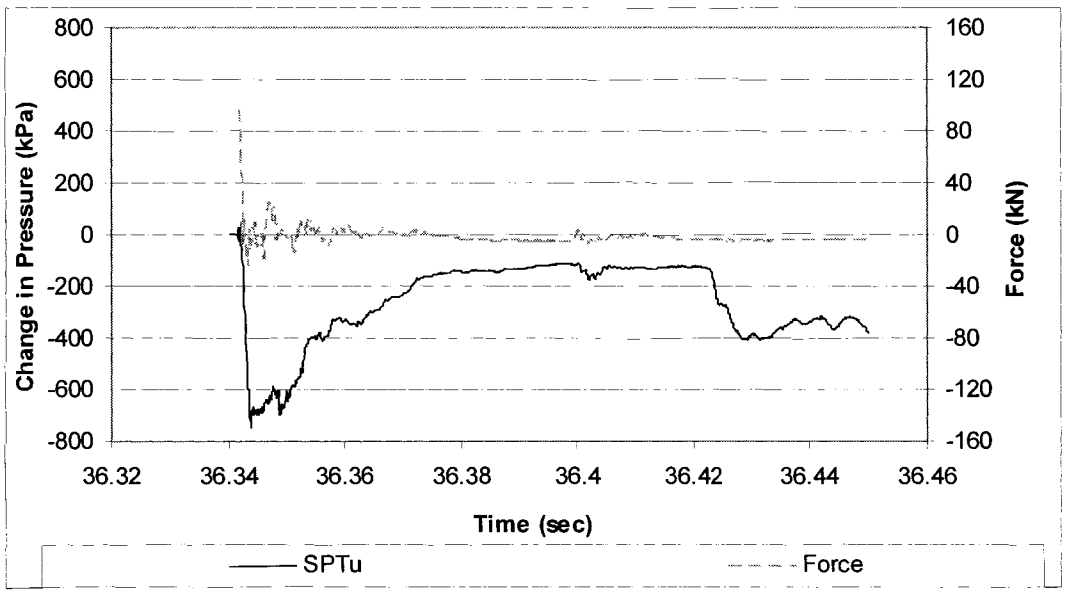

Blow 10 pore pressure response

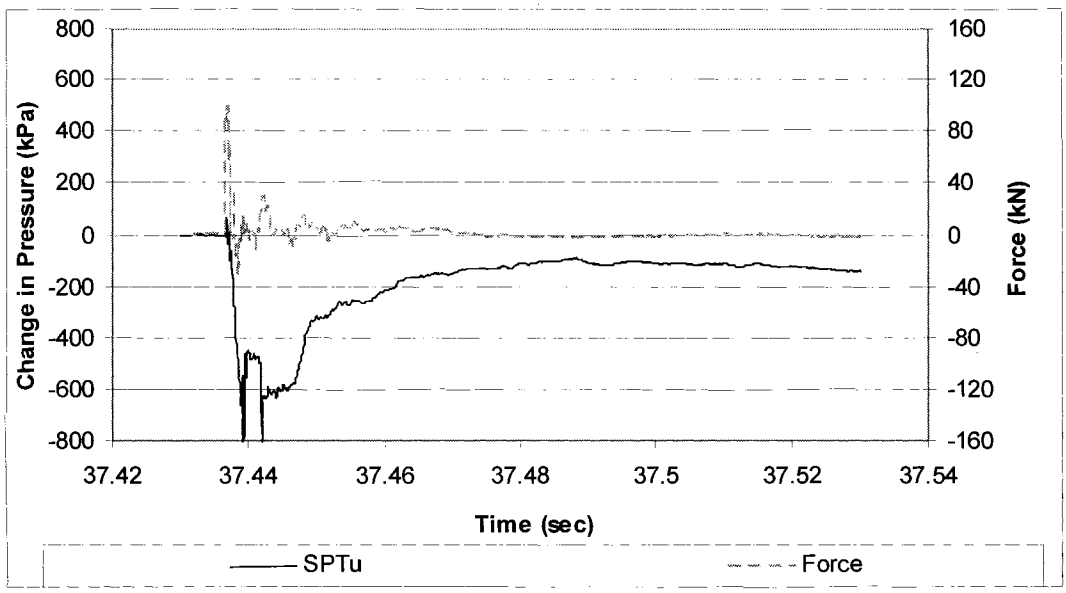

Blow 11 pore pressure response

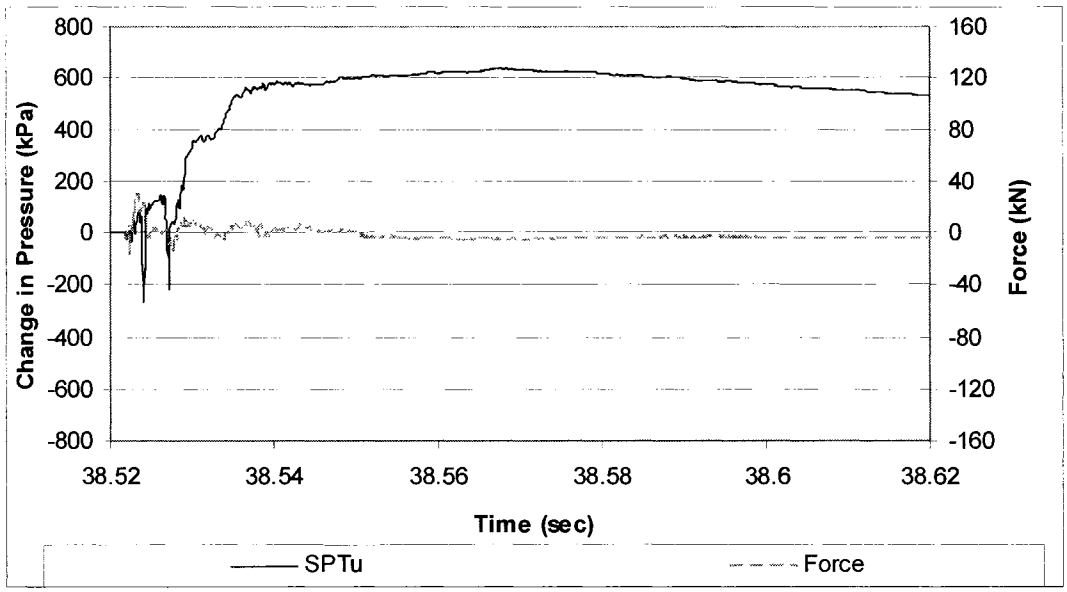

Blow 12 pore pressure response

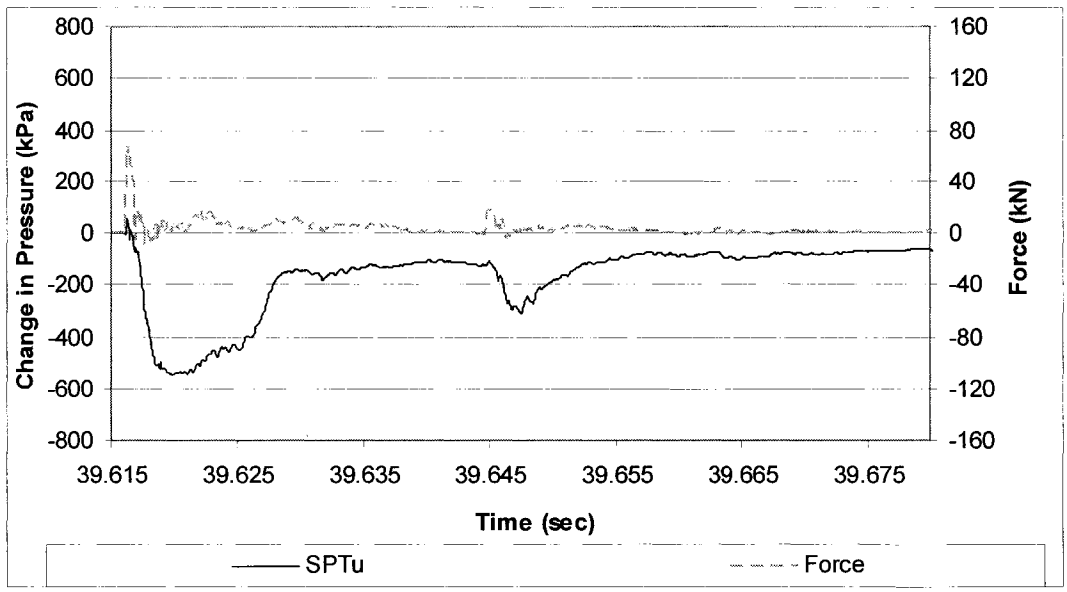

SPTu Pore Pressure Response From 8.56 m Depth

Blow 1 pore pressure response

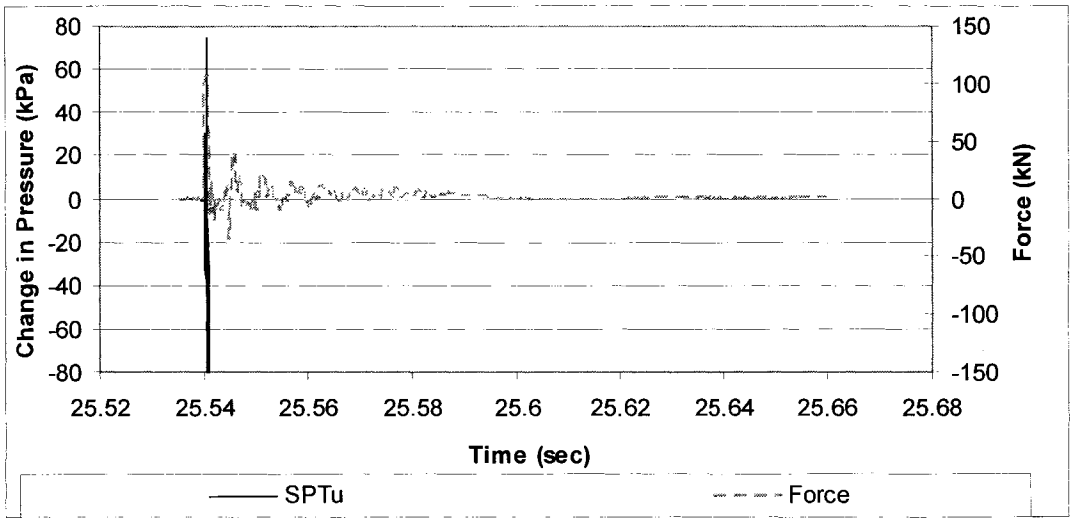

Blow 2 pore pressure response

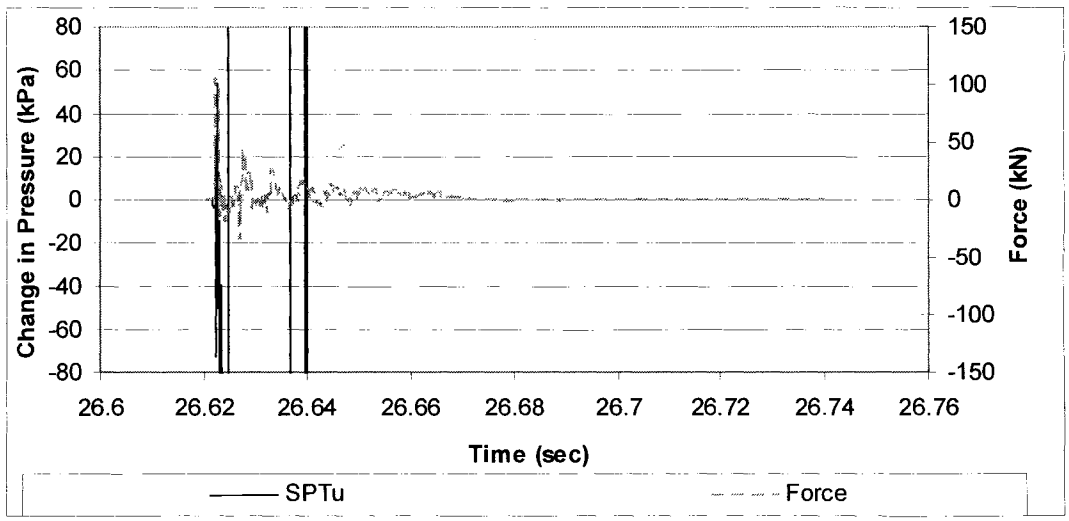

Blow 3 pore pressure response

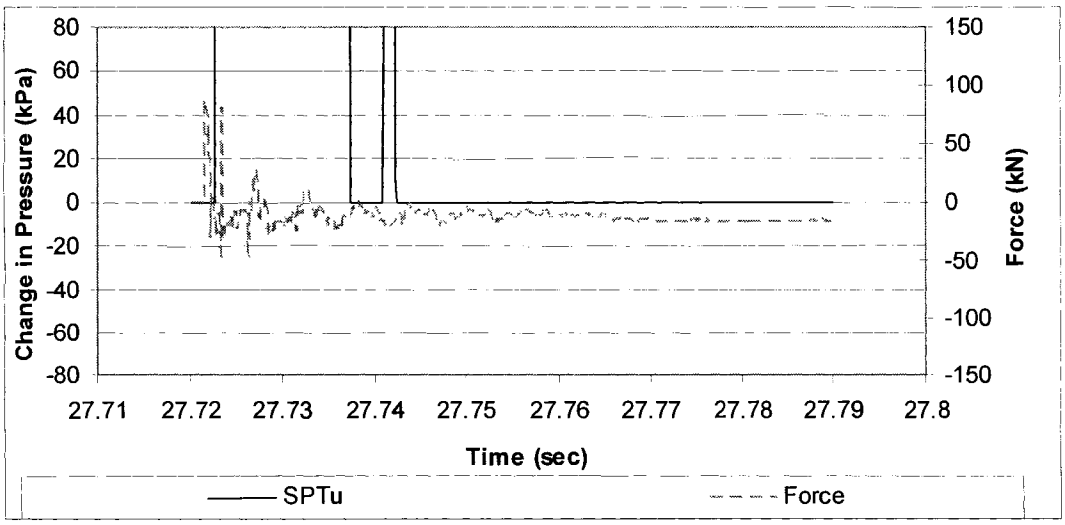

Blow 4 pore pressure response

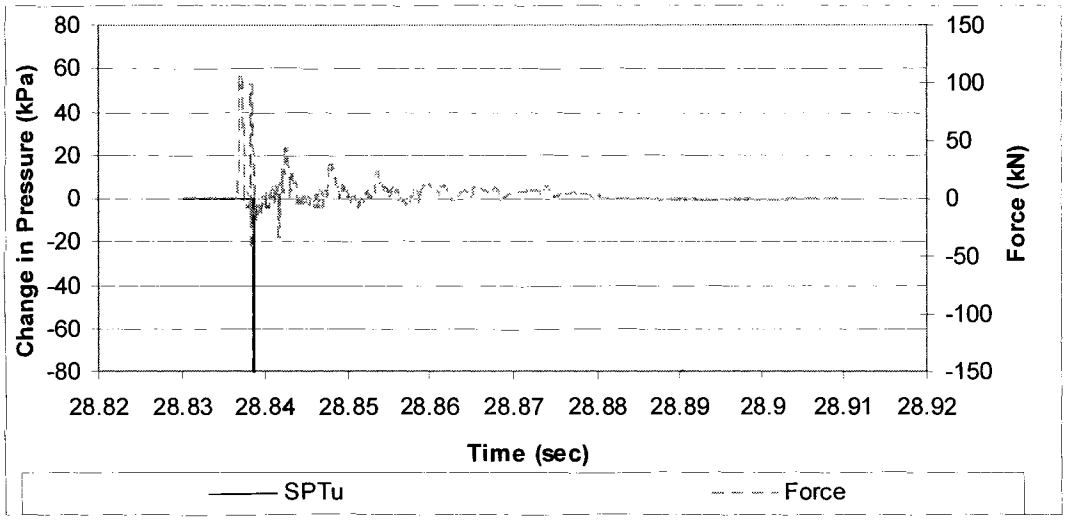

Blow 5 pore pressure response

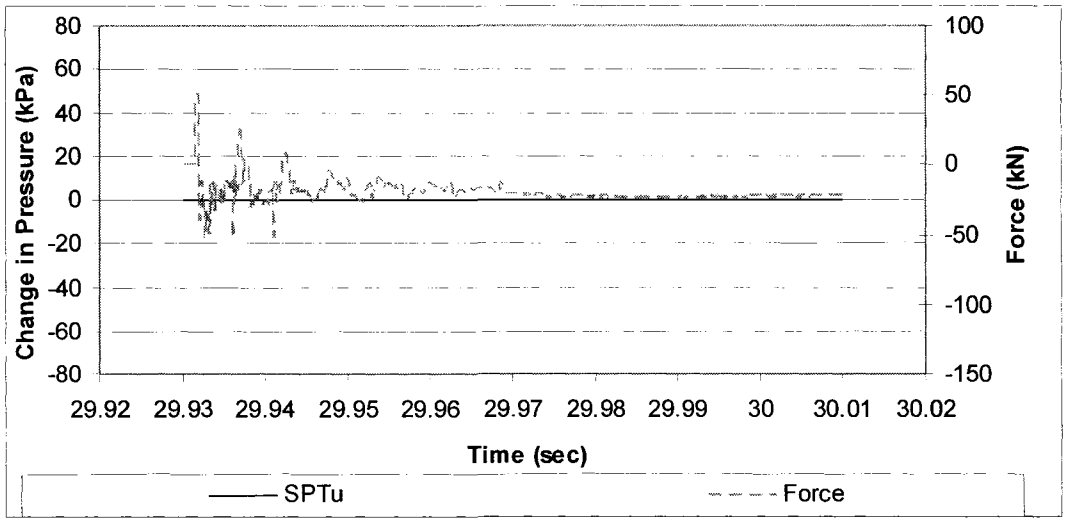

Blow 6 pore pressure response

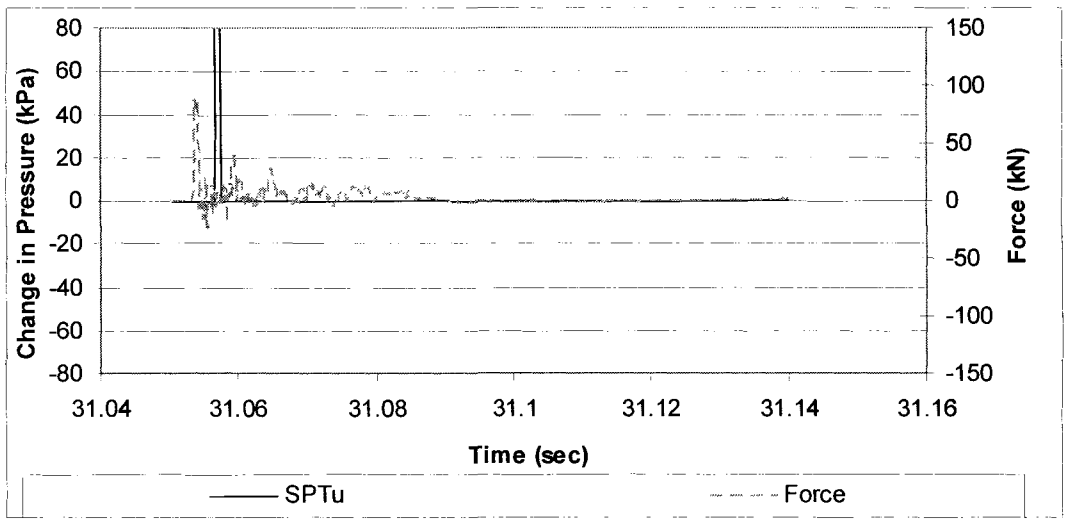

Blow 7 pore pressure response

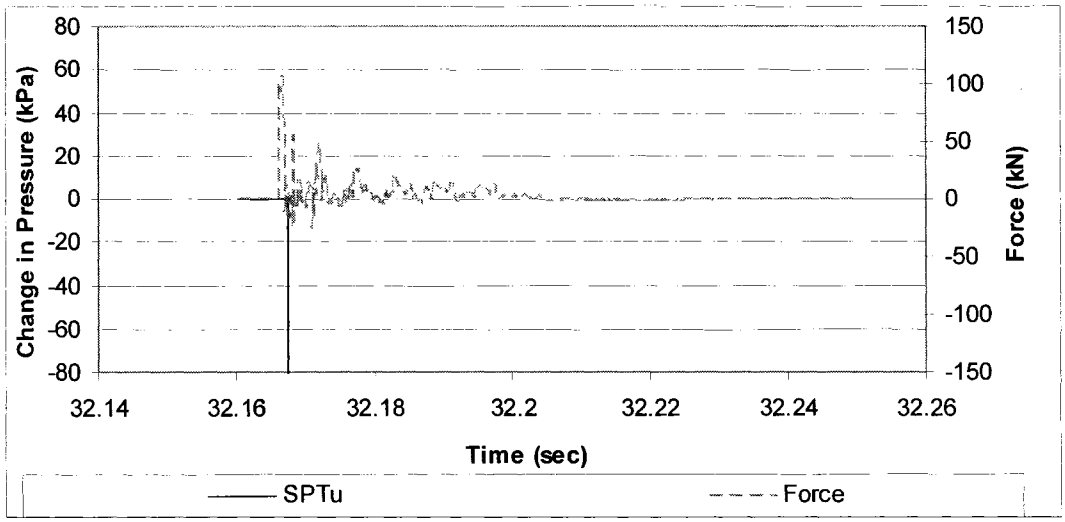

Blow 8 pore pressure response

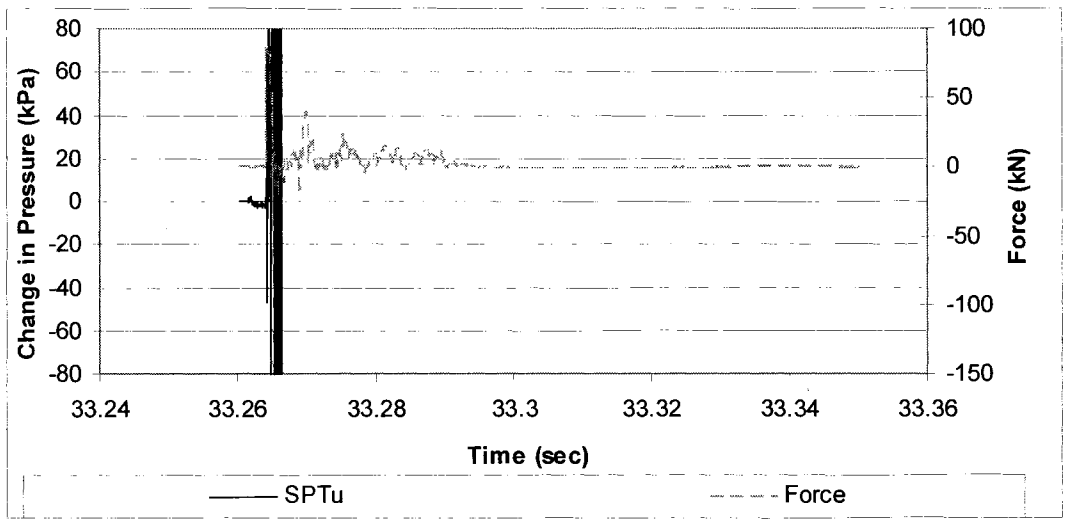

Blow 9 pore pressure response

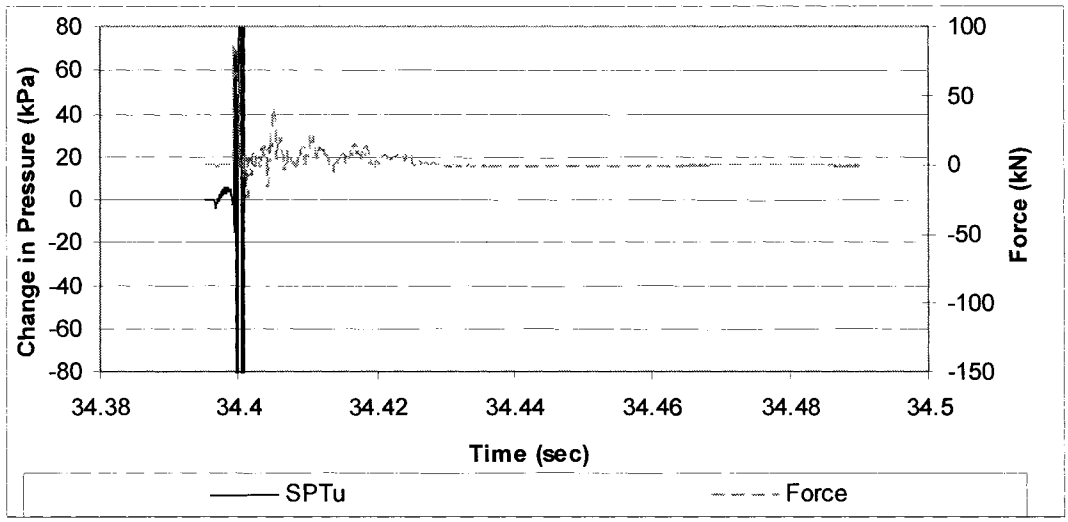

SPTu Pore Pressure Response From 9.33 m Depth

Blow 1 pore pressure response

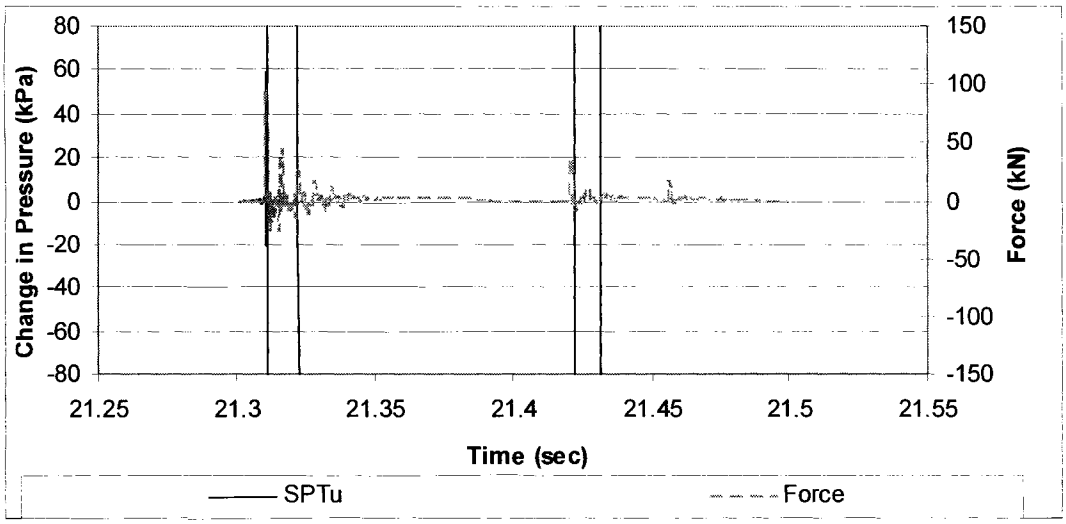

Blow 2 pore pressure response

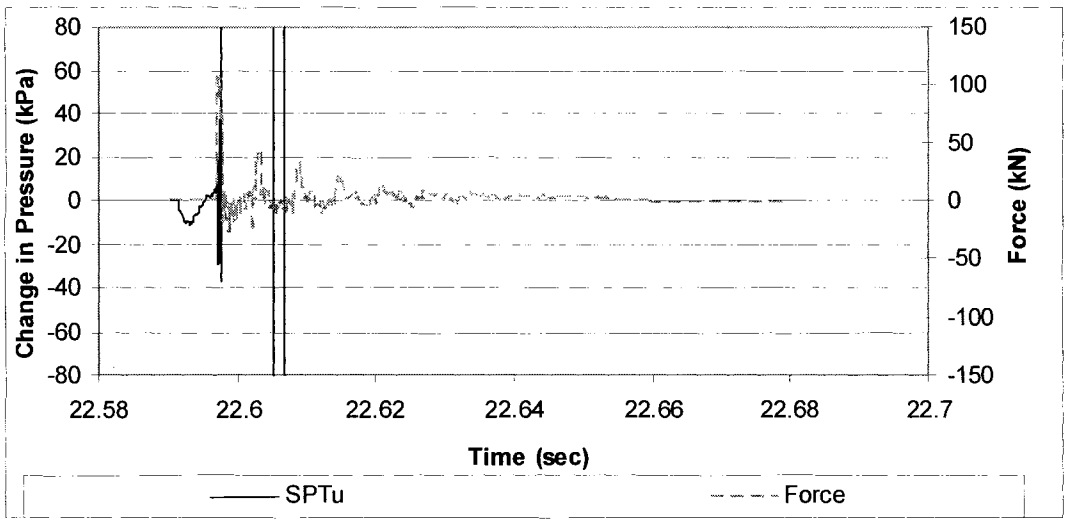

Blow 3 pore pressure response

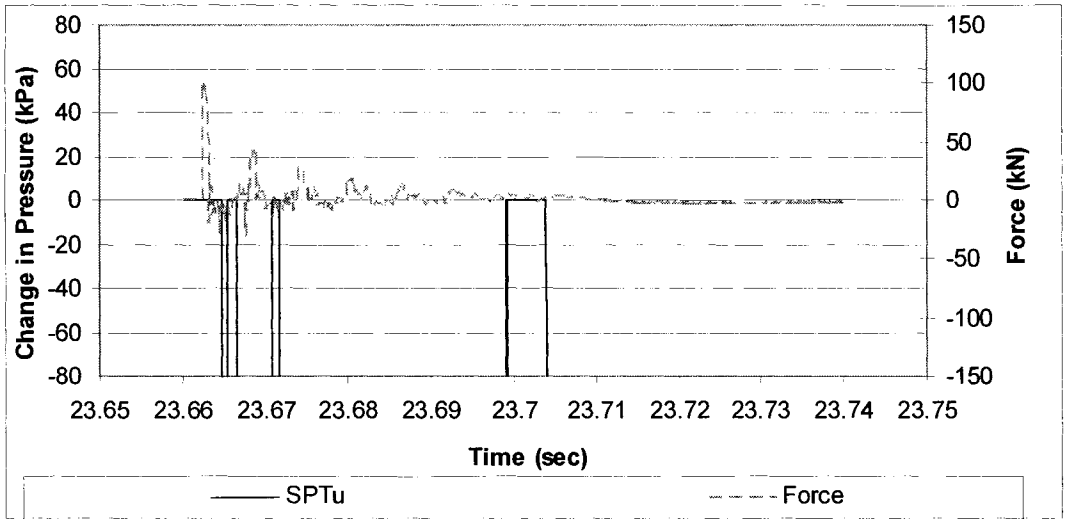

Blow 4 pore pressure response

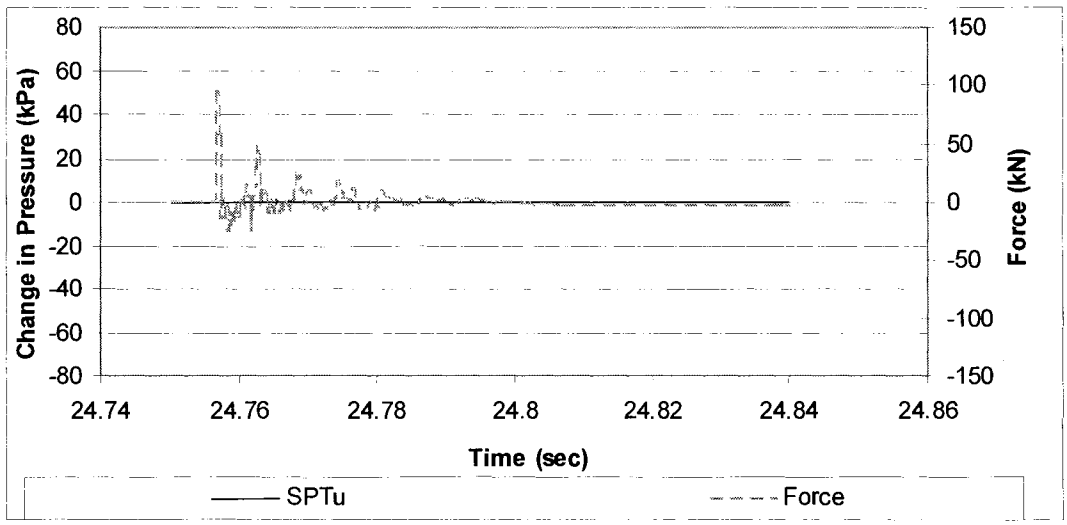

Blow 5 pore pressure response

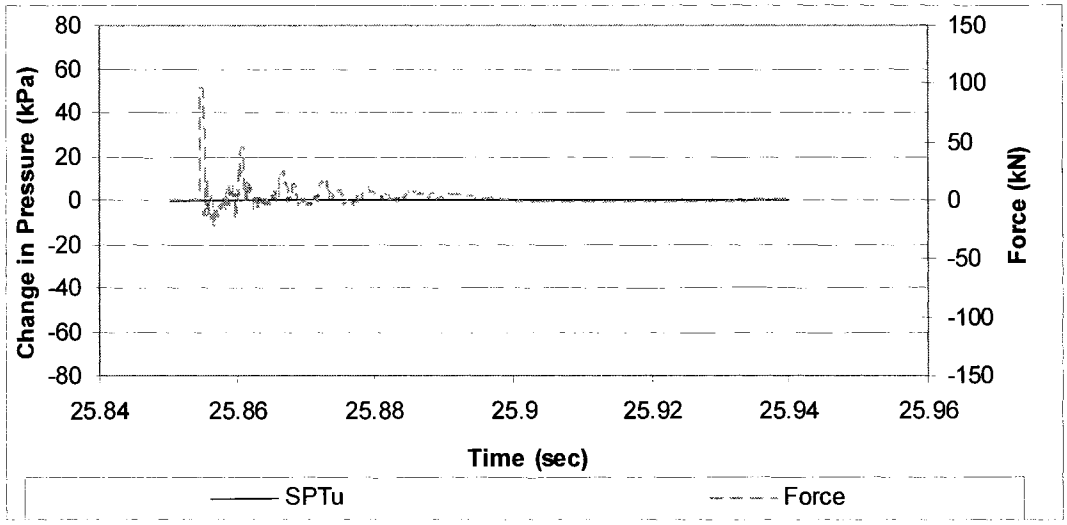

Blow 6 pore pressure response

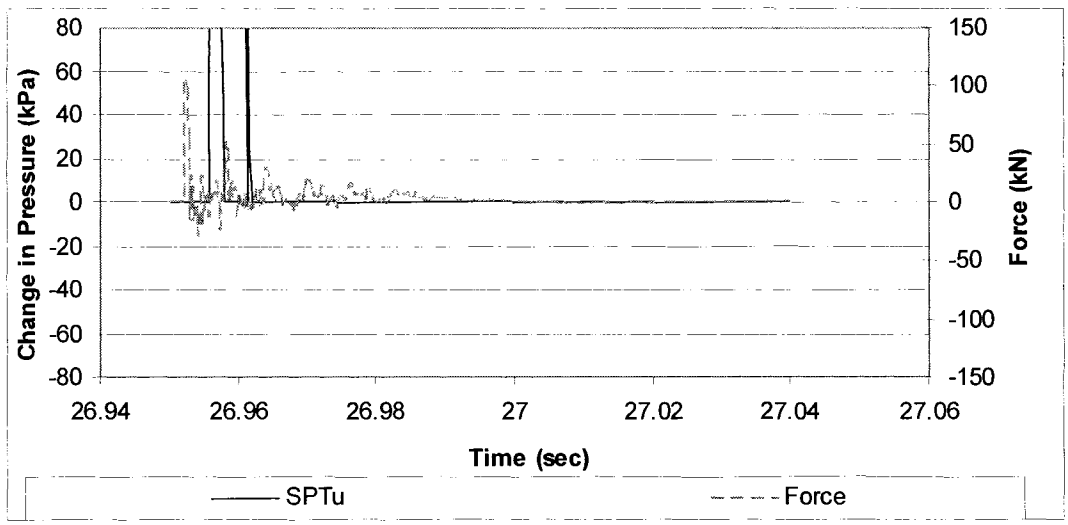

Blow 7 pore pressure response

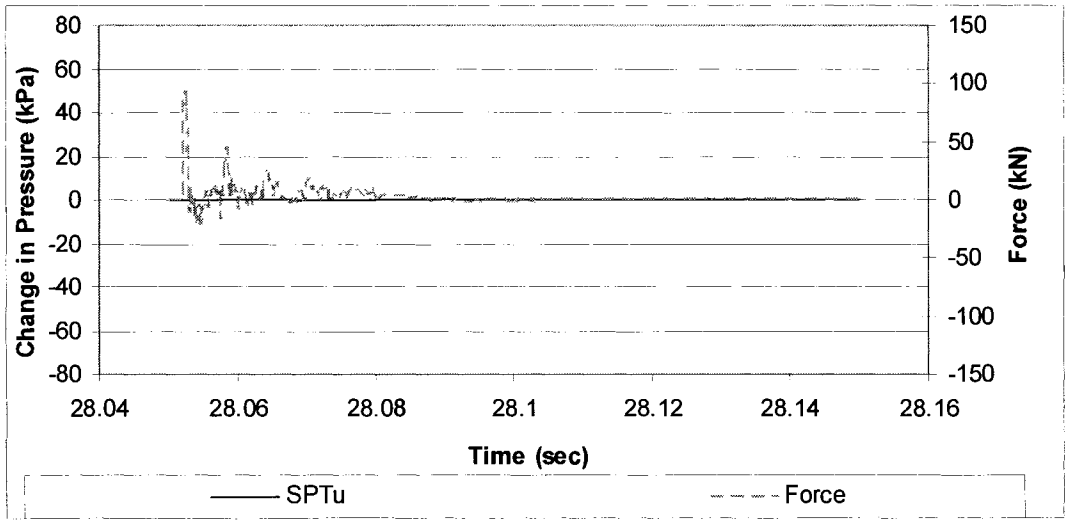

Blow 8 pore pressure response

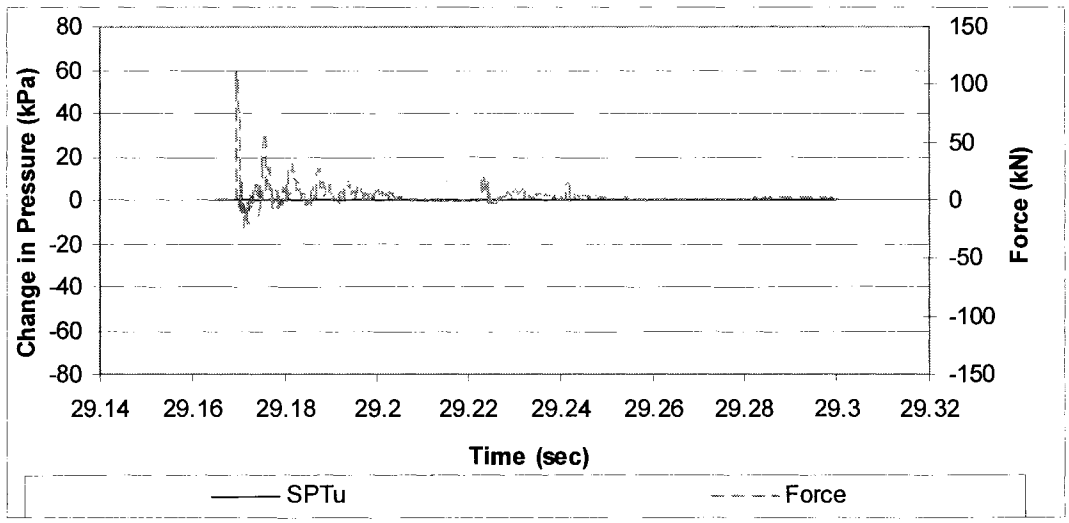

SPTu Pore Pressure Response From 10.80 m Depth

Blow 1 pore pressure response

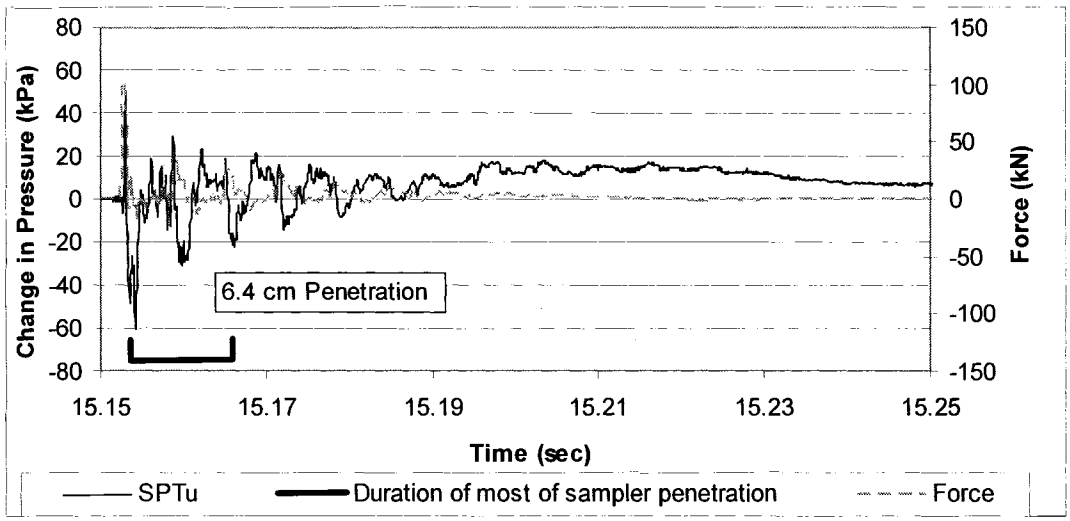

Blow 2 pore pressure response

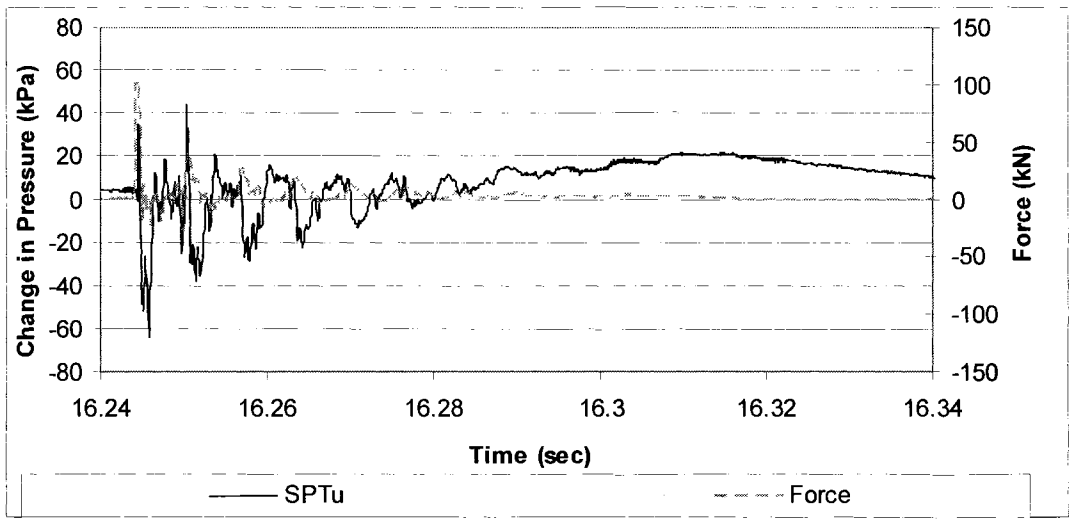

Blow 3 pore pressure response

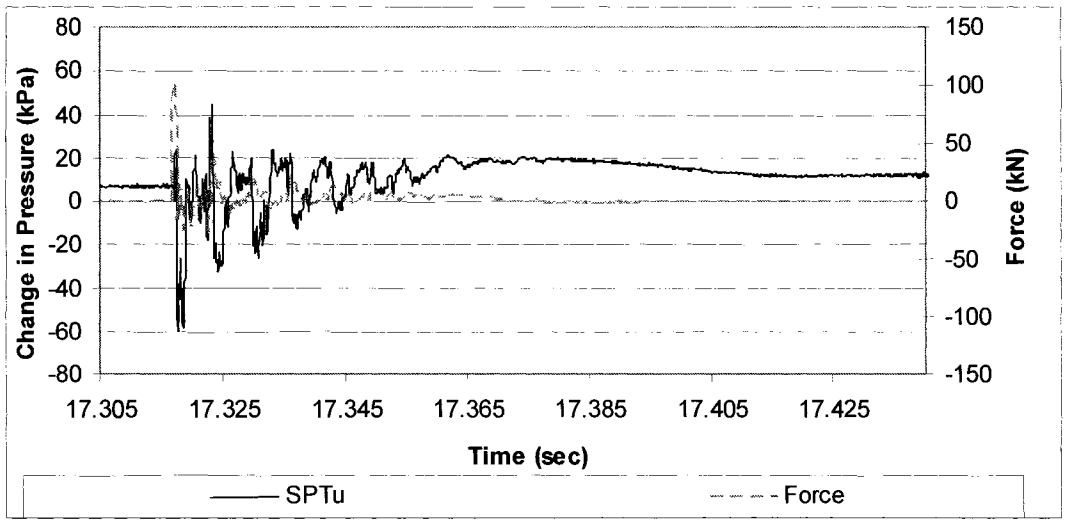

Blow 4 pore pressure response

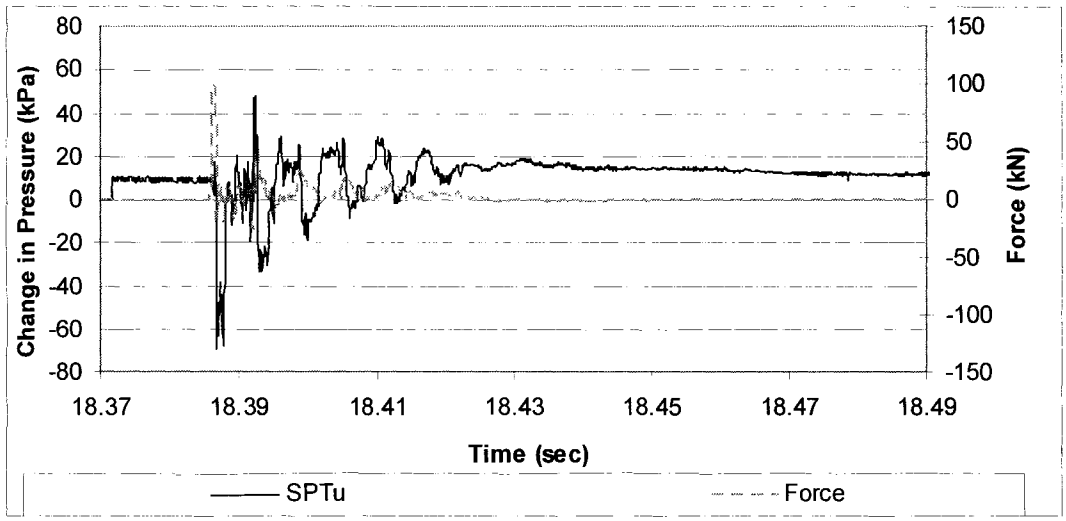

Blow 5 pore pressure response

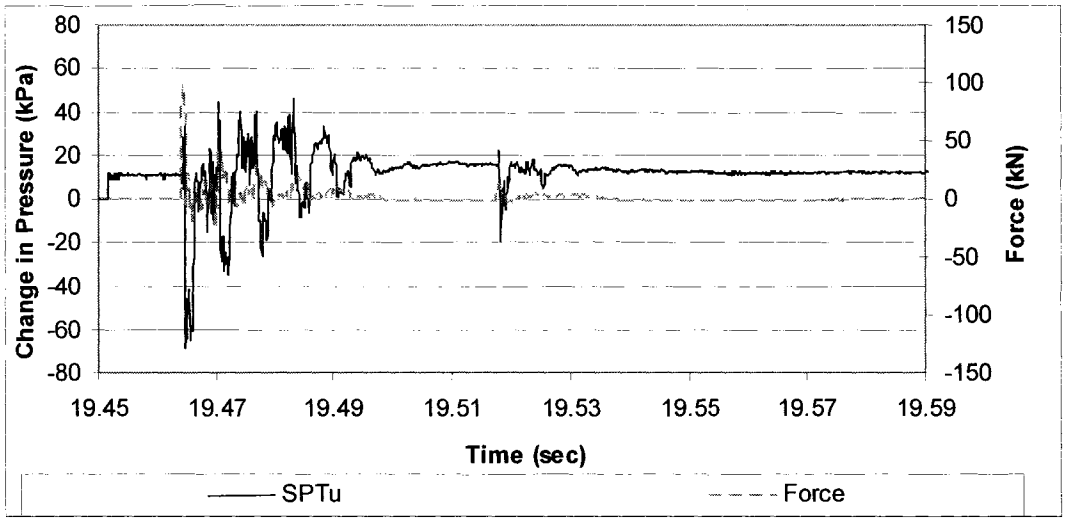

Blow 6 pore pressure response

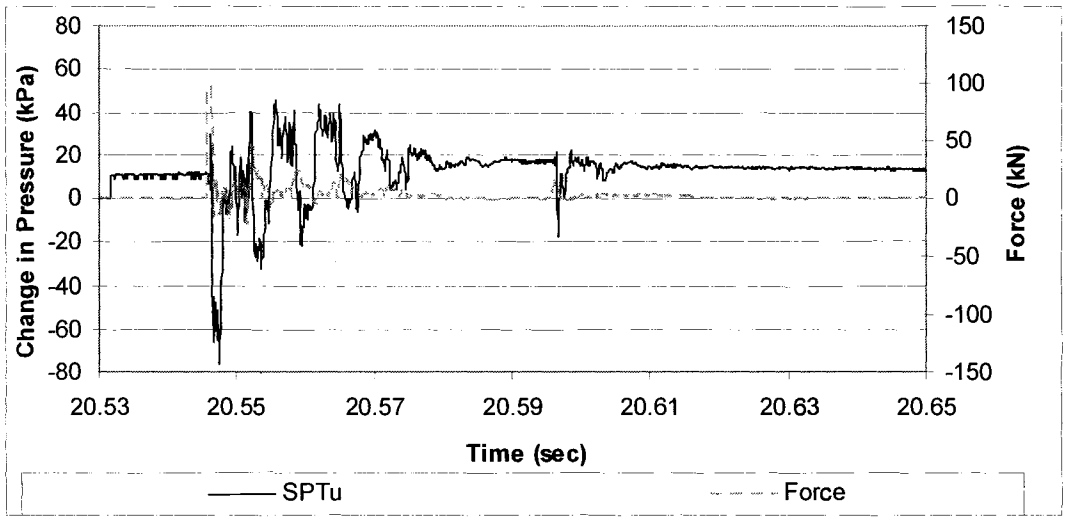

Blow 7 pore pressure response

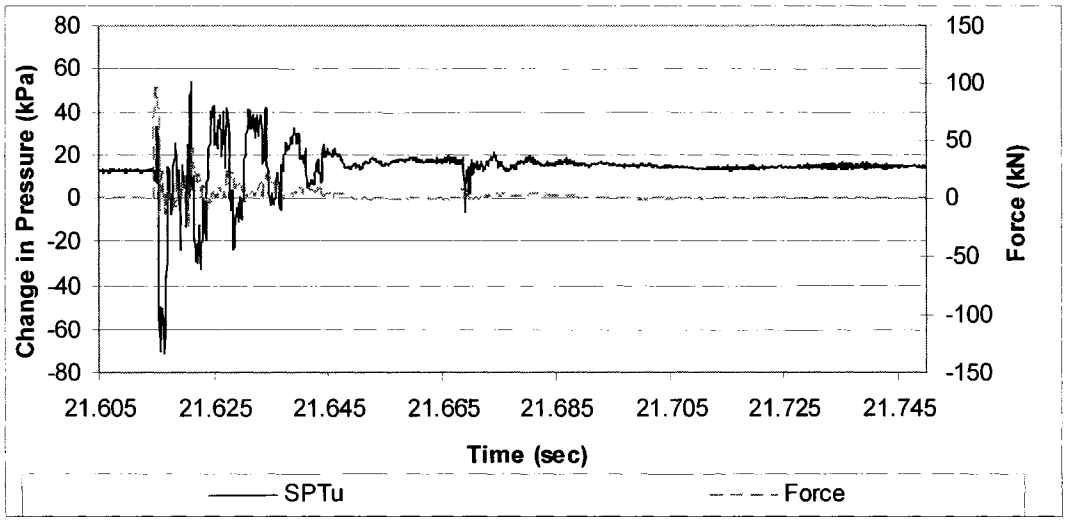

Blow 8 pore pressure response

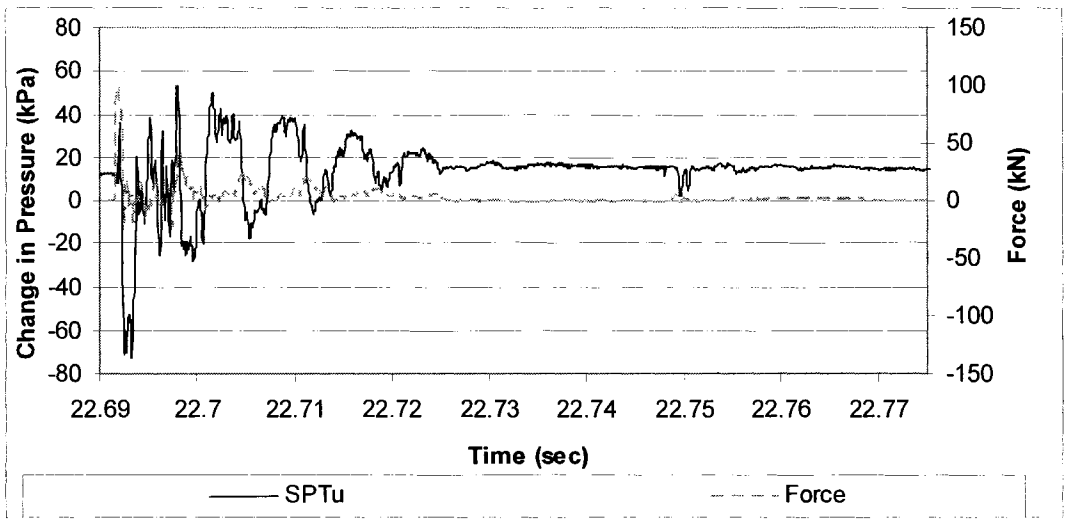

Blow 9 pore pressure response

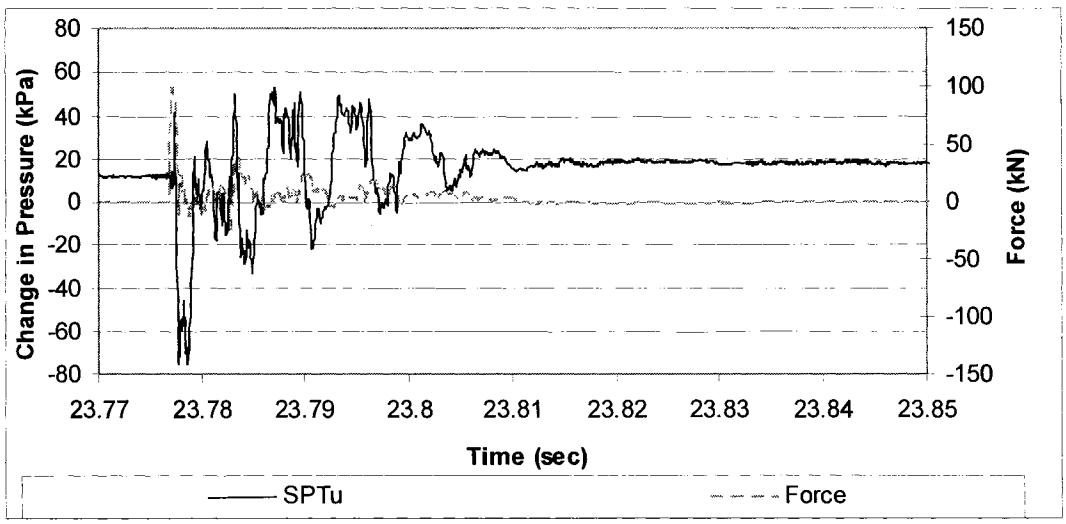

Blow 10 pore pressure response

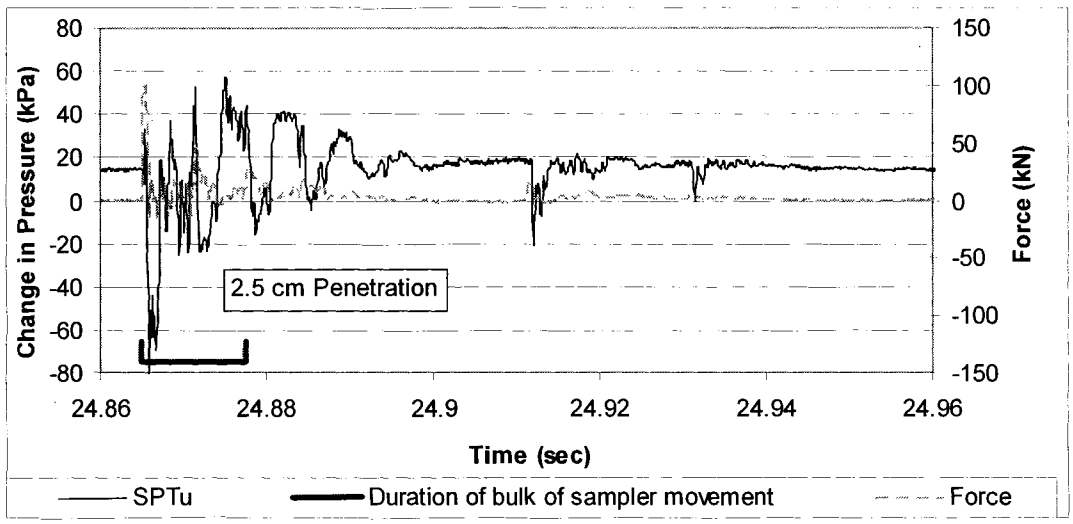

SPTu Pore Pressure Response From 12.41 m Depth

Blow 1 pore pressure response

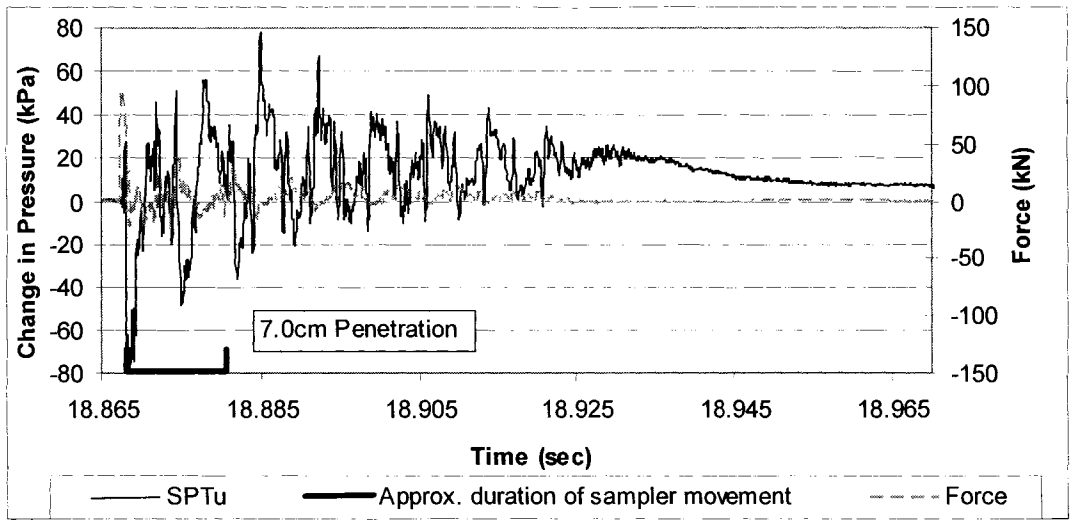

Blow 2 pore pressure response

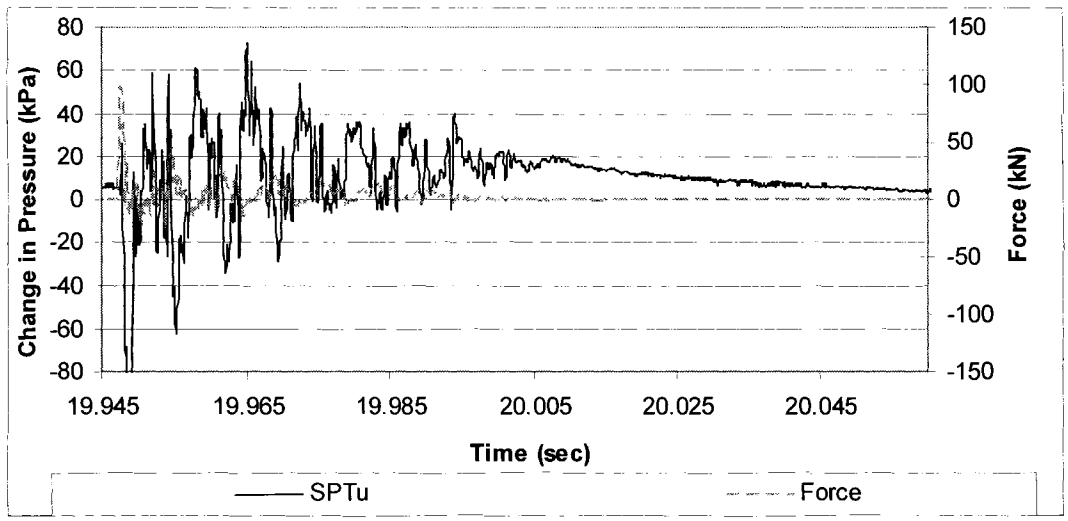

Blow 3 pore pressure response

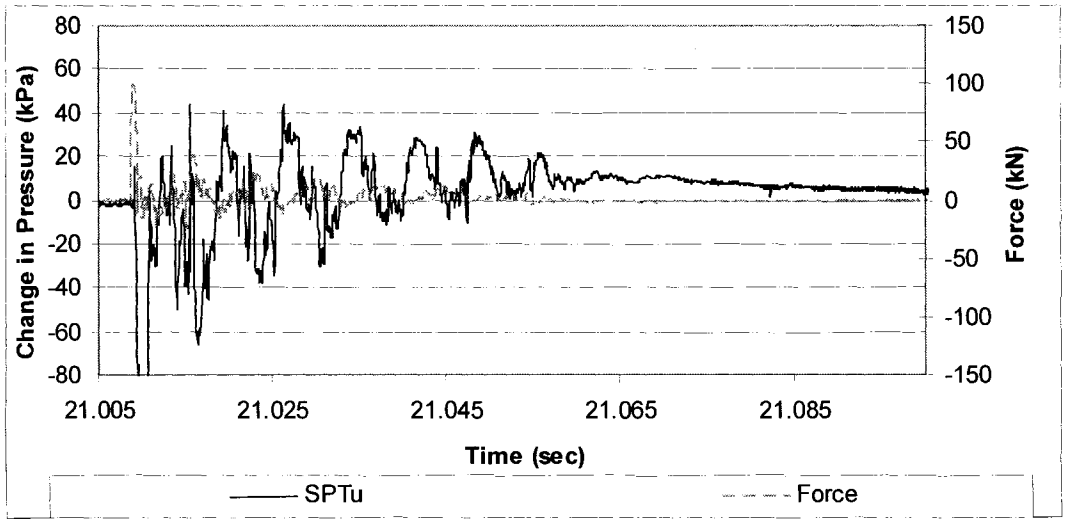

Blow 4 pore pressure response

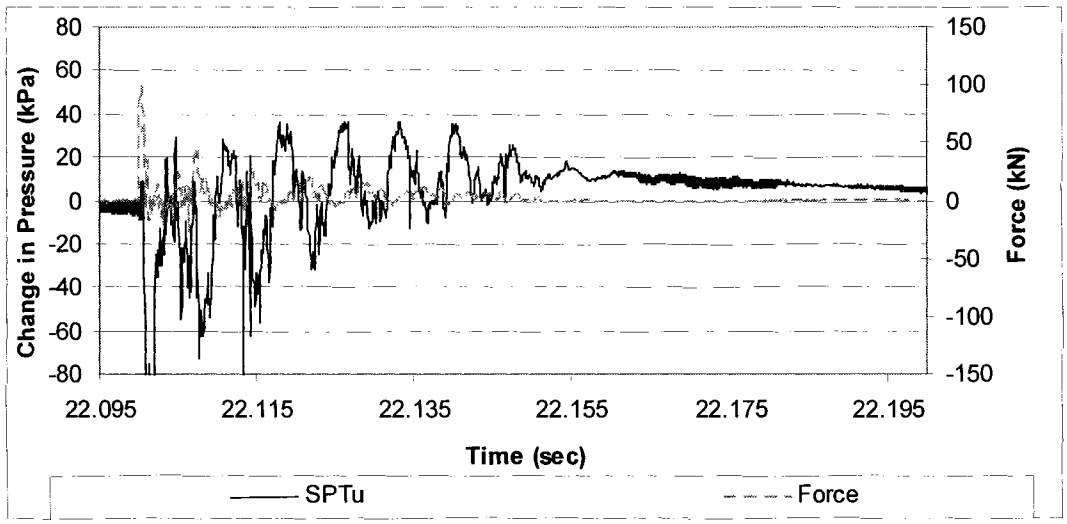

Blow 5 pore pressure response

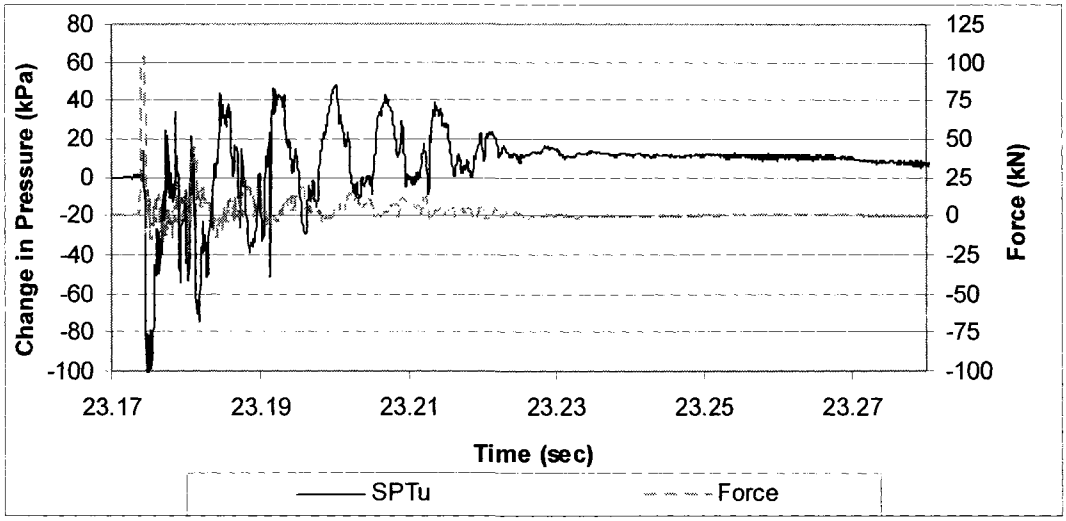

Blow 6 pore pressure response

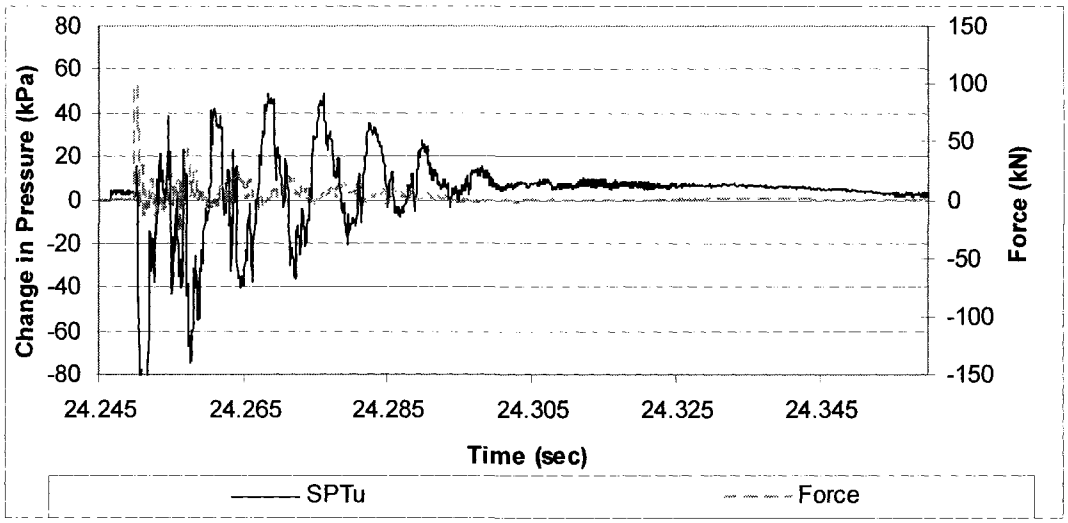

Blow 7 pore pressure response

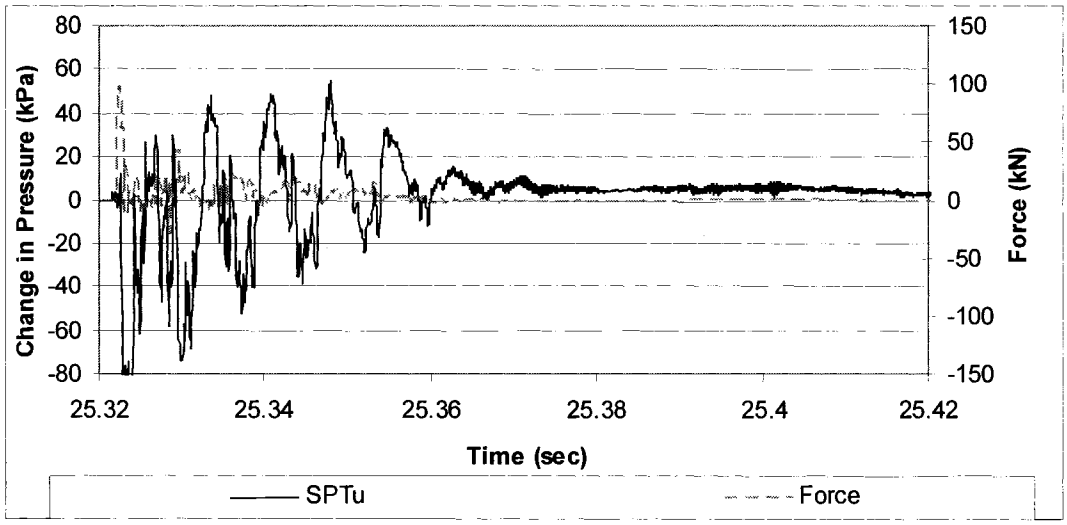

Blow 8 pore pressure response

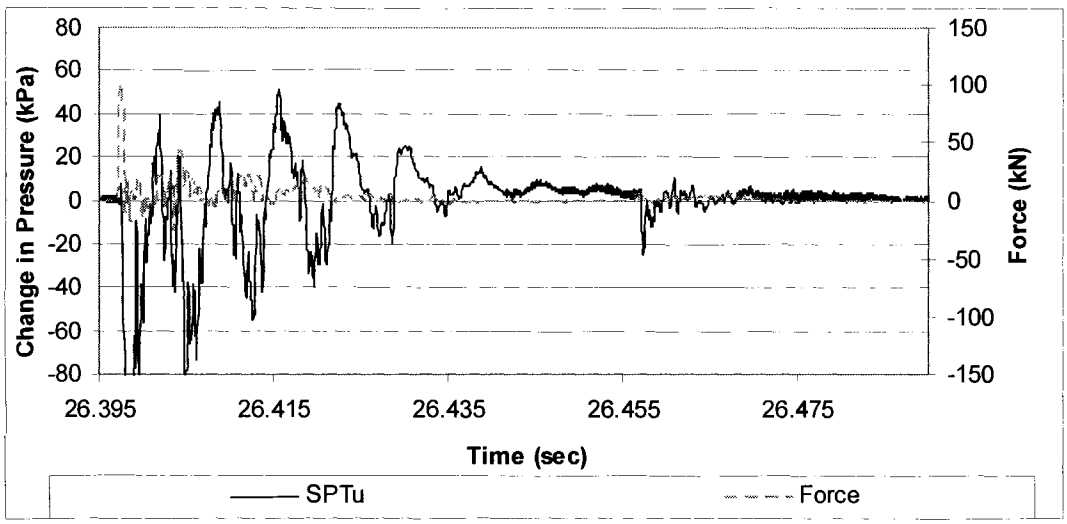

Blow 9 pore pressure response

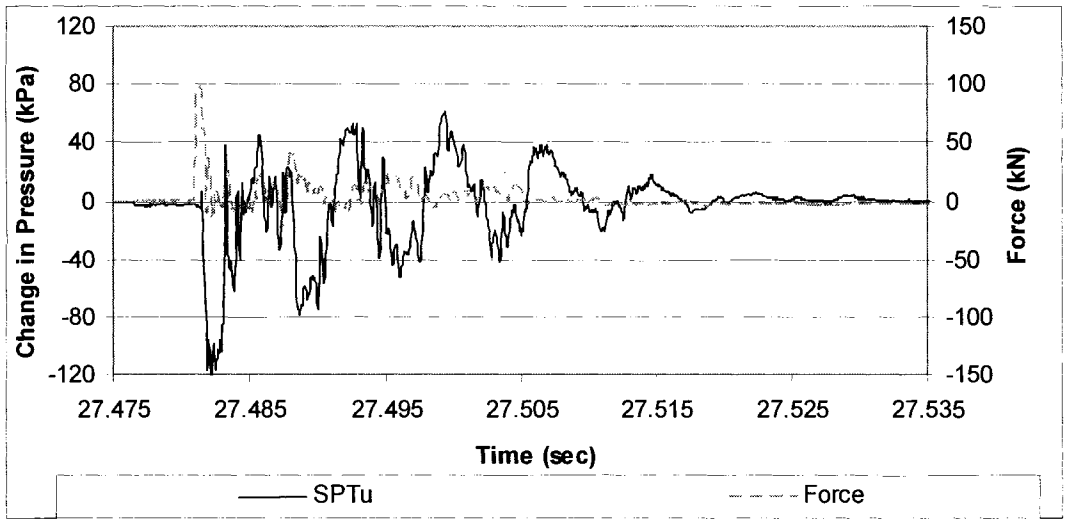

Blow 10 pore pressure response

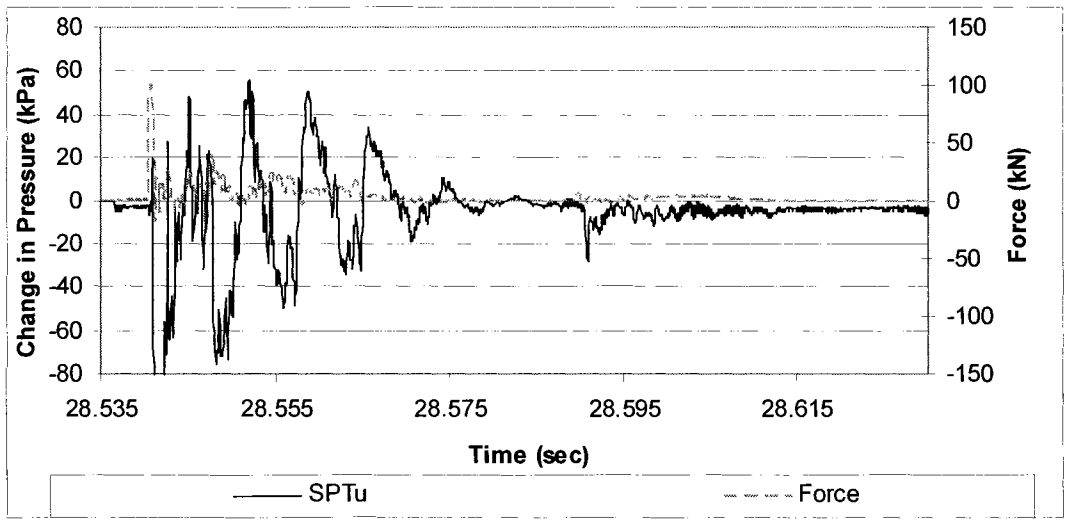

Blow 11 pore pressure response

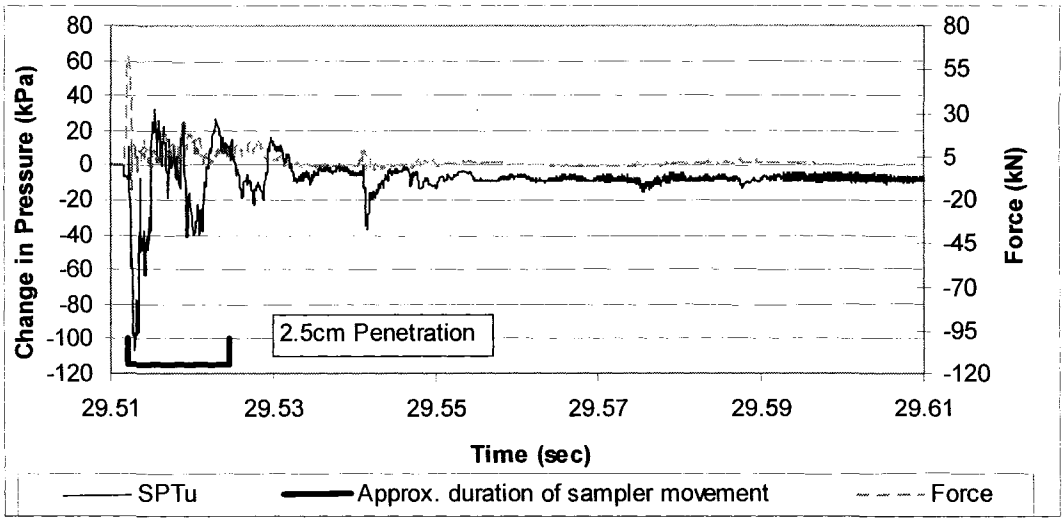

SPTu Pore Pressure Response From 13.92 m Depth

Blow 1 pore pressure response

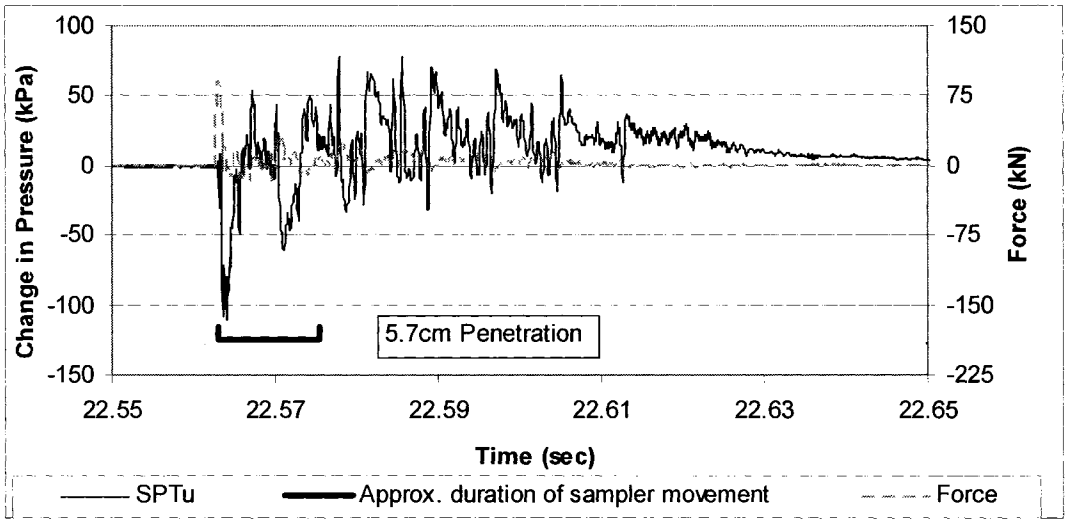

Blow 2 pore pressure response

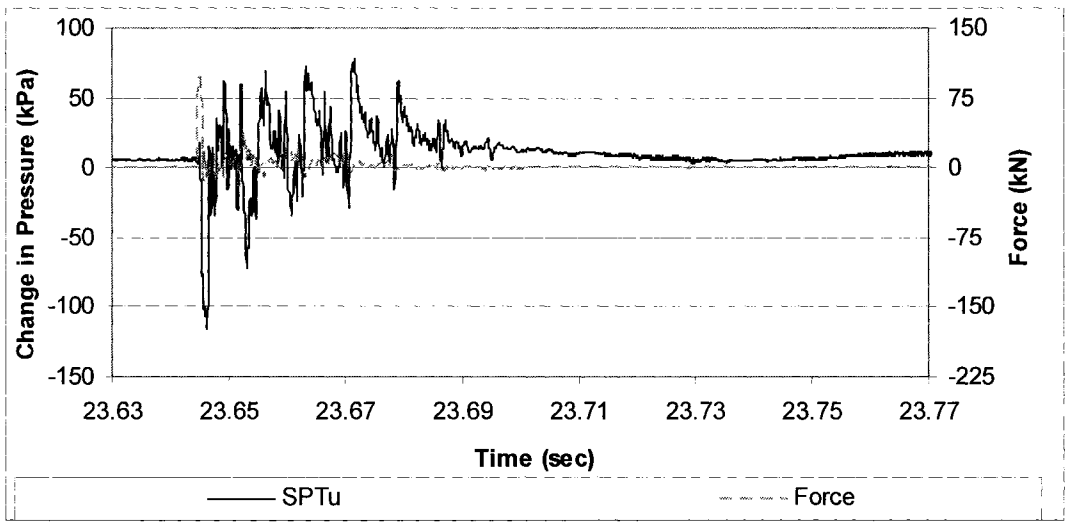

Blow 3 pore pressure response

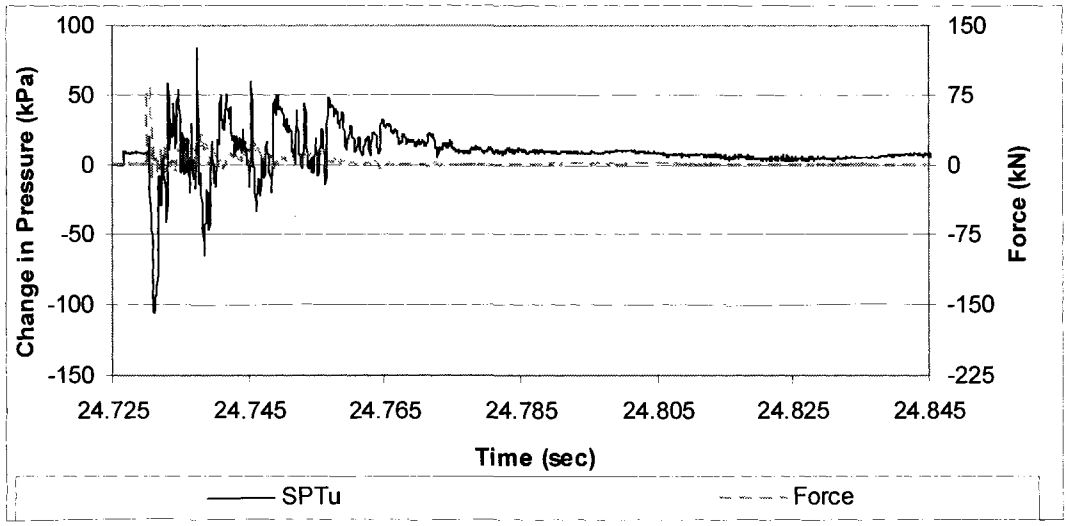

Blow 4 pore pressure response

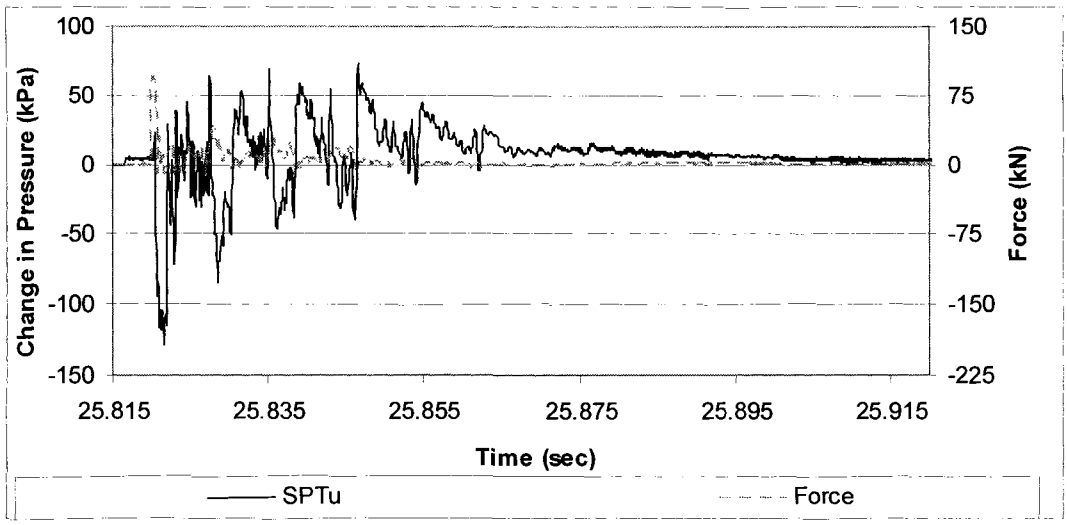

Blow 5 pore pressure response

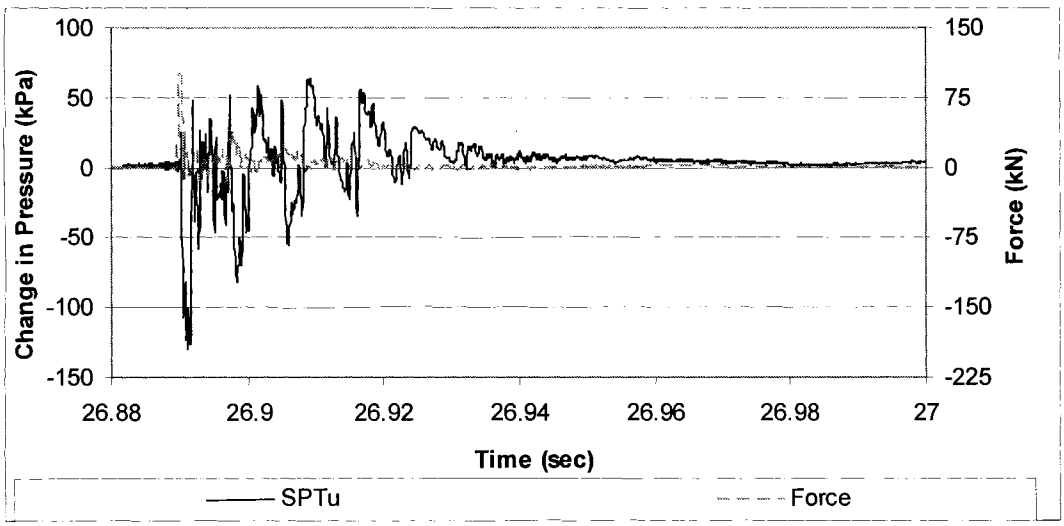

Blow 6 pore pressure response

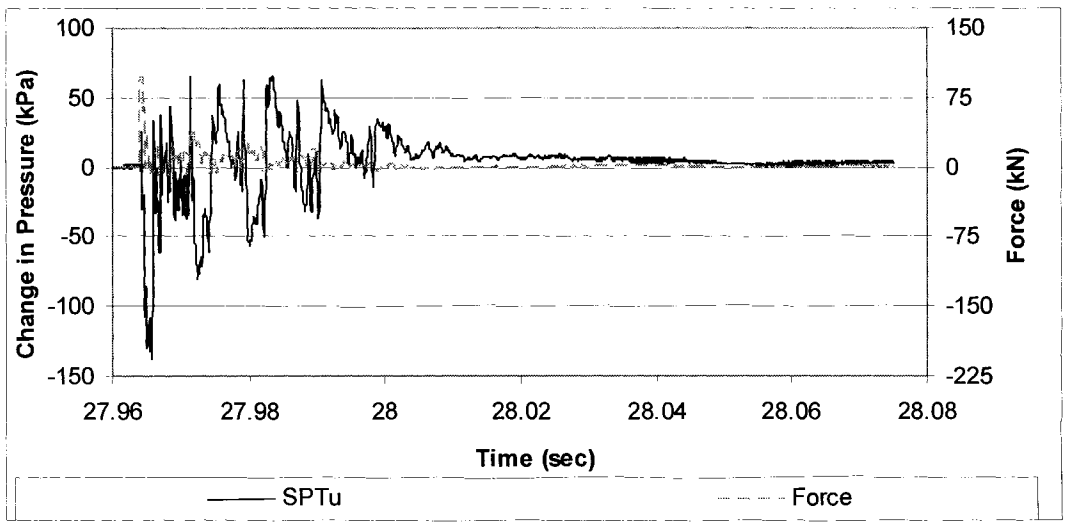

Blow 7 pore pressure response

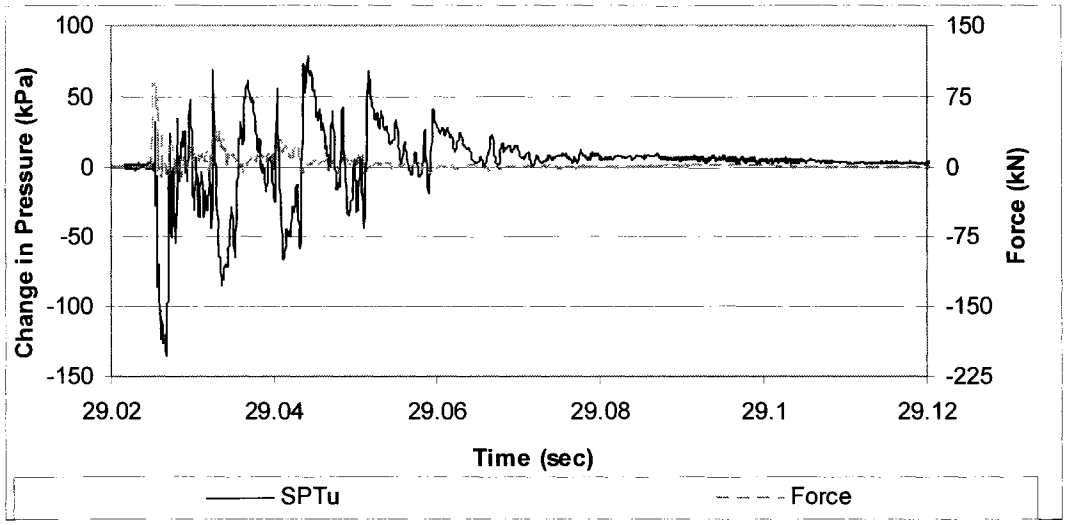

Blow 8 pore pressure response

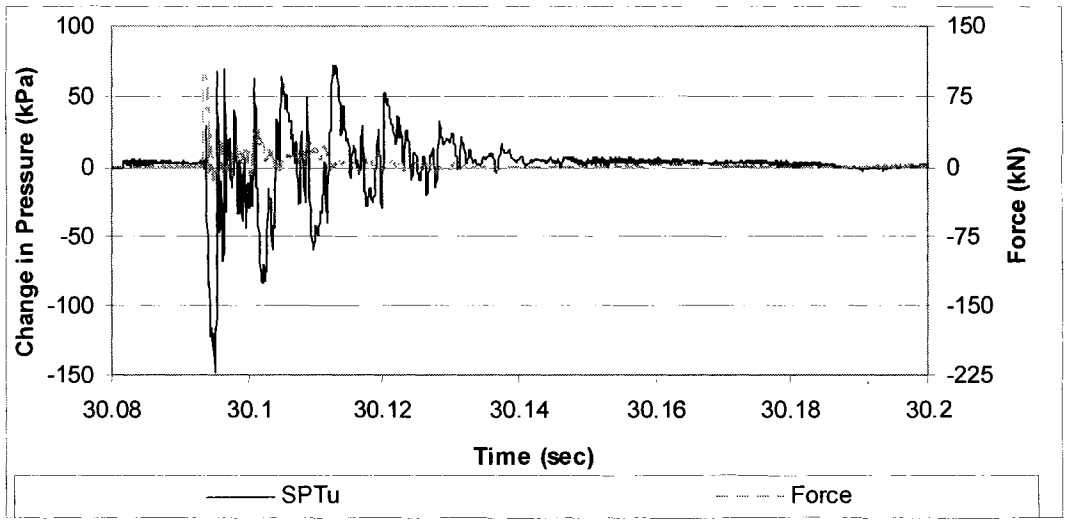

Blow 9 pore pressure response

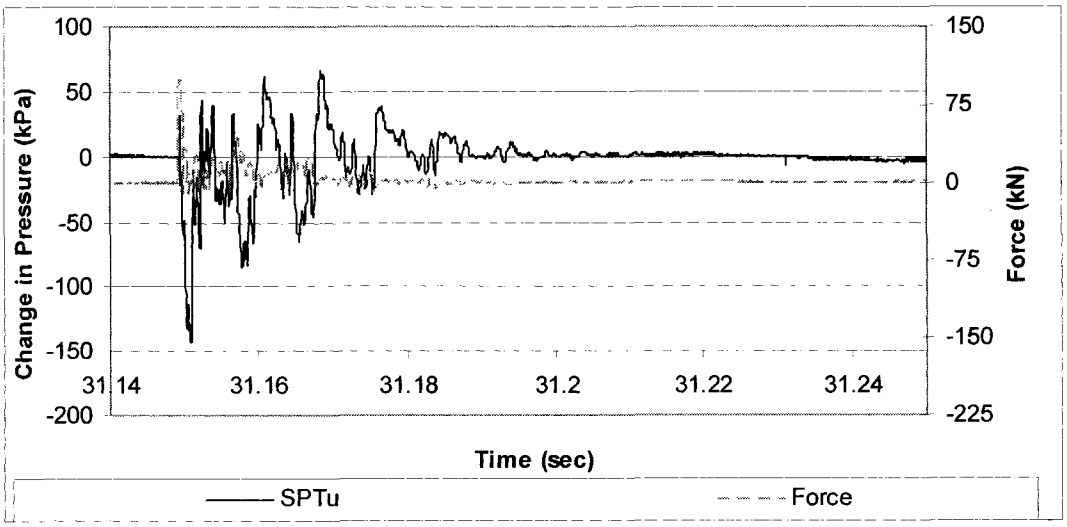

Blow 10 pore pressure response

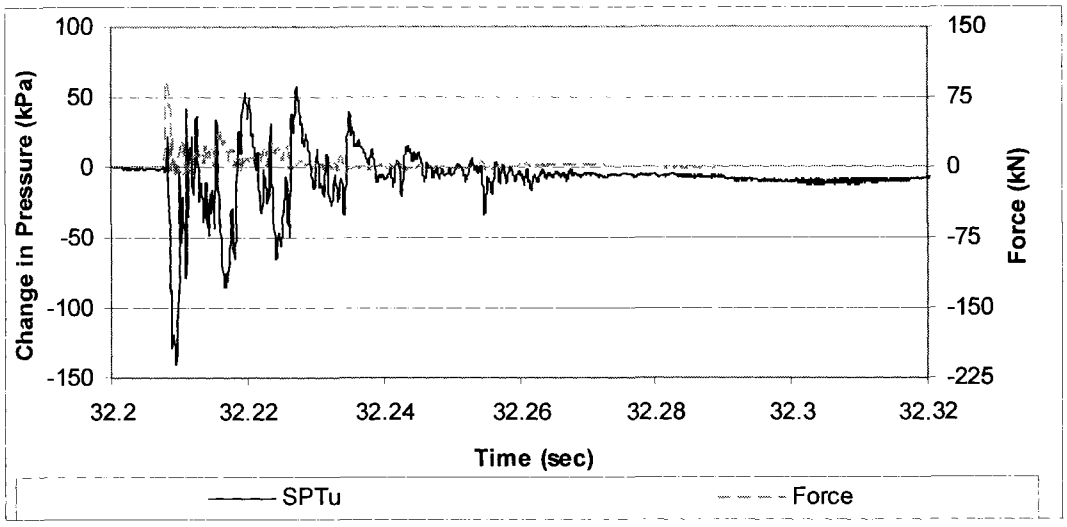

Blow 11 pore pressure response

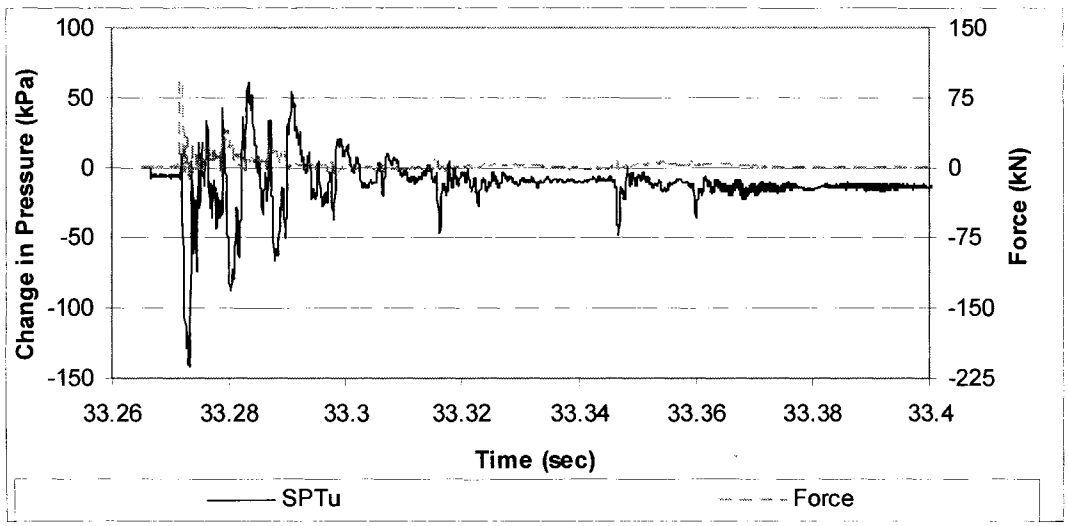

Blow 12 pore pressure response

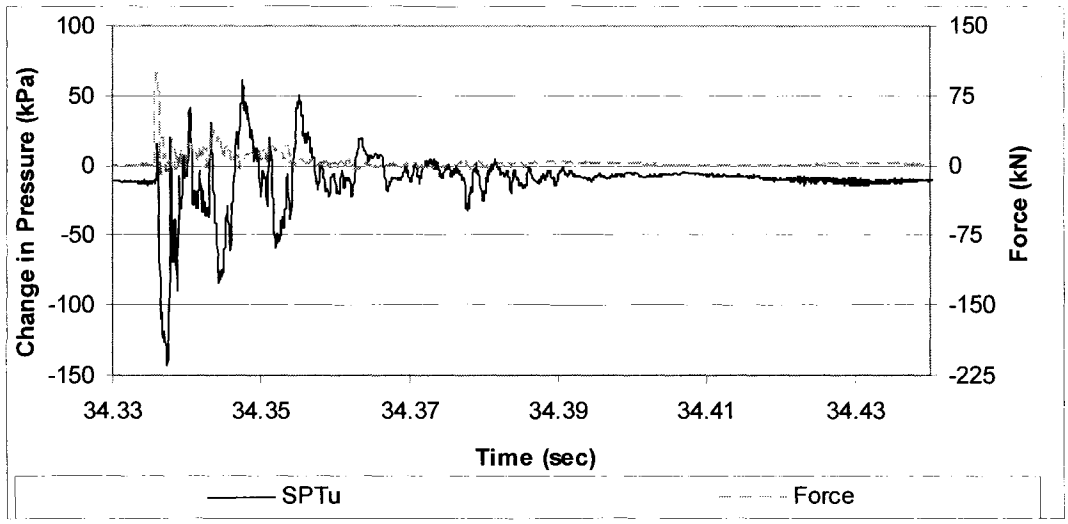

Blow 13 pore pressure response

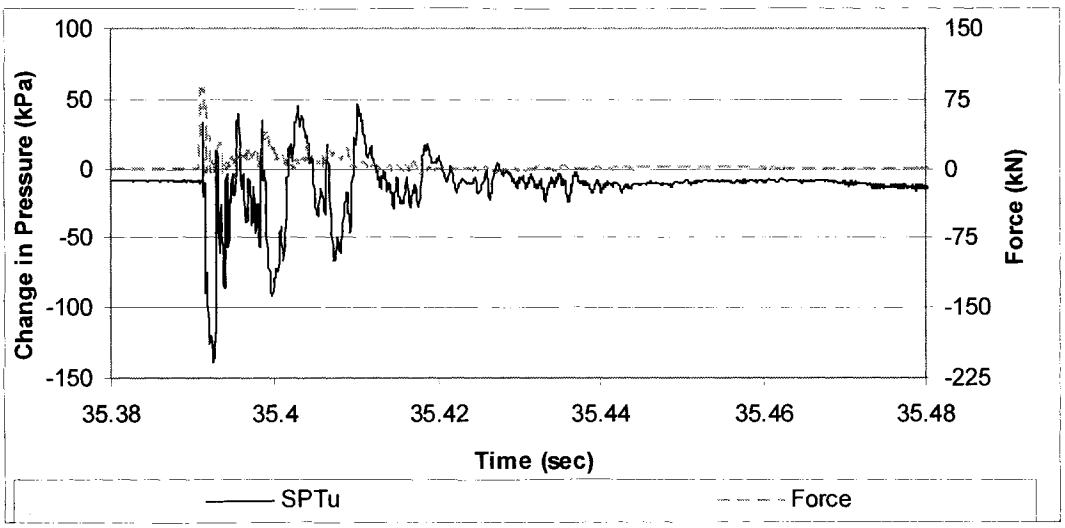

Blow 14 pore pressure response

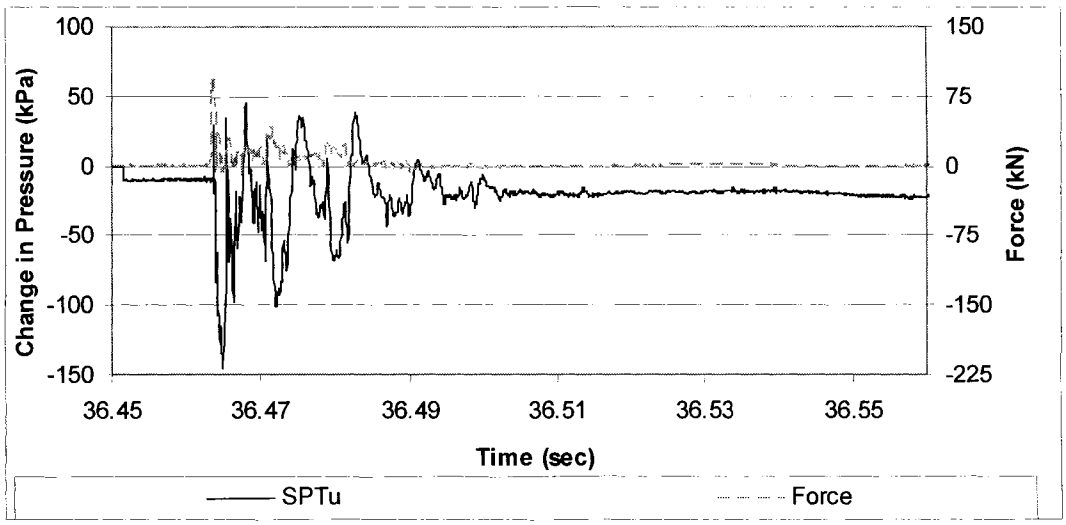

Blow 15 pore pressure response

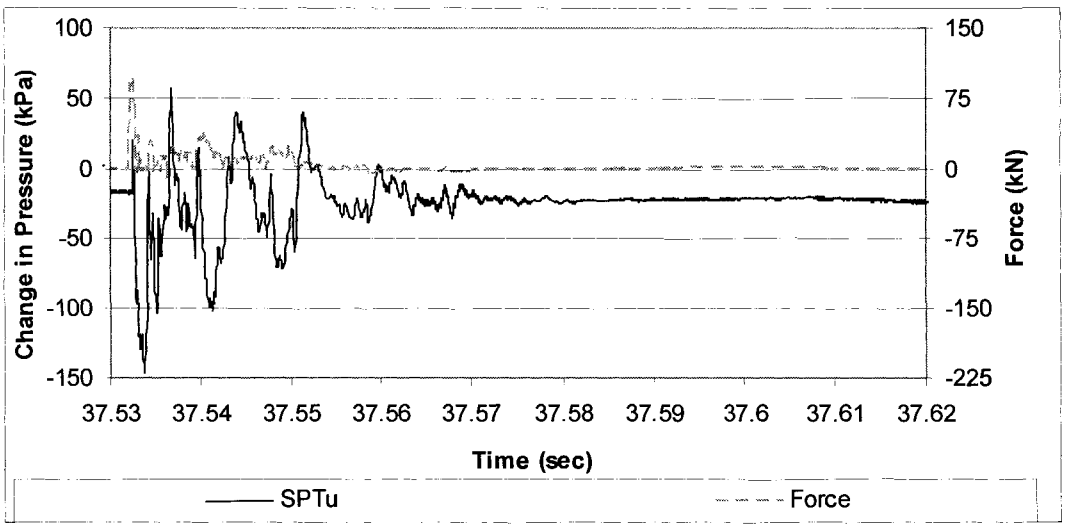

Blow 16 pore pressure response

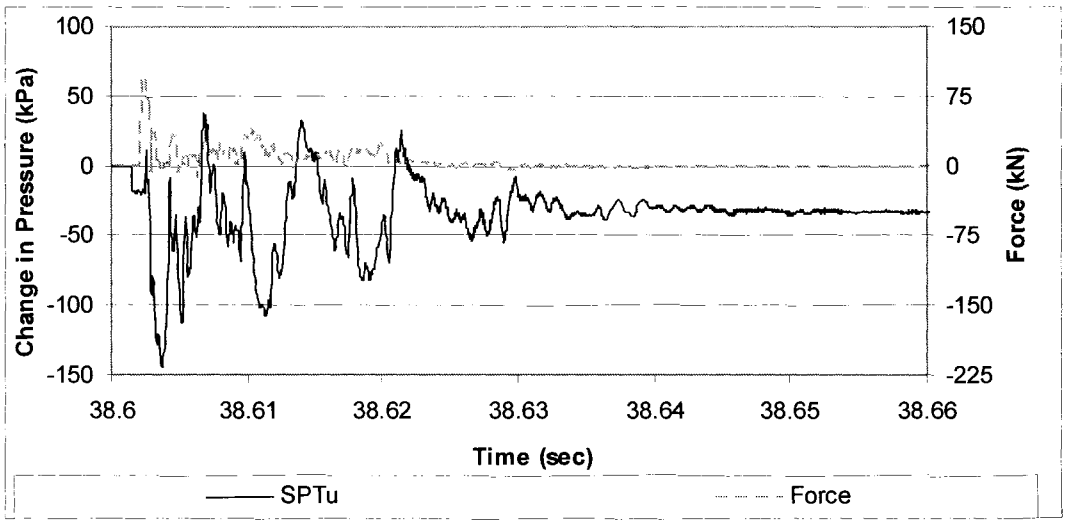

Blow 17 pore pressure response

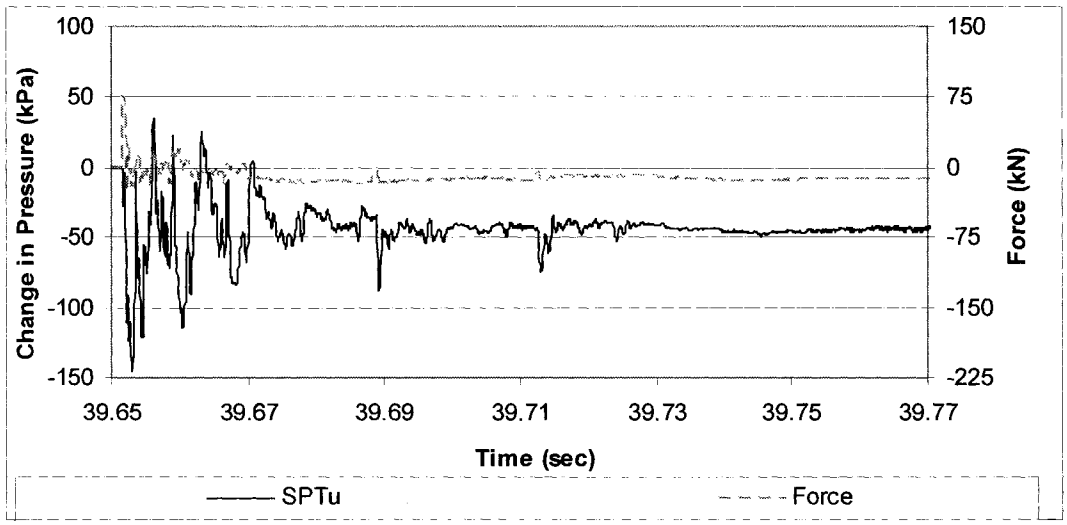

Blow 18 pore pressure response

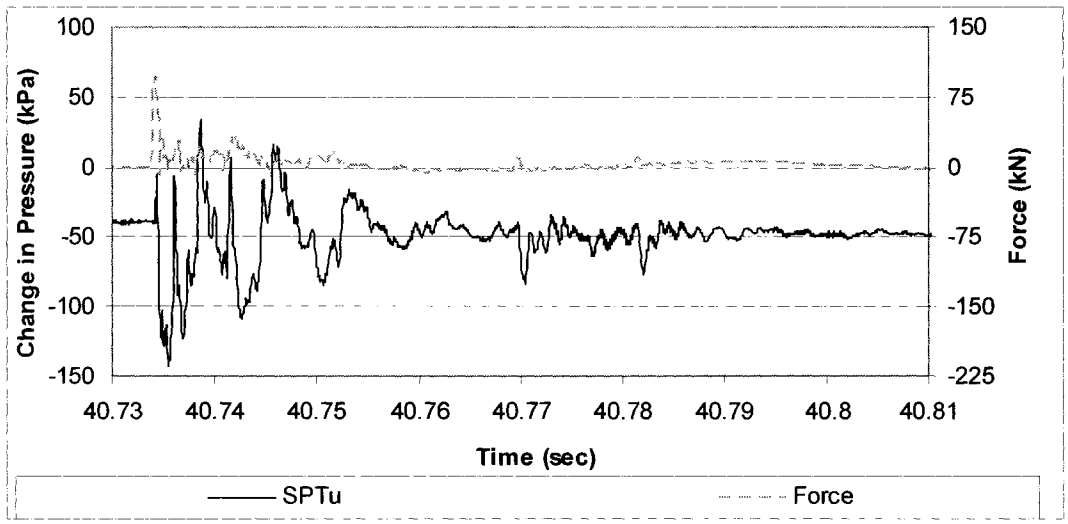

Blow 19 pore pressure response

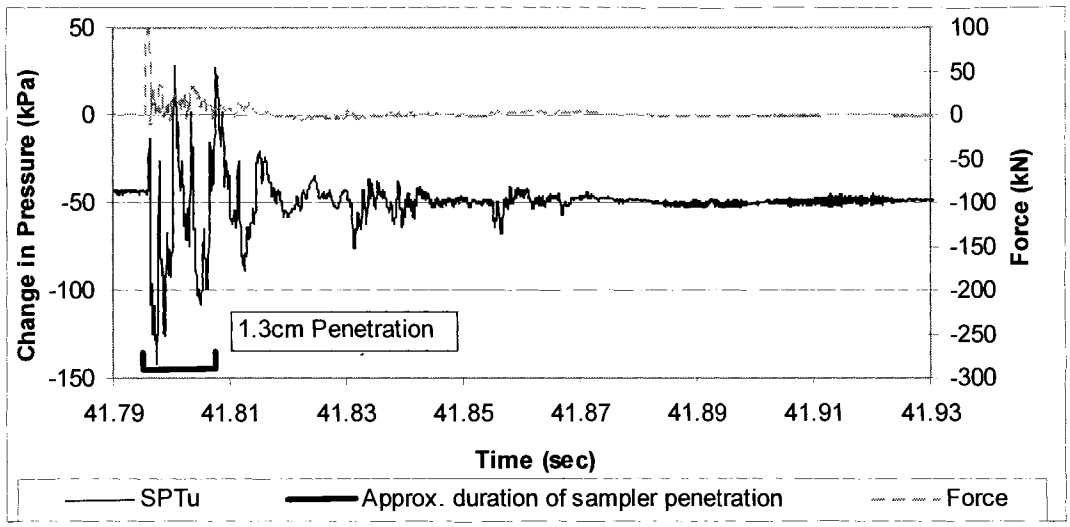

APPENDIX D: BLAST PROBE PORE PRESSURE MEASUREMENTS

Blast Probe Pore Pressure Response from 1.52 m Depth

Blow 1 blast probe pore pressure response:

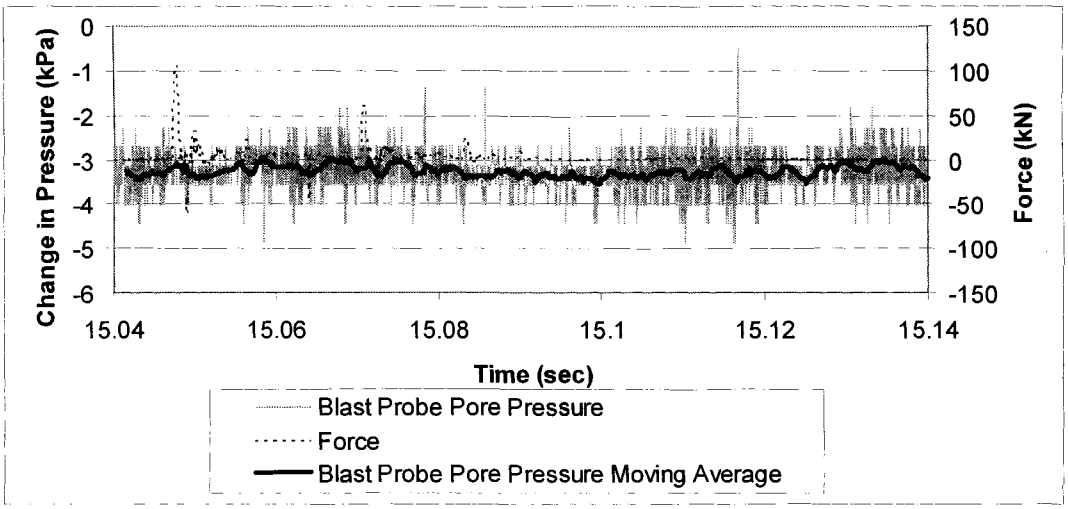

Blow 2 blast probe pore pressure response:

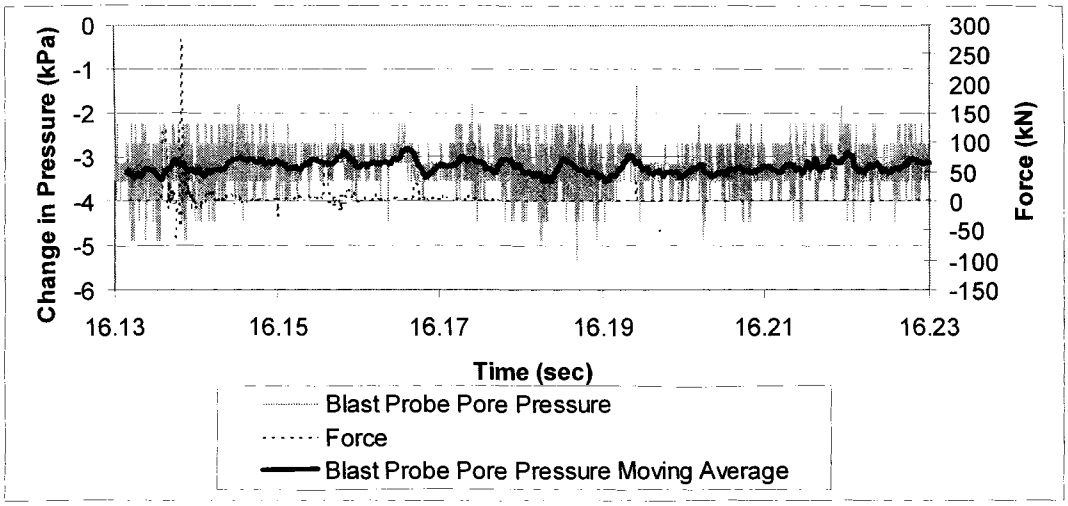

Blow 3 blast probe pore pressure response:

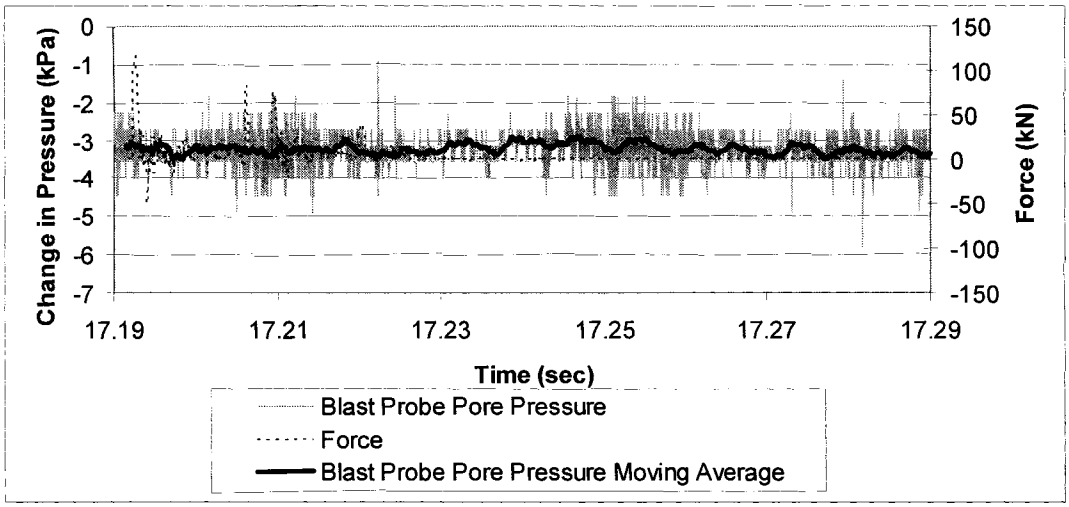

Blow 4 blast probe pore pressure response:

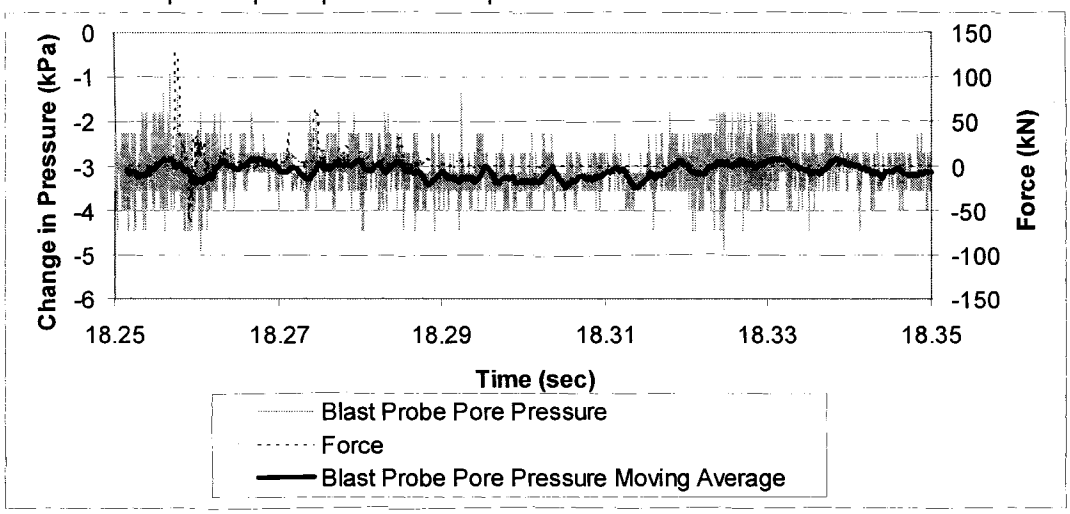

Blow 5 blast probe pore pressure response:

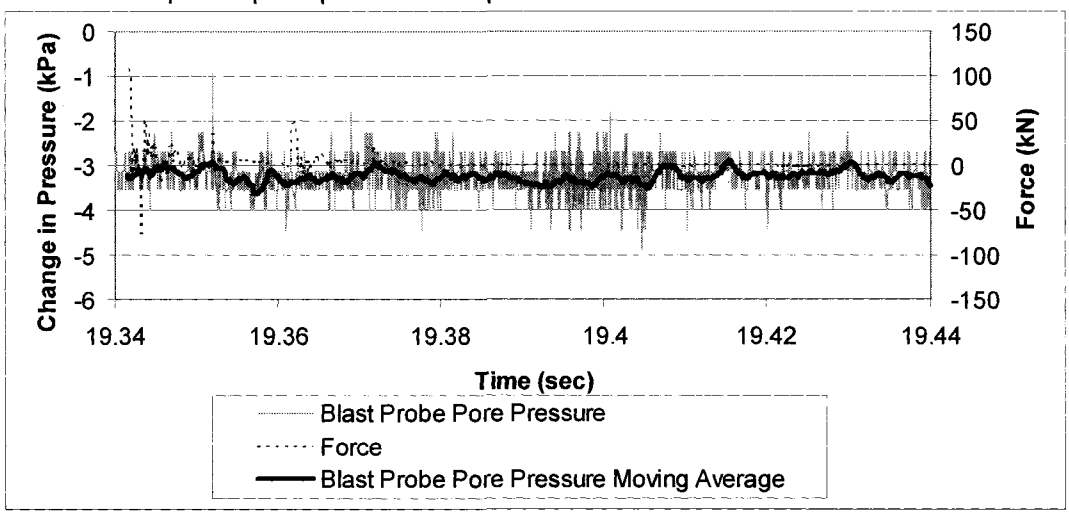

Blow 6 blast probe pore pressure response:

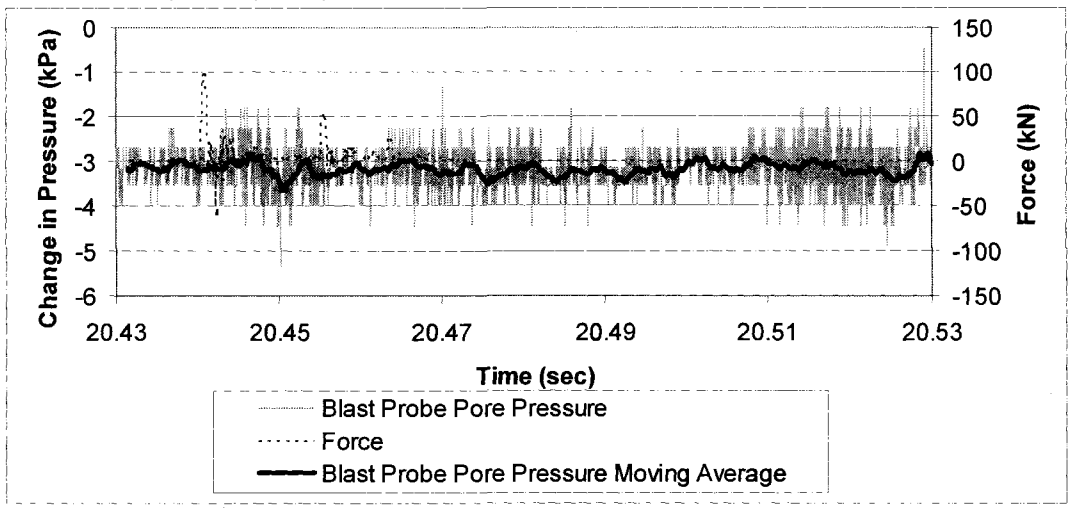

Blow 7 blast probe pore pressure response:

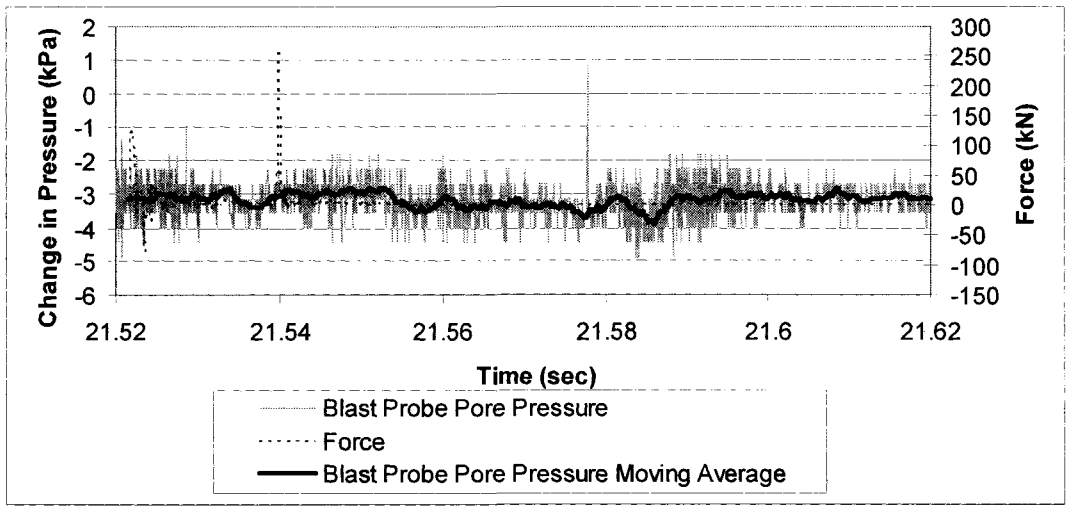

Blow 8 blast probe pore pressure response:

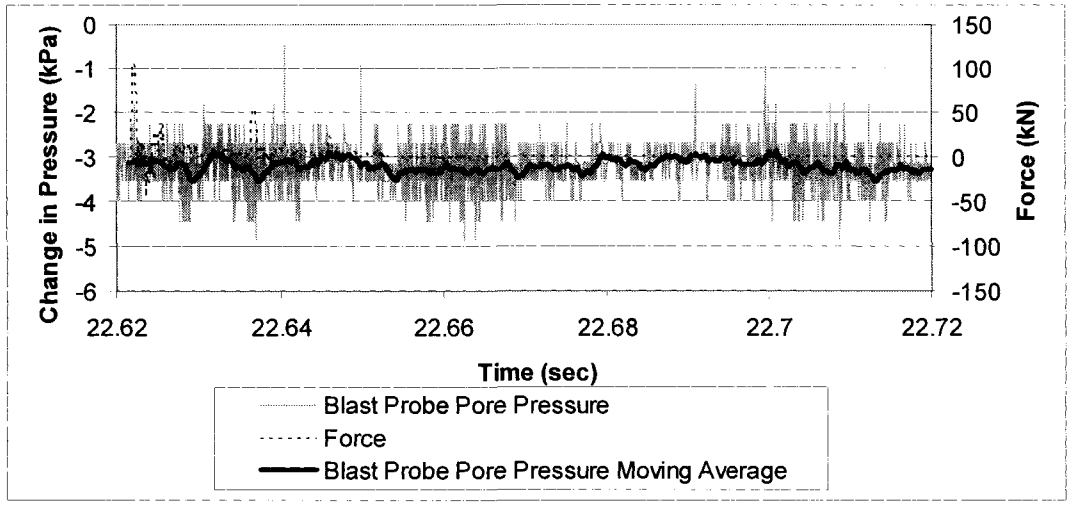

Blow 9 blast probe pore pressure response:

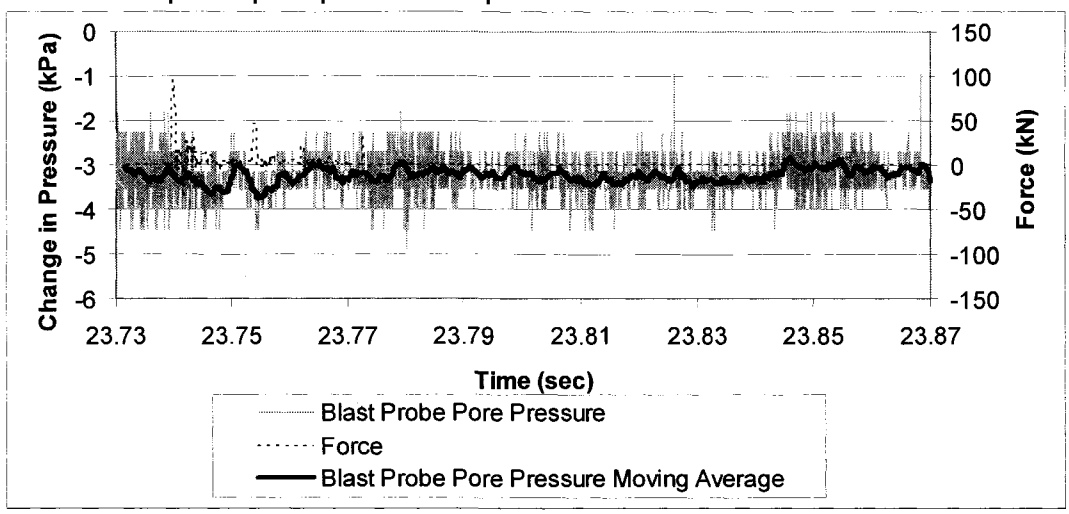

Blow 10 blast probe pore pressure response:

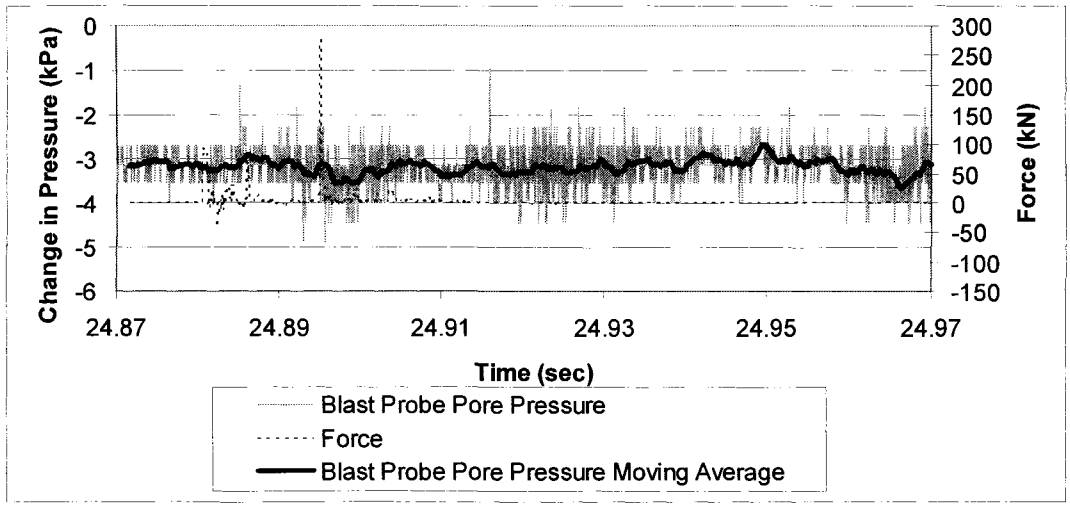

Blow 11 blast probe pore pressure response:

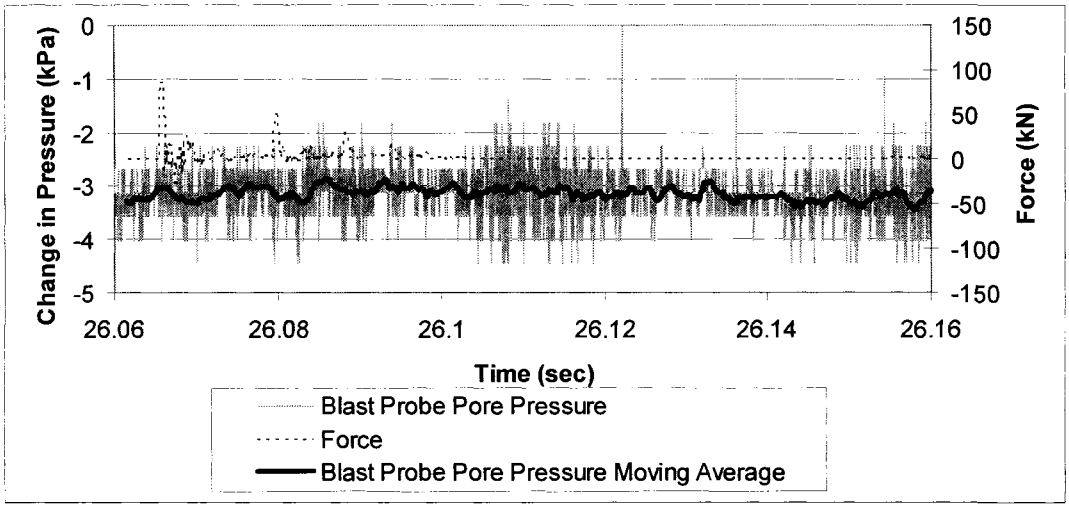

Blast Probe Pore Pressure Response from 7.72 m Depth

Blow 1 blast probe pore pressure response:

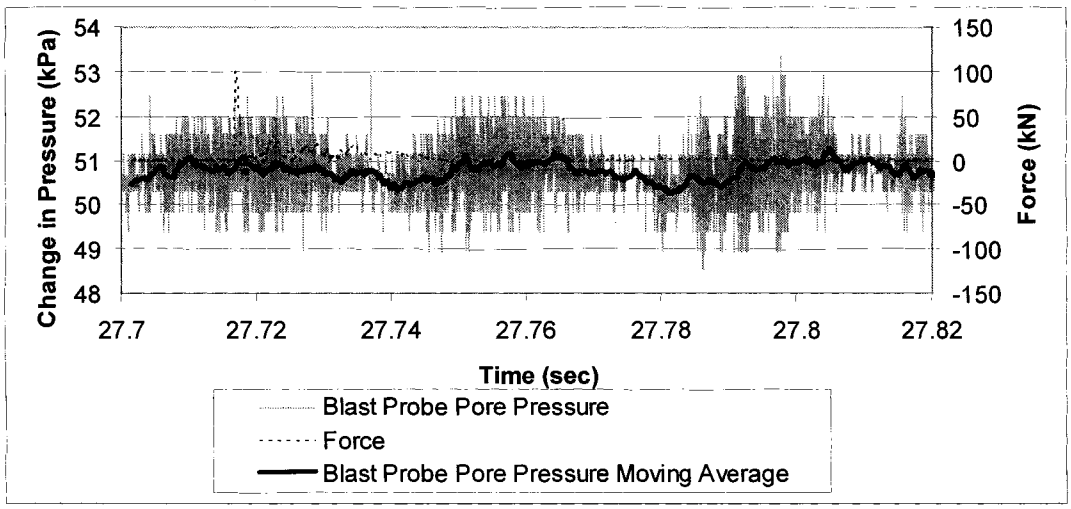

Blow 2 blast probe pore pressure response:

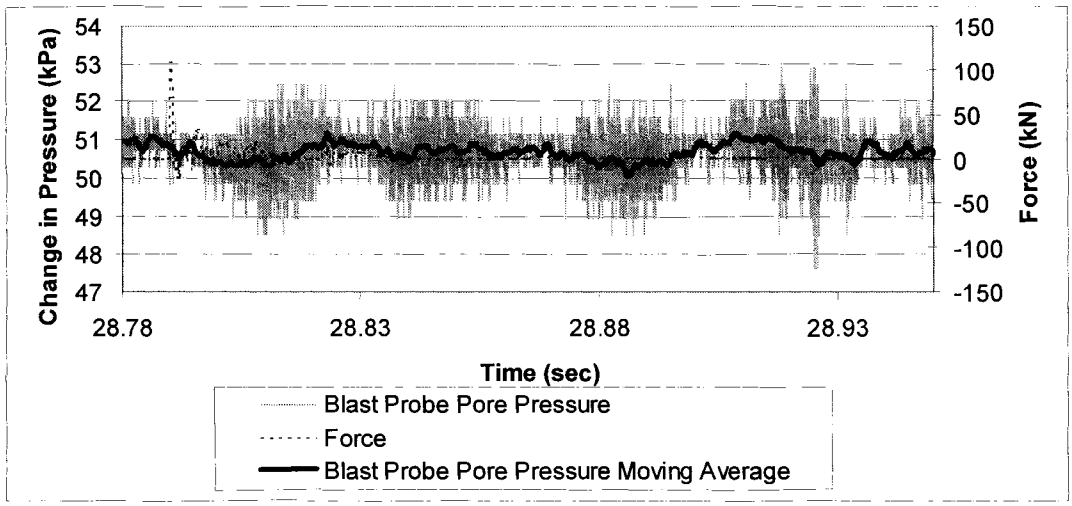

Blow 3 blast probe pore pressure response:

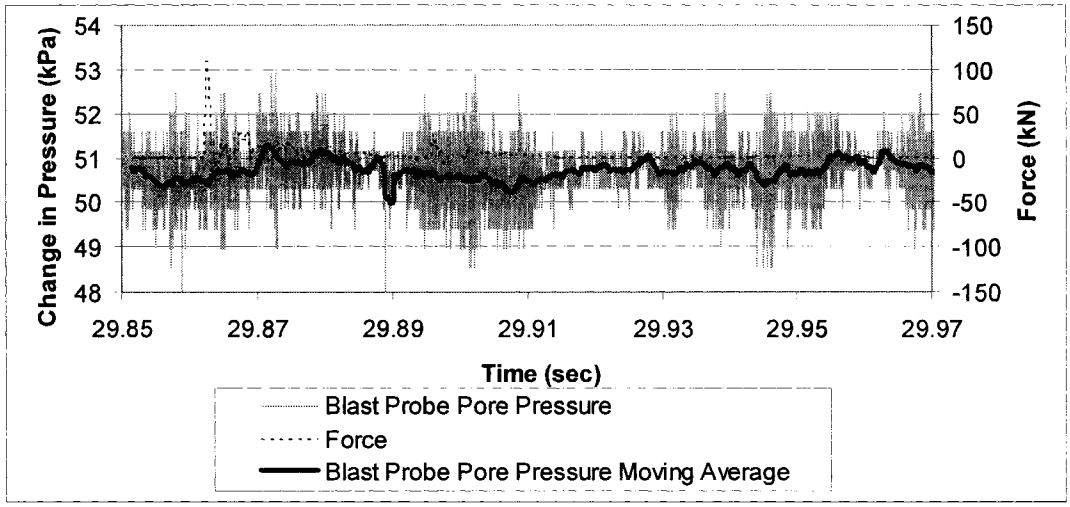

Blow 4 blast probe pore pressure response:

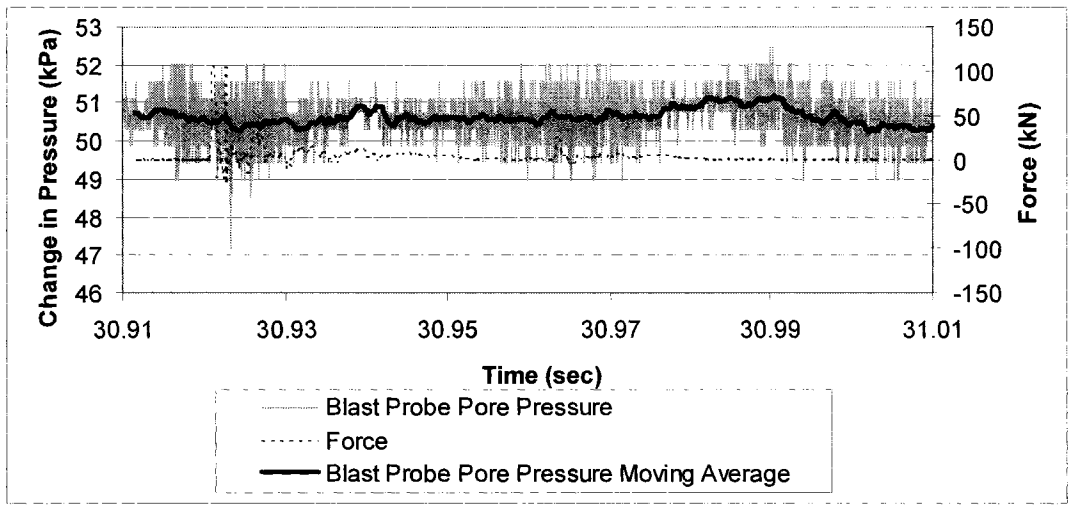

Blow 5 blast probe pore pressure response:

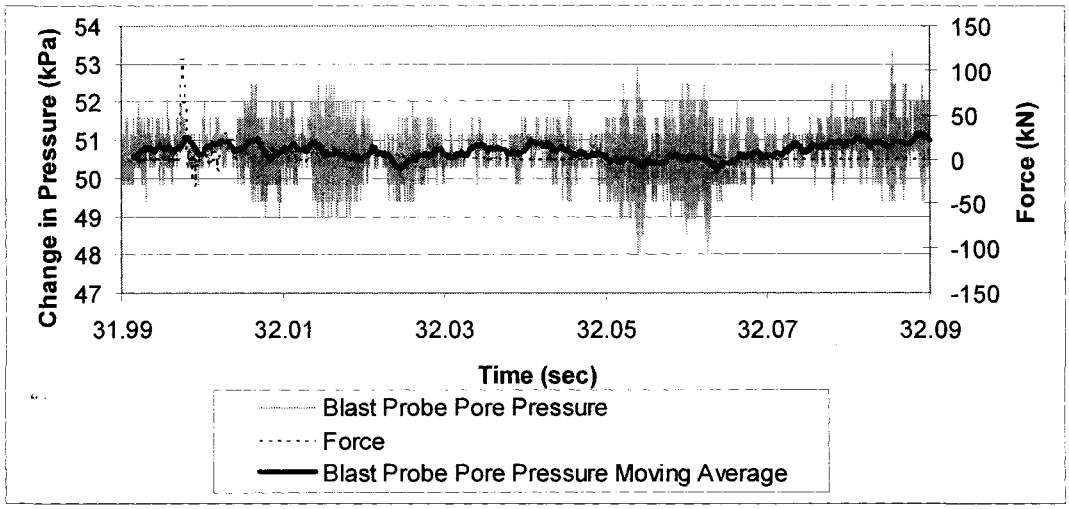

Blow 6 blast probe pore pressure response:

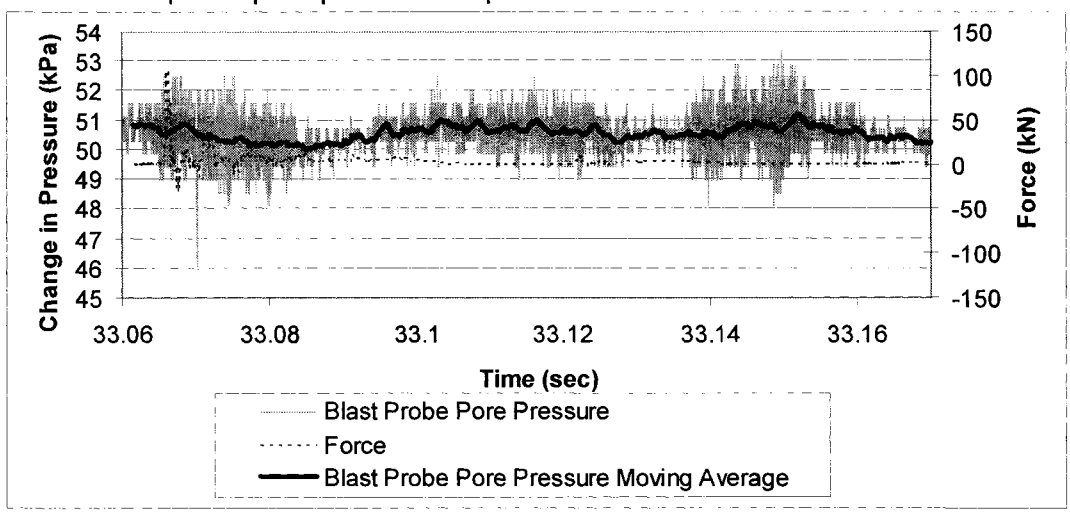

Blow 7 blast probe pore pressure response:

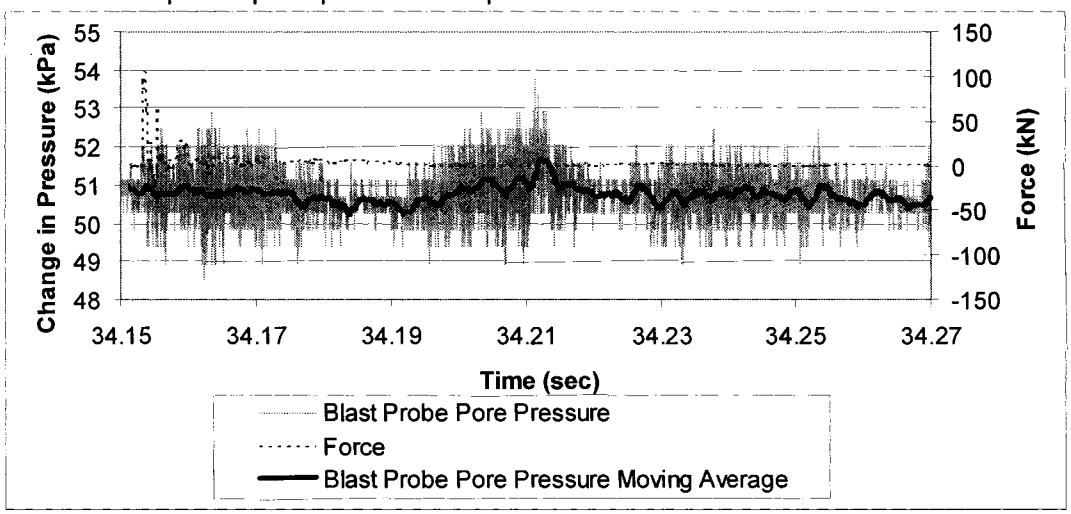

Blow 8 blast probe pore pressure response:

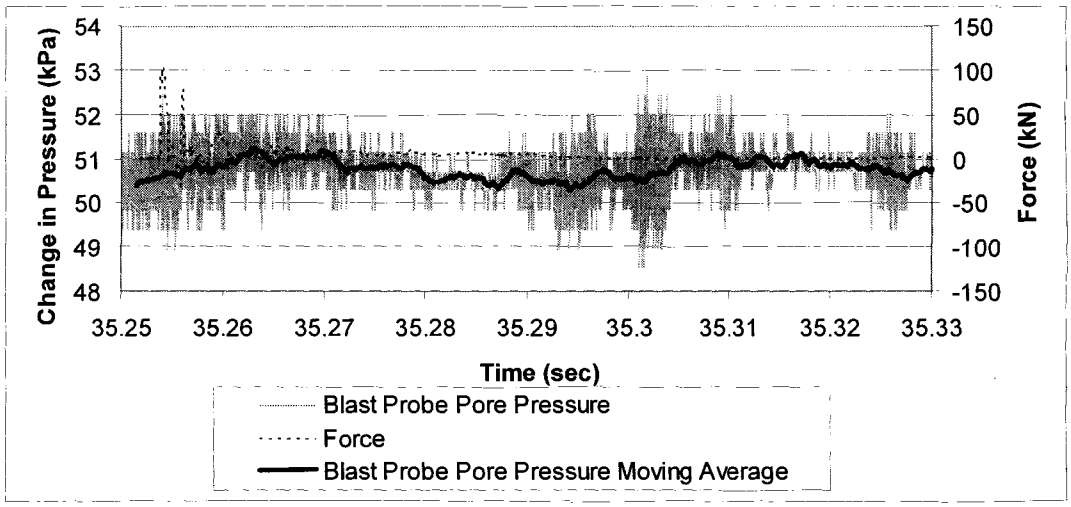

Blow 9 blast probe pore pressure response:

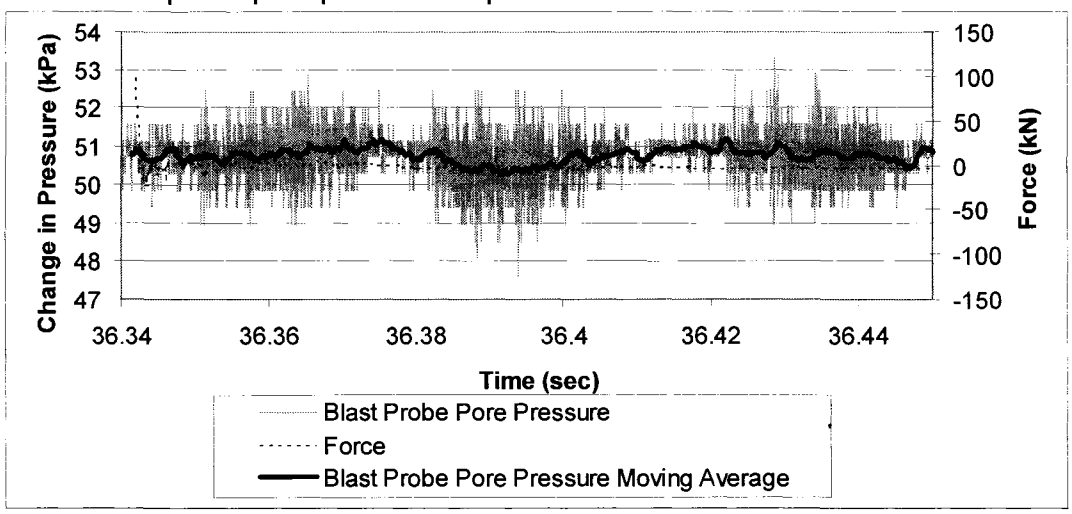

Blow 10 blast probe pore pressure response:

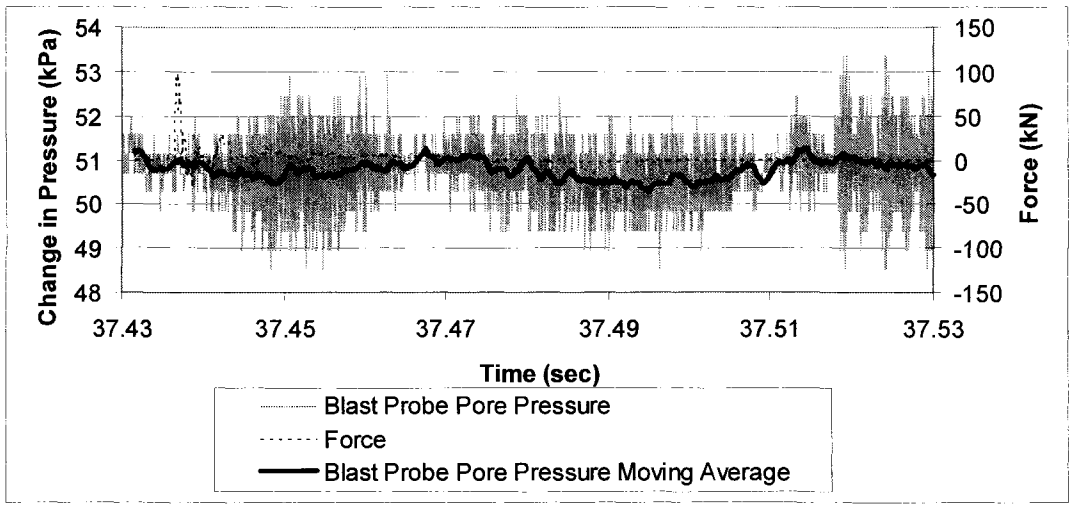

Blow 11 blast probe pore pressure response:

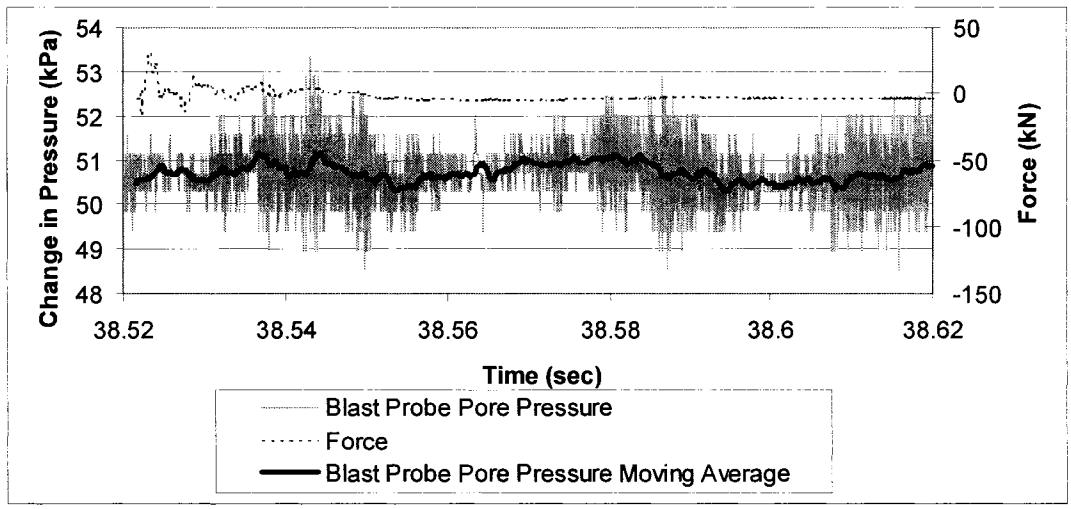

Blow 12 blast probe pore pressure response:

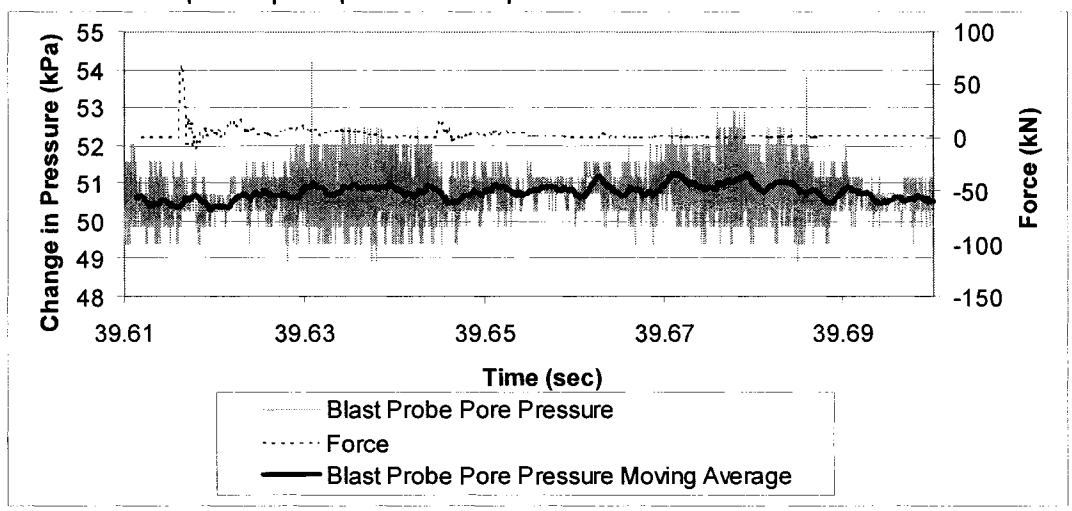

Blast Probe Pore Pressure Response from 8.56 m Depth

Blow 1 blast probe pore pressure response:

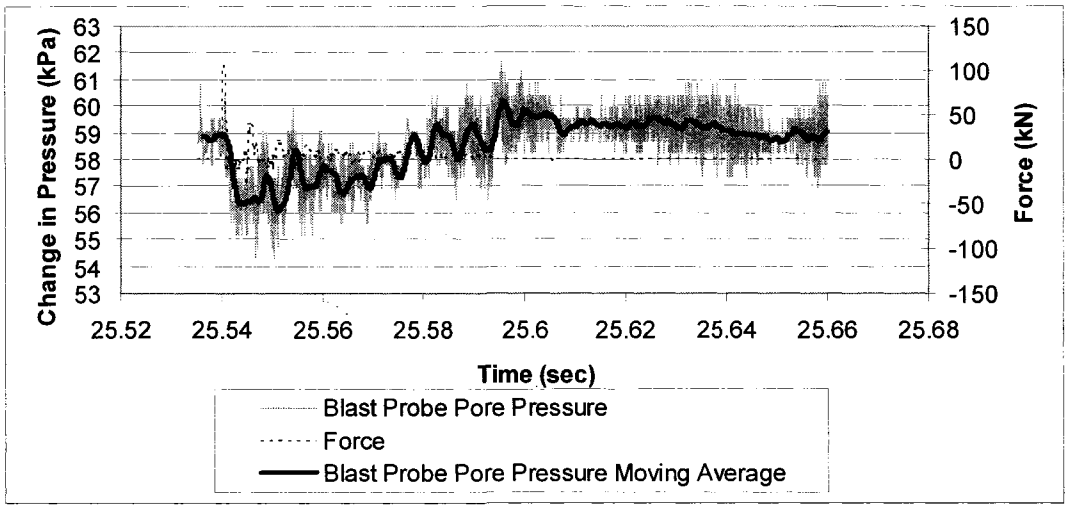

Blow 2 blast probe pore pressure response:

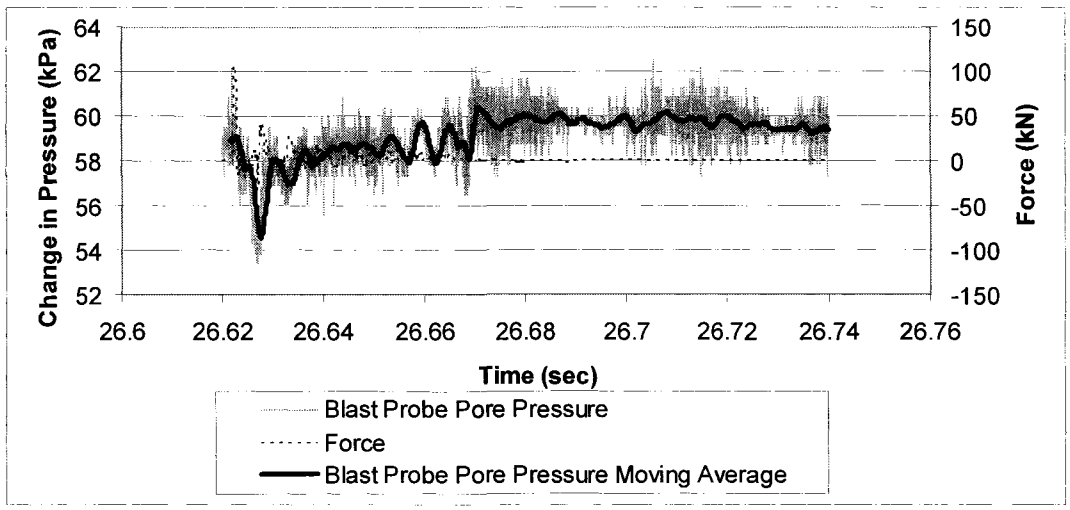

Blow 3 blast probe pore pressure response:

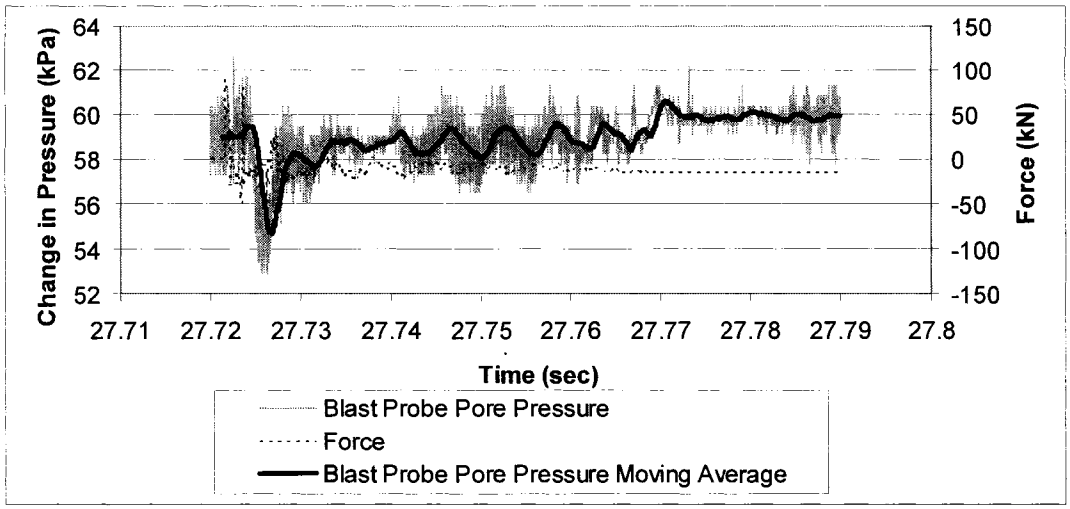

Blow 4 blast probe pore pressure response:

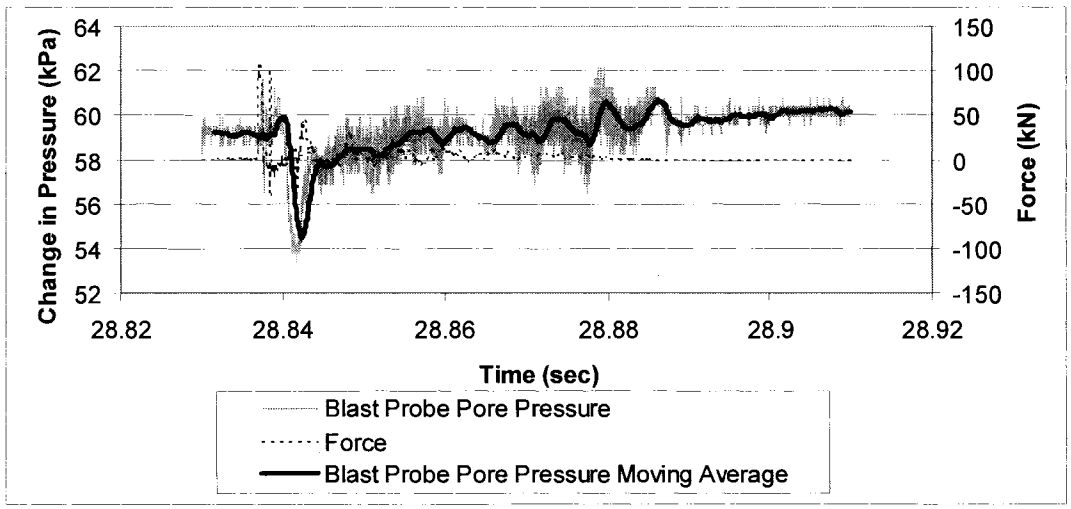

Blow 5 blast probe pore pressure response:

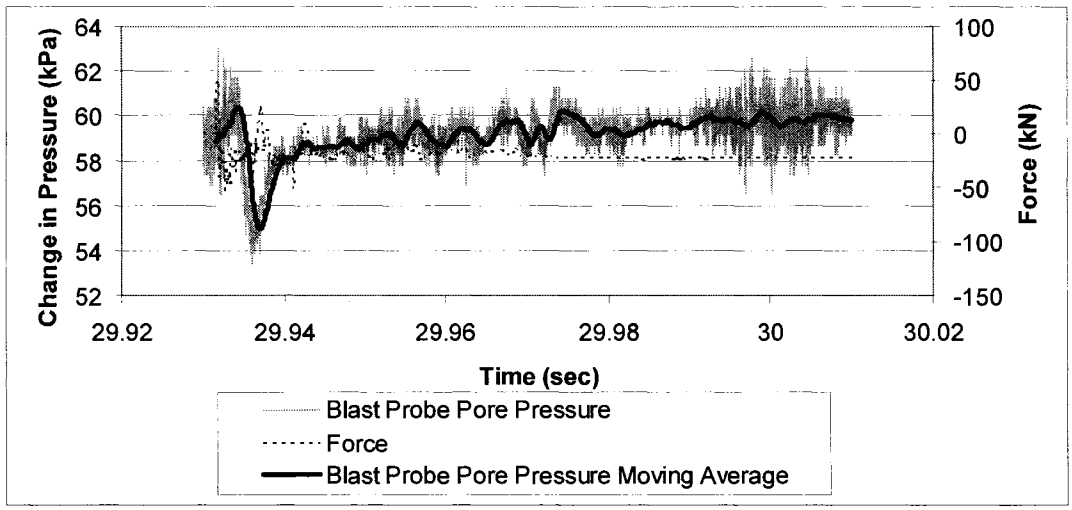

Blow 6 blast probe pore pressure response:

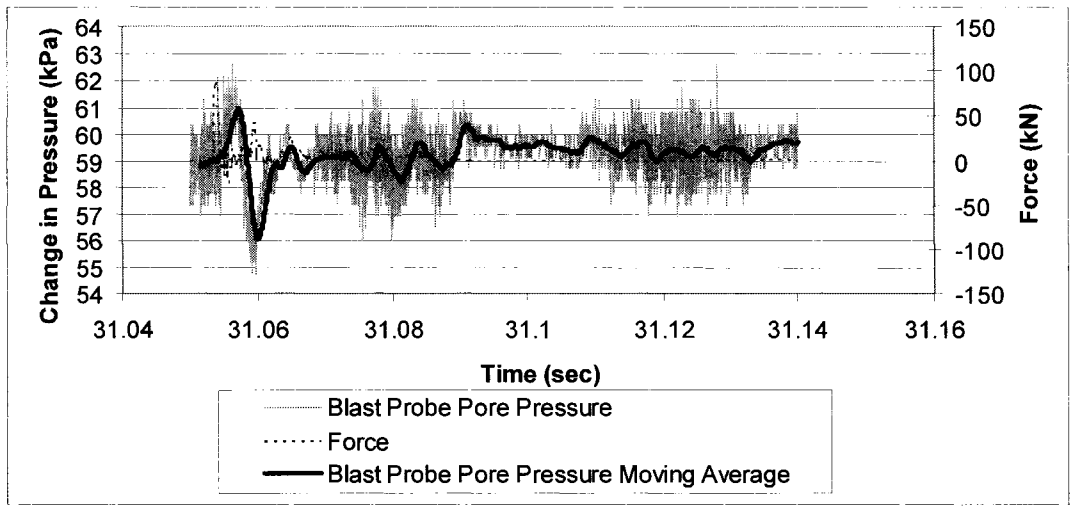

Blow 7 blast probe pore pressure response:

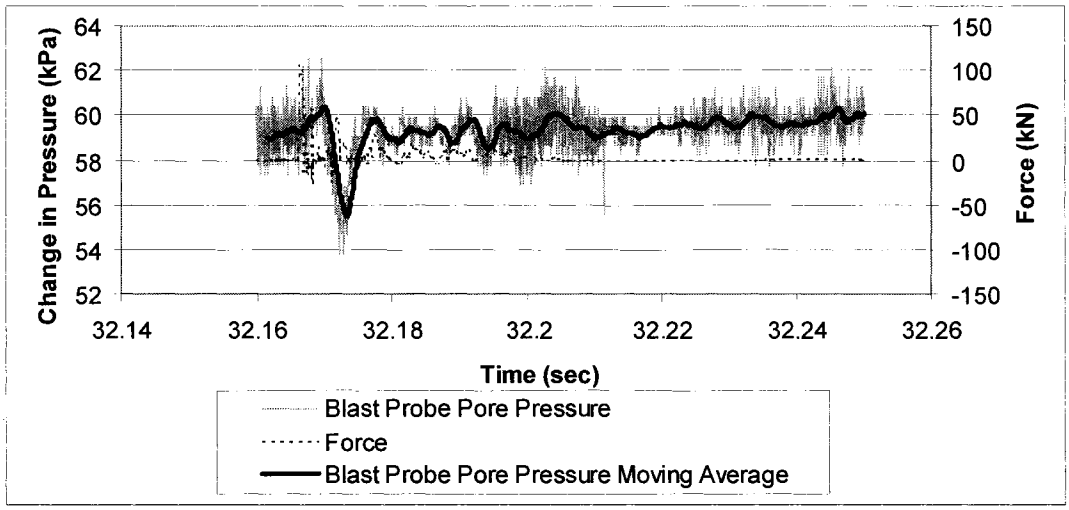

Blow 8 blast probe pore pressure response:

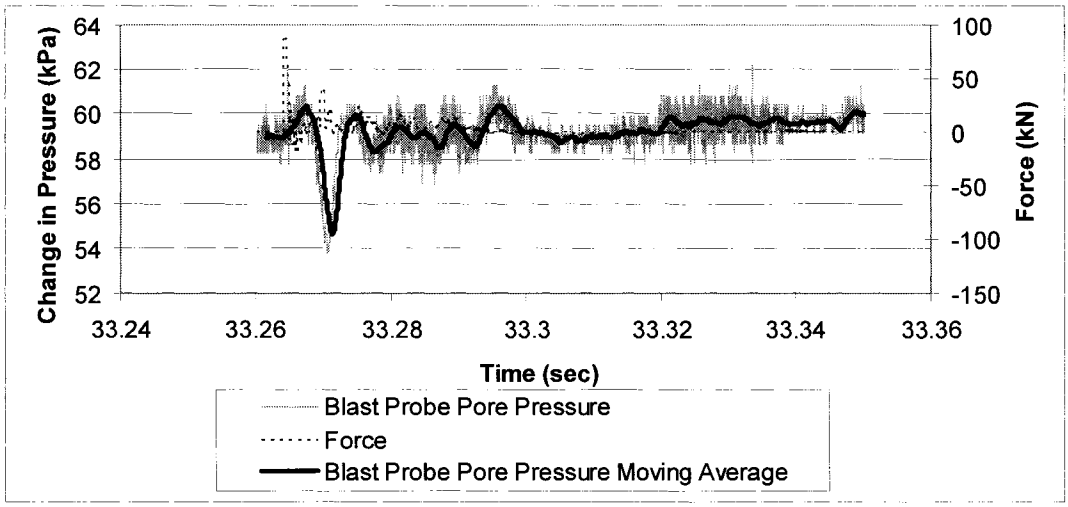

Blow 9 blast probe pore pressure response:

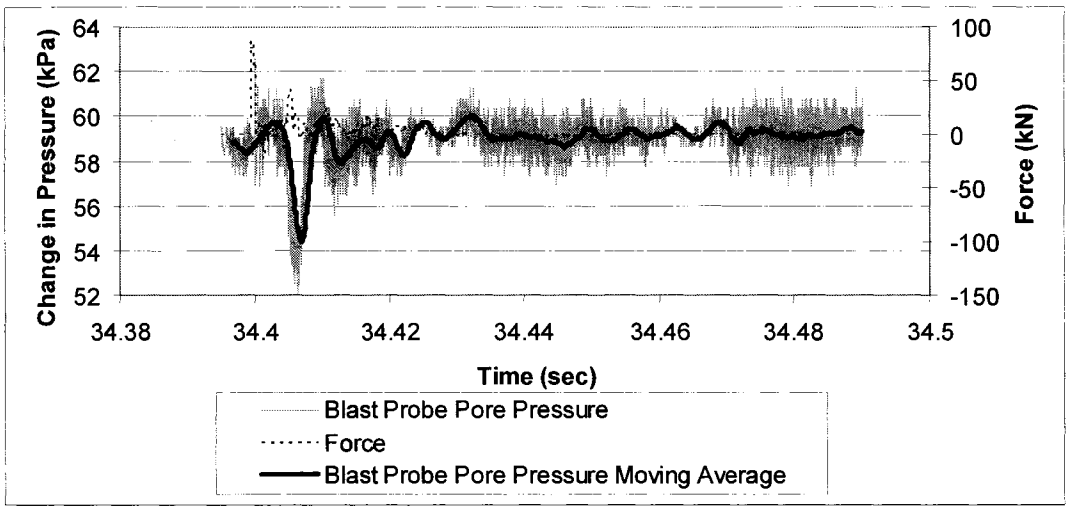

Blast Probe Pore Pressure Response from 9.33 m Depth

Blow 1 blast probe pore pressure response:

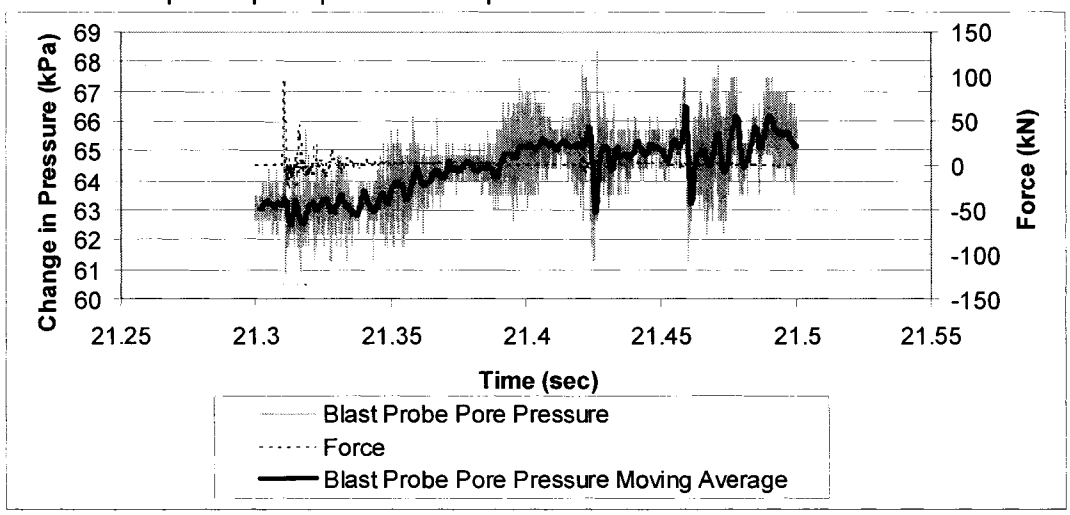

Blow 2 blast probe pore pressure response:

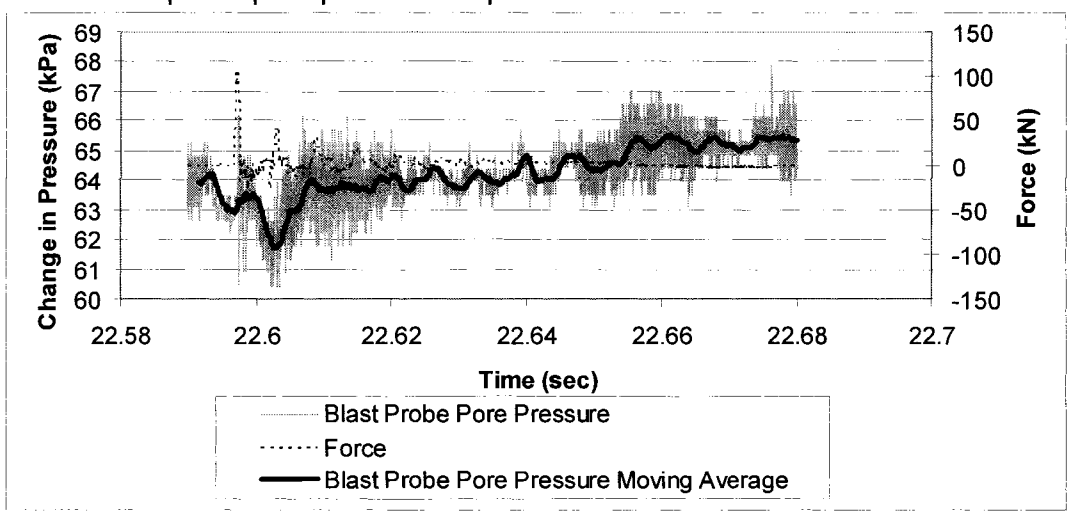

Blow 3 blast probe pore pressure response:

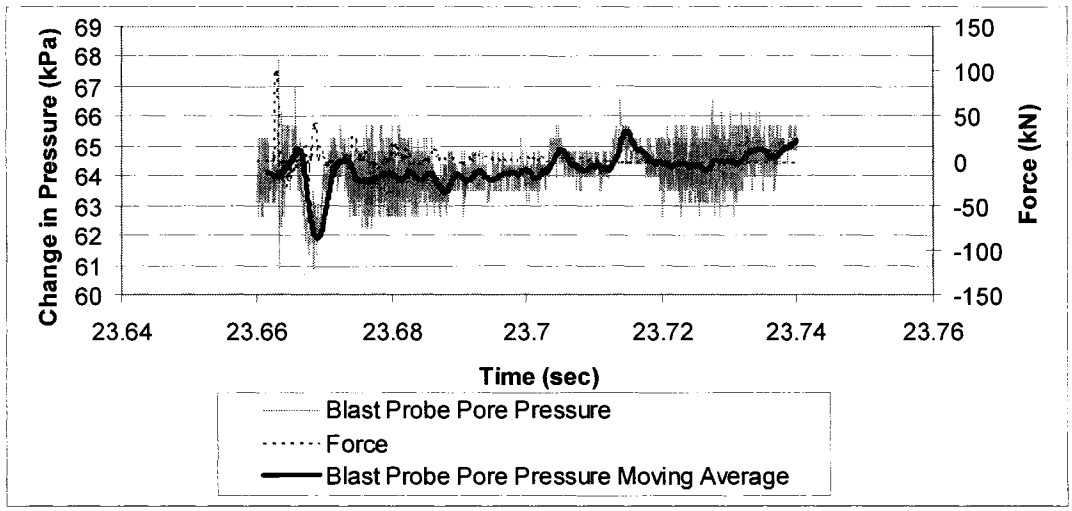

Blow 4 blast probe pore pressure response:

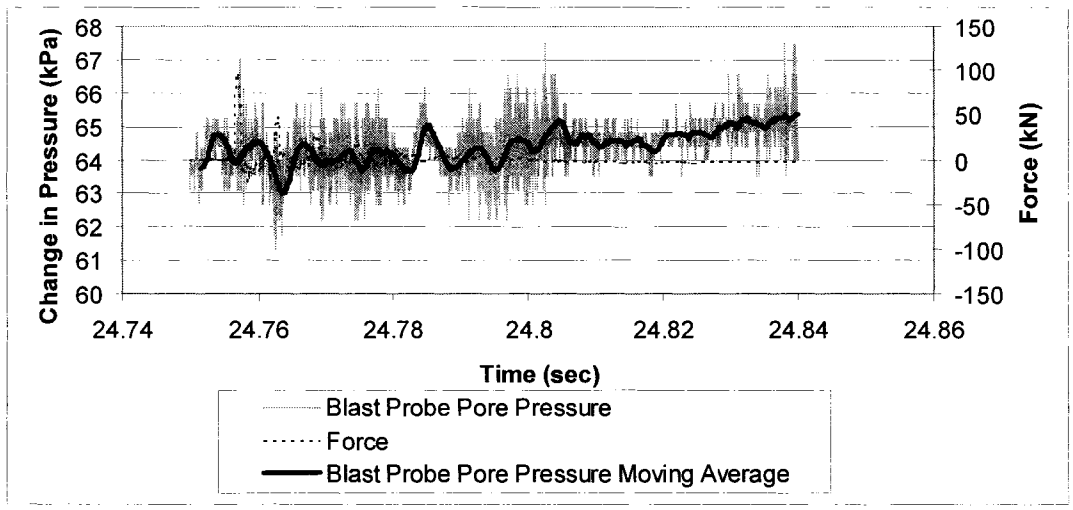

Blow 5 blast probe pore pressure response:

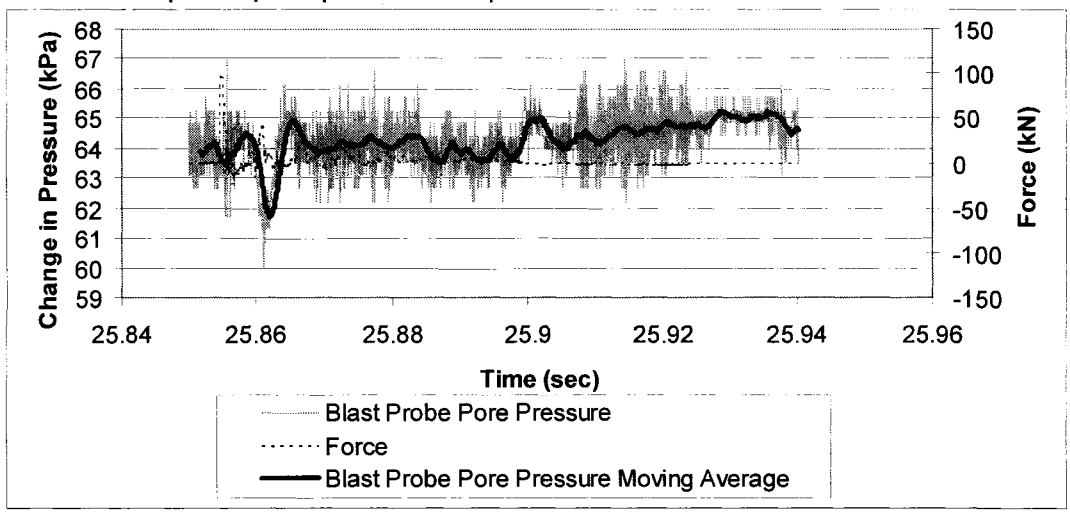

Blow 6 blast probe pore pressure response:

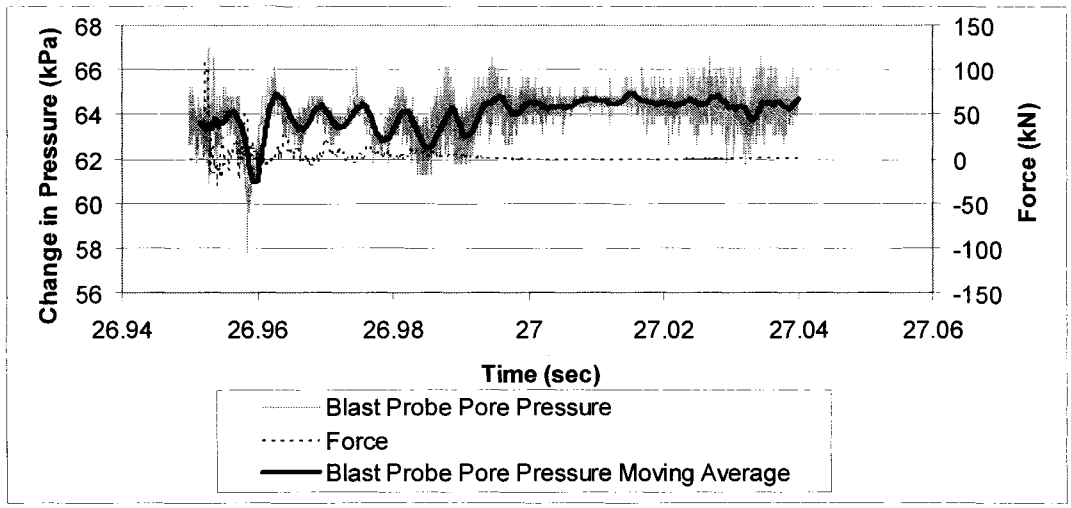

Blow 7 blast probe pore pressure response:

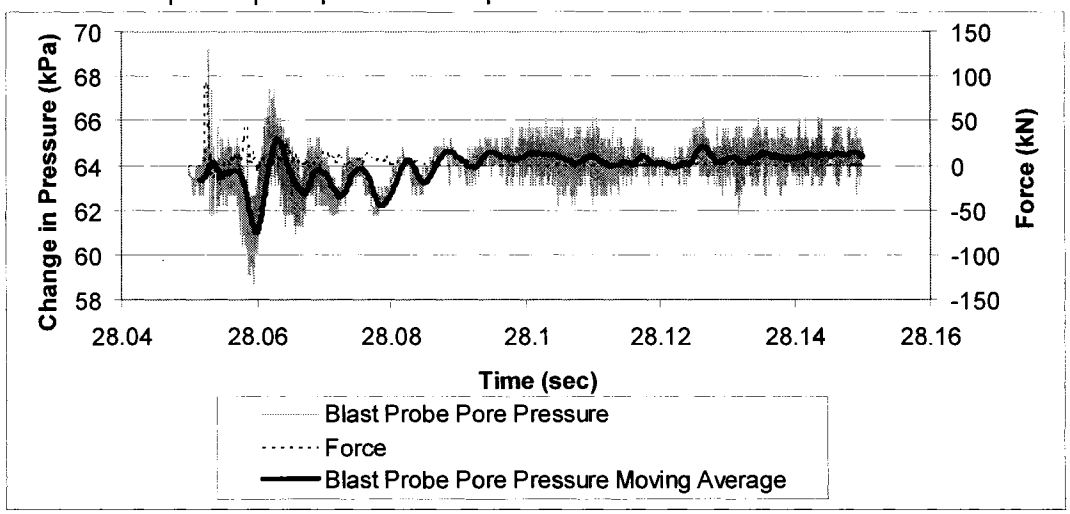

Blow 8 blast probe pore pressure response:

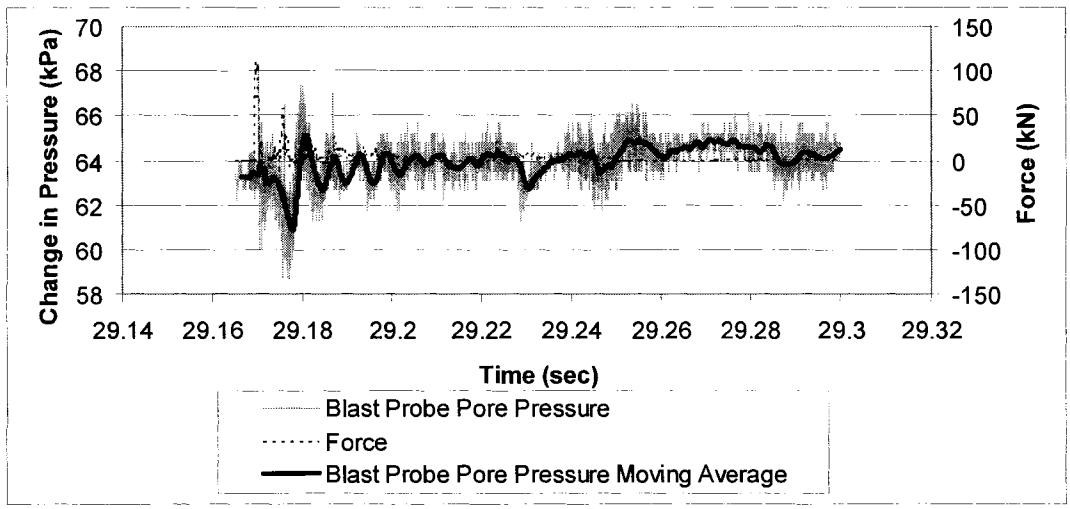

Blast Probe Pore Pressure Response from 10.80 m Depth

Blow 1 blast probe pore pressure response:

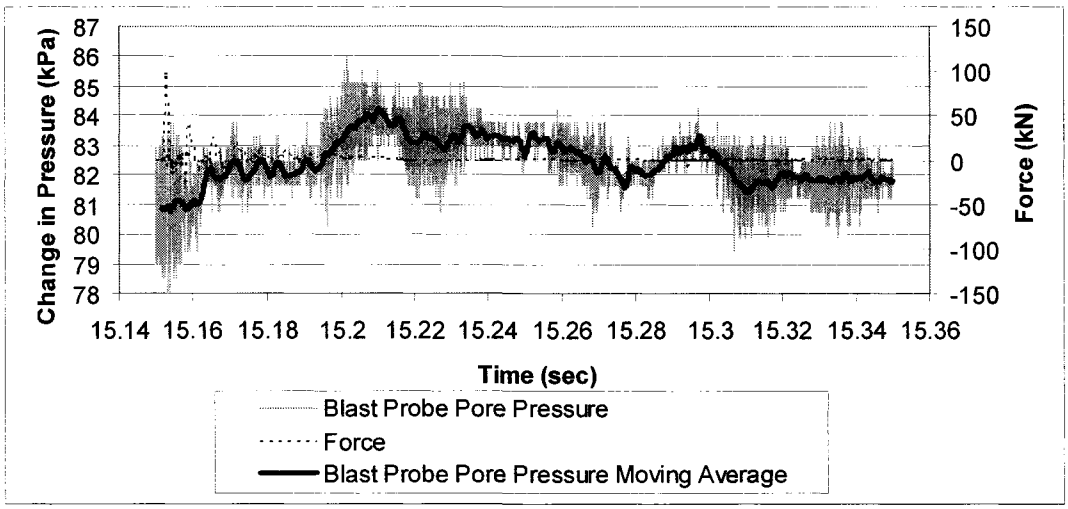

Blow 2 blast probe pore pressure response:

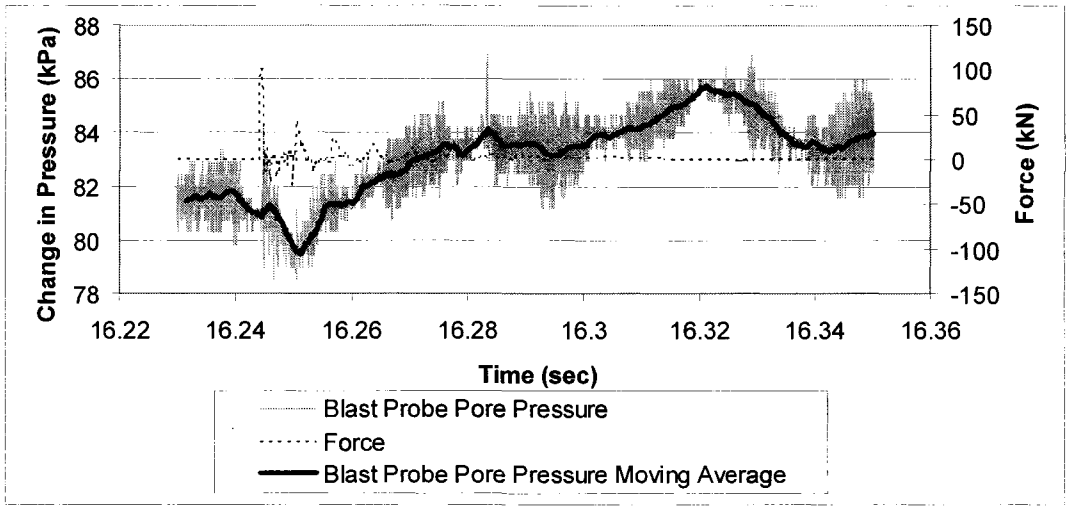

Blow 3 blast probe pore pressure response:

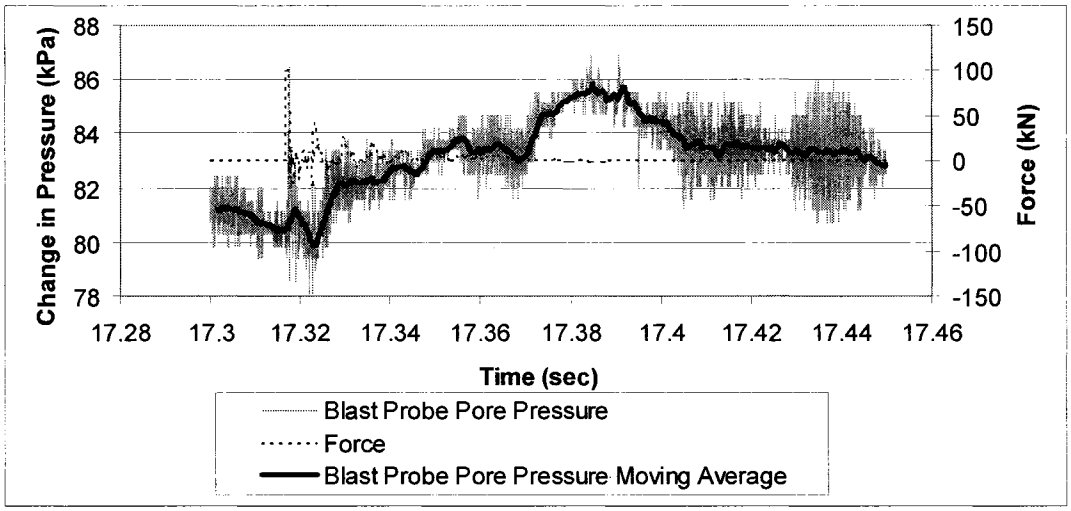

Blow 4 blast probe pore pressure response:

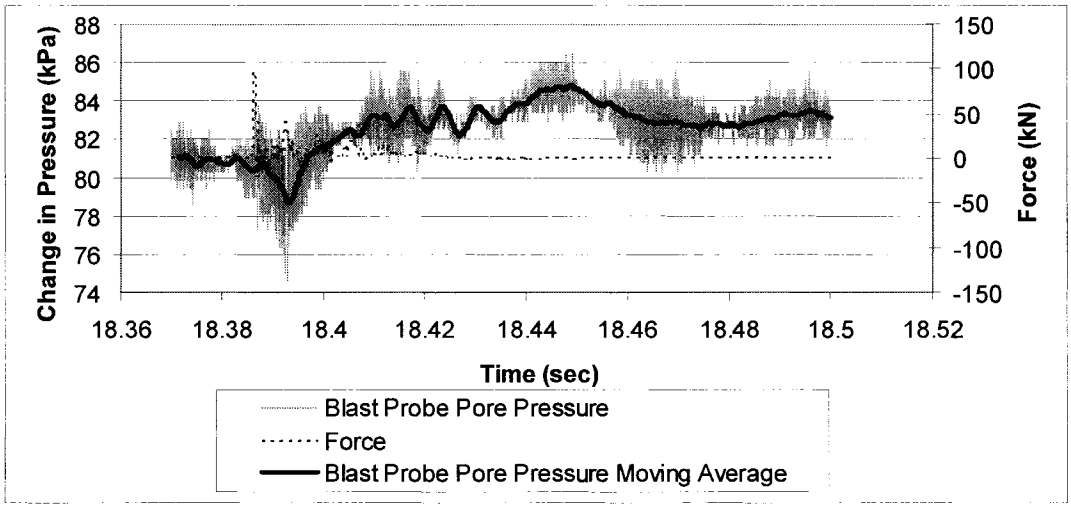

Blow 5 blast probe pore pressure response:

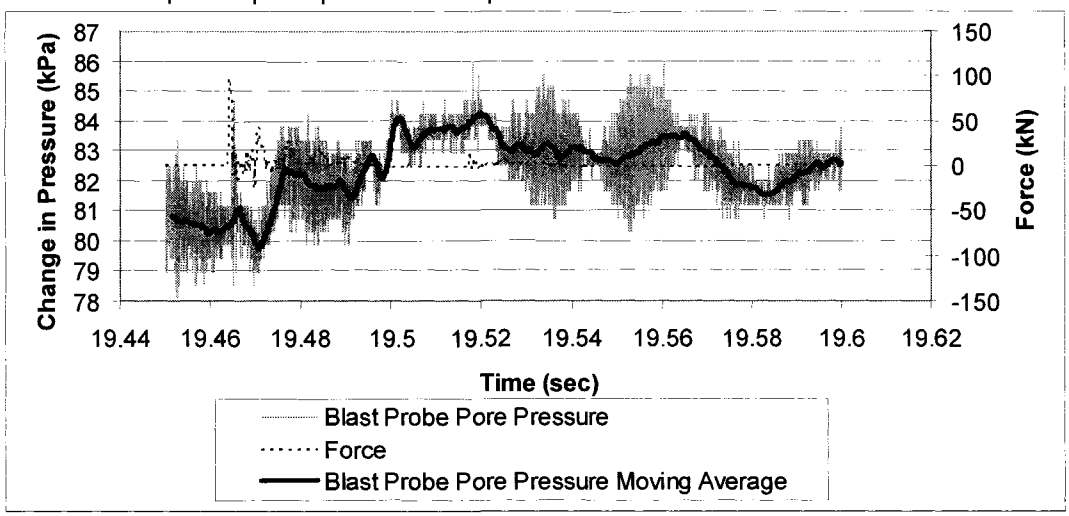

Blow 6 blast probe pore pressure response:

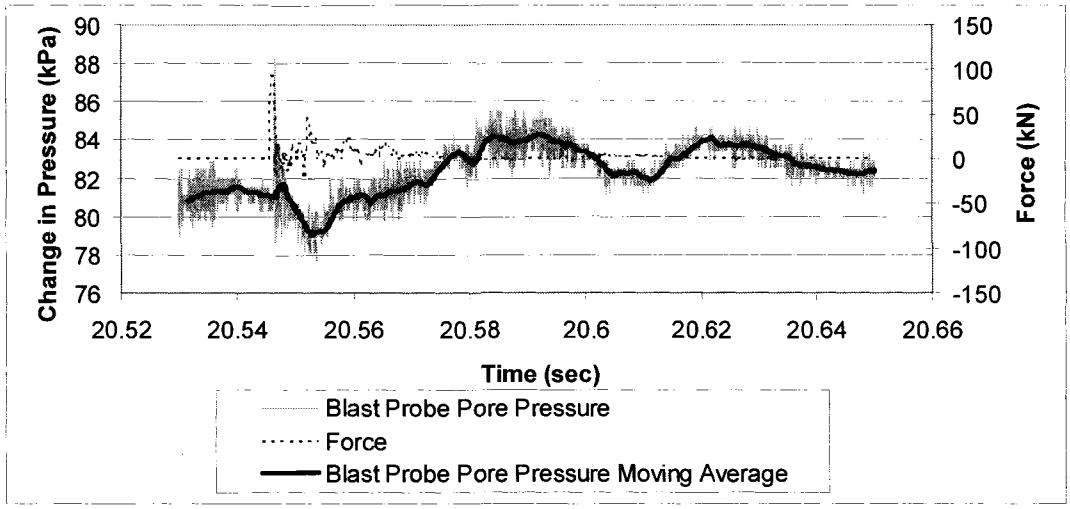

Blow 7 blast probe pore pressure response:

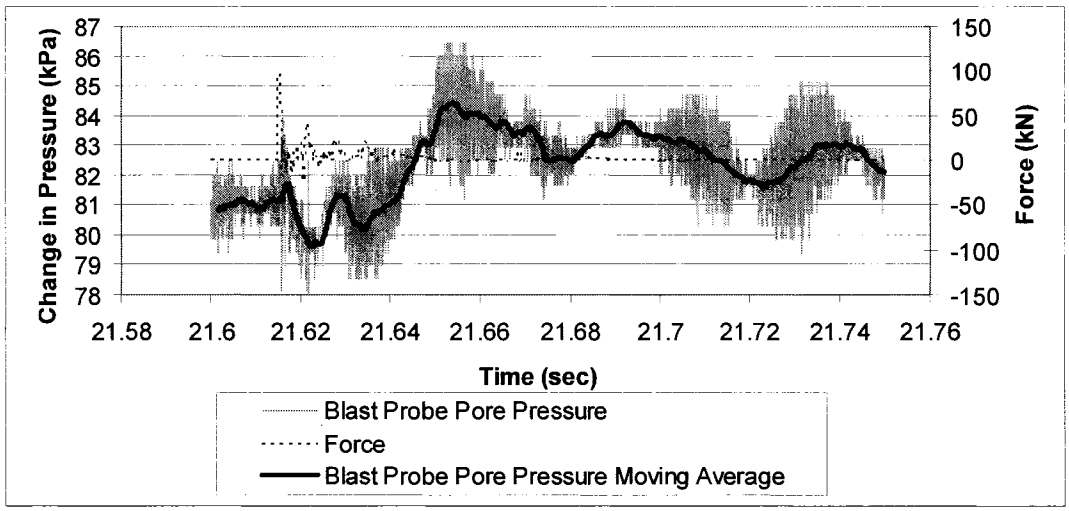

Blow 8 blast probe pore pressure response:

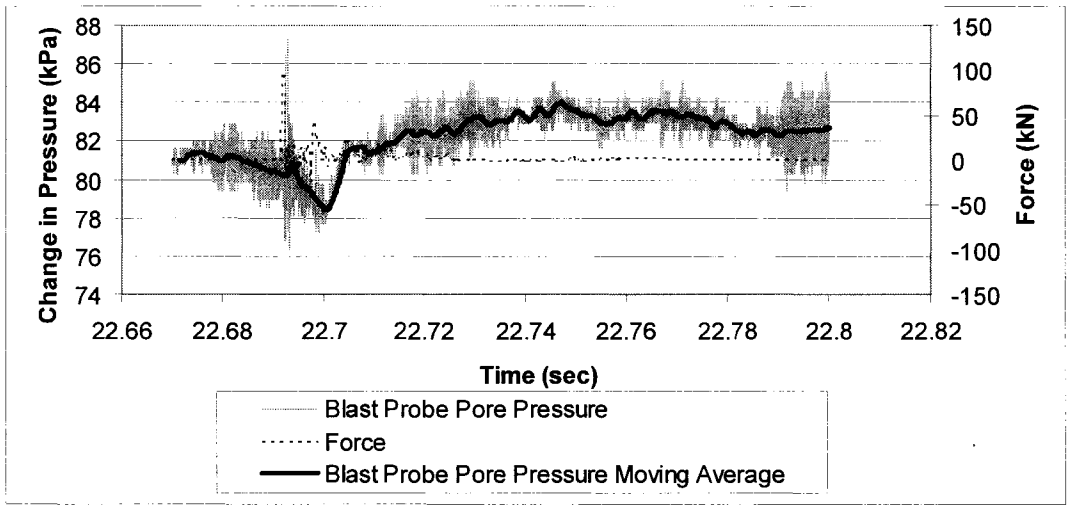

Blow 9 blast probe pore pressure response:

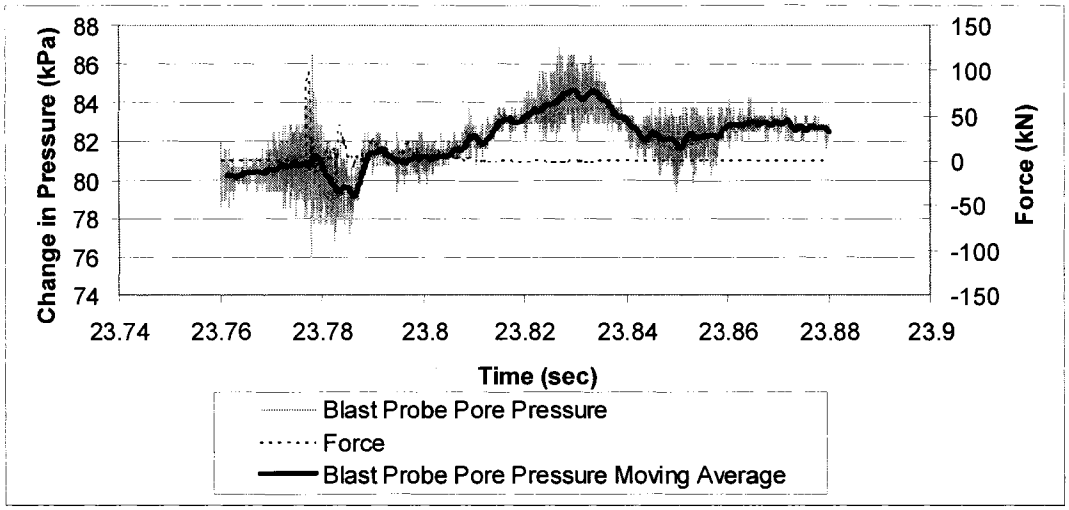

Blow 10 blast probe pore pressure response:

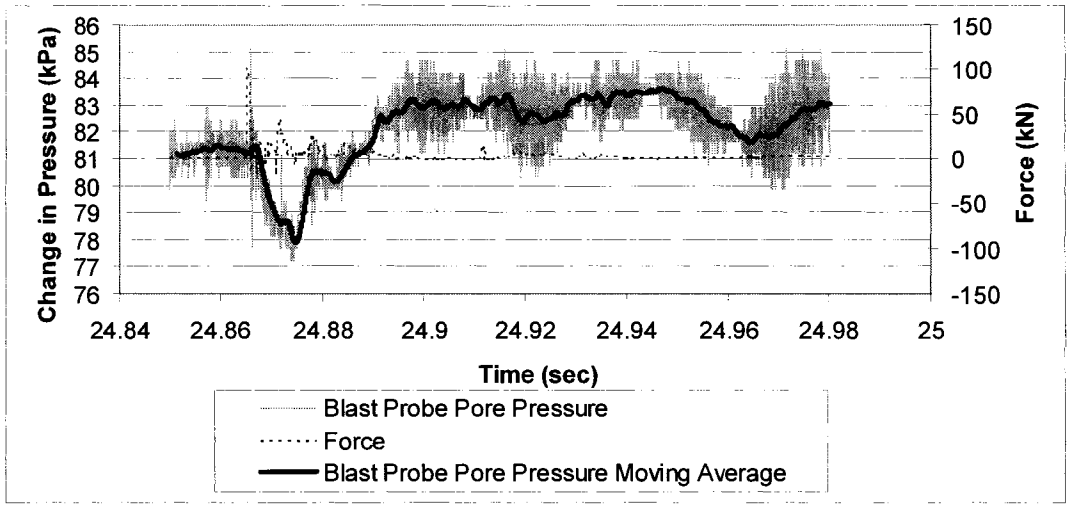

Blast Probe Pore Pressure Response from 12.41 m Depth

Blow 1 blast probe pore pressure response:

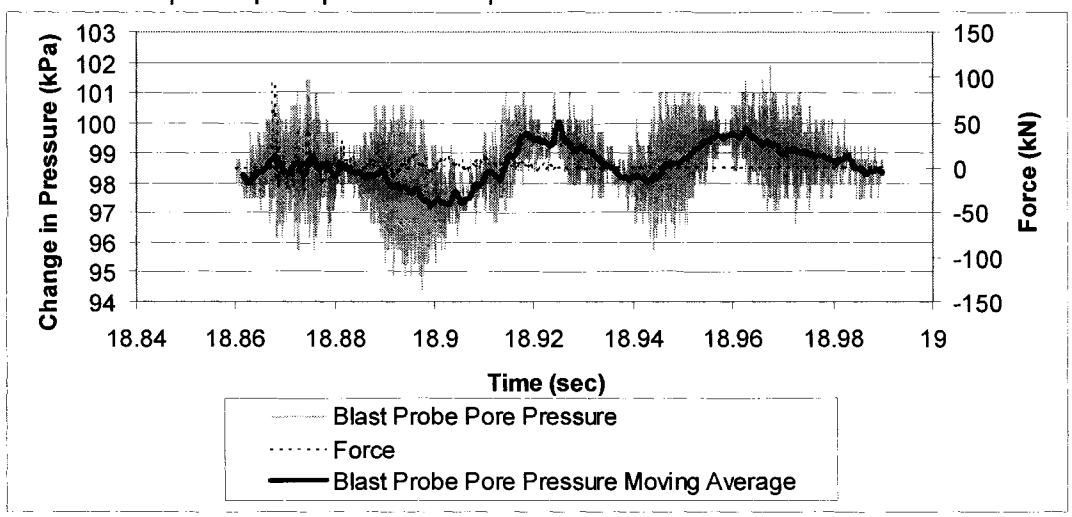

Blow 2 blast probe pore pressure response:

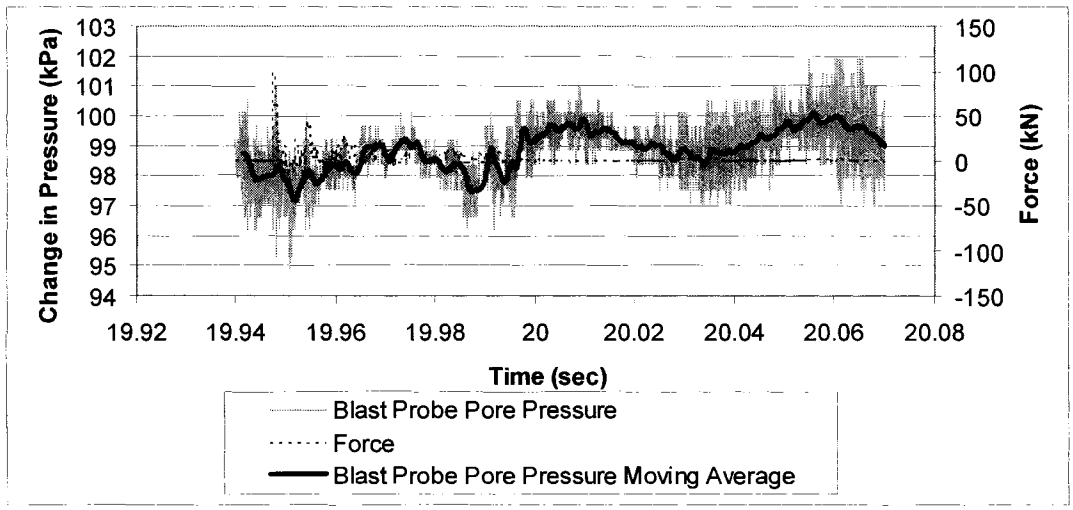

Blow 3 blast probe pore pressure response:

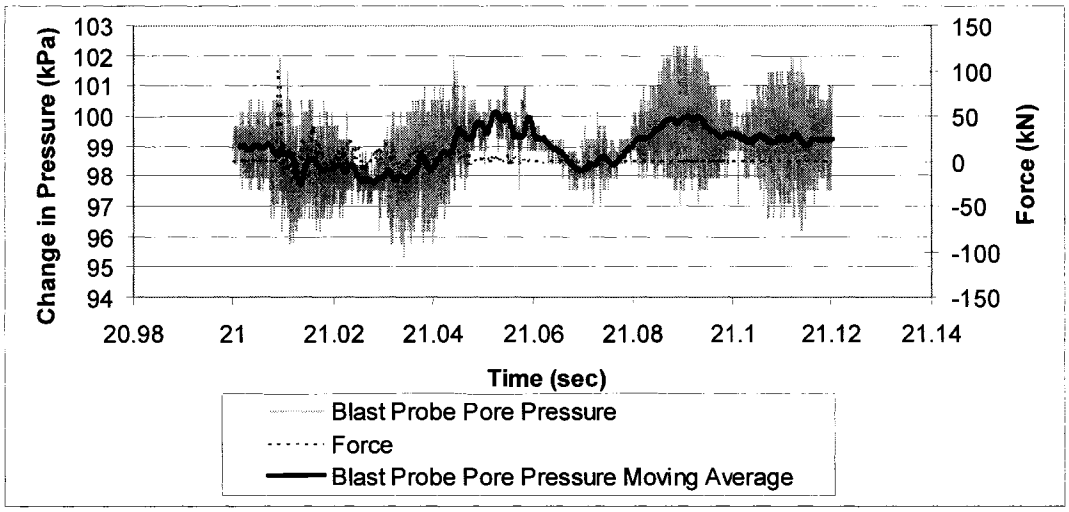

Blow 4 blast probe pore pressure response:

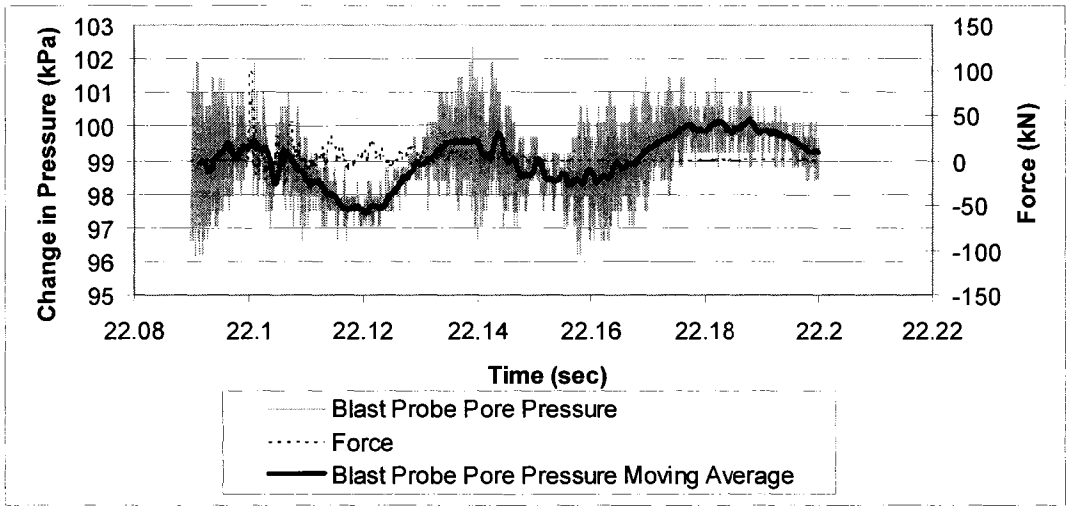

Blow 5 blast probe pore pressure response:

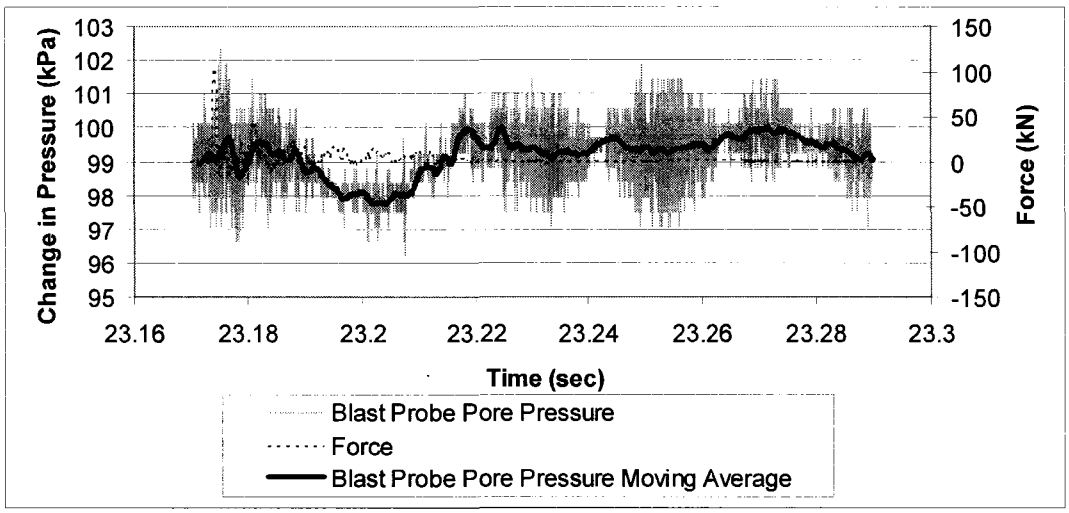

Blow 6 blast probe pore pressure response:

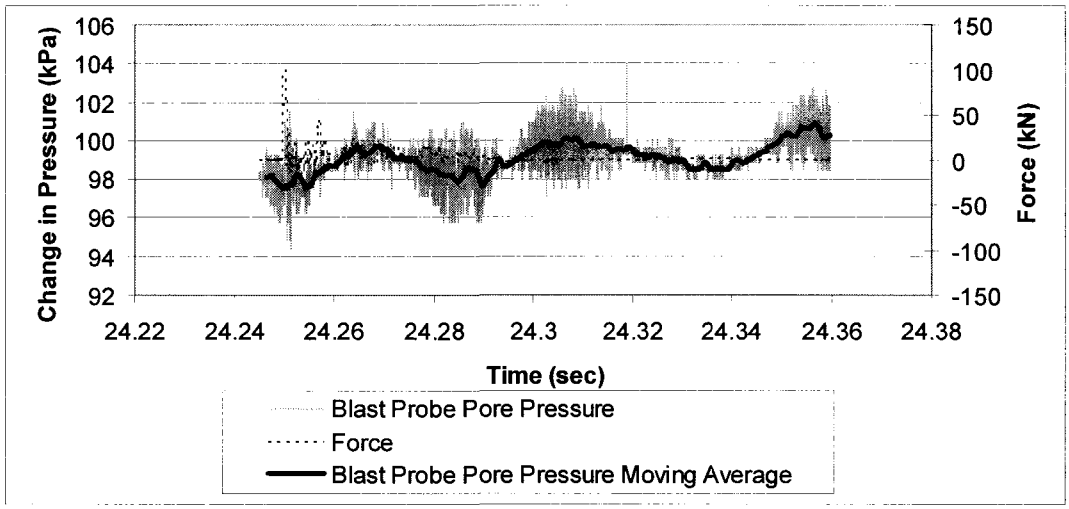

Blow 7 blast probe pore pressure response:

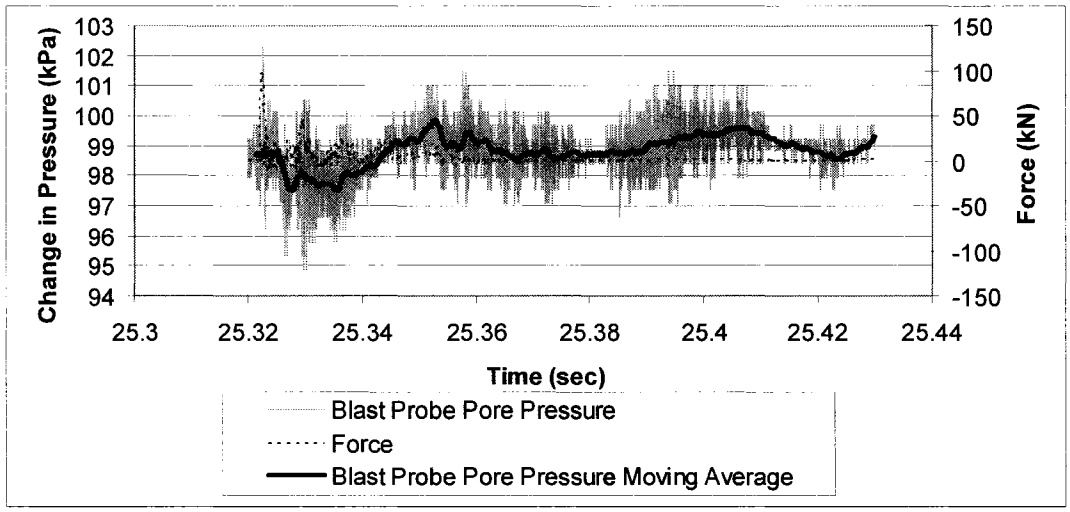

Blow 8 blast probe pore pressure response:

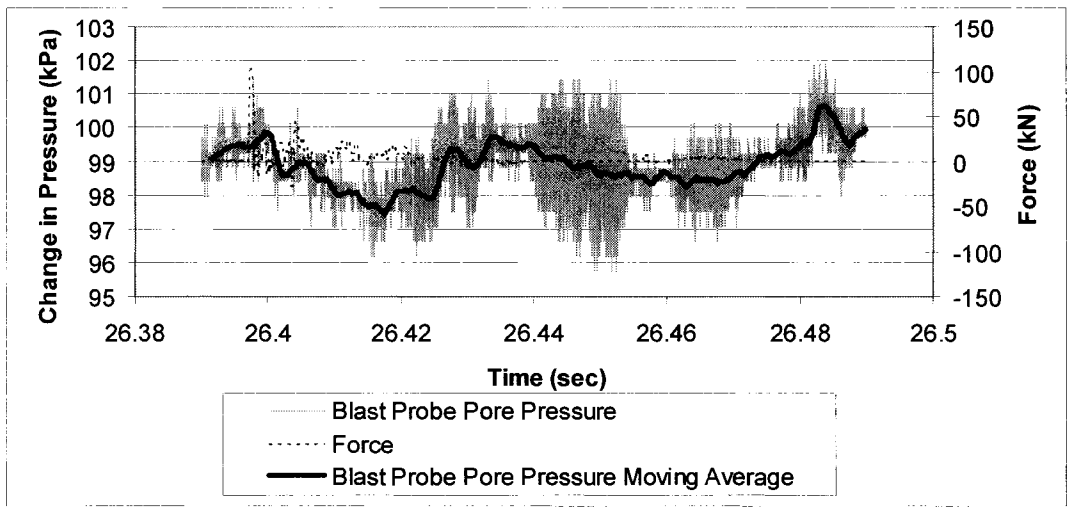

Blow 9 blast probe pore pressure response:

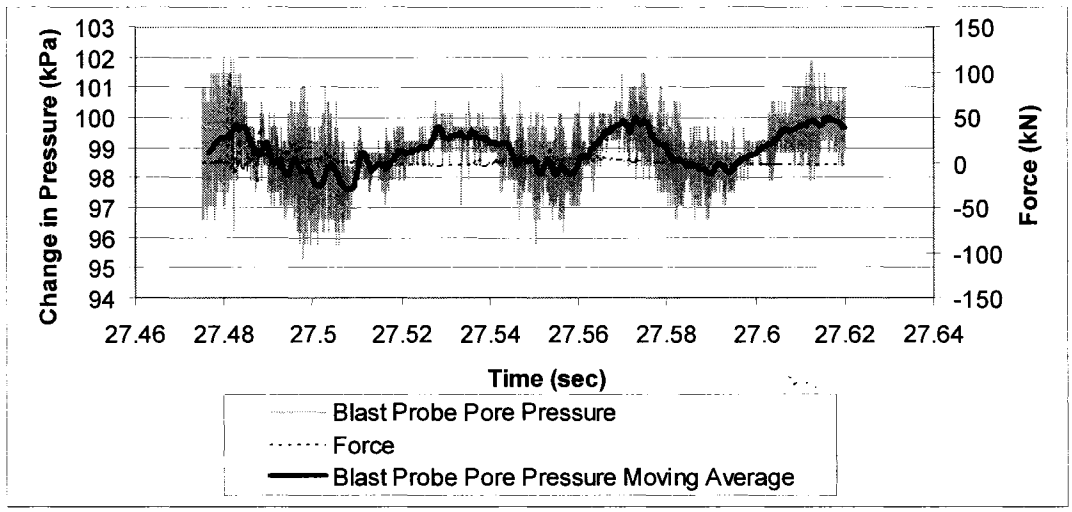

Blow 10 blast probe pore pressure response:

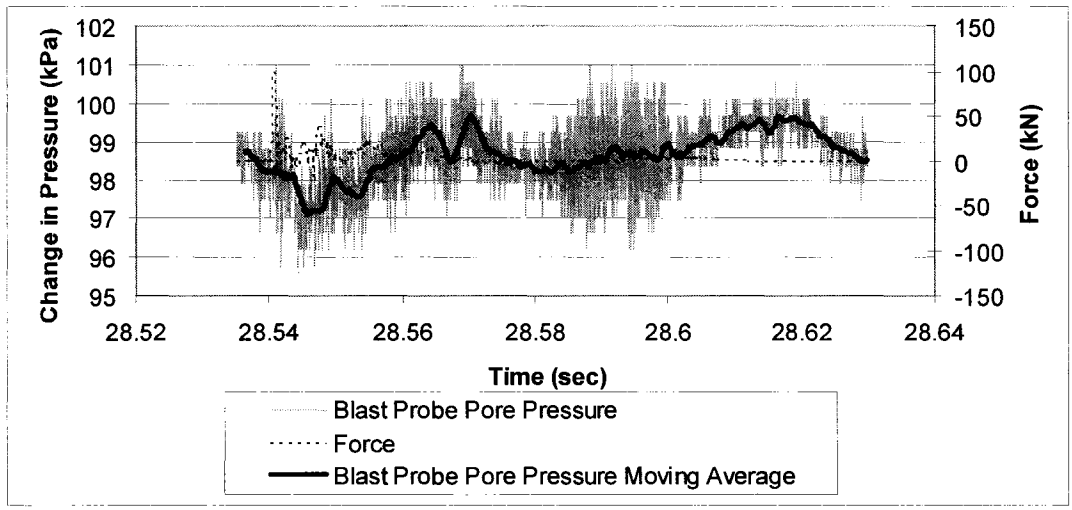

Blow 11 blast probe pore pressure response:

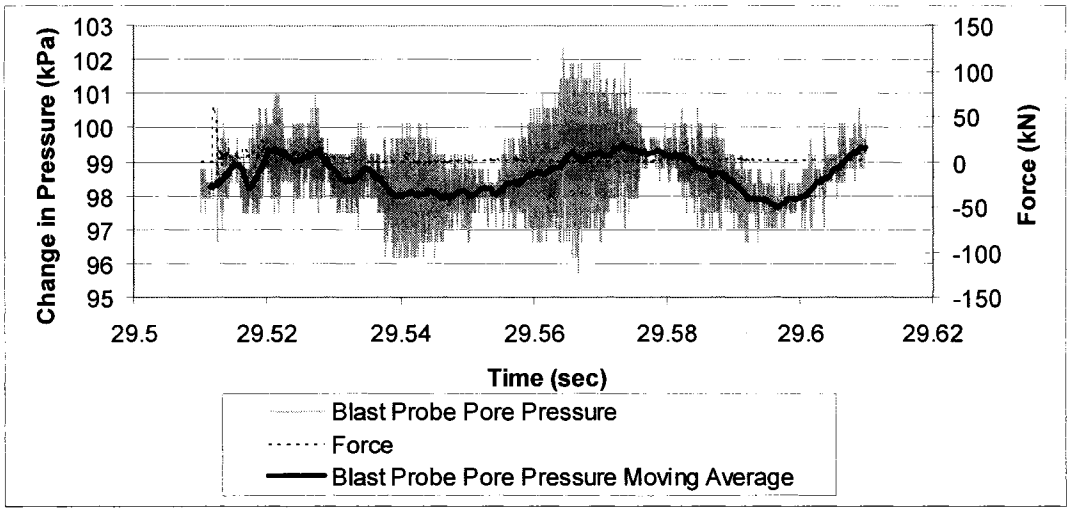

Blast Probe Pore Pressure Response from 13.92 m Depth

Blow 1 blast probe pore pressure response:

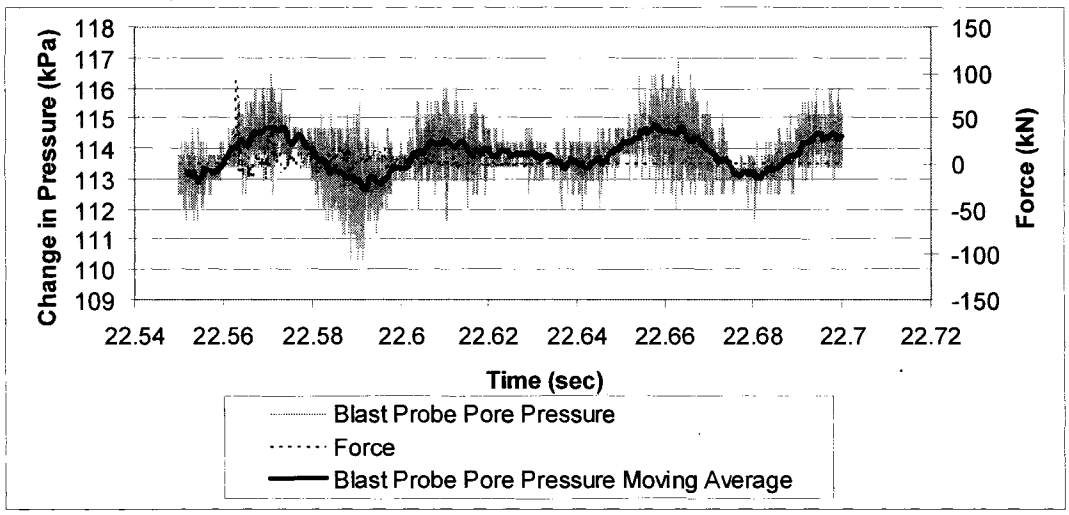

Blow 2 blast probe pore pressure response:

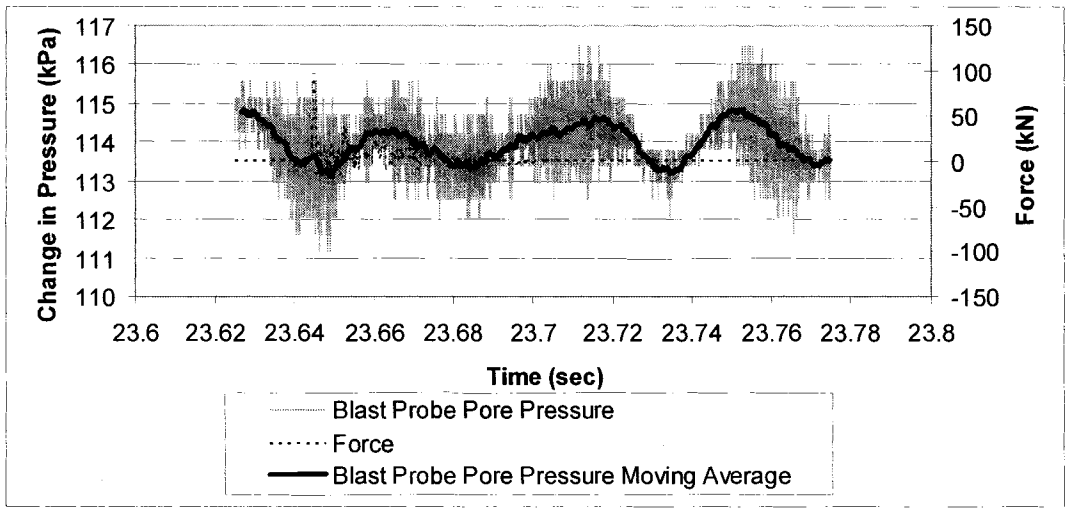

Blow 3 blast probe pore pressure response:

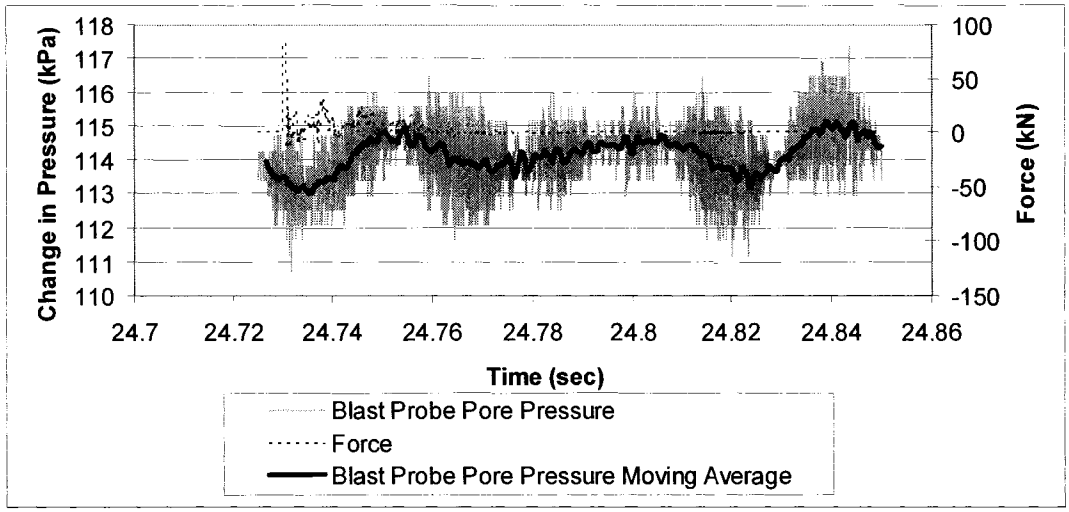

Blow 4 blast probe pore pressure response:

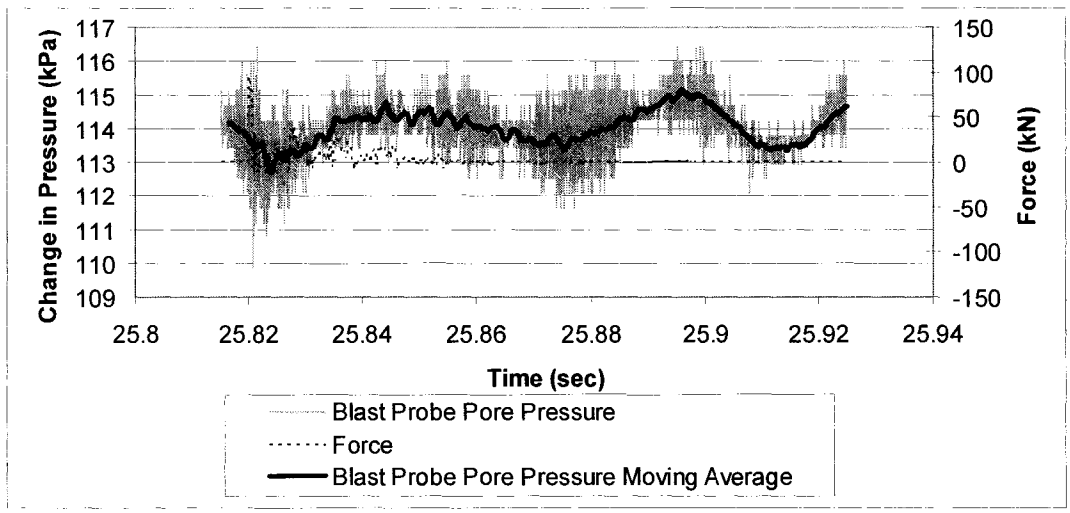

Blow 5 blast probe pore pressure response:

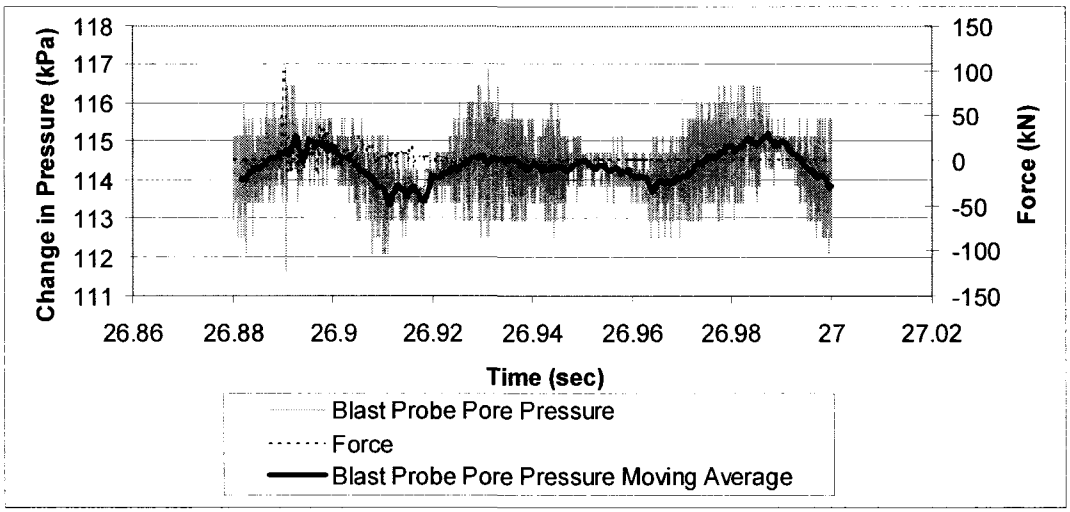

Blow 6 blast probe pore pressure response:

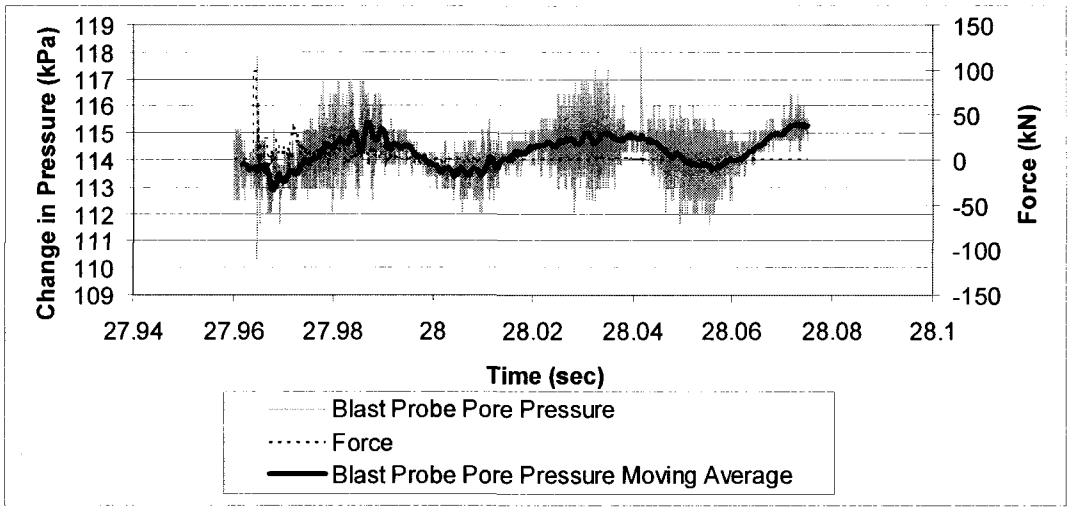

Blow 7 blast probe pore pressure response:

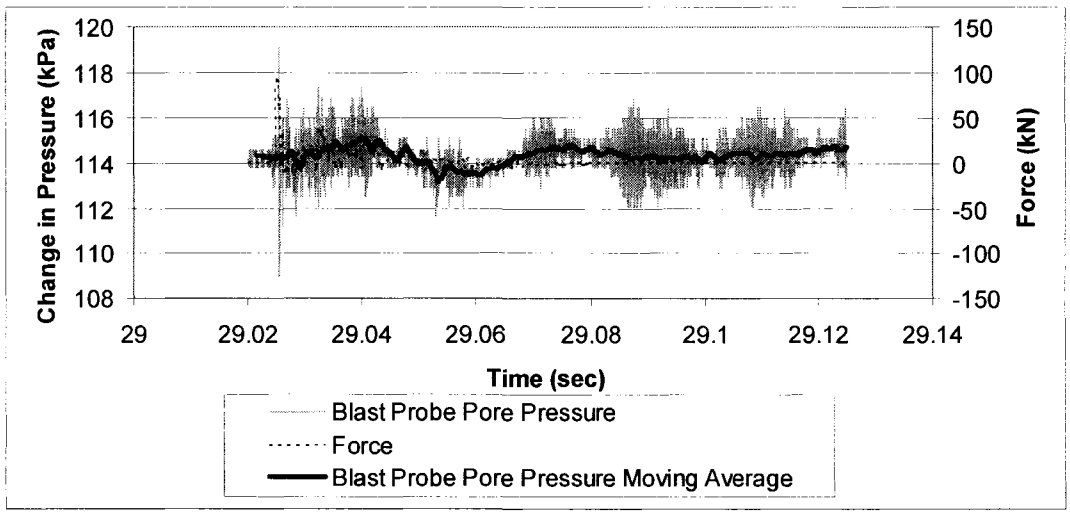

Blow 8 blast probe pore pressure response:

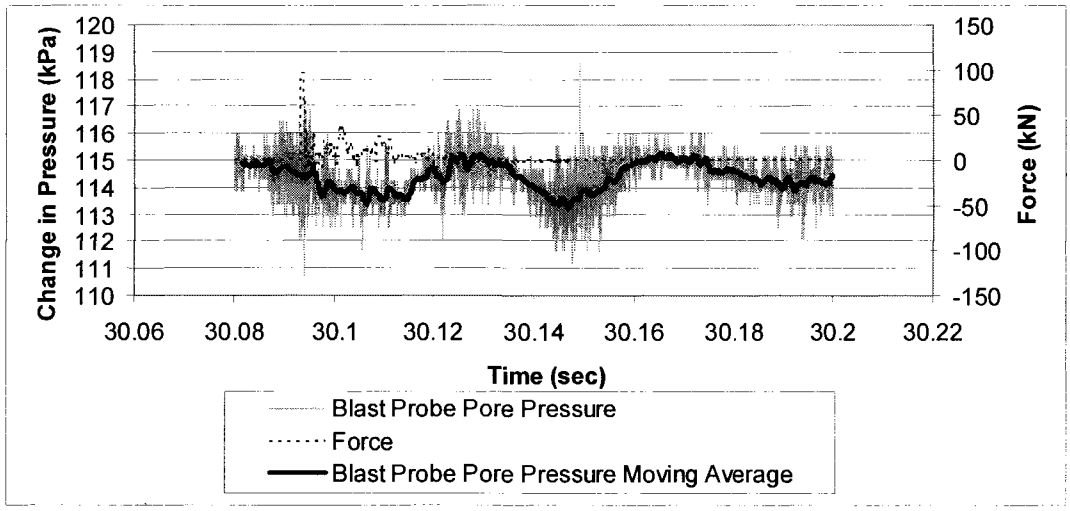

Blow 9 blast probe pore pressure response:

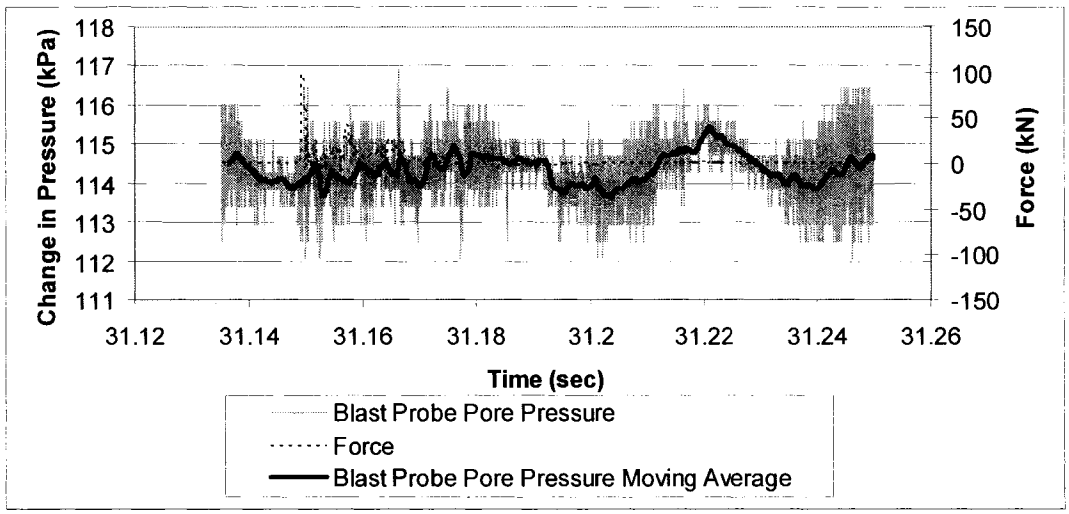

Blow 10 blast probe pore pressure response:

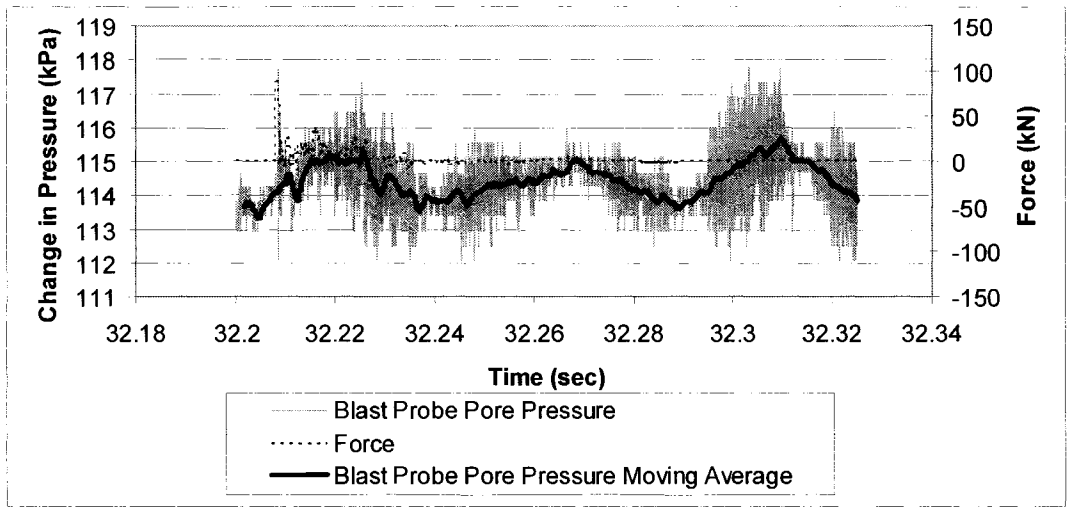

Blow 11 blast probe pore pressure response:

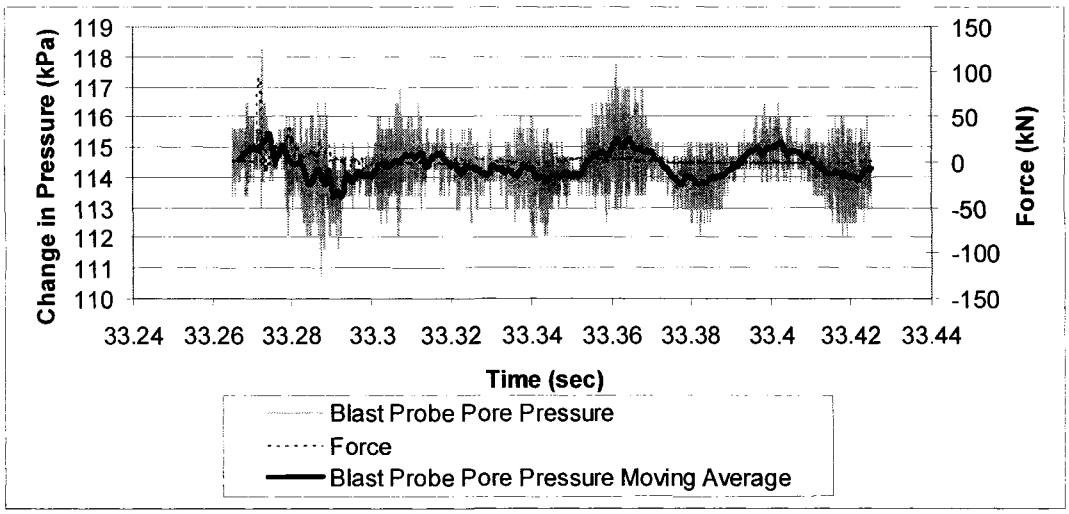

Blow 12 blast probe pore pressure response:

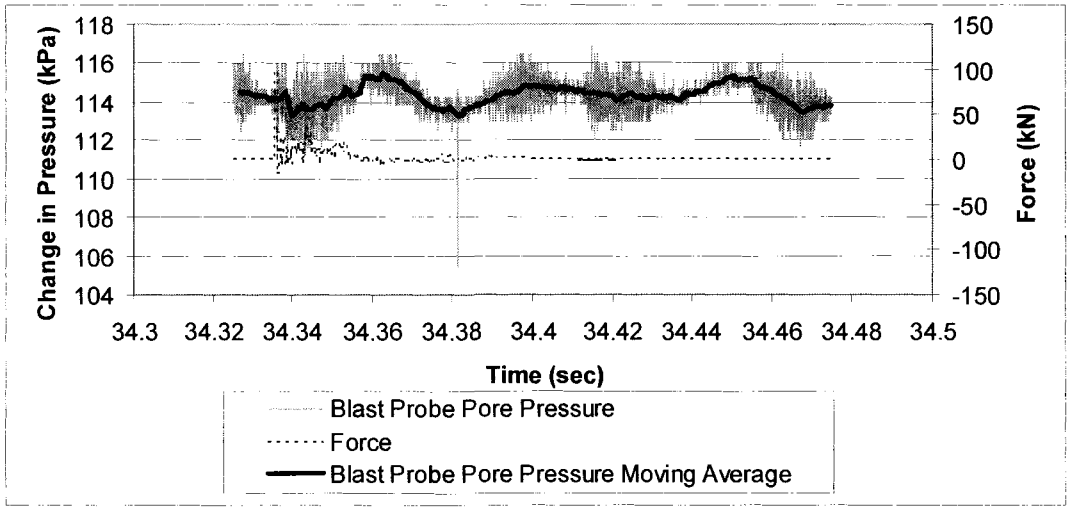

Blow 13 blast probe pore pressure response:

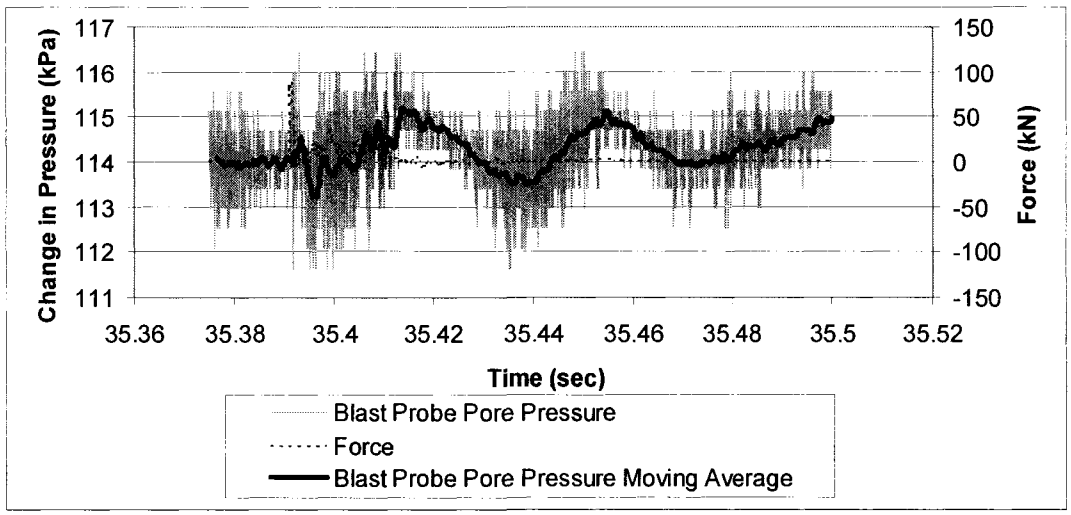

Blow 14 blast probe pore pressure response:

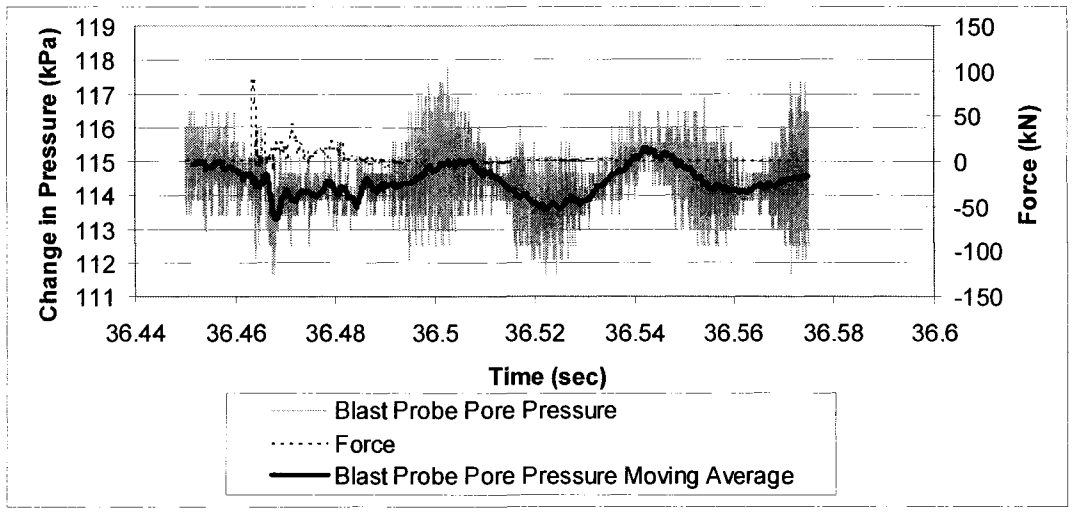

Blow 15 blast probe pore pressure response:

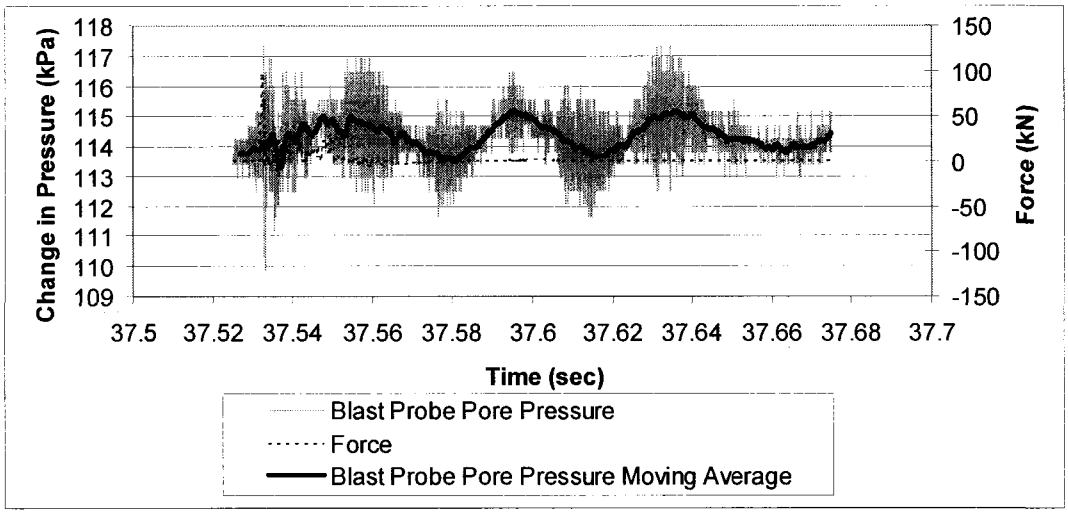

Blow 16 blast probe pore pressure response:

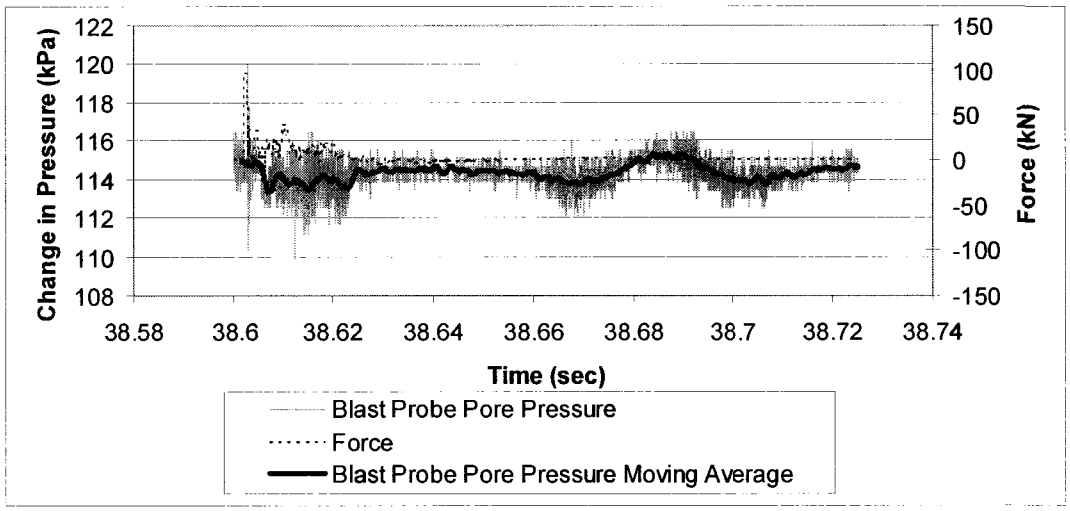

Blow 17 blast probe pore pressure response:

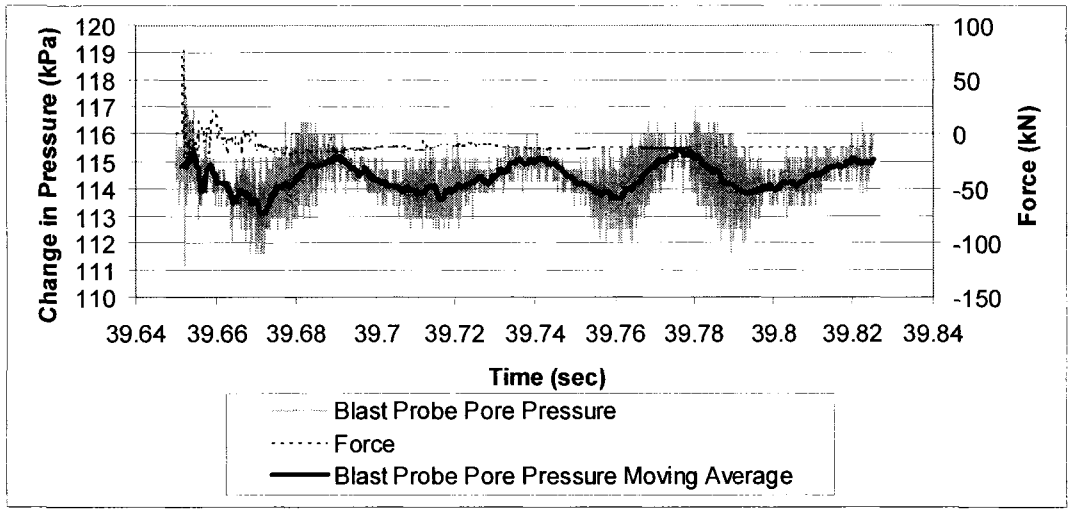

Blow 18 blast probe pore pressure response:

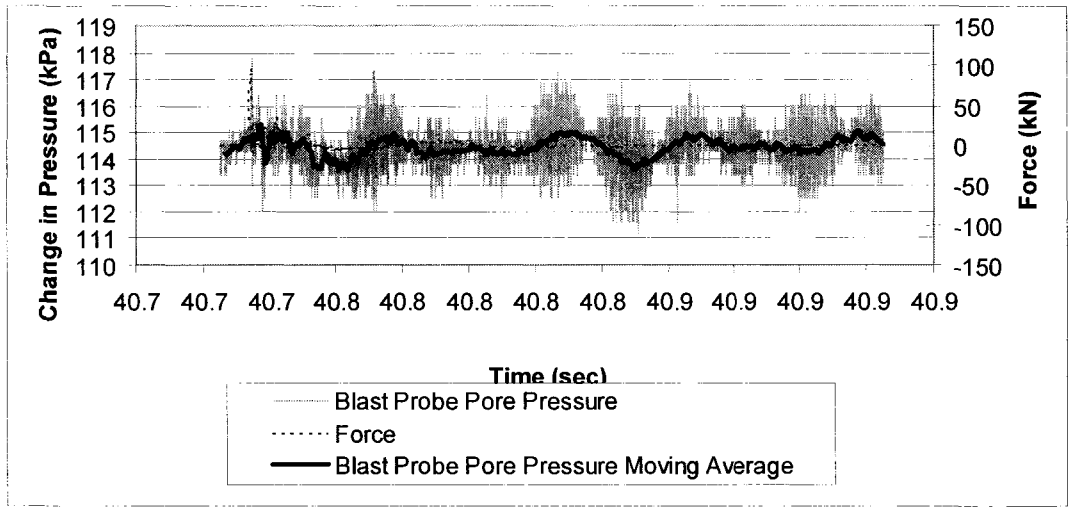

Blow 19 blast probe pore pressure response:

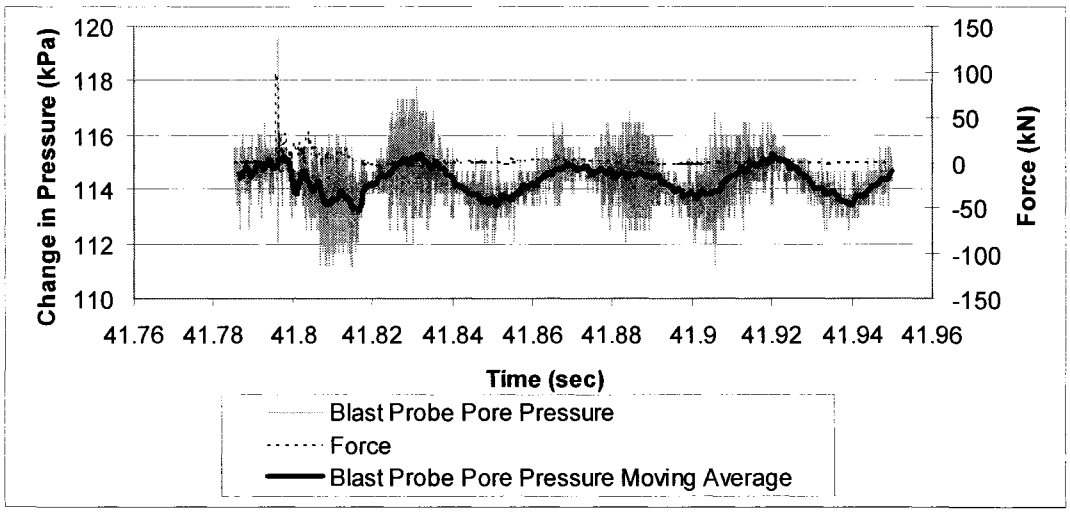

APPENDIX E: BLAST PROBE VIBRATION MEASUREMENTS

Blast Probe Vibration Response from 1.52 m Depth

Blow 1 blast probe vibration response:

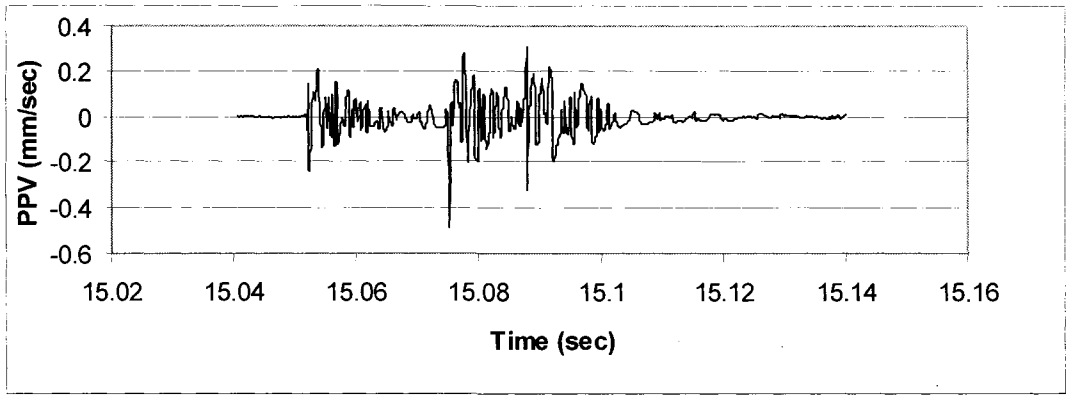

Blow 2 blast probe vibration response:

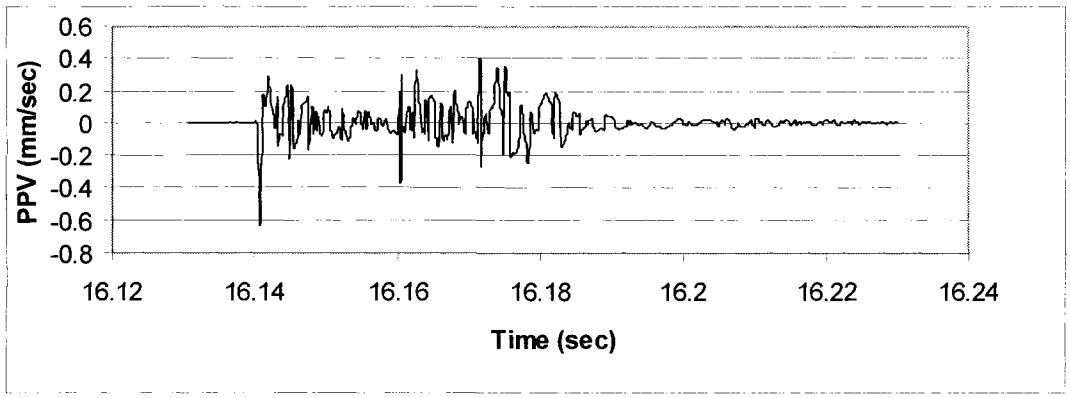

Blow 3 blast probe vibration response:

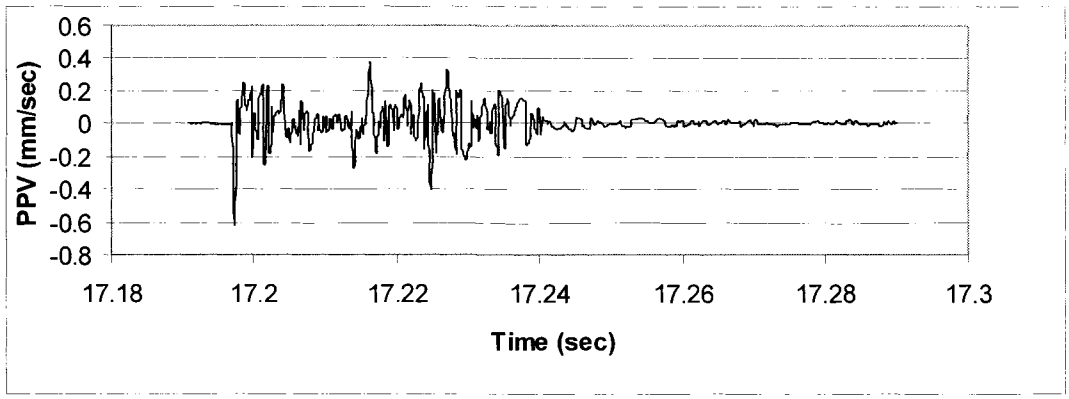

Blow 4 blast probe vibration response:

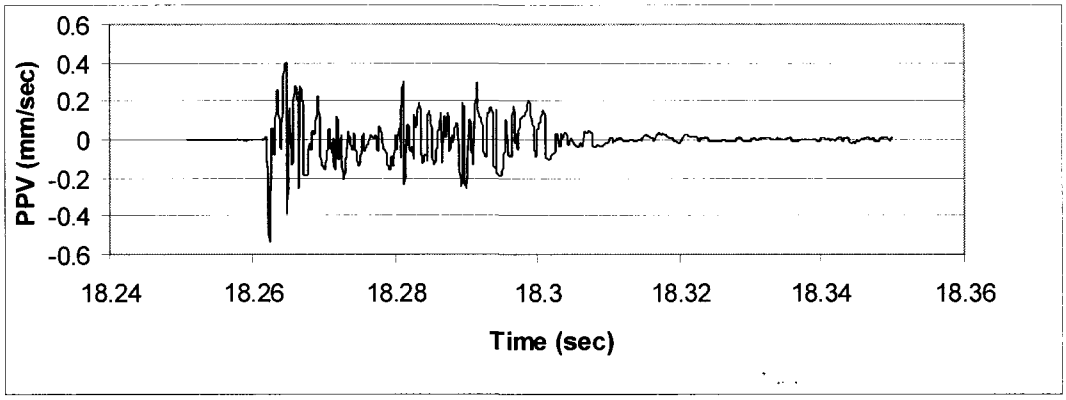

Blow 5 blast probe vibration response:

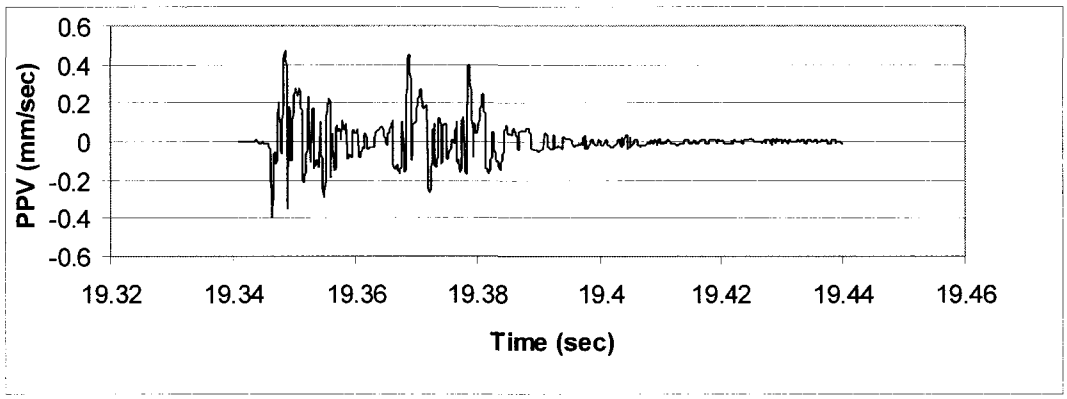

Blow 6 blast probe vibration response:

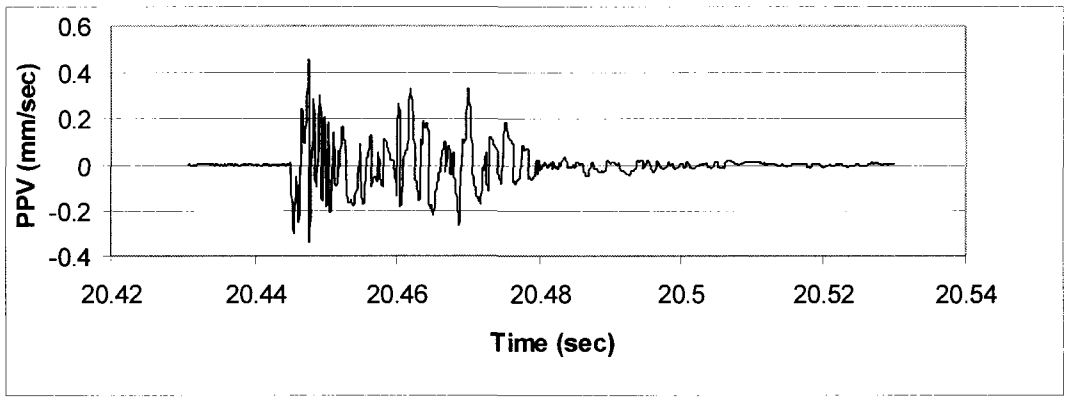

Blow 7 blast probe vibration response:

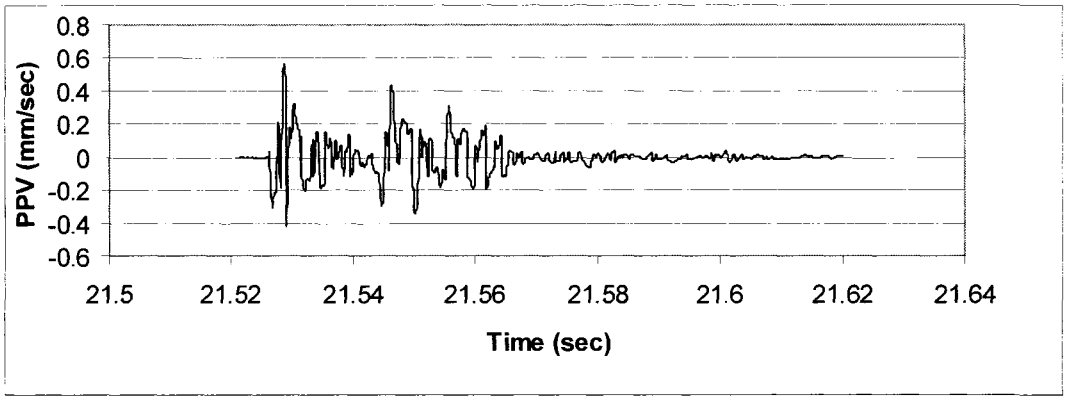

Blow 8 blast probe vibration response:

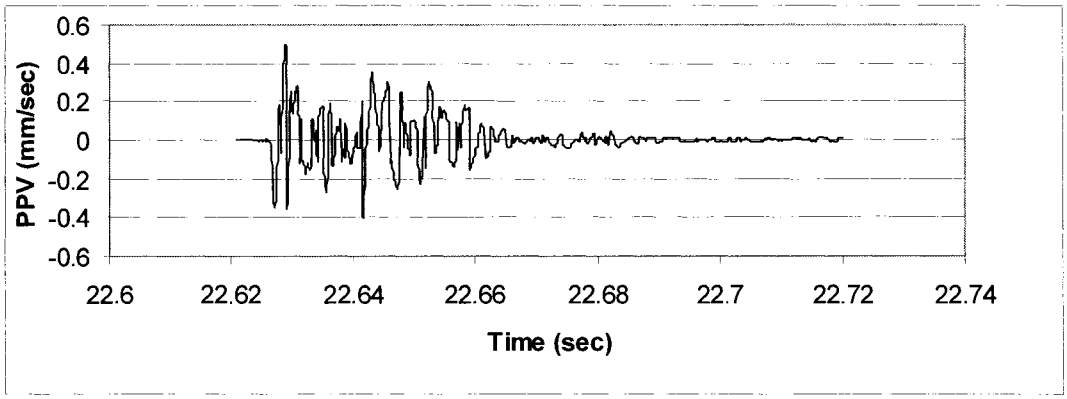

Blow 9 blast probe vibration response:

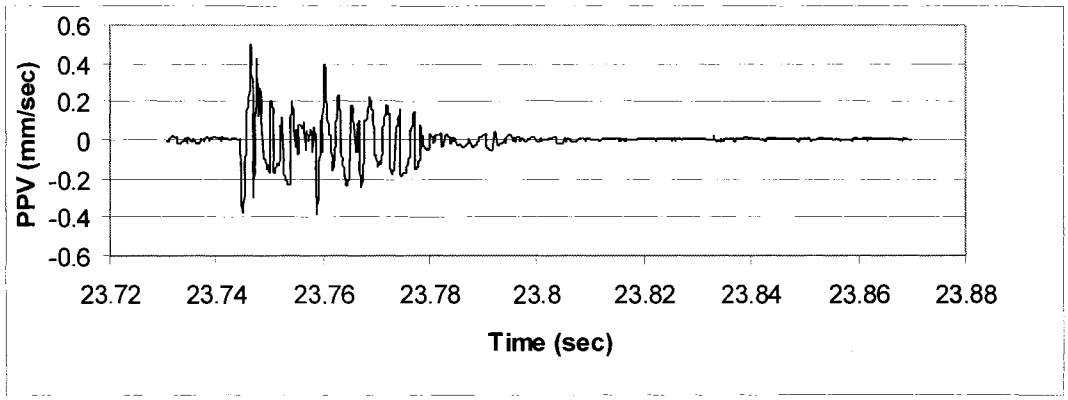

Blow 10 blast probe vibration response:

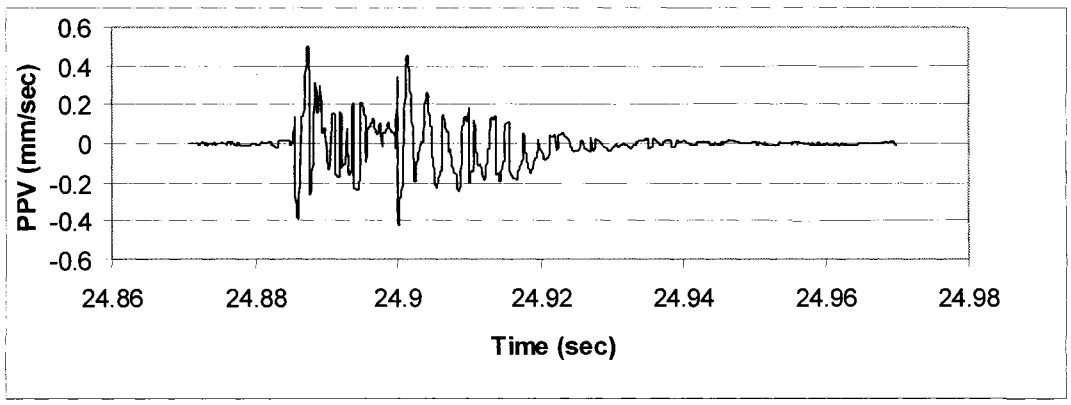

Blow 11 blast probe vibration response:

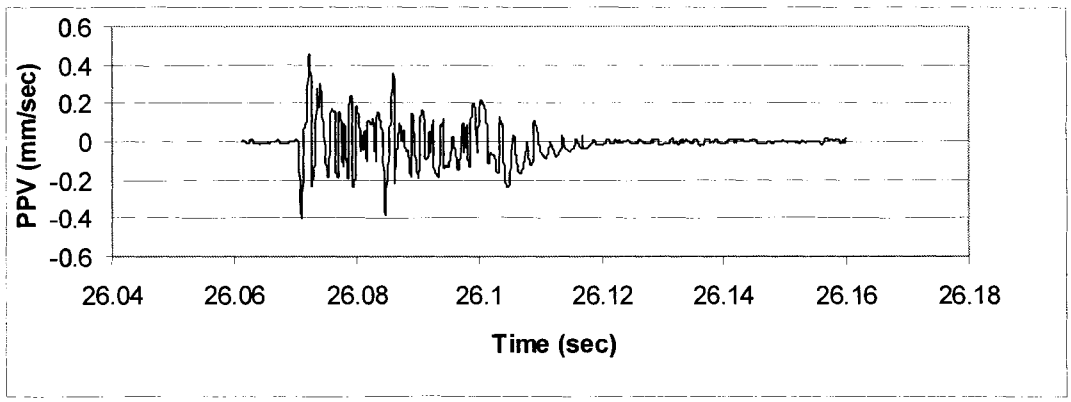

Blast Probe Vibration Response from 7.72 m Depth

Blow 1 blast probe vibration response:

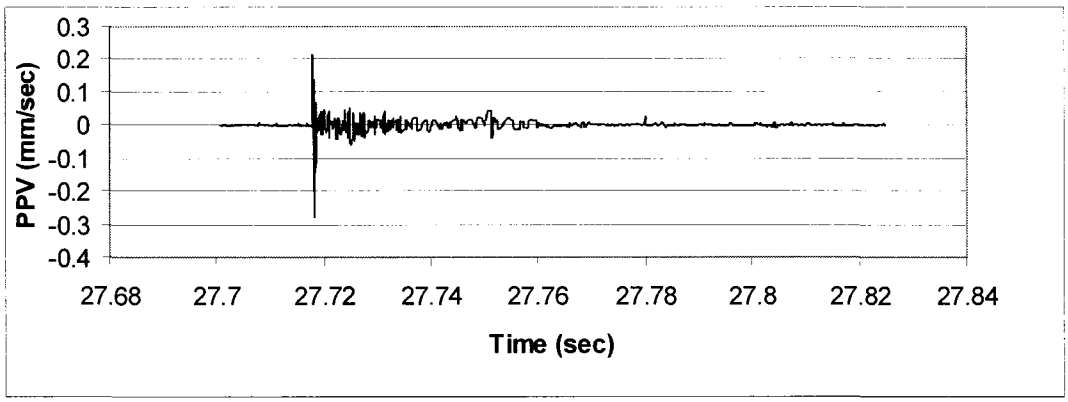

Blow 2 blast probe vibration response:

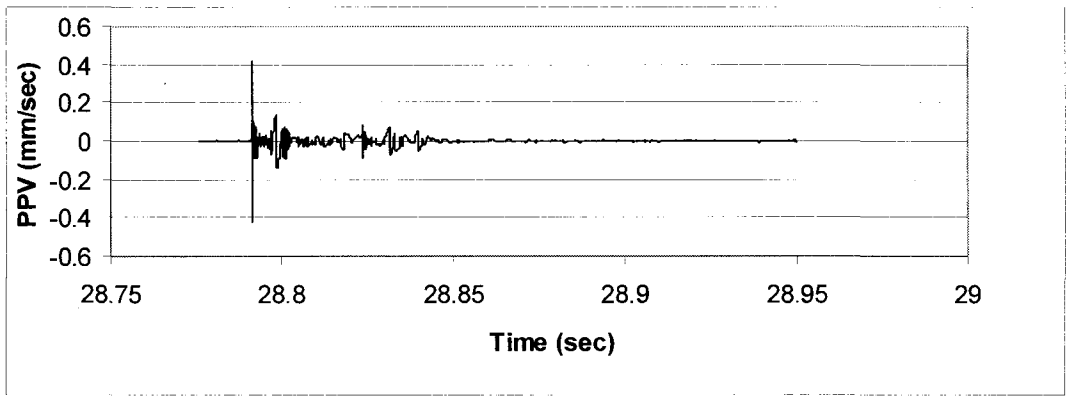

Blow 3 blast probe vibration response:

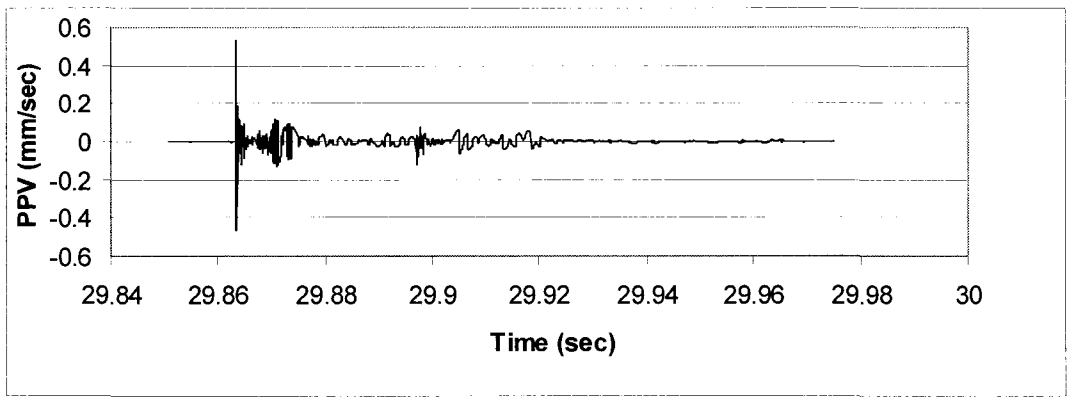

Blow 4 blast probe vibration response:

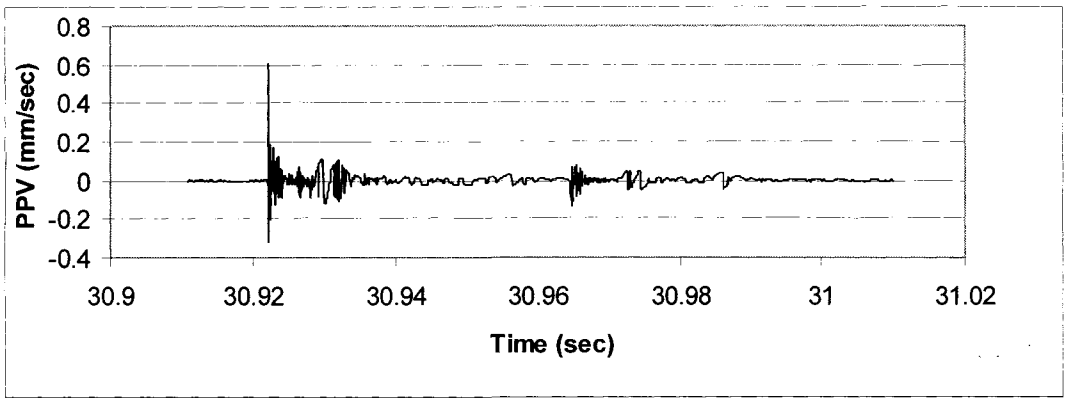

Blow 5 blast probe vibration response:

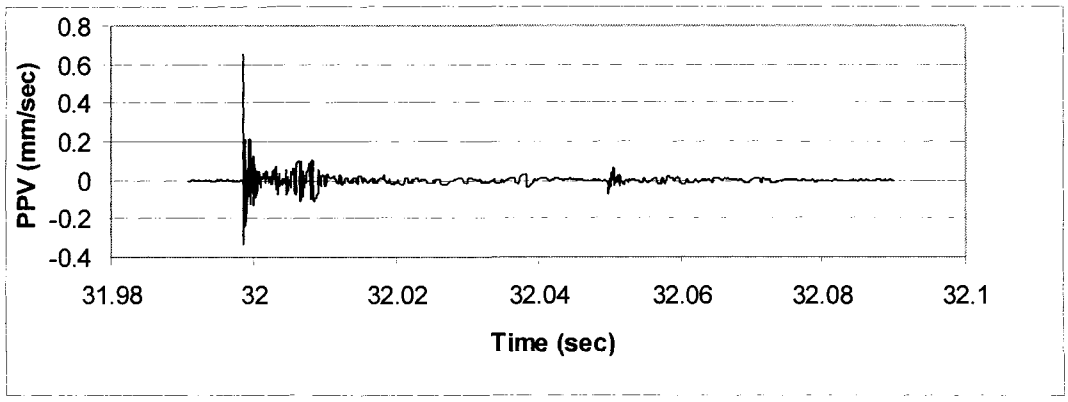

Blow 6 blast probe vibration response:

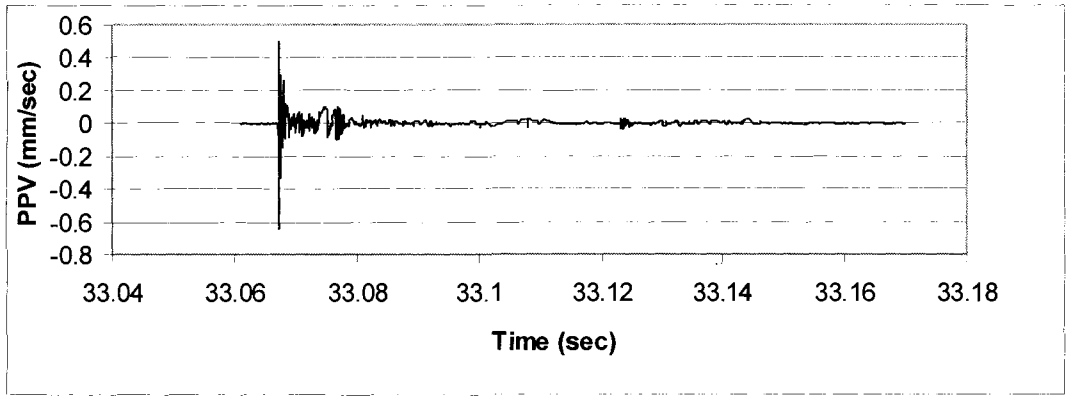

Blow 7 blast probe vibration response:

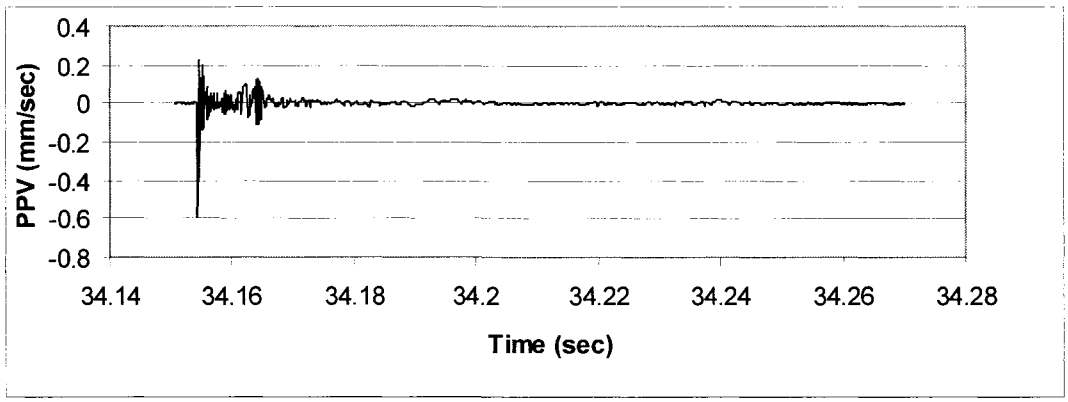

Blow 8 blast probe vibration response:

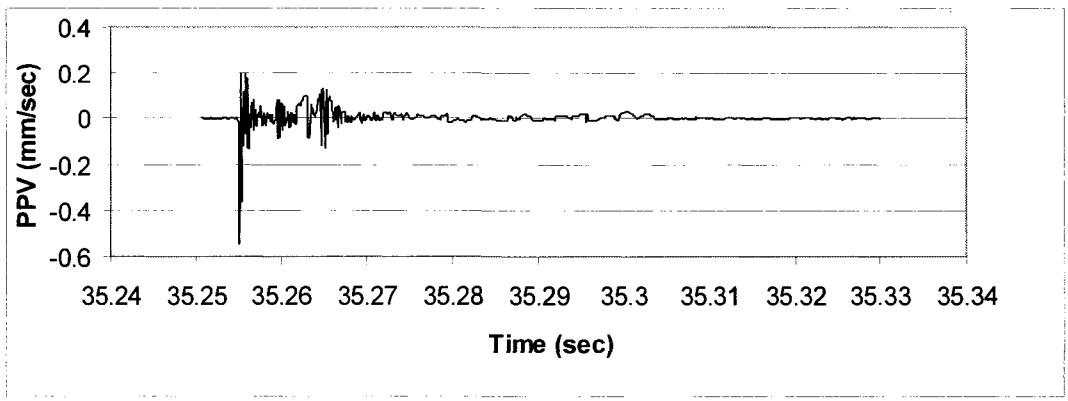

Blow 9 blast probe vibration response:

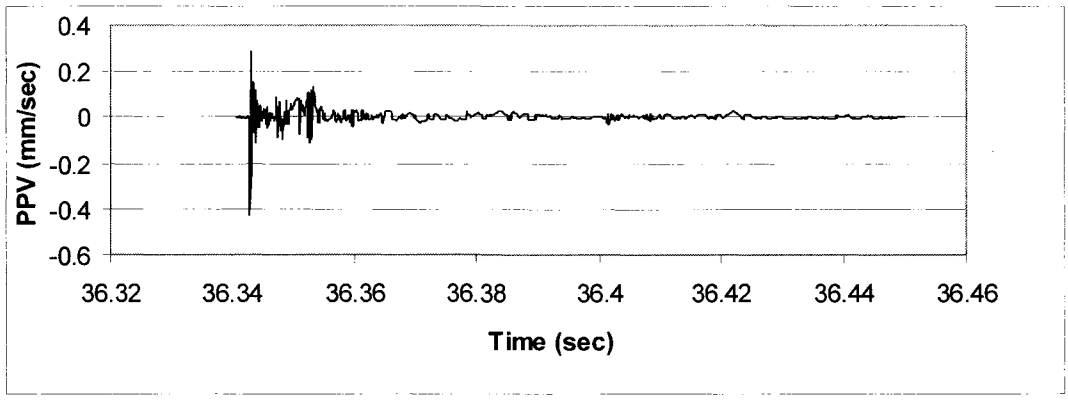

Blow 10 blast probe vibration response:

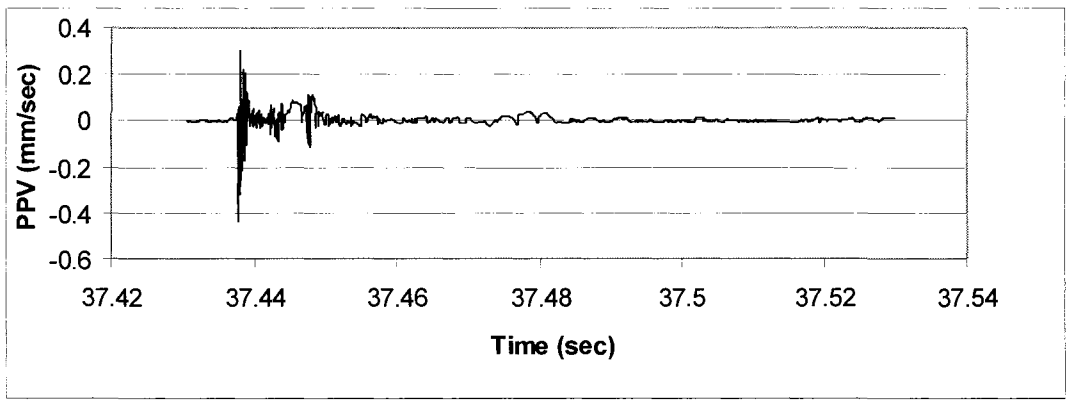

Blow 11 blast probe vibration response:

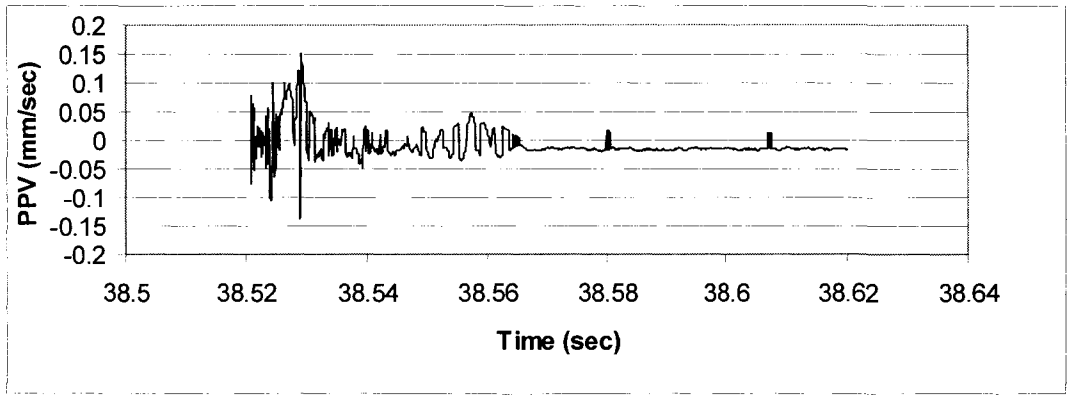

Blow 12 blast probe vibration response:

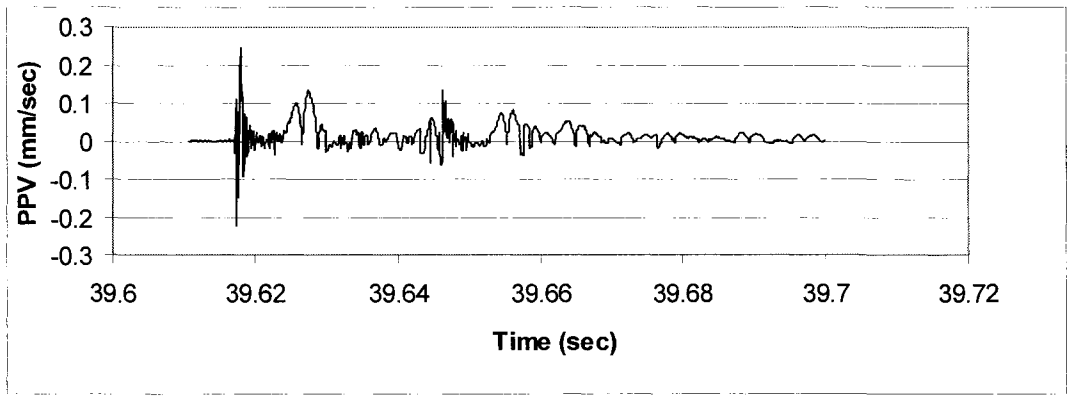

Blast Probe Vibration Response from 8.56 m Depth

Blow 1 blast probe vibration response:

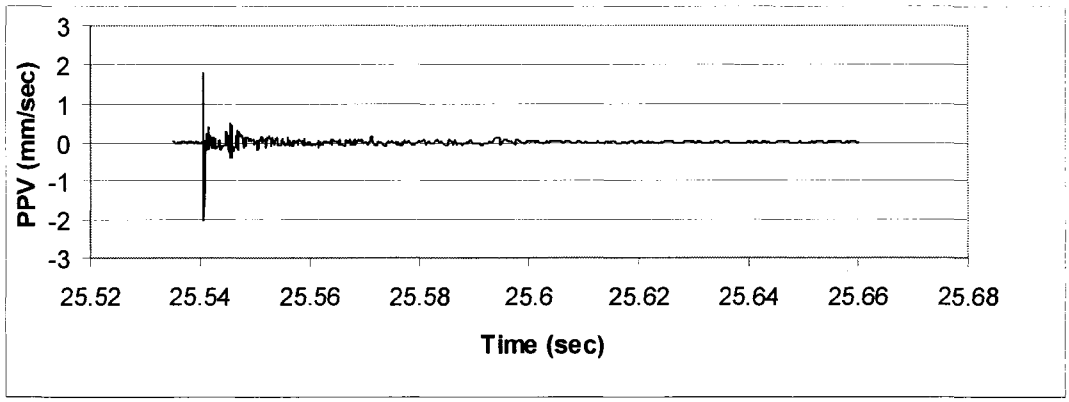

Blow 2 blast probe vibration response:

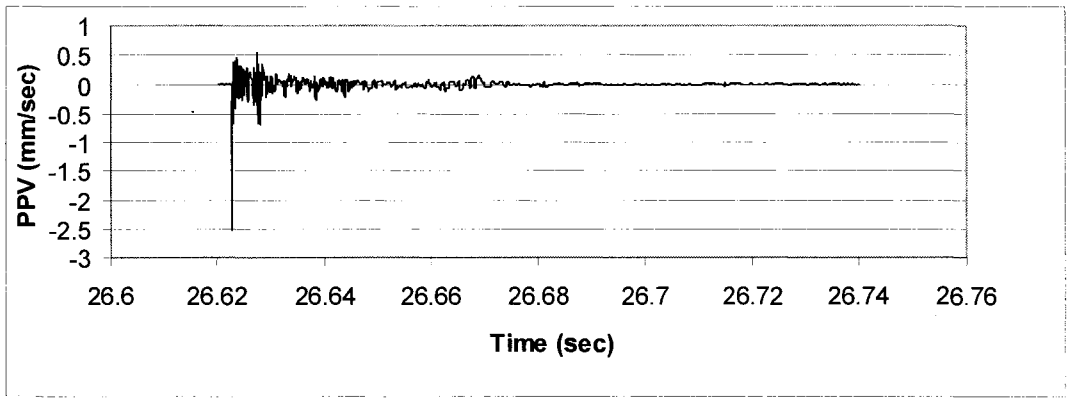

Blow 3 blast probe vibration response:

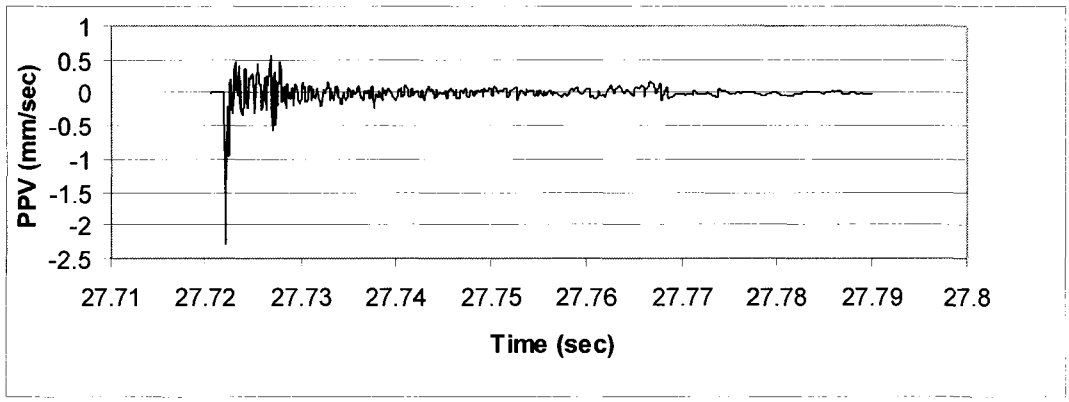

Blow 4 blast probe vibration response:

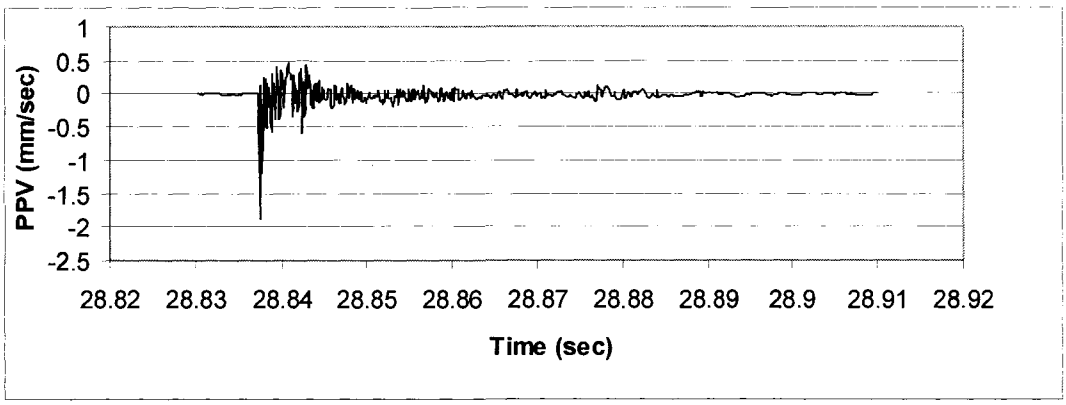

Blow 5 blast probe vibration response:

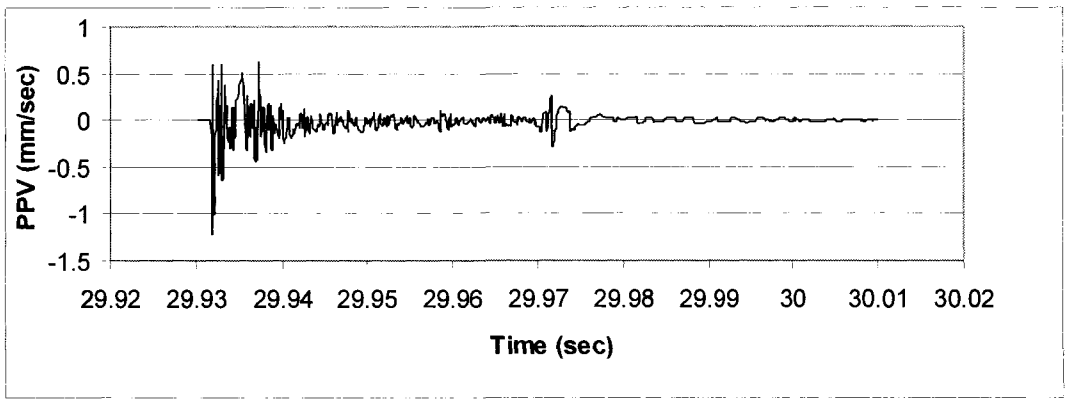

Blow 6 blast probe vibration response:

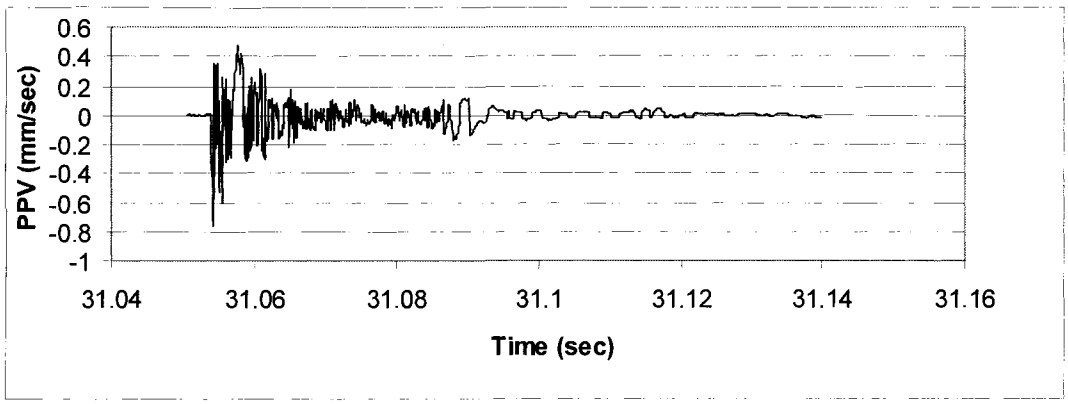

Blow 7 blast probe vibration response:

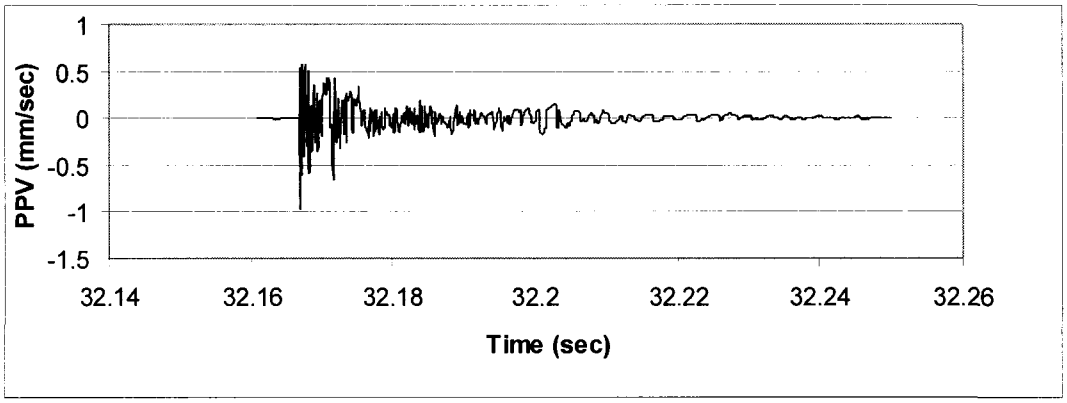

Blow 8 blast probe vibration response:

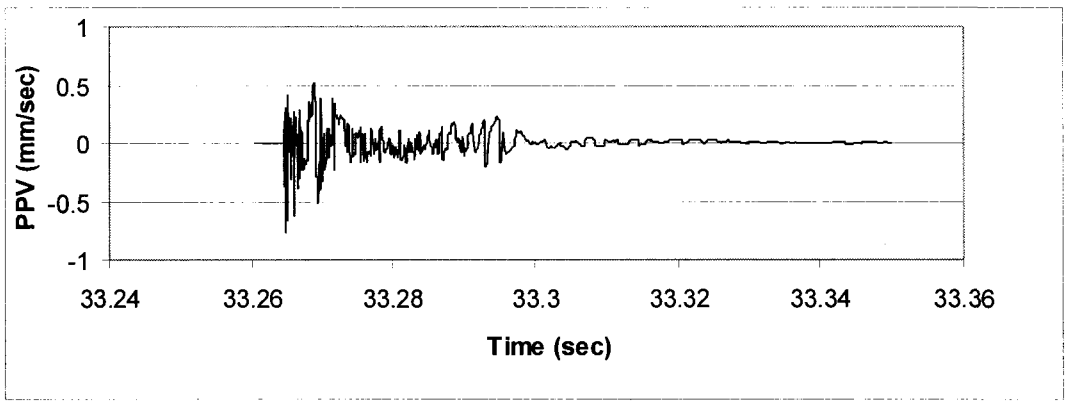

Blow 9 blast probe vibration response:

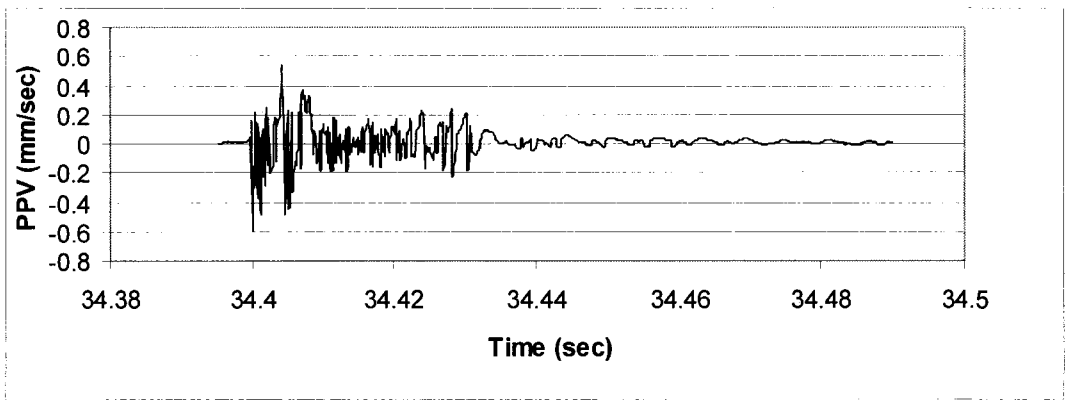

Blast Probe Vibration Response from 9.33 m Depth

Blow 1 blast probe vibration response:

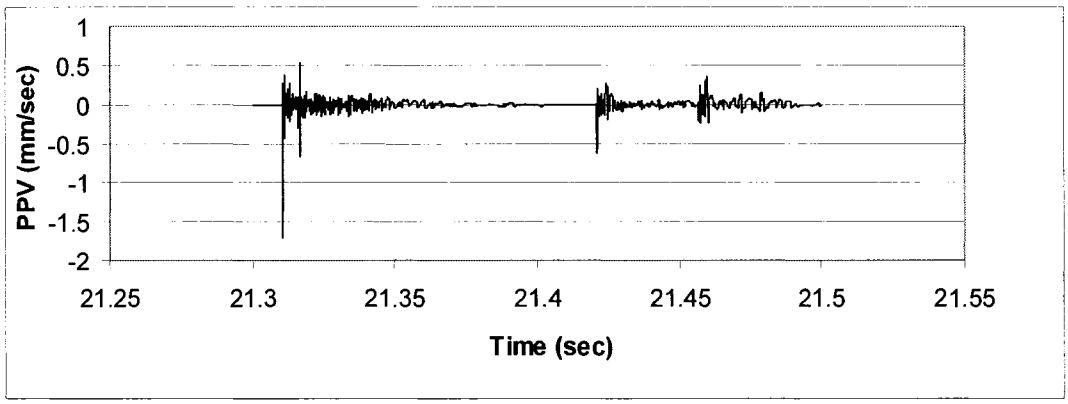

Blow 2 blast probe vibration response:

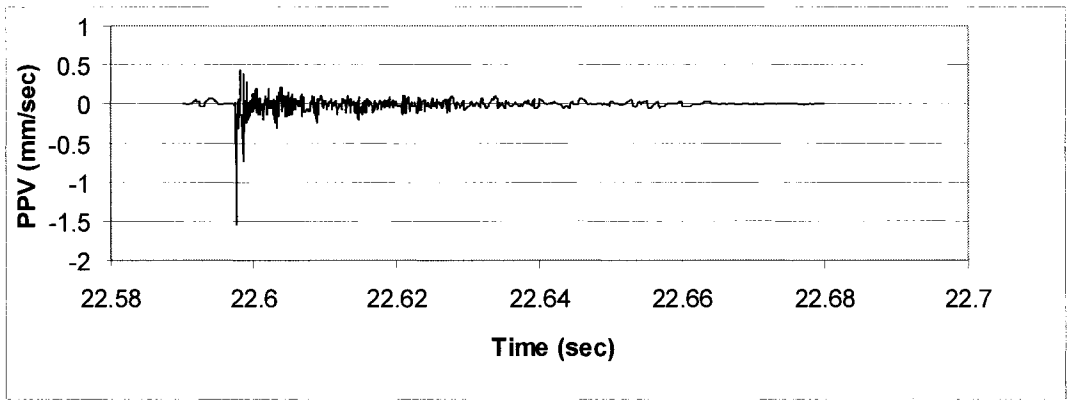

Blow 3 blast probe vibration response:

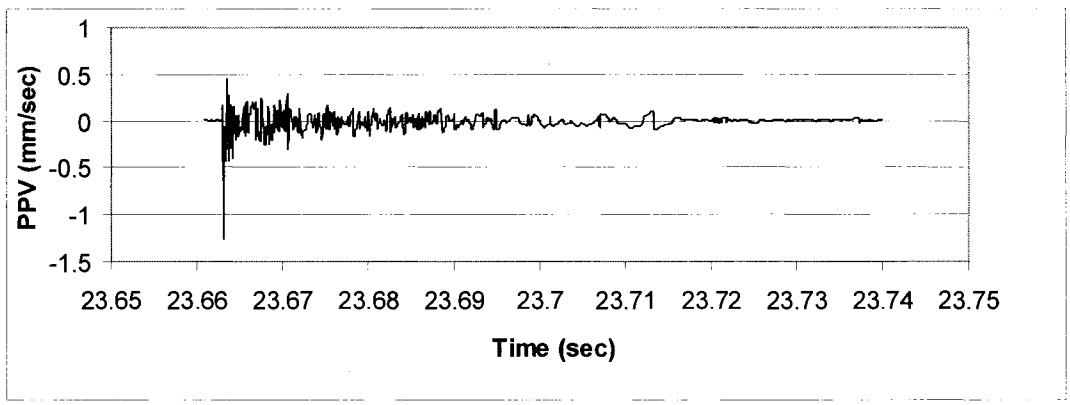

Blow 4 blast probe vibration response:

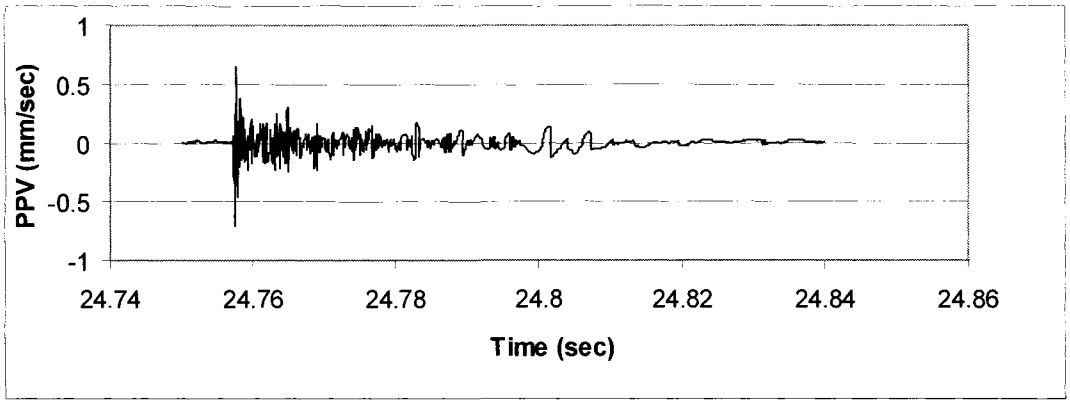

Blow 5 blast probe vibration response:

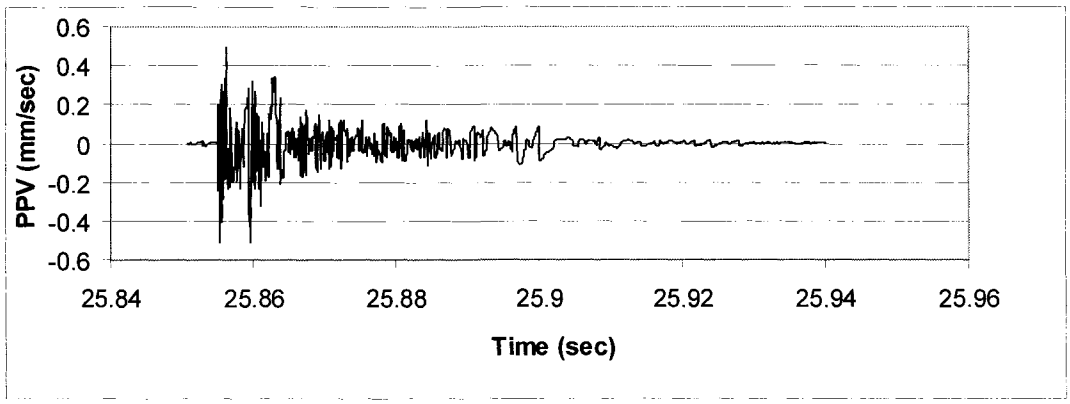

Blow 6 blast probe vibration response:

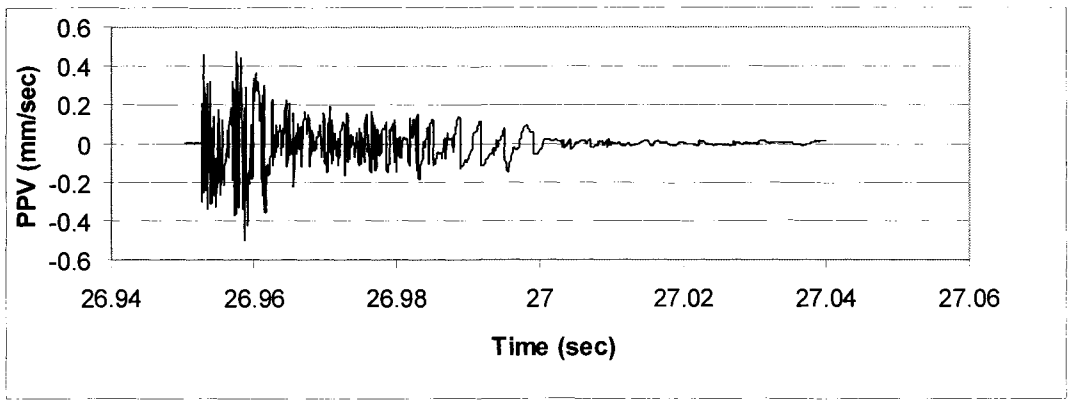

Blow 7 blast probe vibration response:

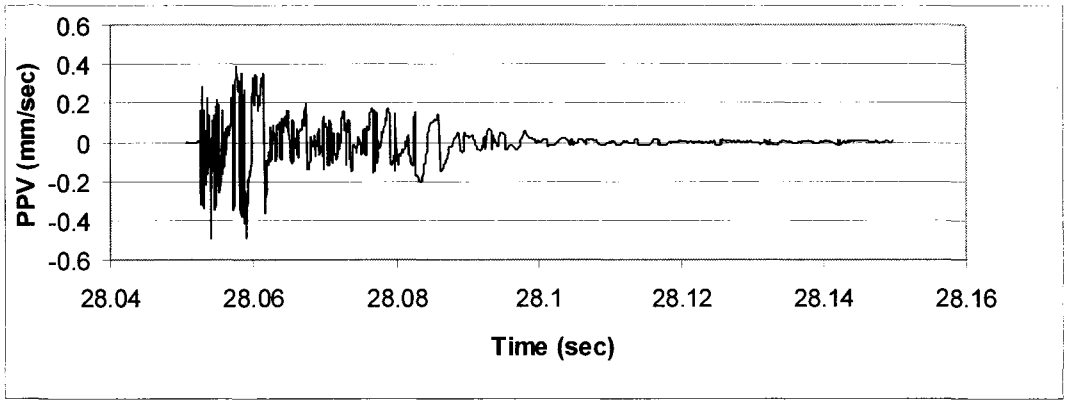

Blow 8 blast probe vibration response:

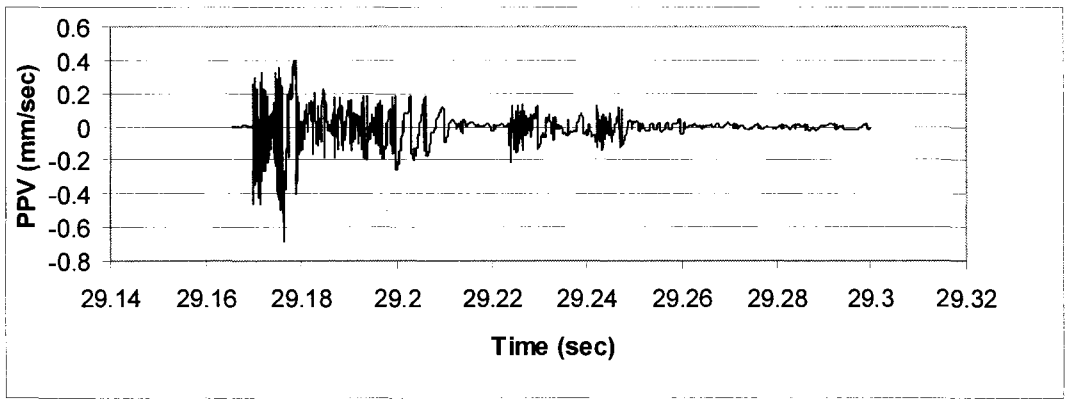

Blast Probe Vibration Response from 10.80 m Depth

Blow 1 blast probe vibration response:

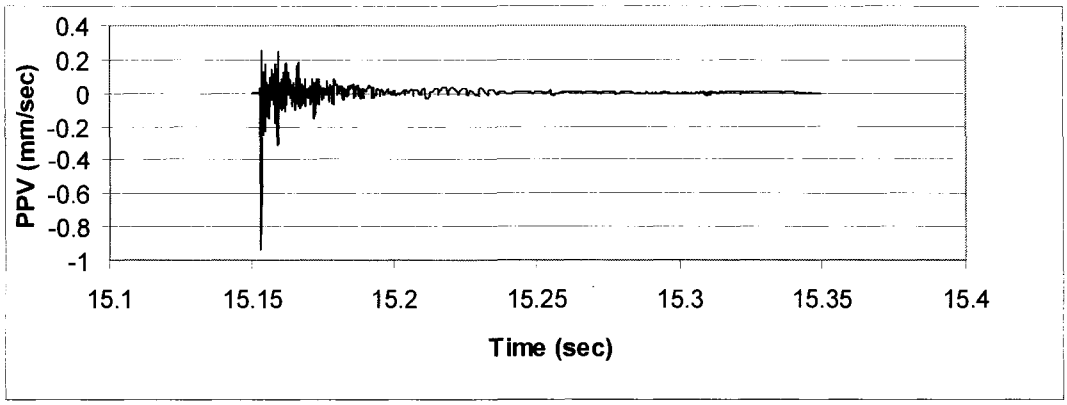

Blow 2 blast probe vibration response:

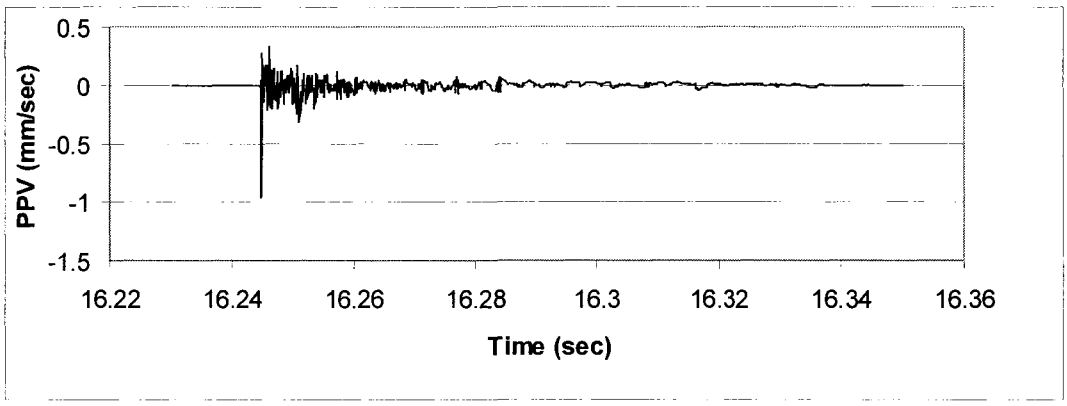

Blow 3 blast probe vibration response:

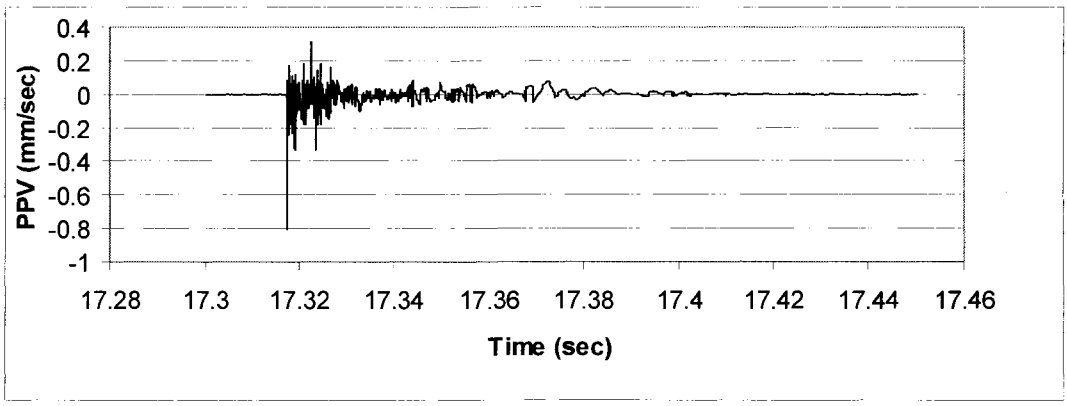

Blow 4 blast probe vibration response:

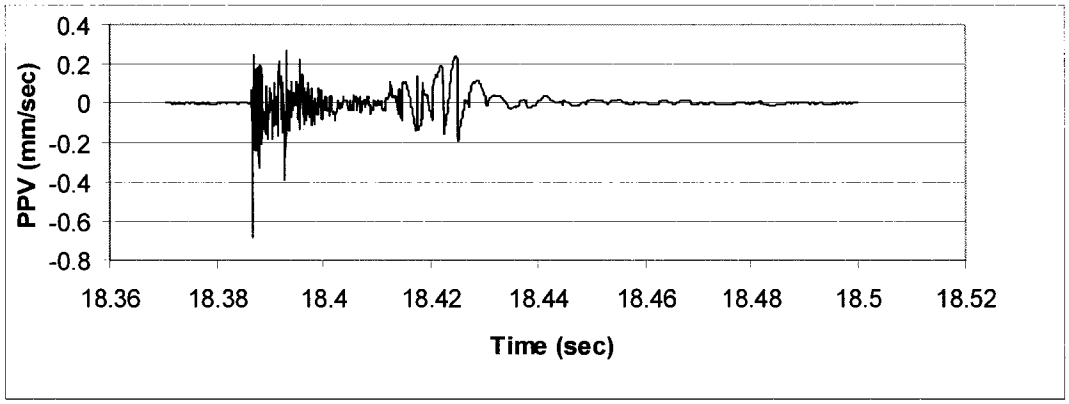

Blow 5 blast probe vibration response:

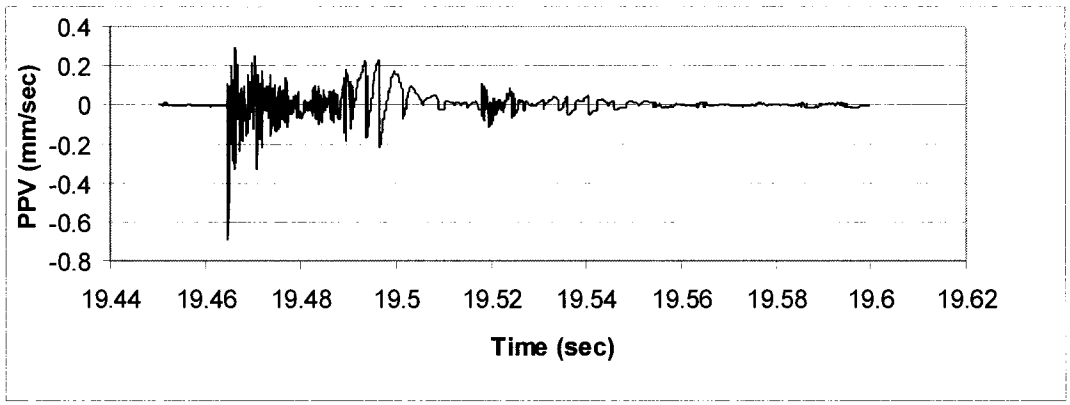

Blow 6 blast probe vibration response:

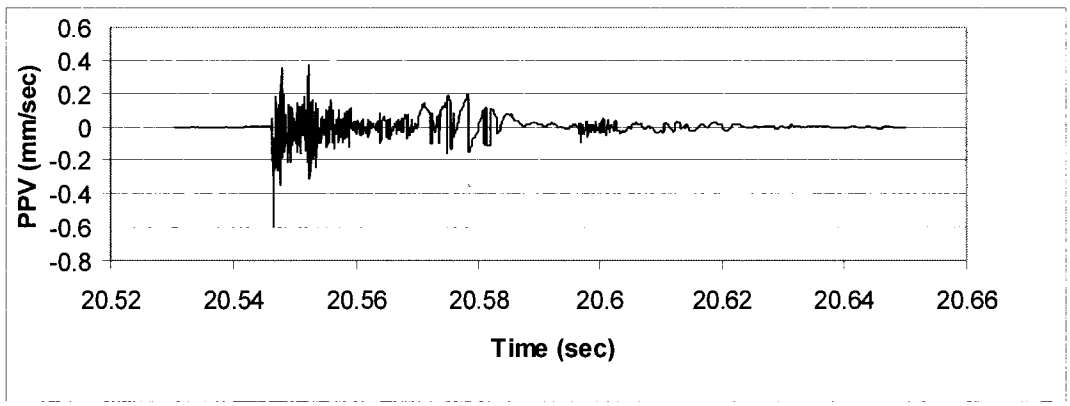

Blow 7 blast probe vibration response:

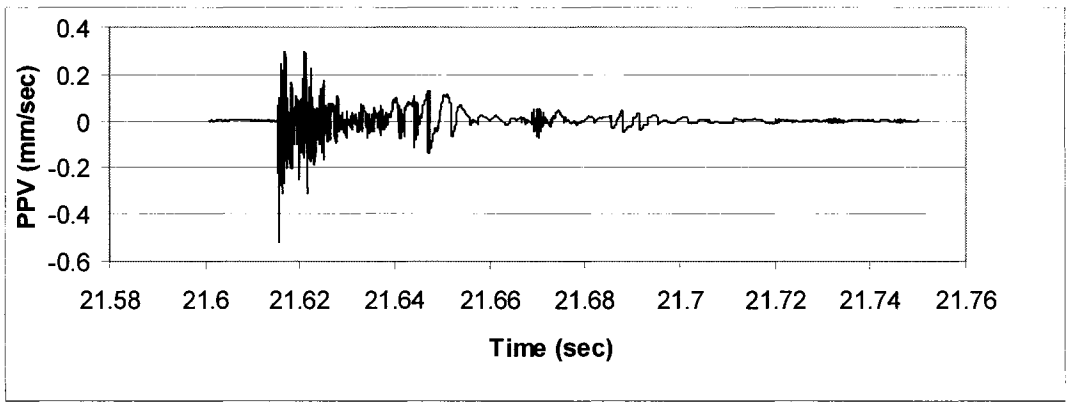

Blow 8 blast probe vibration response:

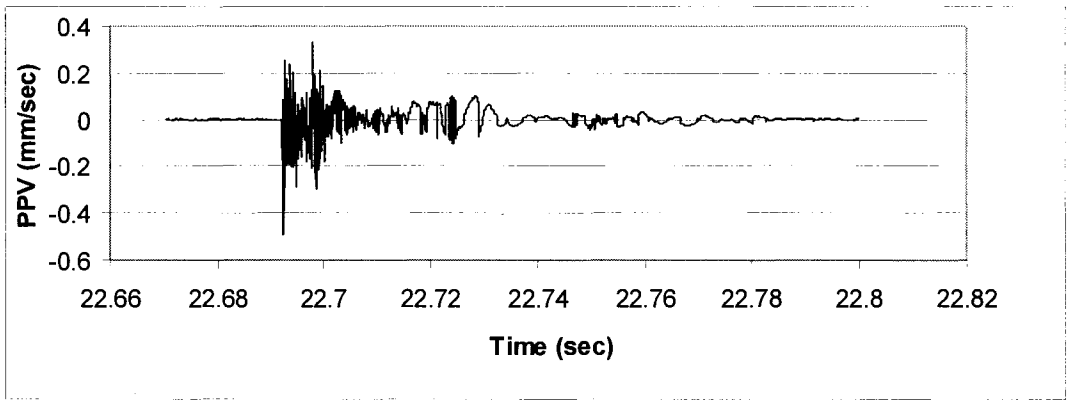

Blow 9 blast probe vibration response:

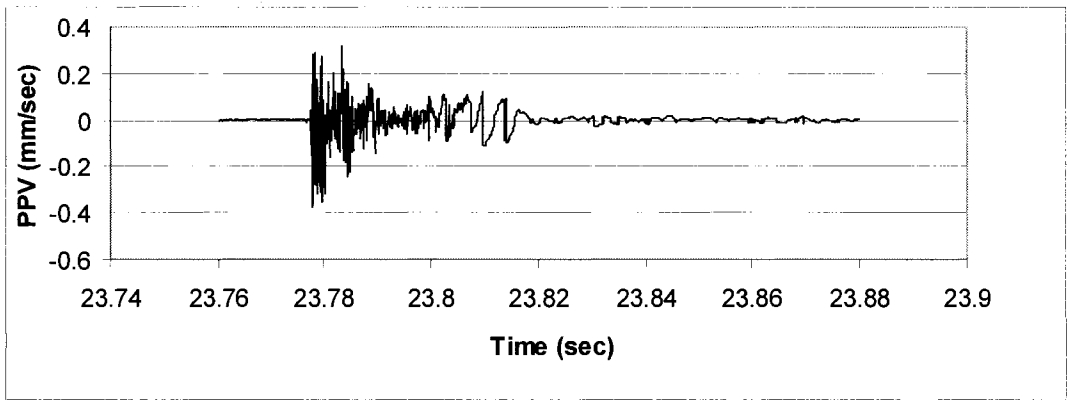

Blow 10 blast probe vibration response:

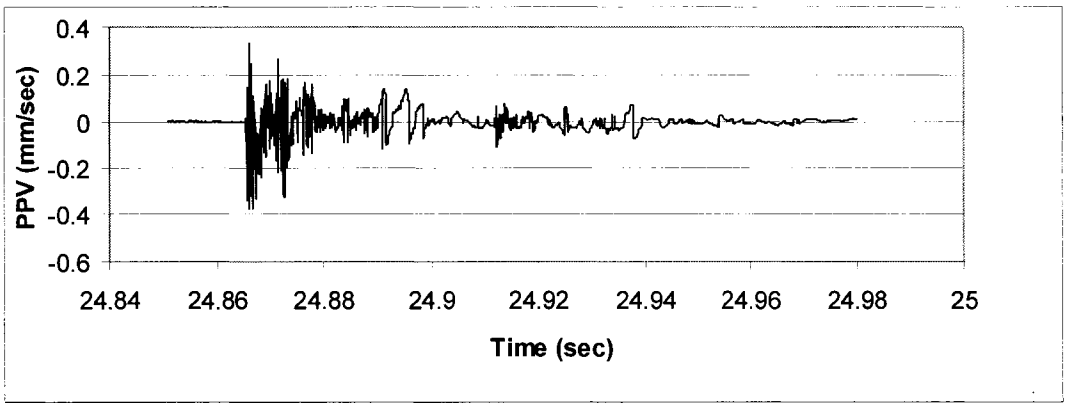

Blast Probe Vibration Response from 12.41 m Depth

Blow 1 blast probe vibration response:

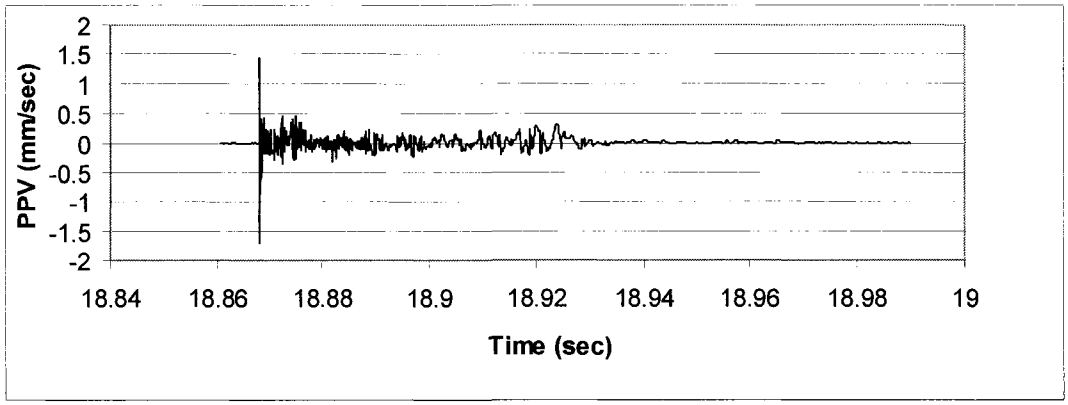

Blow 2 blast probe vibration response:

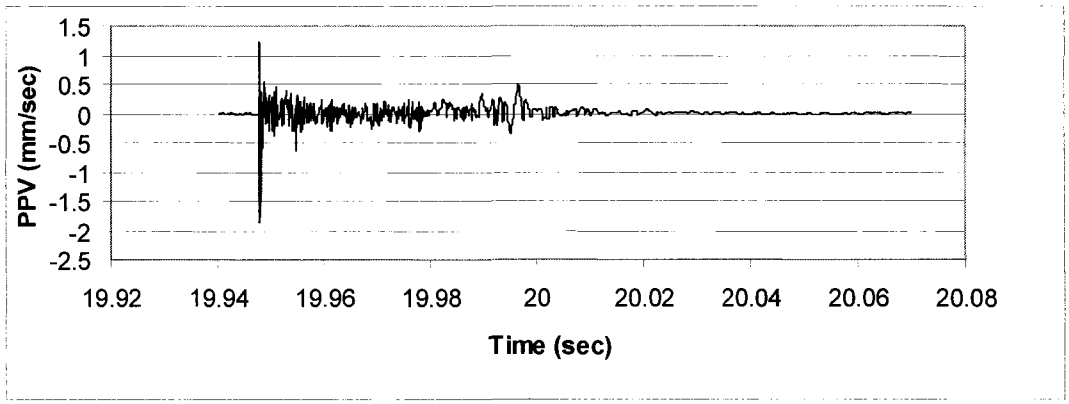

Blow 3 blast probe vibration response:

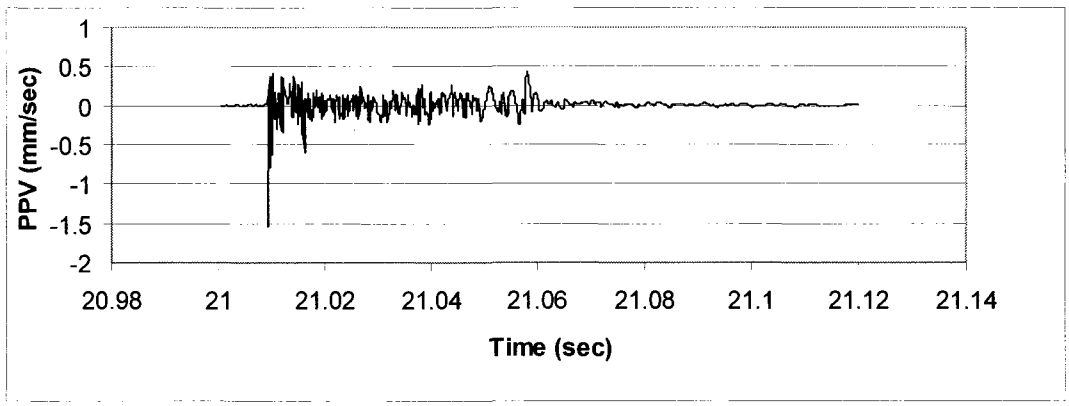

Blow 4 blast probe vibration response:

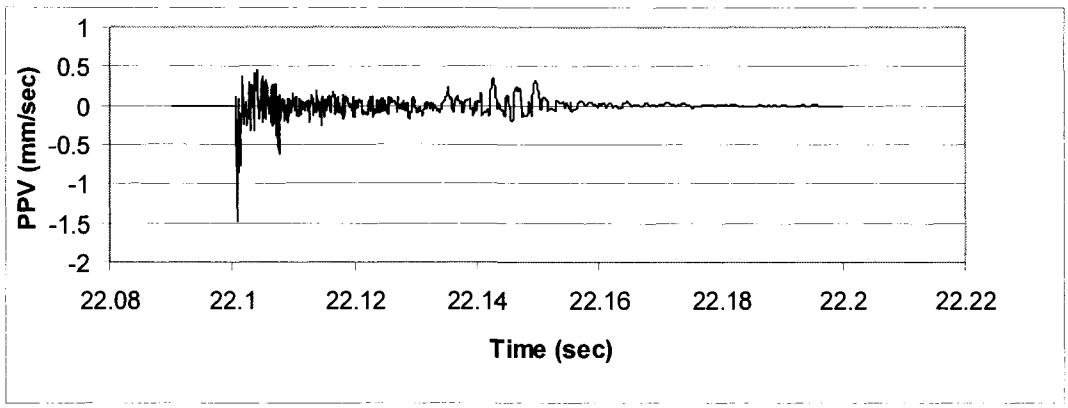

Blow 5 blast probe vibration response:

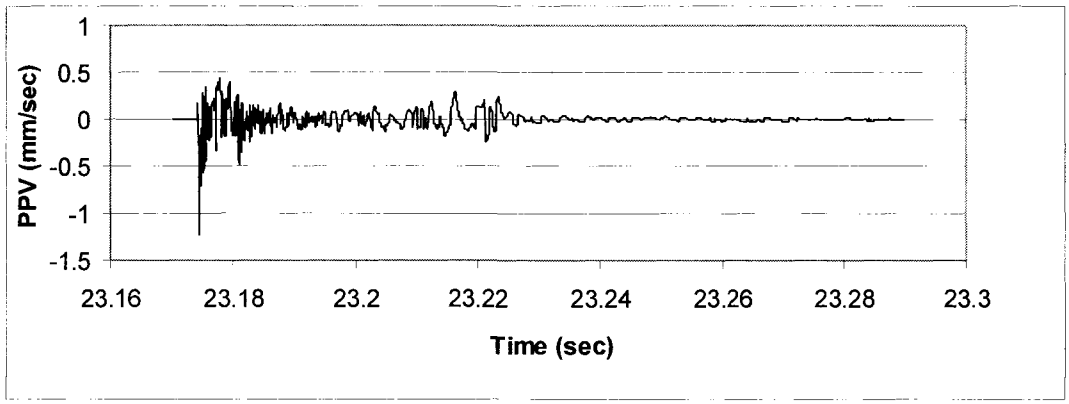

Blow 6 blast probe vibration response:

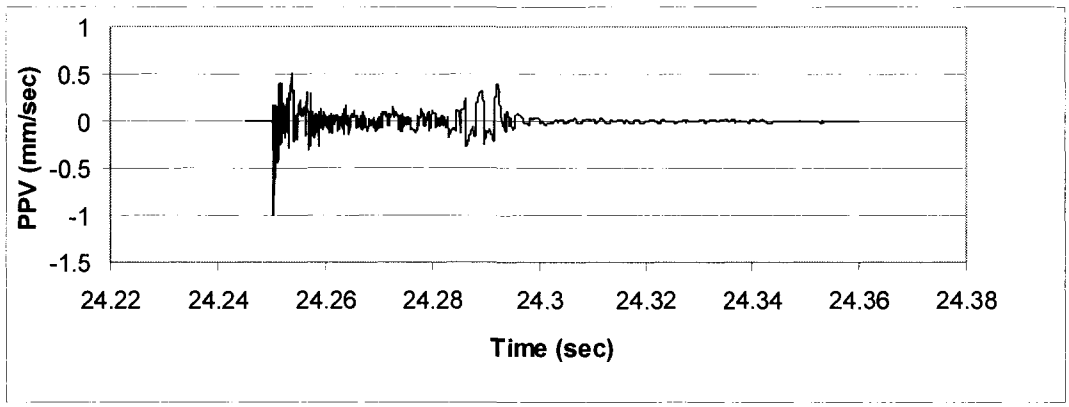

Blow 7 blast probe vibration response:

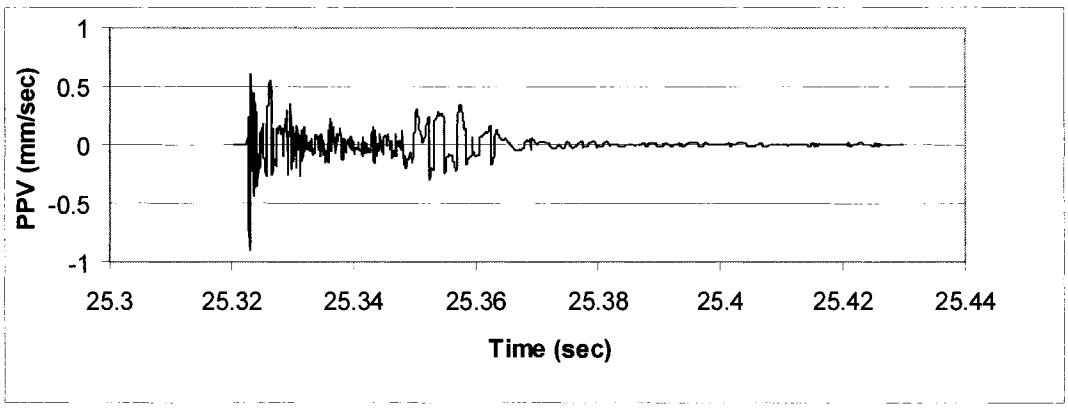

Blow 8 blast probe vibration response:

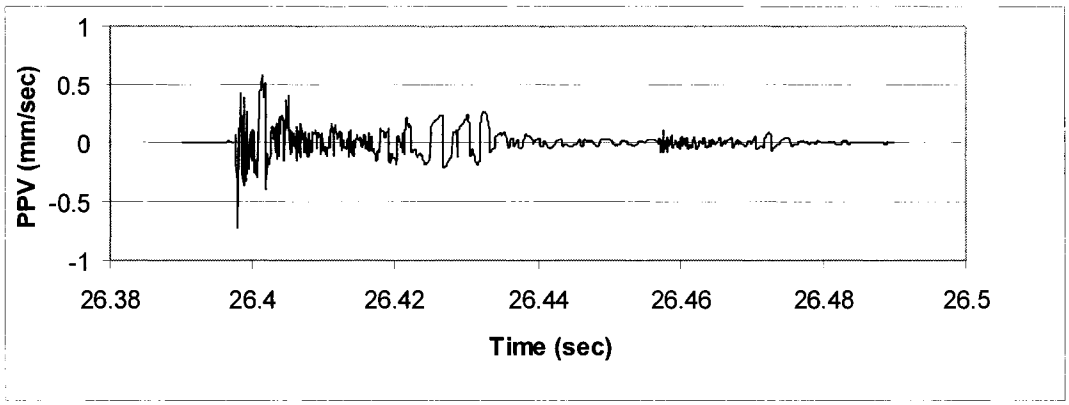

Blow 9 blast probe vibration response:

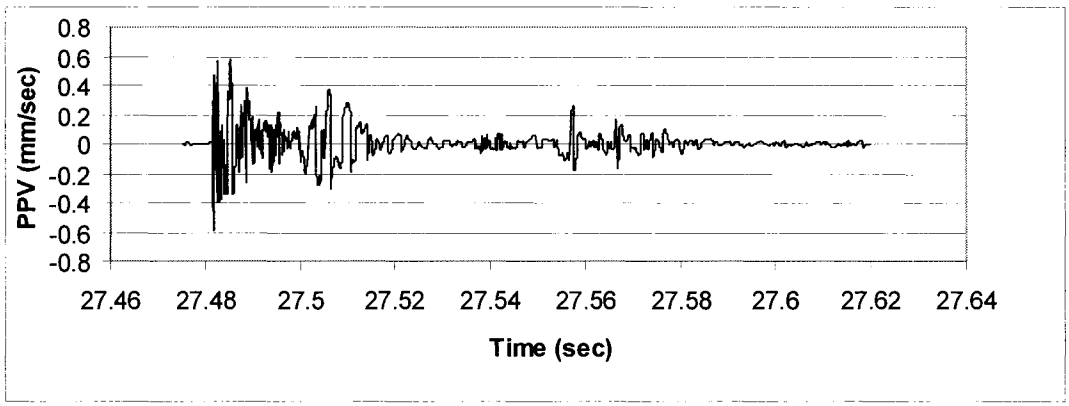

Blow 10 blast probe vibration response:

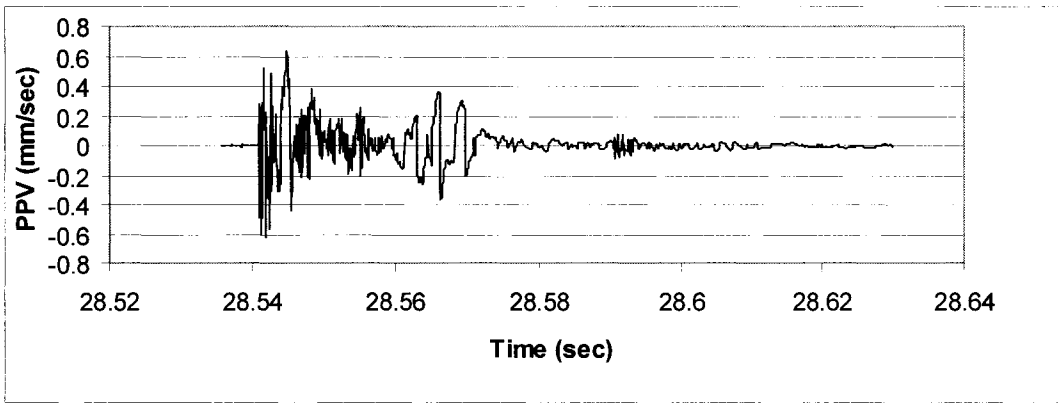

Blow 11 blast probe vibration response:

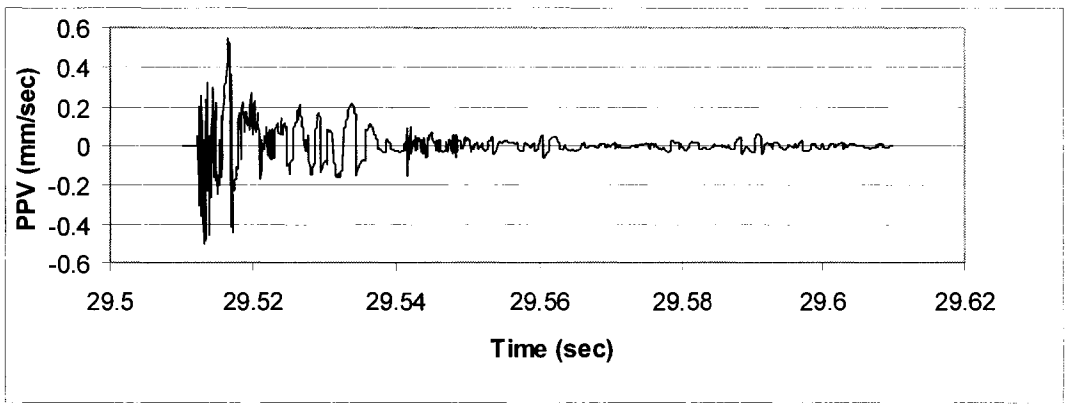

Blast Probe Vibration Response from 13.92 m Depth

Blow 1 blast probe vibration response:

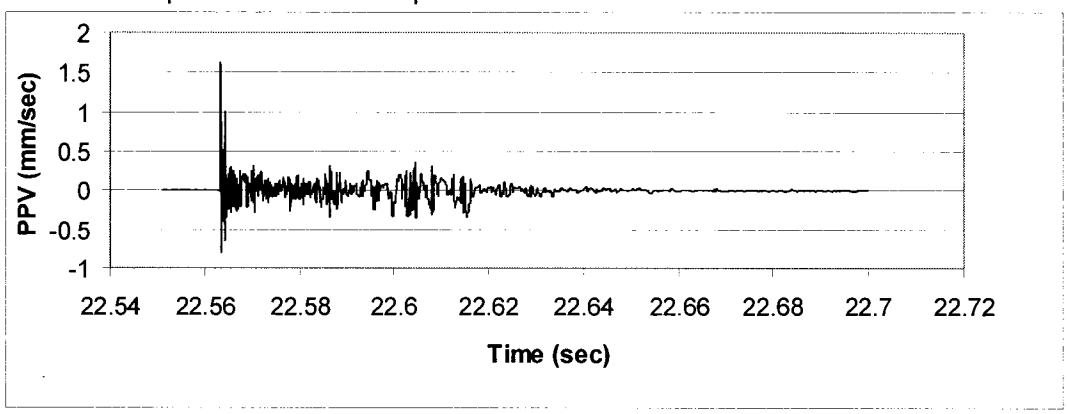

Blow 2 blast probe vibration response:

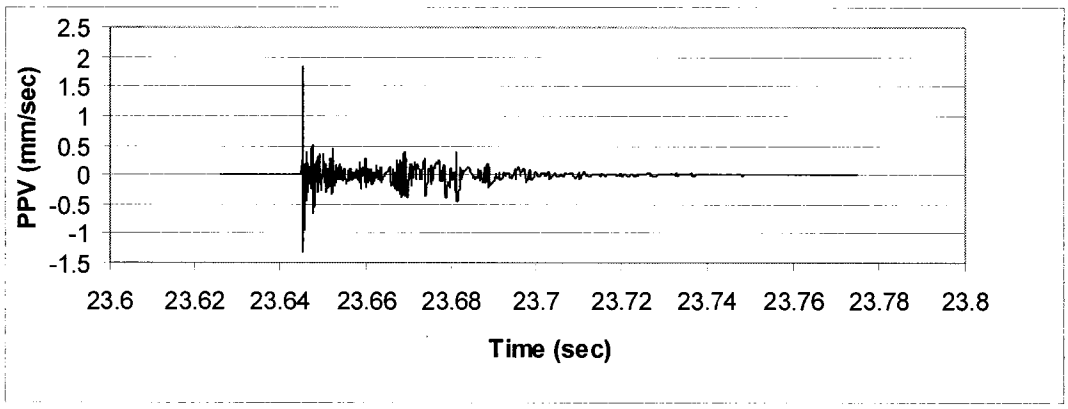

Blow 3 blast probe vibration response:

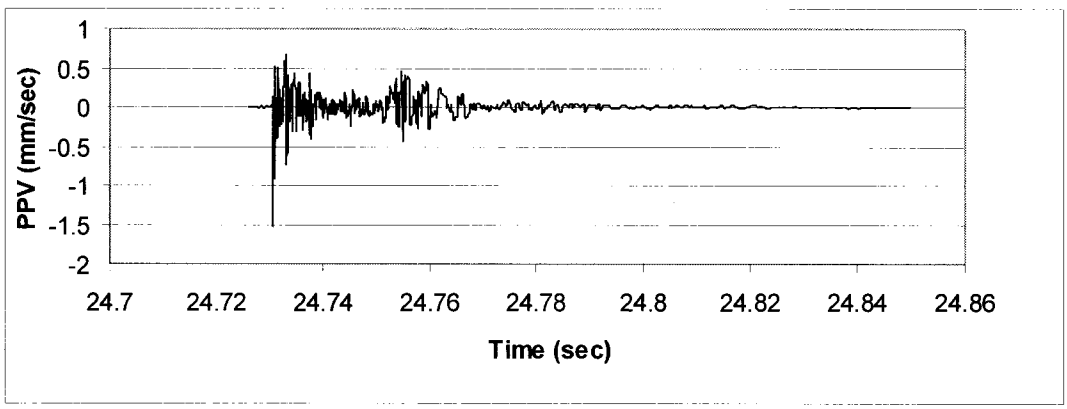

Blow 4 blast probe vibration response:

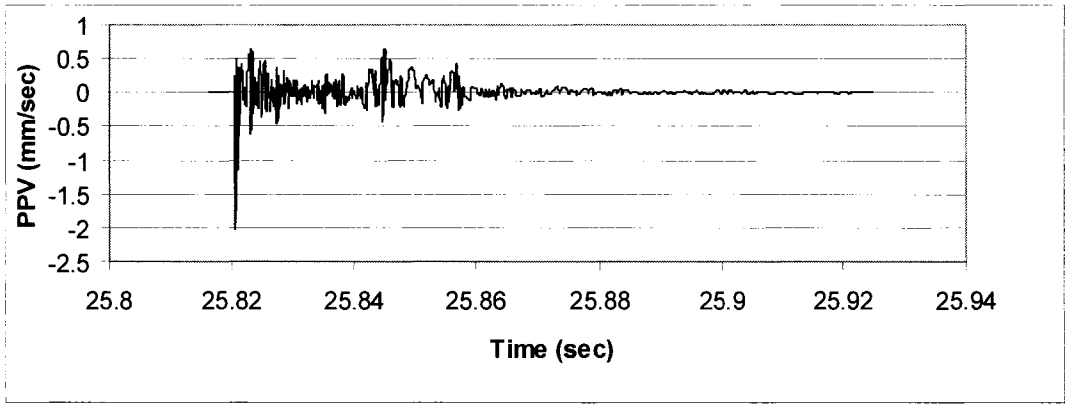

Blow 5 blast probe vibration response:

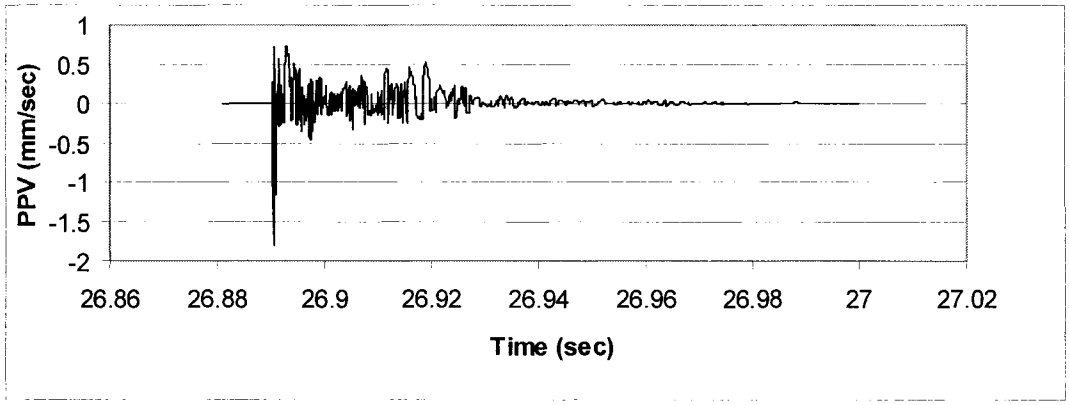

Blow 6 blast probe vibration response:

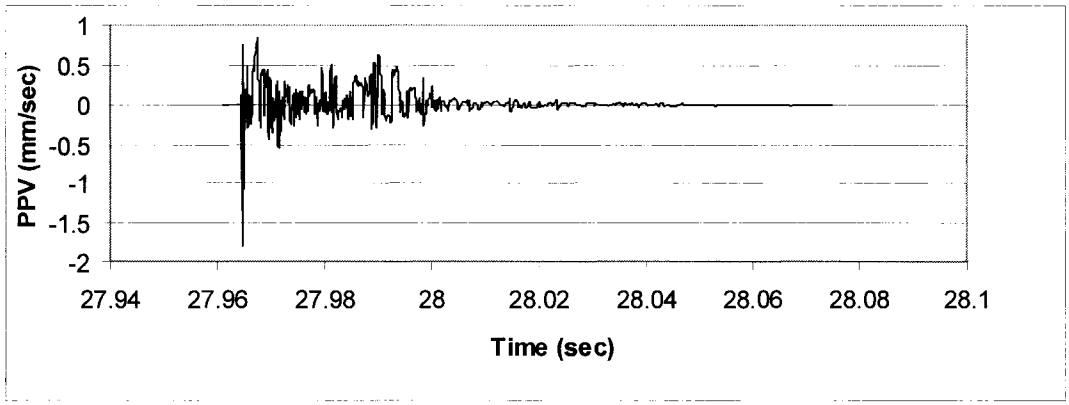

Blow 7 blast probe vibration response:

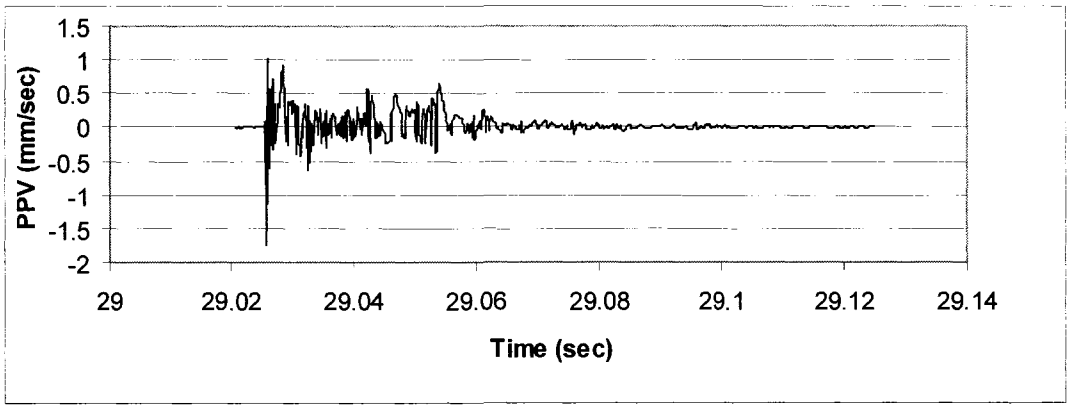

Blow 8 blast probe vibration response:

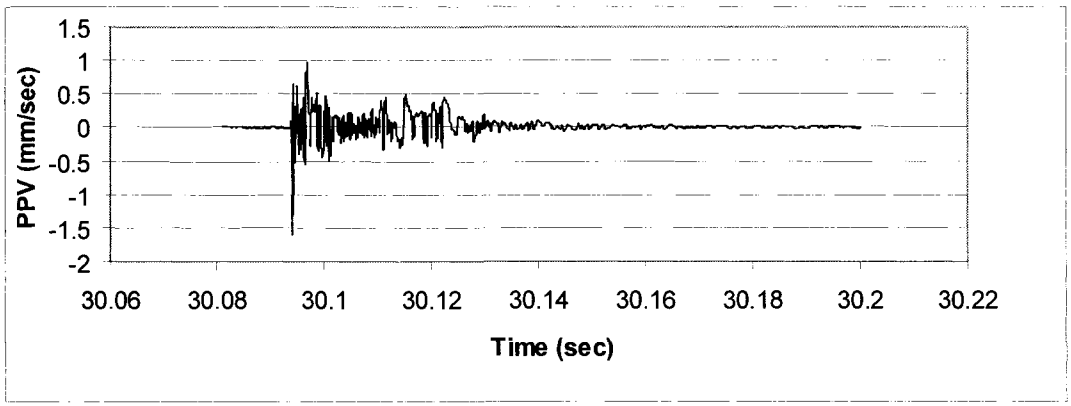

Blow 9 blast probe vibration response:

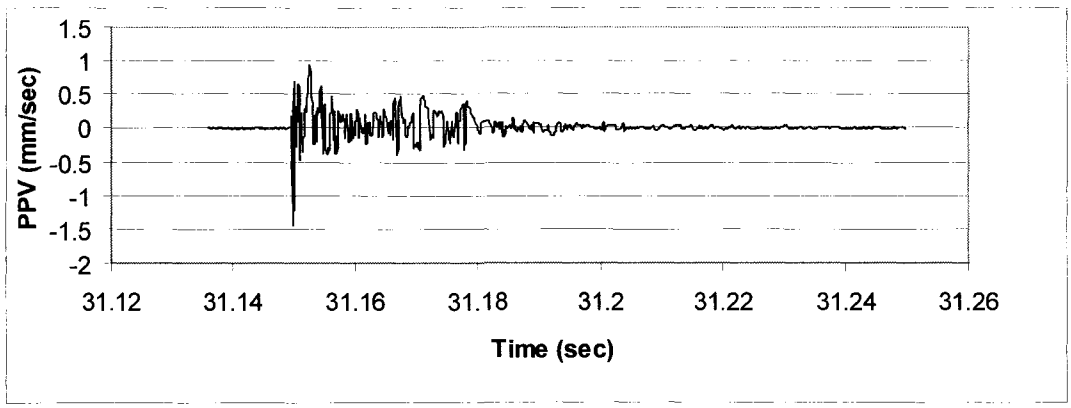

Blow 10 blast probe vibration response:

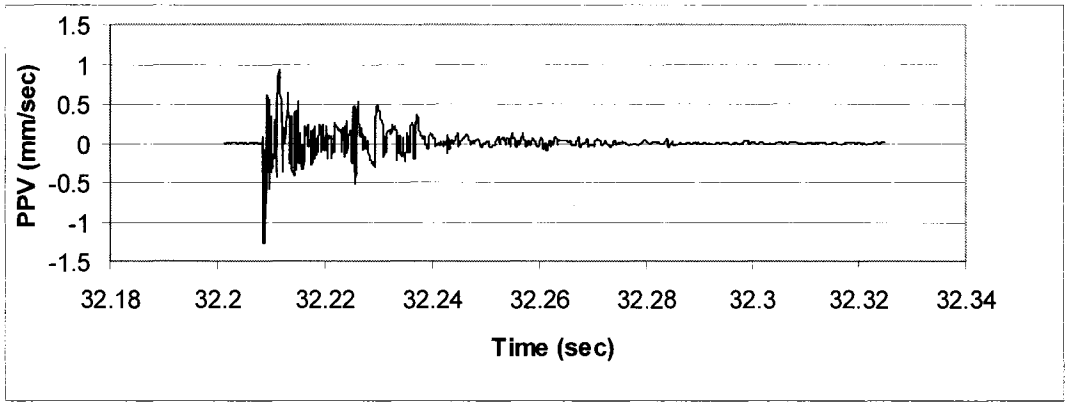

Blow 11 blast probe vibration response:

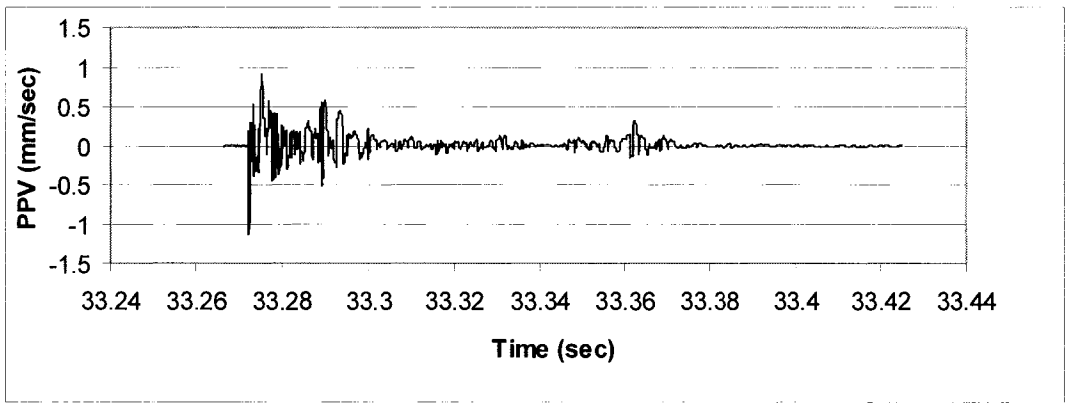

Blow 12 blast probe vibration response:

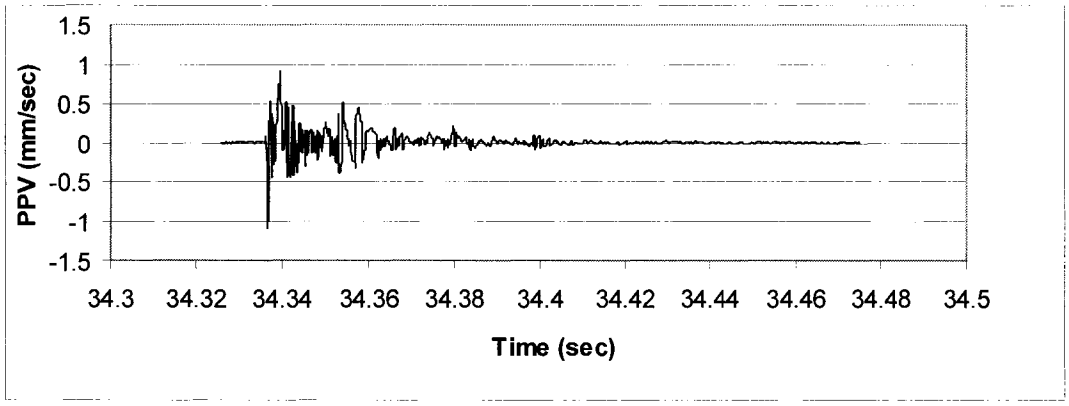

Blow 13 blast probe vibration response:

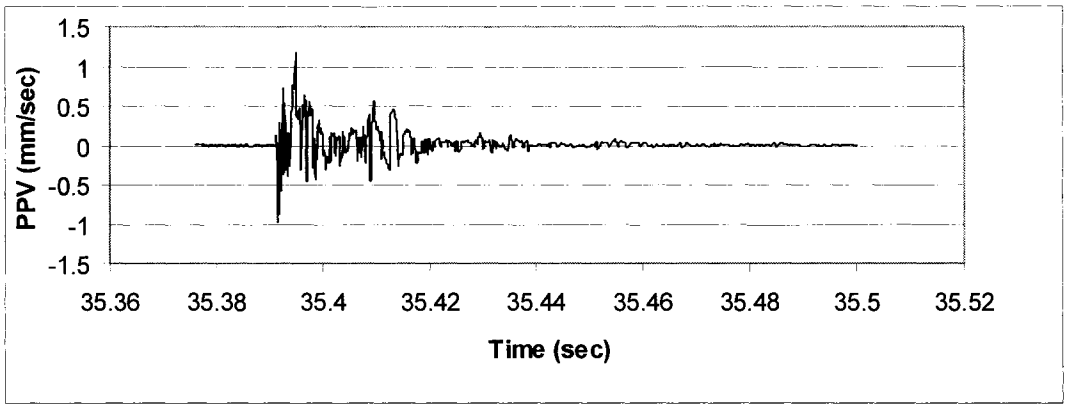

Blow 14 blast probe vibration response:

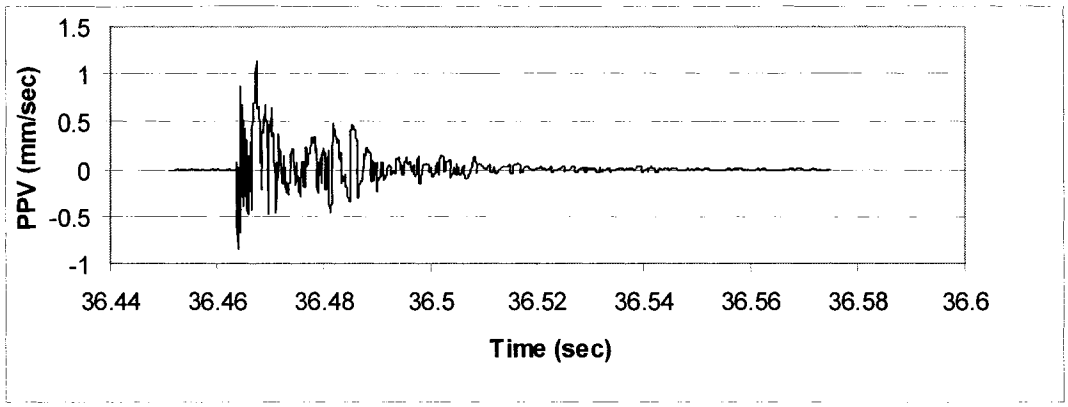

Blow 15 blast probe vibration response:

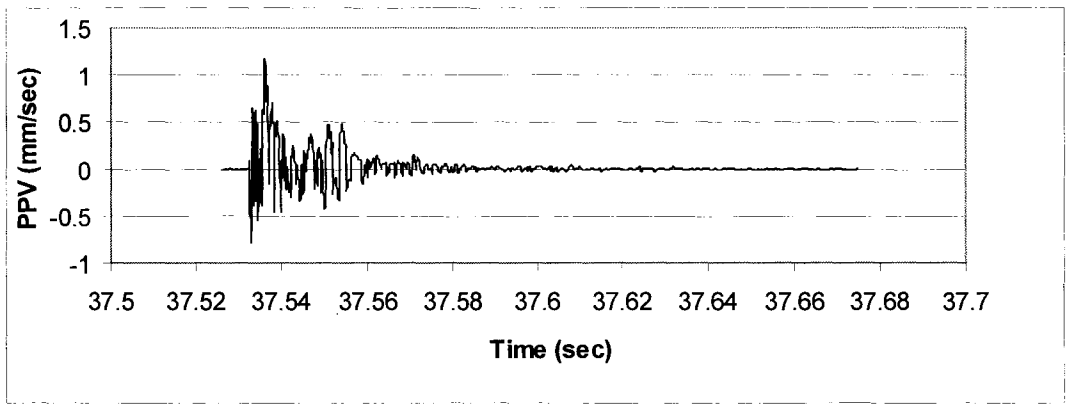

Blow 16 blast probe vibration response:

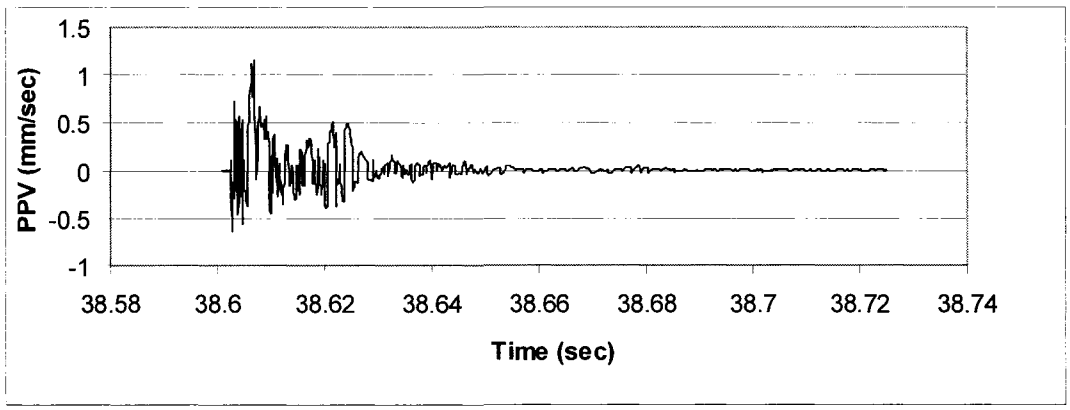

Blow 17 blast probe vibration response:

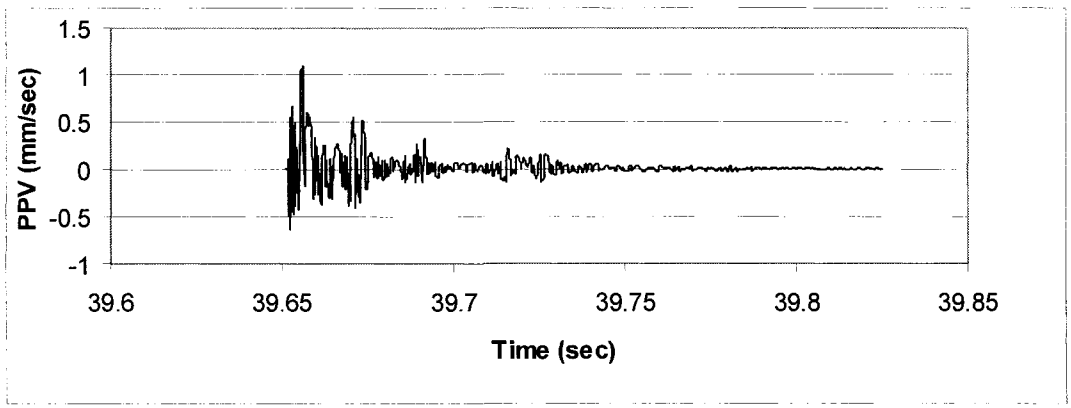

Blow 18 blast probe vibration response:

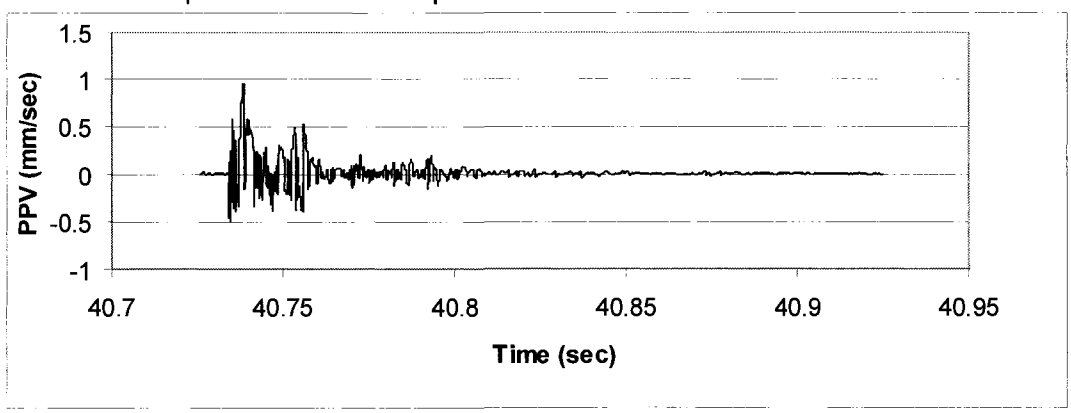

Blow 19 blast probe vibration response: